ORNL/TM-6609

Characterization of Time-Independent Properties of Formed and Welded Pipe for Breeder Reactor Applications

J. W. McEnerney
V. K. Sikka

OAK RIDGE NATIONAL LABORATORY
CENTRAL RESEARCH LIBRARY
CIRCULATION SECTION
4500N ROOM 175
LIBRARY LOAN COPY
DO NOT TRANSFER TO ANOTHER PERSON
If you wish someone else to see this report, send in name with report and the library will arrange a loan.

OAK RIDGE NATIONAL LABORATORY
OPERATED BY UNION CARBIDE CORPORATION · FOR THE DEPARTMENT OF ENERGY

Printed in the United States of America. Available from
the Department of Energy,
Technical Information Center
P.O. Box 62, Oak Ridge, Tennessee 37830
Price: Printed Copy $6.50; Microfiche $3.00

This report was prepared as an account of work sponsored by an agency of the United States Government. Neither the United States Government nor any agency thereof, nor any of their employees, contractors, subcontractors, or their employees, makes any warranty, express or implied, nor assumes any legal liability or responsibility for any third party's use or the results of such use of any information, apparatus, product or process disclosed in this report, nor represents that its use by such third party would not infringe privately owned rights.

ORNL/TM-6609
Distribution
Category UC-79b,-h,-k

Contract No. W-7405-eng-26

METALS AND CERAMICS DIVISION

CHARACTERIZATION OF TIME-INDEPENDENT PROPERTIES OF FORMED AND WELDED PIPE FOR BREEDER REACTOR APPLICATIONS

J. W. McEnerney V. K. Sikka

Date Published: April 1979

OAK RIDGE NATIONAL LABORATORY
Oak Ridge, Tennessee 37830
operated by
UNION CARBIDE CORPORATION
for the
DEPARTMENT OF ENERGY

CONTENTS

ABSTRACT 1

1. INTRODUCTION 2

2. DESCRIPTION OF THE FIVE FORMED AND WELDED PIPES 5

3. ECONOMIC EVALUATION 12

4. DESCRIPTION OF THE FORMING AND WELDING PROCESS 13

5. NONDESTRUCTIVE EVALUATION 21

   5.1 Dimensional Evaluation 21
   5.2 Determination of Weld Ferrite Number 33
   5.3 Radiographic Inspection 34

6. DESTRUCTIVE EVALUATION 35

   6.1 Sectioning of Pipes 35
   6.2 Metallographic Characterization 36
   6.3 Ferrite Evaluation 53

7. MECHANICAL PROPERTY CHARACTERIZATION 67

   7.1 Test Procedure 69
   7.2 Data 70
   7.3 Engineering Stress-Strain Curves 70
   7.4 Comparison of Weld Properties with Upper and Lower Bounds for the Wrought Material 70
   7.5 Comparison of Weld Properties with Base-Metal Properties 75
   7.6 Comparison between GTA (E-13) and SA (H-22) Welded Pipes 84
   7.7 Estimate of Residual Cold Work in the Base Metal and Weld 85
   7.8 Role of Carbon and Nitrogen on Tensile Properties 87
   7.9 Stress-Strain Behavior (up to 5% Strain) 91
   7.10 Photographs of Tensile-Tested Specimens 92
   7.11 Summary of Mechanical Property Characterization 108

8. CONCLUSIONS 109

ACKNOWLEDGMENTS 110

REFERENCES 110

CHARACTERIZATION OF TIME-INDEPENDENT PROPERTIES OF FORMED AND WELDED PIPE FOR BREEDER REACTOR APPLICATIONS*

J. W. McEnerney V. K. Sikka

ABSTRACT

Five commercially available large-diameter, thin-wall, formed and welded pipes were procured to characterize their time-independent properties for breeder reactor applications. The pipes were 0.91-m-OD by 12.77-mm-wall by 1.83-m-long type 316 stainless steel with solution-annealed longitudinal seam welds made by the gas tungsten-arc (GTA) or submerged-arc (SA) processes with types 16-8-2 or 316 stainless steel, or with no filler metal. A comparison between the pipe used for the Fast-Flux Test Facility (FFTF) and these pipes showed the latter to be less expensive.

Nondestructive evaluation of the pipes included dimensional characterization, determination of weld ferrite number, and radiographic inspection. The dimensional evaluation indicated that the majority of the pipes did not fully comply with the commercial specifications for which they were procured. Based upon this evaluation, a recommendation is made that direct measurements in the restrained condition should be used to characterize pipe ends for weld fitup. Three of the five pipes had a magnetically determined weld ferrite number of zero, while the other two had values of approximately 4 or less.

Destructive evaluation of the pipes included metallographic characterization and ferrite content determination. The metallographic characterization included evaluation of both macro- and microstructural details. The macrostructural analysis highlighted the differences that can occur between welds made by the same process. In addition, it revealed some end discontinuities which were not detected by the normal inspection techniques. The microstructural analysis indicated that the welds contained mixed substructures which ranged from dendritic to cellular. The ferrite evaluation indicated that values obtained by calculation of the ferrite number from chemical analysis can be deceptive due to the effects of solution annealing and is also dependent upon dilution effects and the inclusion of nitrogen in analyses for GTA welds. A difference was shown to exist between magnetically determined ferrite number and optically determined ferrite content. A good correlation was shown between destructively and nondestructively determined ferrite number based upon magnetic permeability measurements.

Tensile testing of base-metal and weldment specimens in the as-received condition was performed at room temperature, 427, 538, and 649°C, while reannealed specimens were tested at room temperature and 649°C. Significant differences were shown to exist between the stress-strain curves of the base metal and weld. A comparison of weldment properties with scatter bands of eight wrought heats showed that yield strength (YS) was comparable, but ultimate tensile strength (UTS), uniform, and total elongation and reduction in area had values which fell outside the scatter band. Direct comparison of the weldment and base-metal properties of the pipes showed the same trend as indicated above. A comparison of a pipe welded by GTA and one welded by SA showed the latter to be weaker. Based upon models which predict creep and stress-rupture properties for base metal from UTS, the weldments are predicted to be weaker than the base metal, with GTA better than SA. An evaluation of the residual cold work in the pipes indicates that YS is more affected than UTS, with the welds generally having higher levels of residual stress than the base metal. The effect of this residual stress on elevated-temperature properties is not considered to be significant. Carbon and nitrogen are shown to play an important role in determining the YS and UTS of the base metal and weld. We showed that it is possible to predict the stress-strain behavior for both the base metal and weld, using base-metal constants. However, for accurate prediction of weld behavior, a modified steady-state strain-hardening constant is needed. Photographs of the tensile-tested transverse weld specimens show that the weld is the weakest link, because this was the location of all failures.

*Work performed under DOE/RRT 189a OH103, Piping and Fittings Development.

1. INTRODUCTION

In current United States[1,2] designs for breeder reactors (BR), primary and intermediate coolant systems operate at high temperature and low pressure and utilize sodium as the heat transfer medium. Due to this medium, operating temperatures in the creep range, and potentially rapid thermal transients, design considerations for BR primary and intermediate coolant piping are significantly different than for light-water reactors (LWR).

Figure 1 shows a schematic diagram of one of the three loops in the Clinch River Breeder Reactor Plant (CRBRP) heat transport system. Since the CRBRP was designed as an intermediate step toward a commercial BR,[1] the design considerations applicable to its primary and intermediate sodium coolant systems should be generic of loop systems. The schematic of the CRBRP heat transport system shows that the hot leg of the primary sodium system will operate at about 535°C, while the hot leg of the intermediate sodium system will operate at about 500°C. Both of these operating temperatures are within the creep range and therefore exceed temperatures for which allowable stress values are given in ASME Code, Section III, Division 1.[3]

ASME Code Case N-47, formerly Code Case 1592,[4] provides rules for materials, design, fabrication, and inspection. This code case considers time-dependent material properties and guards against time-dependent rupture modes such as creep rupture, creep fatigue, and gross distortion due to ratchetting. The design of components is based upon the control of both load and deformation. Because of the potential for reduced ductility and strain concentration in weldments, Code Case N-47 limits the calculated strain for the weld region to one-half the values permitted for the base metal. However, base material properties are used in the

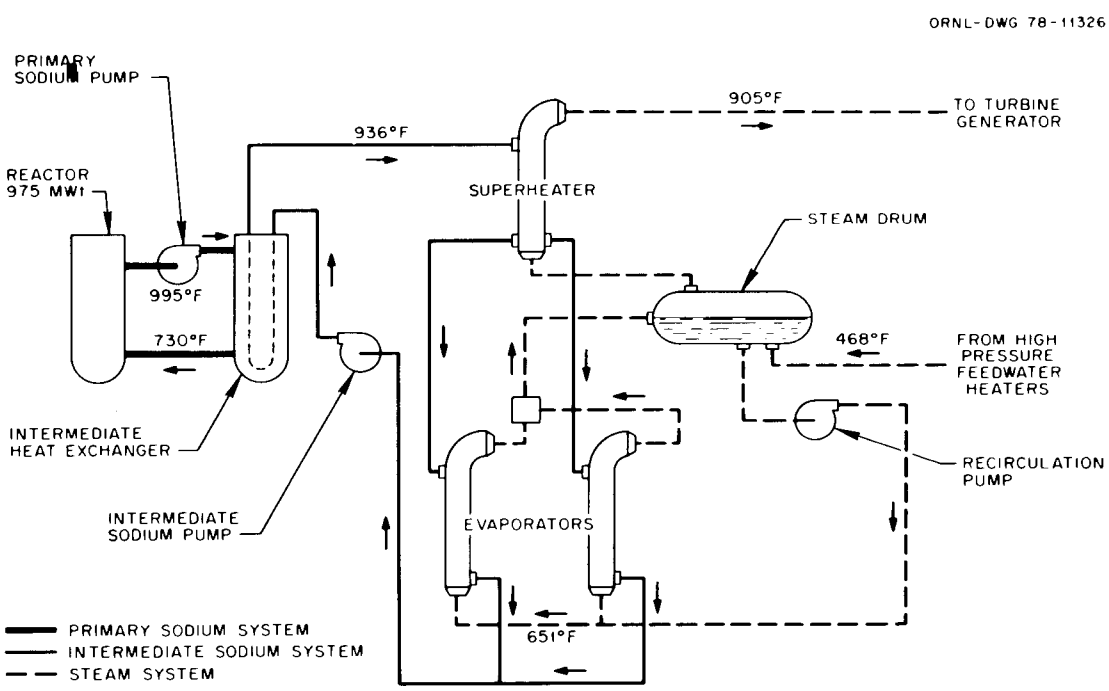

Fig. 1. Schematic diagram of one of three loops in the Clinch River Breeder Reactor Plant heat transport system, showing the primary and intermediate sodium circuits and portions of the steam circuit (ref. 1).

design of weldments. In addition, time-dependent metallurgical structure changes are considered, for example, by limiting the amount of delta ferrite in austenitic stainless steel welds.

Figure 2 shows the primary and portions of the intermediate sodium piping system in one of the three loops in the CRBRP. The hot-leg piping for both the primary and intermediate sodium systems will be type 316 stainless steel, while the cold leg will be type 304 stainless steel. Type 316 stainless steel was selected for the hot-leg piping in both the CRBRP and the FFTF because of its superior elevated-temperature properties.[2,5] However, the use of sodium as the cooling medium imposes additional material and design requirements. The sodium can cause interstitial transfer (decarburization) and mass transfer (corrosion) to occur on the inside surface of the austenitic stainless steel pipe.[2] To account for the interstitial transfer, high-carbon or H-grade materials are used to assure that a specified minimum level of carbon is present at the end-of-life. Additional material is used to provide an allowance for mass transfer.

Because of potentially rapid thermal transients and the low operating pressure in BR primary and intermediate sodium systems, thin-walled piping (9.5 mm for FFTF and 12.7 mm for CRBRP) is used to reduce the thermal stress gradient across the wall thickness. The control of wall thickness variations is also important in reducing thermal stress gradients. Code Case N-47 specifically cautions the designer that since dimensional standards for piping components do not control the maximum wall thickness, additional controls may have to be imposed when significant thermal transients are anticipated.

Because of the high thermal output and low operating pressure of BRs, large-diameter piping will be required to provide the necessary coolant flow. The FFTF utilized 0.71-m-OD primary coolant piping. Figure 2 shows that the CRBRP primary hot-leg piping from the reactor to the primary sodium pump is

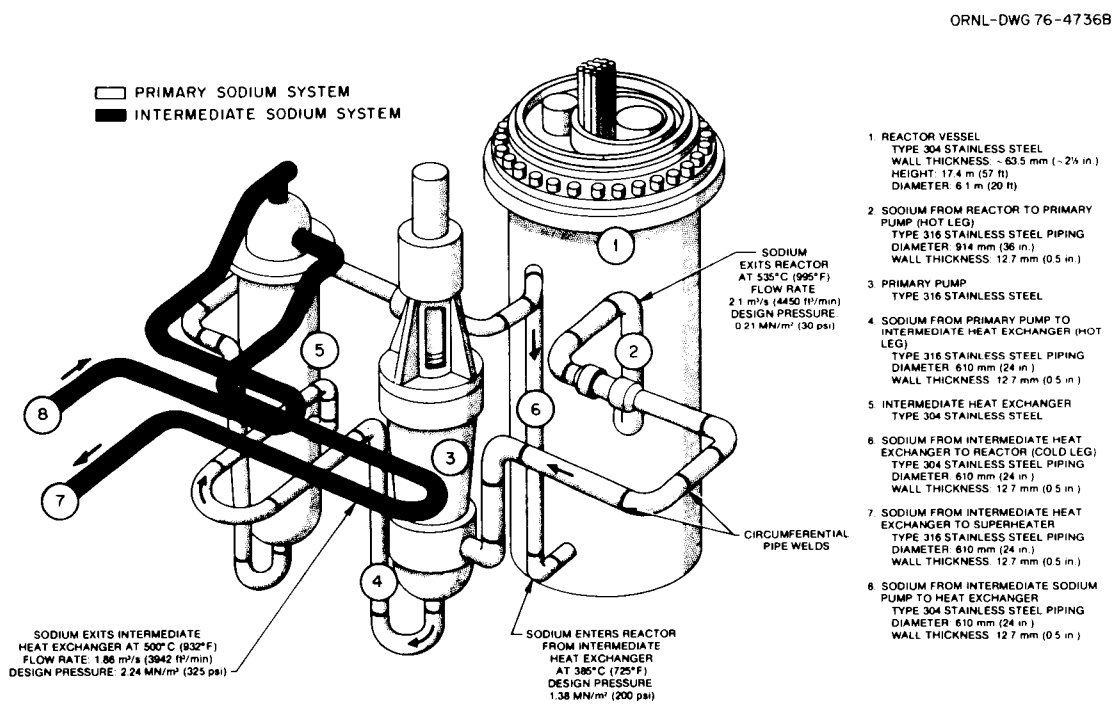

Fig. 2. Primary and portions of intermediate sodium piping system in one of the three loops in the Clinch River Breeder Reactor Plant (ref. 5).

0.91 m in outside diameter. Commercial-size BRs have been projected to have piping which could range from 0.91 to 1.32 m in outside diameter. The combination of the large diameter and the thin wall introduces problems in both the manufacturing of the pipe and the shop and field fabrication. The methods used to manufacture this pipe must provide good dimensional control to reduce variations in wall thickness and diameter. Tight control of the wall thickness is primarily necessary because of the previously discussed effects of thermal transients. Diametral and wall thickness control are important for fitup during shop and field welding. The need for diametral control is also important because circumferential and axial bending stresses can be produced in out-of-round pipe due to internal pressure.[6,7] These stresses are classified as peak and are only considered in the fatigue analysis.[7] In addition to dimensional control, the manufacturing and fabrication techniques must provide base-metal and weldment properties which are adequate for the service conditions. However, it is also important that the cost of the piping be minimized to enable a commercial BR to be economically competitive.

The FFTF utilized hot-extruded and -worked and hot-extruded and -machined pipe to achieve the integrity required for its primary and intermediate sodium coolant systems. The starting material in both of these manufacturing processes was a heavy-walled, hot-extruded pipe section. In the former process, the hot-extruded pipe was reduced to the desired thickness and diameter by performing several cold-working sequences with intermediate anneals. The cold reduction is accomplished by a rotary point extrusion process in which rotating rollers or stationary rollers with a rotating preform move axially over the inside or outside surface, applying both reduction and extrusion forces. This process provides tight dimensional control of the piping as shown by dimensional data for two sections of FFTF primary coolant piping (Table 1). In addition, extensive mechanical properties characterization of the FFTF extruded and worked piping by Hanford Engineering Development Laboratory (HEDL) has demonstrated[10] its acceptable tensile, creep-rupture, and fatigue crack propagation properties. The FFTF extruded and machined pipe was manufactured by machining the extruded pipe to the final dimensions. Dimensional control would therefore be expected to be inherently good. Earlier tensile and stress-rupture testing at HEDL[11] indicated that the strength and ductility of extruded and worked pipe were slightly superior to those of extruded and machined pipe.

Although the two methods for manufacturing the FFTF sodium piping provided high-quality pipe with good dimensional control, the costs were relatively high. Because of these high costs, several different manufacturing methods are being evaluated for follow-on BR sodium coolant systems. These additional methods include forming and welding, centrifugally casting and working, and hot extruding.

A program is in progress at ORNL to characterize large-diameter, thin-wall austenitic stainless steel pipe made by various fabrication methods. As part of this program, five lengths of formed and welded pipe were procured from several commercial suppliers. Pipes manufactured by this process were chosen for

Table 1. Dimensional evaluation of two FFTF 0.71-m-OD × 9.53-mm-wall × 4.57-m-long (28 in. × 0.375 in. × 15 ft) hot-extruded and -worked pipe sections

	Attained tolerance[a] [in. (mm)] (ref. 8)	Required tolerance[a] [in. (mm)] (ref. 9)
Wall thickness	−0.001 to +0.008 (−0.025 to +0.203)	±0.047 (±1.194)
Inside diameter	−0.023 to +0.020 (−0.584 to ±0.508)	±0.031 (±0.787)
Inside diameter ovality	0.009 to 0.026 (0.229 to 0.660)	0.062 max (1.575)
Camber (max in 10 ft)	0.100 (2.540)	0.125 (3.175)

[a]Dimensions given in English units to facilitate comparison with existing specifications.

characterization because they would be representative of a common commercial method for manufacturing pipe in the United States. In addition, this process has a wide range of size capability, limited only by available plate. Since the forming and welding process is generally considered to be one of the most economical methods for manufacturing large-diameter, thin-wall pipe, it has been strongly considered for commercial BR sodium coolant applications. The potential disadvantages of the process are that the ability to control dimensions may not be adequate, and since the pipe is a nonhomogeneous material, separate analytical treatment of the base metal and weldment may be required.

The purpose of this report is to characterize the time-independent properties of the five formed and welded pipes which were procured. Additional work is in progress to characterize their time-dependent properties.

2. DESCRIPTION OF THE FIVE FORMED AND WELDED PIPES

The five formed and welded pipes were procured between August 1976 and February 1977, in accordance with modified ASME code material specifications. The plate used to form the pipes was manufactured in accordance with SA-240, type 316,[12] while the pipes were manufactured in accordance with SA-358[13] and SA-312.[14] The pipes were manufactured and certified in accordance with the requirements of ASME Code, Section III, Division 1, Class 1[15] or 2.[16] Each of the pipe sections was 1.83 m long, with wall thickness and outside diameter prototypic of the CRBRP (0.91-m OD by 12.77-mm wall). Table 2 provides a summary of the identification, material specifications, code class, welding process, filler metal, final heat treatment, and hydrostatic test pressure for these pipes. ORNL modifications to the ASME code material specifications were used to incorporate additional requirements imposed by RDT standards and to obtain material suitable for BR sodium coolant piping applications. Table 3 lists the additional requirements imposed by the ORNL specifications. Several of the fabricators took exception to some of the requirements in both the ASME code and ORNL specifications. These exceptions are shown in Table 4. Although some additional requirements were specified, the five pipes can be considered to be representative of commercially available large-diameter, thin-wall formed and welded pipe. Therefore, the exceptions taken, as shown in Table 4, reflect the commercial practice of the individual fabricators. However, it also must be recognized that since the procurement was small, certain aspects of the manufacturing will not be totally representative of large orders.

Table 2. Fabrication information for formed and welded 1.83-m-long by 0.91-m-OD by 12.70-mm-wall pipes of type 316 stainless steel

Identification	ASME Code, Section II, material specifications		ASME Code, Section III, class	Welding process	Filler metal	Final heat treatment[a]		Hydrostatic test pressure (MPa)
	Plate	Pipe				Temperature (°C)	Time (hr)	
E-13	SA-240[b]	SA-358[c]	1	GTA with both hot and cold wire additions	16-8-2	1060	0.5	2.76
F-14	SA-240[b]	SA-358[c]	1	GTA with cold wire additions	16-8-2	1066	0.2 (min)	3.10
G-15	SA-240[b]	SA-358[c]	1	GTA with cold wire addition and SA	316	1093	0.5	
G-16	SA-240[b]	SA-312[d]	2	Autogenous GTA	None	1038–1066	0.5	
H-22	SA-240[b]	SA-358[c]	1	SA	16-8-2	1066	0.8	3.45

[a]Followed by water quench.
[b]With additional requirements per specification ORNL MET-WB-MS-3 (ref. 17).
[c]With additional requirements per specification ORNL MET-WB-MS-2 (ref. 18).
[d]With additional requirements per specification ORNL MET-WB-MS-4 (ref. 19).
GTA = gas tungsten-arc.
SA = submerged-arc.

Table 3. Additional requirements imposed by ORNL specifications

Additional requirements	ORNL specifications (ASME code specification)		
	MET-WB-MS-3 (SA-240)	MET-WB-MS-2 (SA-358)	MET-WB-MS-4 (SA-312)
1. Minimum carbon content of 0.04%	x	x	x
2. Heat treatment of plate and finished pipe to be solution annealed at 1038 to 1079°C followed by water quench or other rapid cooling; ASTM A-262, practice E corrosion test required to verify adequacy of cooling rate	x	x	x
3. Ultrasonic examination of the starting plate by angle and straight beam	x		
4. Specific surface finish requirements for plate and finished pipe	x	x	x
5. Radiographic examination of welds at two different angles at least 30°, but not more than 150°, apart		x	

Table 4. Fabricator's exceptions to the requirements of the ASME code and ORNL specifications

Identification	ASME code and ORNL specifications	Exceptions
E-13	SA-240, SA-358, MET-WB-MS-3, and MET-WB-MS-2	None
F-14	SA-240, SA-358, MET-WB-MS-3, and MET-WB-MS-2	None
G-15	SA-240, SA-358, MET-WB-MS-3, and MET-WB-MS-2	1. The tolerance on the outside diameter was ±1.0% instead of 0.5% 2. The range of temperature for heat treatment of the plate was 1093 to 1121°C instead of 1038 to 1079°C; the temperature for the heat treatment of the finished pipe was 1093°C instead of 1038 to 1079°C 3. Hydrostatic test was not performed
G-16	SA-240, SA-312, MET-WB-MS-3, and MET-WB-MS-4	Same as pipe G-15
H-22	SA-240, SA-358, MET-WB-MS-3, and MET-WB-MS-2	The temperature for the heat treatment of the plate was 1038°C minimum instead of 1038 to 1079°C

Figures 3 through 7 show front and end views of the five pipes with a close-up of one of the ends of the longitudinal seam weld. The ASME code plate can be seen on the pipes in Figs. 4(*a*) and 7(*b*). The person shown standing in Fig. 5(*a*) provides a good perspective of the overall size of the pipe. The weld end cross section can be seen in Figs. 3(*c*), 4(*c*), and 5(*c*) as a result of the pickling operation. However, it cannot be seen in Fig. 6(*c*) due to grinding, and in Fig. 7(*c*) due to machining. Internal and/or external surface grinding marks can be seen on all five pipes.

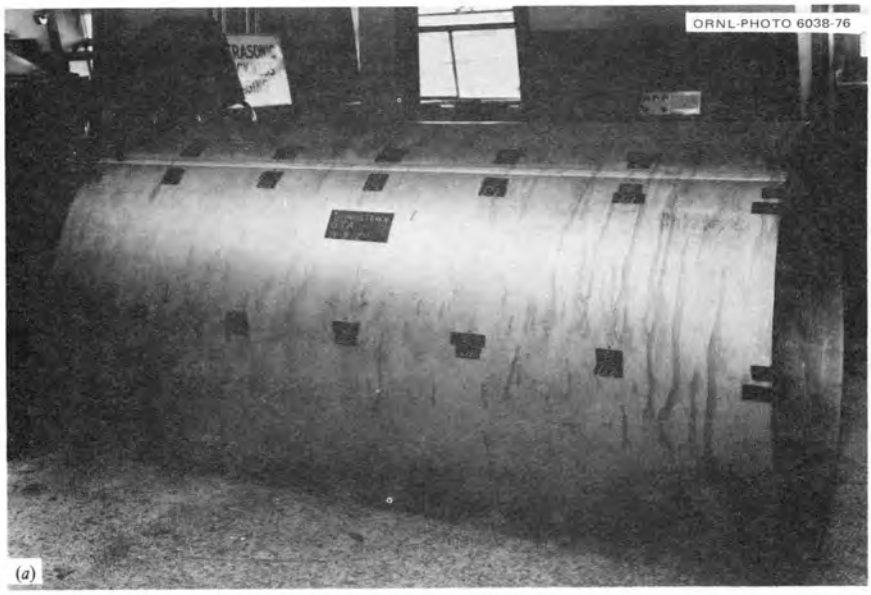

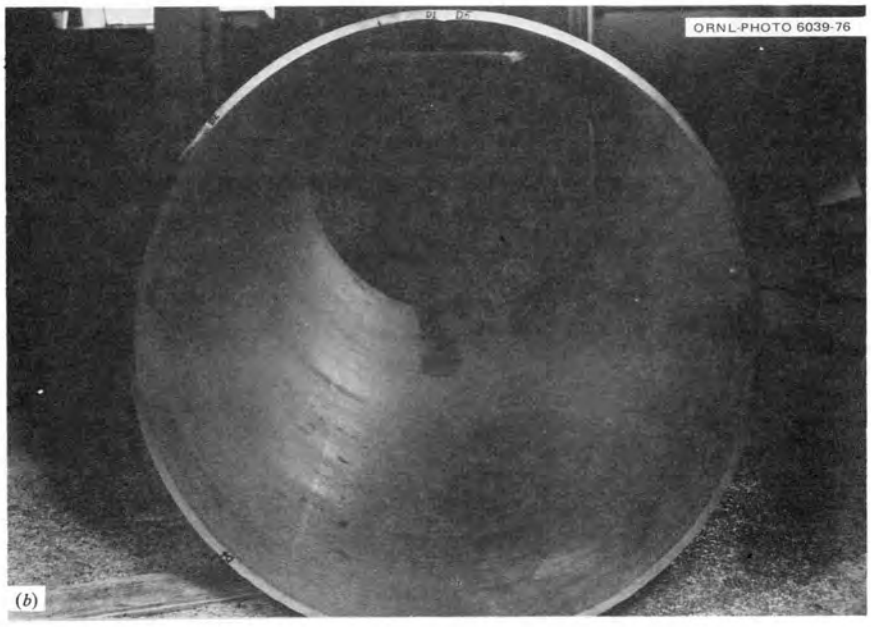

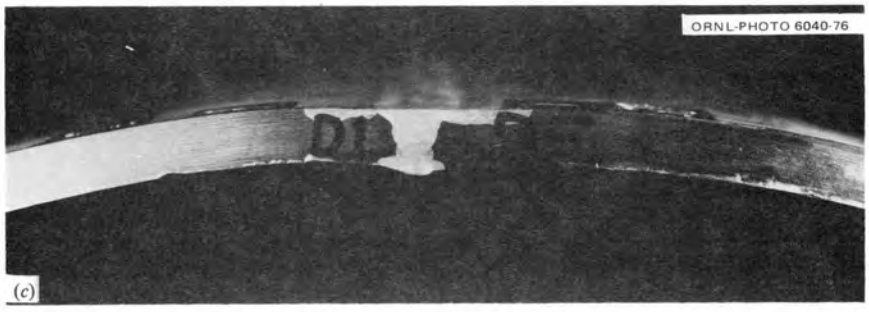

Fig. 3. Pipe E-13, type 316 stainless steel formed and welded pipe, GTA welded with type 16-8-2 filler metal, 0.91-m OD by 12.7-mm wall by 1.83-m length. (*a*) Front view showing dimensional inspection grid, (*b*) end view with diametral inspection locations, (*c*) close-up of weld end.

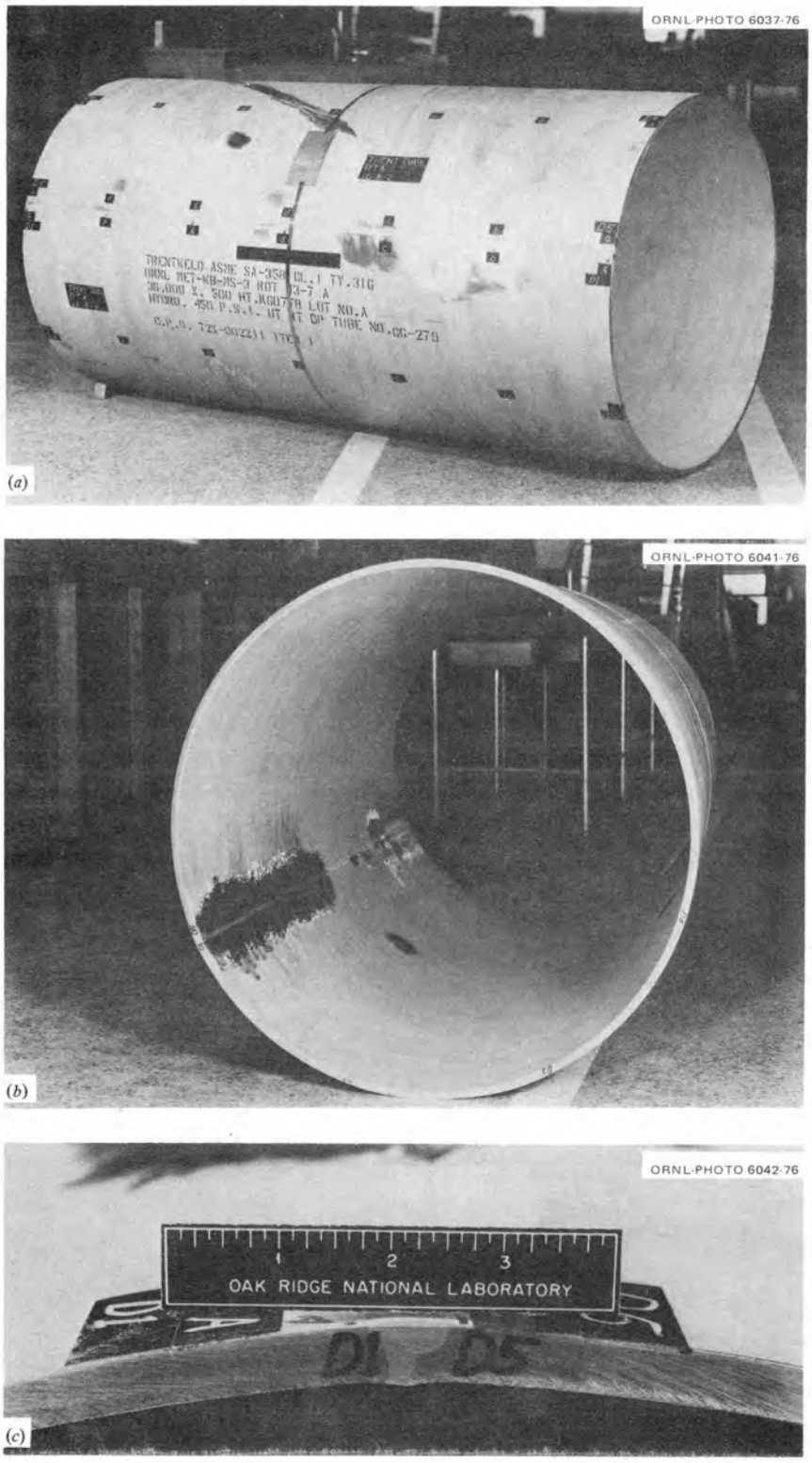

Fig. 4. Pipe F-14, type 316 stainless steel formed and welded pipe, GTA welded with type 16-8-2 filler metal, 0.91-m OD by 12.7-mm wall by 1.83-m length. (*a*) Front view showing dimensional inspection grid, (*b*) end view with diametral inspection locations, (*c*) close-up of weld end.

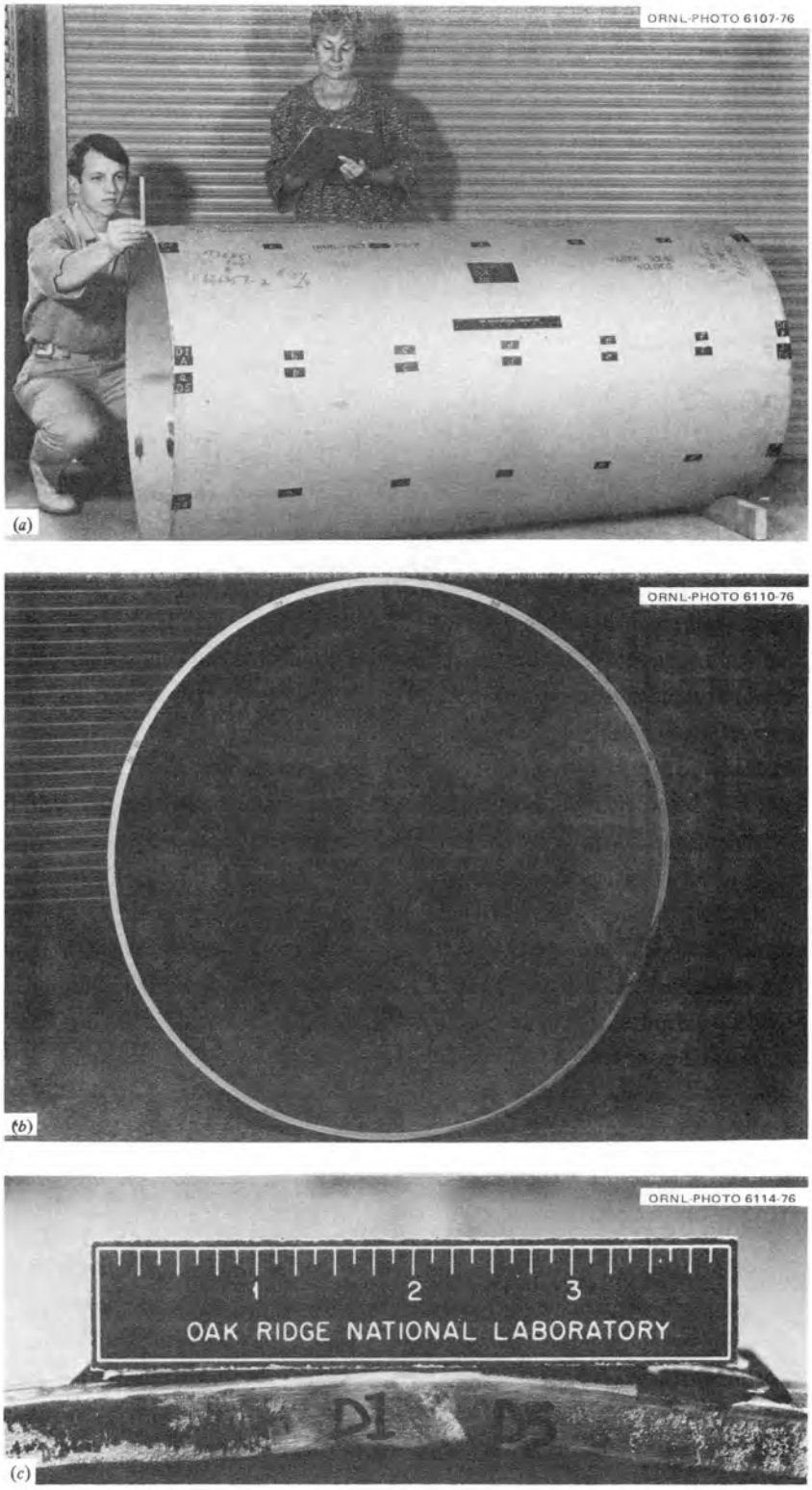

Fig. 5. Pipe G-15, type 316 stainless steel formed and welded pipe, GTA and SA welded with type 316 filler metal, 0.91-m OD by 12.7-mm wall by 1.83-m length. (*a*) Front view showing dimensional inspection grid, (*b*) end view with dimensional inspection locations, (*c*) close-up of weld end.

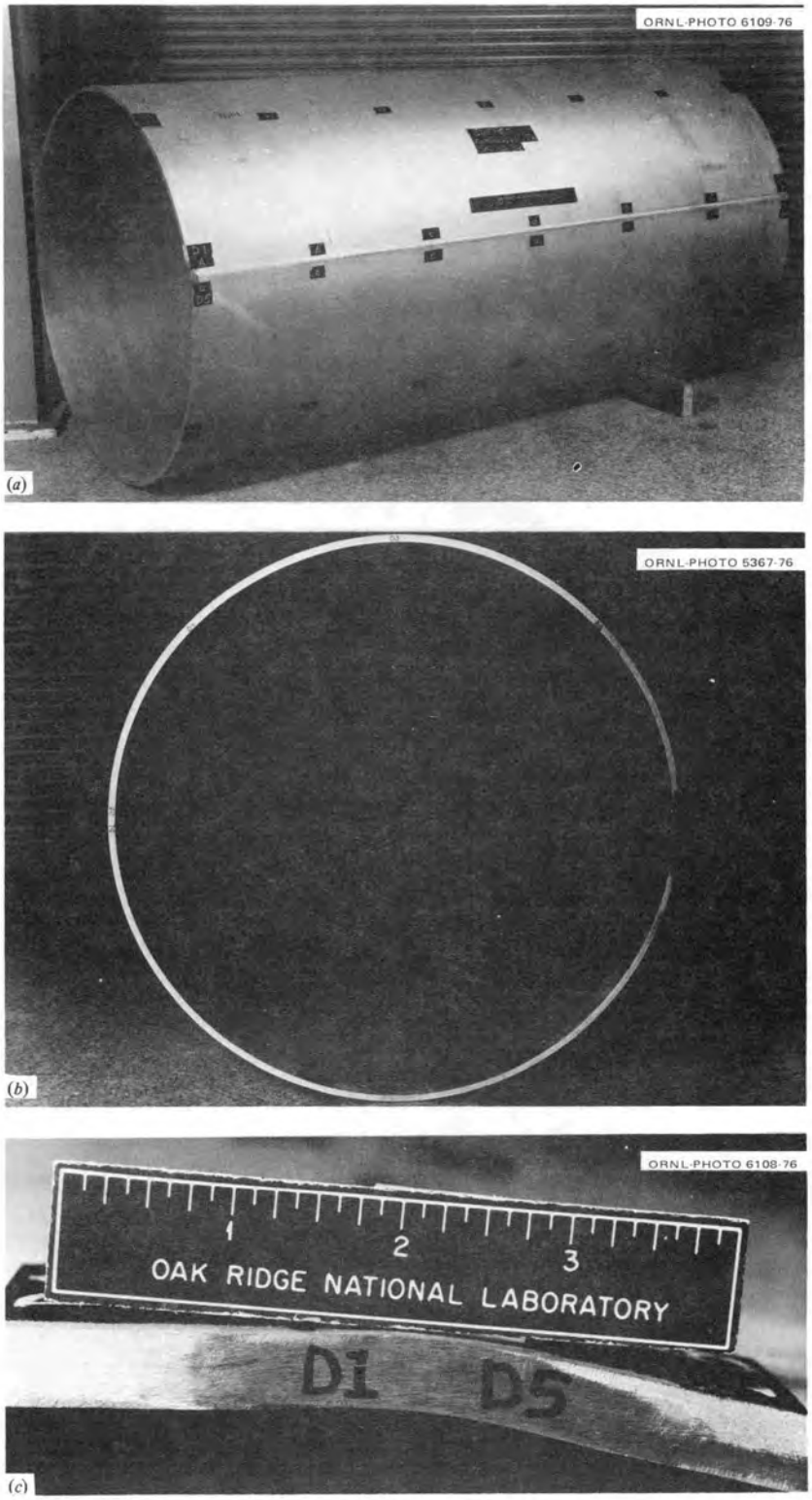

Fig. 6. Pipe G-16, type 316 stainless steel formed and welded pipe, autogenously GTA welded, 0.91-m OD by 12.7-mm wall by 1.83-m length. (*a*) Front view showing dimensional inspection grid, (*b*) end view with diametral inspection locations, (*c*) close-up of weld end.

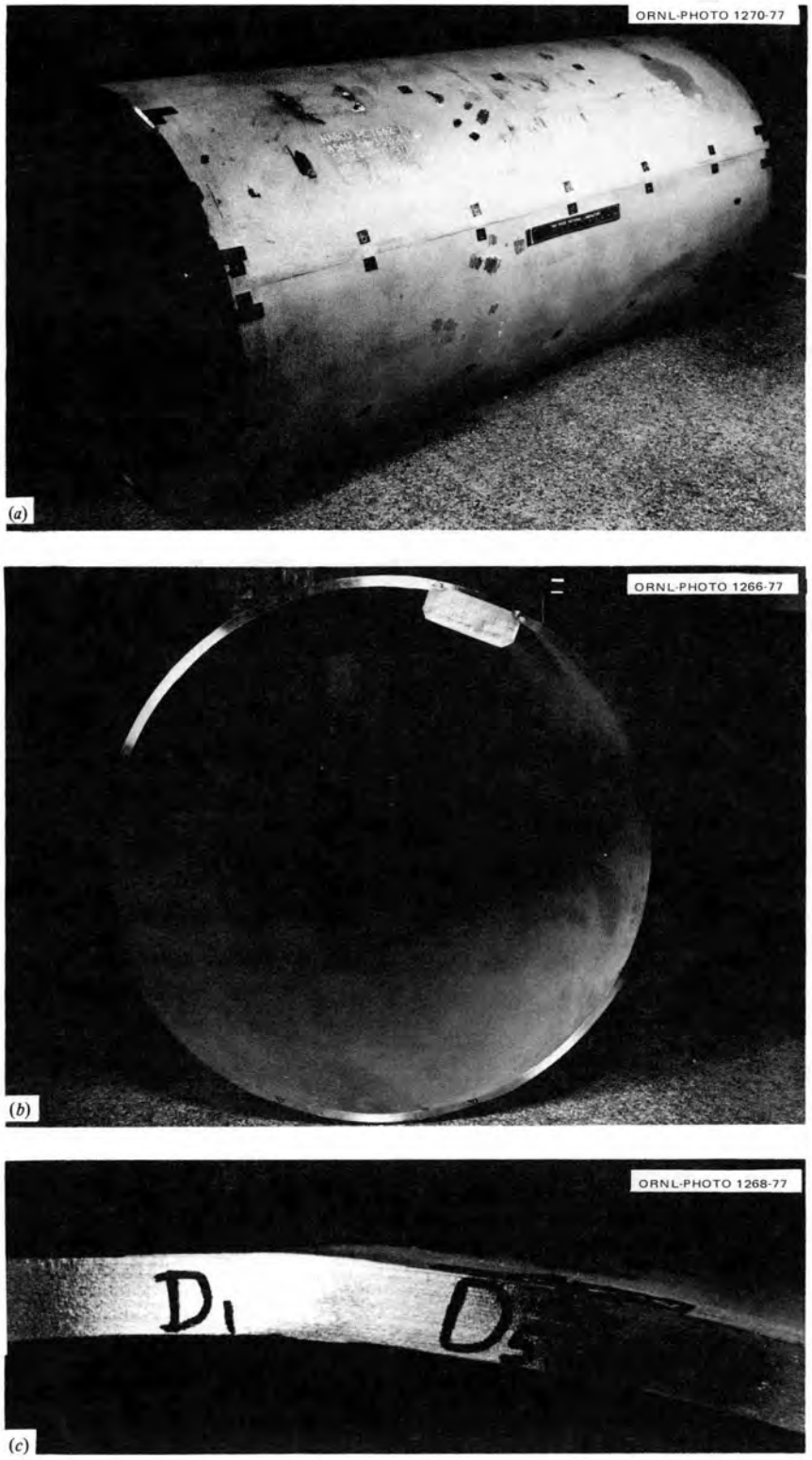

Fig. 7. Pipe H-22, type 316 stainless steel formed and welded pipe, SA welded with type 16-8-2 filler metal, 0.91-m OD by 12.7-mm wall by 1.83-m length. (*a*) Front view showing dimensional inspection grid, (*b*) end view with diametral inspection locations, (*c*) close-up of weld end.

3. ECONOMIC EVALUATION

As a part of the procurement of the five formed and welded pipes, the fabricators were also requested to bid on the cost per unit length for the manufacturing of 30.48 m, to be supplied in five 6.10-m lengths, of the same type of pipes as described in Table 2. Two optional requirements were specified for manufacturing this pipe. Only three of the four fabricators were requested to bid on the 30.48 m of pipe with the two optional requirements. The fabricator of pipe H-22 was asked to bid without the optional requirements. The first optional requirement specified that the inside diameter of the pipe be controlled to a maximum of 35.09 in.* at any point as measured by an inside micrometer, caliper, or equivalent. The second optional requirement included the requirement of the first option and added that the inside-diameter ovality within 0.30 m from each end should be controlled to 0.030 in. maximum (i.e., the difference between the maximum and minimum inside diameters cannot exceed 0.030 in.). The purpose of requesting bids on 30.48 m of pipe with these additional dimensional control requirements was to obtain more meaningful economic data on piping representative of that which would be required for BRs.

The three fabricators that were asked to bid on the optional requirements would not agree to meet these requirements. However, the fabricator of pipe F-14 did agree to tighten the ovality requirement from 1% to 0.5% of the outside diameter. This increased dimensional control also applied to the 1.83-m length of pipe which was procured.

Table 5 shows the quotations that were received from the various fabricators for both the 1.83 and 30.48 m of pipe. These quotations indicate that there is a wide degree of variation between different

Table 5. Summary of quotations[a] for type 316 stainless steel formed and welded pipe

Fabricator code	ASME Code, Section II, pipe specification	ASME Code Section III, class	Welding process	Quotation ($/m)	
				1.83-m length	30.48-m length
E	SA-358	1	GTA	3807	No response
F	SA-358	1	GTA	4954	2008
G (distributor 1)	SA-358	1	GTA or SA	4482	No response
G (distributor 2)	SA-358	1	GTA or SA	5154	3648
G (distributor 1)	SA-312	2	GTA	3245	No response
G (distributor 2)	SA-312	2	GTA	5154	3648
H	SA-358	1	SA	6762	4029

[a]Quotations made between March and June of 1976 for 1.83 and 30.48 m of 0.91-m-OD by 12.70-mm-wall pipe.

fabricators and even between different distributors for the same fabricator. As expected, these quotations show that the price per unit length of pipe decreases as the total length of the order increases. Because the FFTF primary hot-leg piping was smaller in diameter and wall thickness and was purchased approximately four years earlier, it is impossible to make a direct cost comparison. However, an estimated comparison can

*All dimensions which deal with dimensional tolerance control will be given in English units to facilitate comparison with existing specifications.

be made by adjusting the price of the FFTF pipe to account for these differences. The adjustments made to the cost per unit length of the FFTF primary hot-leg pipe (0.71-m-OD by 9.53-mm-wall) are:

1. Multiply the original unit cost by the ratio of the cross-sectional area of 0.91-m-OD by 12.70-mm-wall pipe to 0.71-m-OD by 9.53-mm-wall pipe to account for differences in material.
2. Add 30% of the original unit cost to the value determined in item 1 to account for additional manufacturing costs.
3. Multiply the value obtained in item 2 by a compound interest factor to account for 7% inflation per year for four years.

Table 6 shows a comparison of the costs for FFTF piping and formed and welded pipe prototypic of CRBRP, using the adjustment calculation outlined above. In addition, after normalizing both costs in terms of 1976 dollars, they were both adjusted to indicate the cost in 1978. Because several assumptions were utilized, the cost comparisons shown in Table 6 are subject to some degree of error. However, these comparisons do indicate that the use of formed and welded pipe has the potential for significantly lowering the material cost per unit length. The specific cost for formed and welded pipe would still be a function of the requirements imposed for a particular BR and would therefore vary accordingly.

Although the preceding evaluation has indicated that formed and welded pipe is economically desirable, a thorough investigation of its other characteristics is necessary before identifying it as a favorable method. The refusal of three manufacturers to bid on pipe with increased dimensional control is indicative of an area of weakness for this manufacturing method.

Table 6. Comparison of costs for FFTF piping[a] and formed and welded pipe prototypic of CRBRP

Piping	1974 cost ($/m)	1976 cost ($/m)	1978 cost ($/m)
FFTF[a]	1602[b]	4218[c]	4809[d]
Formed and welded prototypic of CRBRP		2008–4029[e]	2289–4593[d]

[a]0.71-m-OD by 9.53-mm-wall, type 316H stainless steel, hot-extruded and -worked pipe.

[b]Bechtel Power Corporation purchase order No. 8776-M-106AC (ref. 20).

[c]Obtained by adjusting the 1974 cost as follows: (1) multiply 1974 cost by the ratio of CRBRP/FFTF pipe cross-sectional area (× 1.71); (2) add 30% of the 1974 cost to item 1; (3) multiply item 2 by the compound interest factor to account for 7% inflation per year for four years (× 1.31).

[d]Obtained by adjusting the 1976 cost as follows: Multiply by the compound interest factor to account for 7% inflation per year for two years (× 1.14).

[e]Obtained from Table 5.

4. DESCRIPTION OF THE FORMING AND WELDING PROCESS

Forming and welding of plate is a common commercial method for producing pipe in the United States. Plate can either be formed into a cylinder with a longitudinal seam, or it can be wound such that it has a spiral seam which follows a helical path along the pipe. Figure 8 shows a schematic representation of formed and welded pipes with longitudinal and spiral seams. The spiral winding of plate into pipe is limited

ORNL-DWG 78-11327

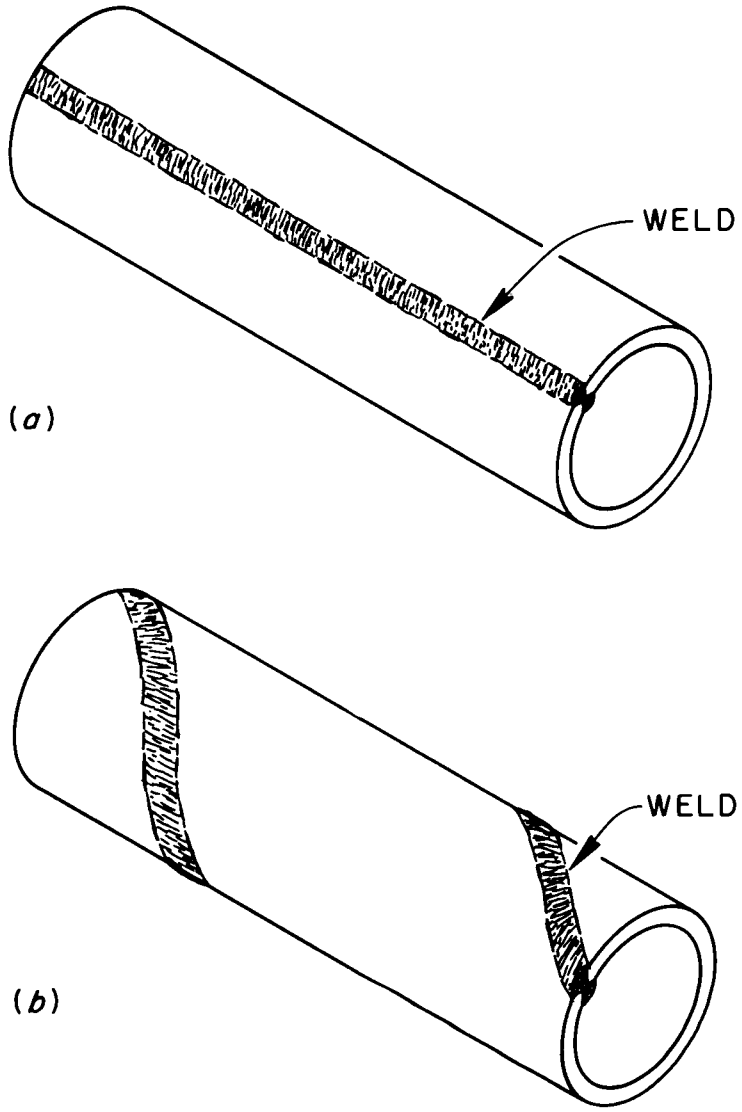

Fig. 8. Schematic representation of formed and welded pipe with (*a*) longitudinal seam, (*b*) spiral seam.

to thin plate or sheet. In addition, the uniformity of the spiral seam can be difficult to control if camber or bowing is present.[21] Because of these limitations, spiral-wound pipe has not been utilized for nuclear applications. This discussion will therefore concentrate on formed and welded pipe with a longitudinal seam.

The first consideration in making formed and welded pipe is the starting plate. The size of formed and welded pipe is usually only limited by the size of the available plate. Generally the size limitation would be a function of the desired diameter and length of the pipe (i.e., as the diameter increased, the available length would decrease). However, for heavy-wall thicknesses, ingot yield capacity at the rolling mill might also become a limiting factor. Wall thickness might also be limited by the forming capability of the manufacturer, although hot forming can essentially remove this limitation. In general, the diameter is the

most flexible dimension, followed by wall thickness and length. Since the forming operations during the manufacturing of the pipe are not designed to appreciably affect the wall thickness, the plate rolling-mill operations determine the control of this dimension. Such factors as roll crown and type of finishing operation (hot or cold) determine the mill's capability to control the wall thickness. Generally the mills are accustomed to manufacturing plate in accordance with specifications which only limit the minimum wall thickness. By aiming the rolling operations to produce a heavier wall thickness than that required, the adverse effects of crowning can be avoided while still complying with the requirements. Obviously, it is not economically advantageous for the mill to supply plate that is significantly thicker than the minimum requirement. It is also possible to pay a premium price to obtain plate with a greater degree of thickness control.

For ASME Code, Section III, Class 1 material,[22] the plate is ultrasonically inspected prior to being formed into a cylinder. This operation would usually be performed by the material supplier.

The first operation that the pipe manufacturer would perform is to gas or plasma-arc cut or shear the plate to the required blank size, which is generally determined by the length and mean circumference (circumference taken at the midpoint of the thickness) of the pipe to be manufactured.[23] However, for greater dimensional control, the exact location of neutral bending axis is used to calculate the circumference and thereby establish the blank size.[23] For example, it is reported[23] that during cold forming, the neutral axis shifts inward approximately 26% from the mean plate thickness. During hot forming, the effects of both a shift in the neutral axis and thermal expansion must be accounted for if tight dimensional control is required.[23]

Once the blank is cut to the required size, the next operation is to prepare the two edges to be welded. This edge preparation involves imparting the desired weld joint configuration and is usually performed by gas or plasma-arc cutting or planing. Figure 9 shows some of the typical weld joint configurations, with welding passes superimposed, which would be used.

ORNL-DWG 78-11328

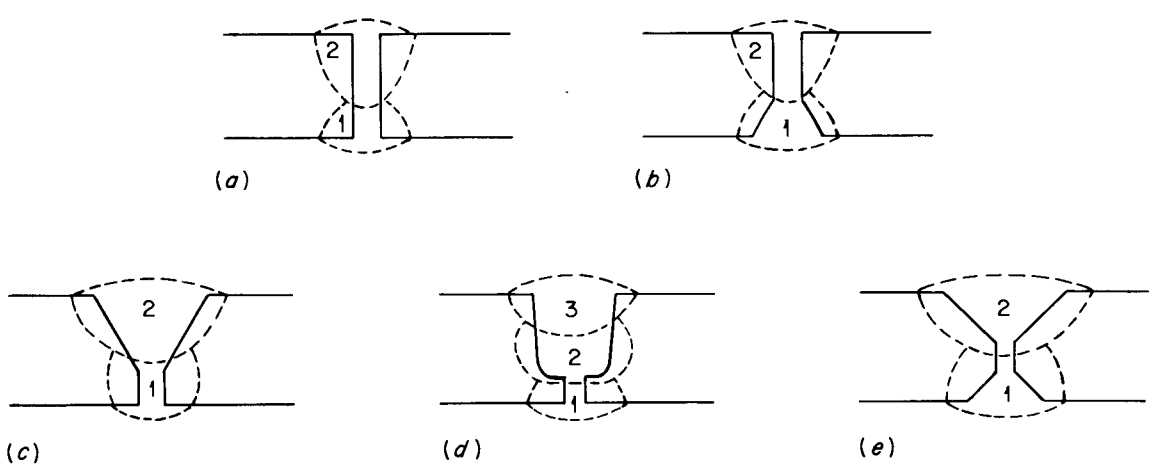

Fig. 9. Typical weld joint configurations for longitudinal seam welds with welding passes superimposed; (*a*) square butt, (*b*) single V-groove on ID, (*c*) single V-groove on OD, (*d*) single U-groove on OD, (*e*) double V-groove. The outside surface of the pipe is up in all cases.

The first operation for forming plate into a cylindrical shape is normally crimping the edges to be welded.[24] Crimping consists in bending the edges to the proper radius so that there will not be a flat surface near the longitudinal seam. Figure 10 shows a plate with both ends crimped and ready for forming. Crimping of the plate is usually performed on a press or rolls.[24] However, not all plate is necessarily crimped before forming into a cylinder. Pipes which are not crimped would be expected to contain some degree of flatness near the longitudinal seam.

ORNL-DWG 78-11329

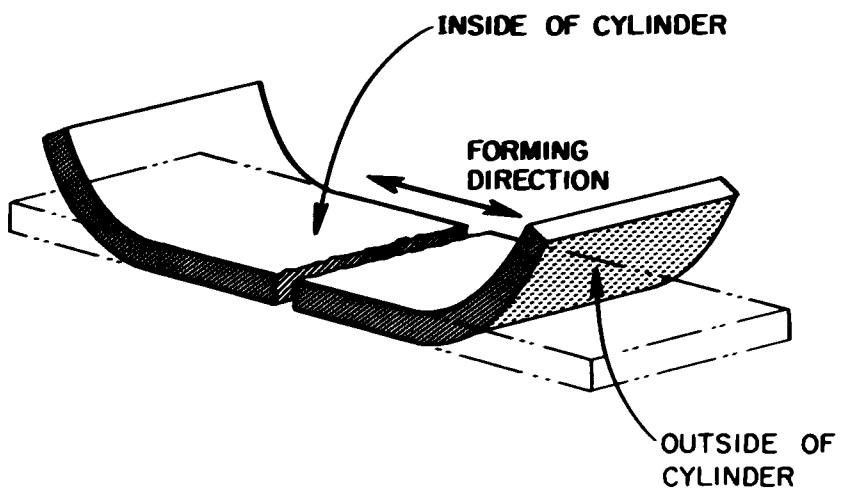

Fig. 10. Typical plate with both ends crimped and ready for forming.

After the plate has been crimped, the next operation is the roll or press forming of the plate into a cylinder. Roll forming is generally used for short, heavy-wall pipe sections, while press forming is used for longer, thinner-wall sections. Press forming is preferred for high-production-rate mills, whereas roll forming is more suited for smaller production runs with frequent size changes. Roll forming is usually performed with three forming rolls. The three-roll forming machines can be either of two basic types: pinch roll or pyramid roll.[23] Figure 11, as adopted from ref. 23, shows schematic diagrams of cylinders being roll formed in a conventional pinch-roll, shoe-type pinch-roll, and a pyramid-roll machine. The pinch-roll machine can provide greater dimensional control and cover a wider range of thicknesses than the pyramid roll.[23] The shoe-type pinch roll can reduce fattening effects on noncrimped plate and is suited for larger production runs of a given size cylinder.[23] However, it is limited in size capability and can only be used for cold forming. The conventional pinch-roll machine is therefore the most likely equipment to be utilized for roll-forming BR piping.

Press forming is generally accomplished by a process referred to as "U-ing and O-ing." While the initial portion of the forming operation could be performed with a semicylindrical ram and rocker dies or by incremental three-point bending on an open-gap press, the forming principles are the same in both cases.

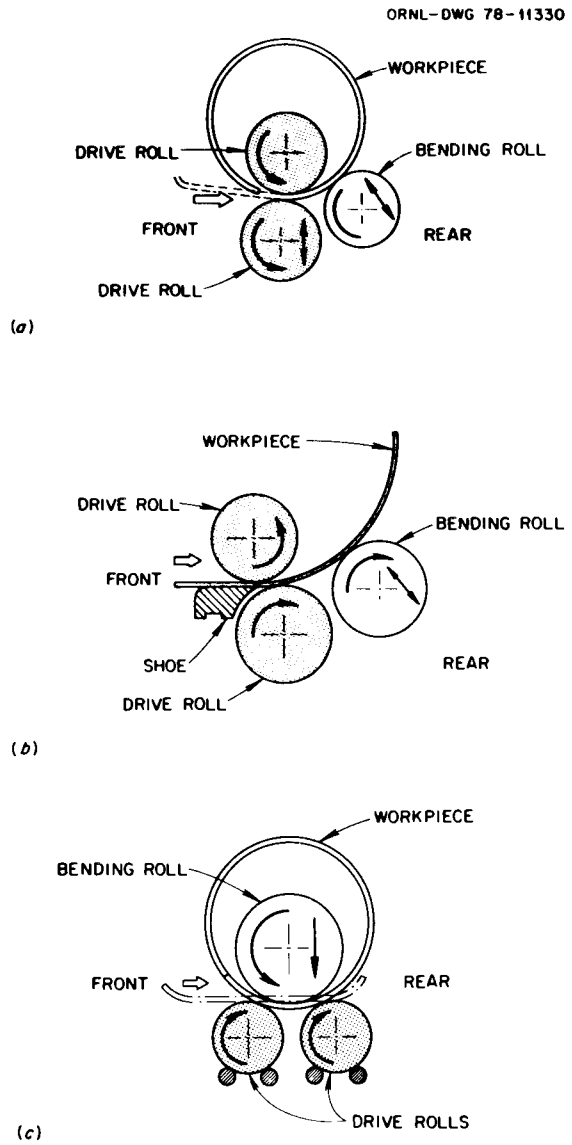

Fig. 11. End view of cylinders being roll formed in various types of machines; (*a*) conventional pinch-roll machine forming an initially crimped plate, (*b*) shoe-type pinch-roll machine forming a noncrimped plate, (*c*) pyramid-roll machine forming an initially crimped plate.

Figure 12 shows schematic diagrams of the end view of cylinders being press formed by U-ing and O-ing, with the initial forming operation being performed with rocker dies and three-point bending. The U-ing and O-ing fabrication technique is used for high-production-rate operations where a large number of pipes of the same size are to be produced. The use of the semicylindrical ram and rocker dies would provide the capability for higher production rates; however, there would be restrictions on the thickness of the plate to be formed. Although the three-point incremental bending technique would not enable as high a production rate, it would be capable of bending heavier plate. With either technique, the plate to be bent would be crimped prior to forming. As shown in Fig. 12, the initial sequence of operations forms the plate into a U-shape, and then the final sequence forms a cylindrical O-shape. The forming operation is normally performed cold.

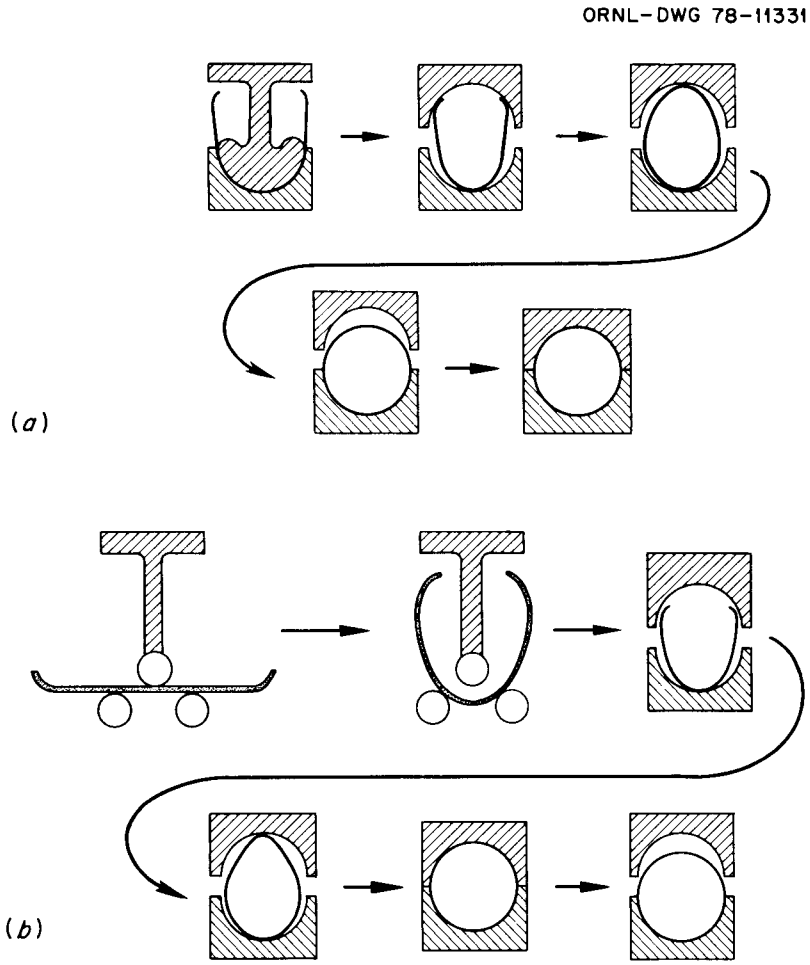

Fig. 12. End view of cylinders being press formed by U-ing and O-ing; (*a*) initial forming operation performed with a semicylindrical ram and rocker dies, (*b*) initial operation performed by three-point bending on an open-gap press.

Once the plate has been formed into a cylindrical shape, the next sequence of operations could take several possible paths. For one path the longitudinal seam between the two butted edges may be cleaned and tack welded. This would enable storage of unwelded cylinders with minimization of shape distortion. The cleaning operation would normally be performed by either shot blasting or grinding. As an alternate path, the longitudinal seam might be cleaned and welded without utilizing a tack weld. The decision to use tack welds would be a function of the joint design and storage requirements. If a joint design is used which would require removal of the material in the vicinity of the tack weld, then the treatment of the tack weld would be simplified because of its complete removal. In this situation the quality of the tack weld would not be a concern, although the cost penalty for utilizing it would be present. Figure 13 shows some typical joint designs which would totally remove the tack weld. Although the joint designs shown in Fig. 9(*c*), (*d*), and (*e*) might use tack welds, the ability to totally remove them would be reduced because of the small amount of base metal present on the lands. However, tack welds can be incorporated in the final weld if qualified procedures are followed and proper controls exercised over the operation. This again, however, adds to the cost. If tack welding is performed, it would be done with the cylinder clamped in a tacking press, which would align the two edges of the longitudinal seam. An additional operation which might be

ORNL-DWG 78-11332

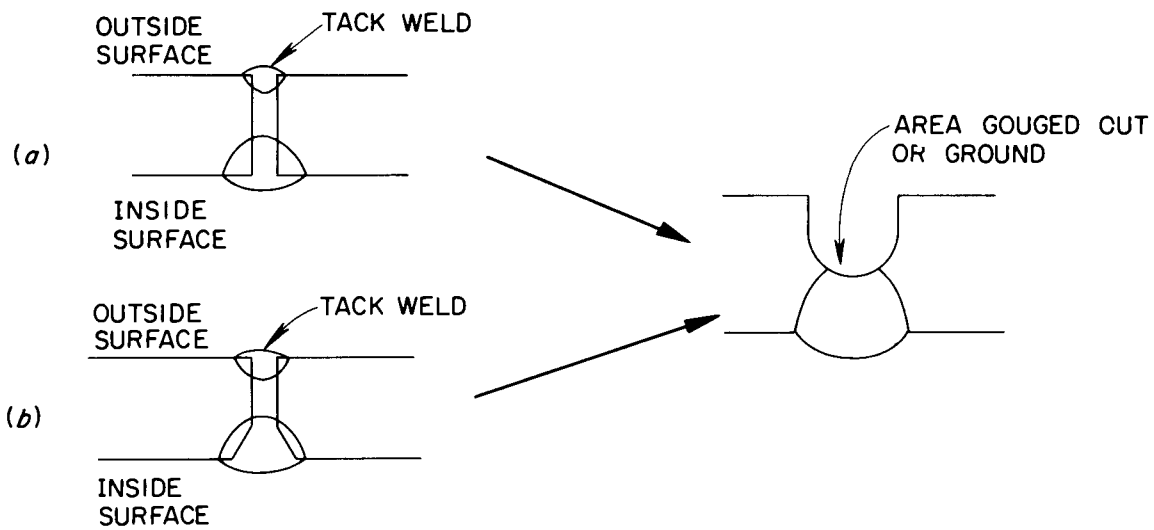

Fig. 13. Typical joint designs which would totally remove tack welds; (*a*) square butt, (*b*) single V-groove on inside surface.

performed at this time is the placement of runoff tabs at the ends of the longitudinal seam. Since these tabs would be welded to the ends, they would in effect act as tack welds. It is therefore likely that runoff tabs would be used prior to any welding if tack welds are being used. However, if tack welds are not being used, then runoff tabs might be added after an initial welding pass is made.[24] The purpose of the runoff tab is to locate arc starting and stopping defects outside of the longitudinal seam weld.

Welding of the longitudinal seam can be accomplished using various welding processes, deposition sequences, and welding equipment. Generally three welding processes would most likely be considered for making the longitudinal seam weld. These would be GTA, SA, and gas metal-arc (GMA). The first two processes are used more frequently. Each process, of course, has inherent characteristics which make it more desirable in certain situations. In addition, there are variations within a process cateogry such as GTA with hot- or cold-wire additions or without filler metal (autogenous). The GTA process with hot- or cold-wire additions would probably be selected instead of SA for longitudinal seam welding of austenitic stainless steel pipe to be used at BR primary coolant system operating temperatures. This is based upon the results of stress-rupture tests which have shown that SA welds typically have lower times to rupture (t_r) than do GTA welds.[25] The higher t_r values for GTA welds are probably due to the lower heat input, which produces a finer weld structure. However, the GTA process also provides an as-deposited weld composition which is different than that for the SA process for a given initial filler metal composition. This is of course due to the slag-metal reactions which occur in the SA process. The Westinghouse Electric Corporation Advanced Reactors Division (WARD) CRBRP equipment specification for welded pipe[26] currently excludes the use of SA welds with type 16-8-2 filler metal.

Generally the deposition sequence would be such that a weld pass would be made on the inside surface of the seam first. This would allow further work such as gouging and/or inspection to be done from the outside surface, where there is more access. In addition, the inside welding would probably be limited to a

single pass to reduce the time spent working in a low-access situation. The welding equipment to make the inside weld would utilize a welding head mounted on a long boom to enable traversing the full length of the pipe. The welding done from the outside surface would probably be multiple pass, depending upon the joint design. The equipment for the welding head would be simpler because the pipe could easily be moved past it. However, the boom used for the inside welding could also be used on the outside. Other techniques could also be used such as welding the outside first or welding the inside and outside at the same time with staggered arcs. Various methods for aligning the seam weld and for tracking and guiding the progress of the welding arc are used. These might include television cameras to enable an operator to make adjustments, or commercially available guidance probes. An integral part of the welding operation might also be the inspection of the weld preparation prior to the start of welding and the inspection of the root of a back-gouged area prior to deposition of further passes.

After welding, the seam weld may be either roll planished or ground to provide the desired surface contour. The roll planishing would involve a roll forging-type operation which might be done cold or hot (i.e., just after welding). In addition to providing the desired surface contour, the roll planishing might also result in refinement of the weld structure.

Inspection of the completed longitudinal seam weld would be made by radiography. This radiographic inspection is performed before the final heat treatment[13] so that if repair welding is required, reheat treatment would not be necessary. The radiographic examination would therefore be followed by a cycle of repair and surface conditioning and additional radiographic examination if necessary. In addition, the runoff tabs would probably be removed at this time.

The next operation would be the heat treatment of the pipe, which would be solution annealed at typically 1038 to 1093°C and then rapidly cooled. The cooling rate required to rapidly pass through the sensitization range (510 to 788°C)[27] would of course be a function of thickness. However, for the thin-wall BR piping, an air quench may be sufficient, although water quenching or spraying will probably be employed. The water quenching operation would generally consist of heating the pipe in a horizontal position, transporting it from the furnace in the horizontal position, and then rolling it into a quench tank. Although heat treatment in the horizontal position can cause diametral distortion, especially in large-diameter pipe, final sizing operations are expected to correct any deviation. In addition, the use of "spiders" near the ends of the pipe can reduce distortion. The use of a symmetrical water spray as the pipe emerges from a horizontal traveling-bed furnace may reduce quench distortion. However, this operation would still be subject to distortion at the solution annealing temperature and therefore might still require spiders. Vertical heat treatment facilities are not readily available and can also limit the length of pipe being produced.

After heat treatment, the pipe is usually sized and straightened. Depending upon the technique used to size the pipe, hydrostatic testing may be performed as a part of the sizing operation. The sizing of the pipe is usually limited to approximately 0.3 m on each end, whereas the straightening operation is normally performed over the entire length. The two techniques used to size the pipe are expansion or die forming. The die-forming technique utilizes an O-ing die as shown in Fig. 12. The pipe ends are placed in the die, and a press forces the pipe to conform to the circular shape of the die. During this press forming the pipe is plastically deformed. When the pipe is released from the die, there is some degree of elastic springback. The amount of deformation used to size the pipe must therefore account for the elastic recovery. Since this technique rounds the pipe from the outside, it would be expected to provide greater control of the outside diameter than of the inside diameter.

The expansion technique is performed by either hydrostatically expanding against retaining jackets or mechanically expanding by a mandrel. Sizing by hydrostatic expansion is performed by forcing mandrels

into each of the pipe ends and pressurizing the body with water.[24] The mandrels expand the ends to the desired inside diameter, while the body is expanded against retaining jackets which control the outside diameter. Hydrostatic expansion also produces some degree of plastic deformation. After the sizing operation is completed, the water pressure can be reduced to enable the hydrostatic test to be performed. The hydrostatic expansion technique would provide sizing over the entire length of the pipe. However, because of the different techniques used at the body and the ends, the sized dimensions of these two areas would be expected to be different. Mechanical expansion is normally performed by a segmented and expandable cylindrical element.[24] The expandable element expands the inside diameter of the pipe to meet the desired dimensions. The amount of deformation imparted to achieve the desired dimensions would again have to account for elastic recovery.

Straightening of the pipe would normally be performed using either dies or rolls. Sizing by hydrostatic expansion or other techniques if incrementally applied along the length of the pipe can be used to both round and straighten. The amount of straightening which is allowed without reannealing is usually limited.

Although the primary goal of sizing and straightening is to obtain the required dimensional control, these operations are also used indirectly to cold work the pipe and therefore improve its mechanical properties. This is analogous to the cold-roll planishing of the longitudinal weld seam to both condition the surface and improve its mechanical properties. Therefore, "annealed" pipe will normally be slightly cold worked. In addition, the amount of cold work is not uniform throughout the pipe, therefore creating some variability in mechanical properties.

If the hydrostatic test is not being performed as a part of the sizing and straightening operations, then it will probably be performed before these operations. As shown in Table 2, the hydrostatic test pressure for the pipes being evaluated was typically 3 to 4 MPa. This stress is well within the elastic range and therefore would not cause any permanent deformation. However, depending upon the equipment used to perform the hydrostatic test, the plugging of the pipe ends may cause distortion, which would make it desirable to size the ends after the test.

The final operations which would be performed on the pipe are end preparation and cleaning. The first step involved in end preparation would be the facing of the ends to assure that they are perpendicular to the axis of the pipe. Once the ends are faced, the desired joint preparation for circumferential welding would be machined. The final cleaning of the pipe would normally be accomplished by either pickling in $HF\text{-}HNO_3$ or blasting with shot or sand.

5. NONDESTRUCTIVE EVALUATION

The nondestructive evaluation of the pipe consisted of three separate examinations, which involved dimensional characterization, determination of weld ferrite number, and radiographic inspection. The purpose of the dimensional characterization was to determine whether formed and welded pipe was capable of meeting the requirements for BR piping. The determination of the weld ferrite number was performed to enable comparison of nondestructive with destructive techniques. The radiographic inspection was performed on a selected number of the pipes as an overcheck of the manufacturers' examination.

5.1 Dimensional Evaluation

In order to establish a standard procedure for dimensionally characterizing the five pipes, an inspection grid system was utilized. A schematic version of this grid system can be seen in Fig. 14, while Figs. 3 through 7 show the pipes with the actual grid points marked on them. The grid was constructed using five diametral planes (D1 through D5) and seven planes perpendicular to the pipe axis (A through G). The points of intersection of these planes on the inside and outside surfaces of the pipes formed the grid system.

ORNL-DWG 78-11333

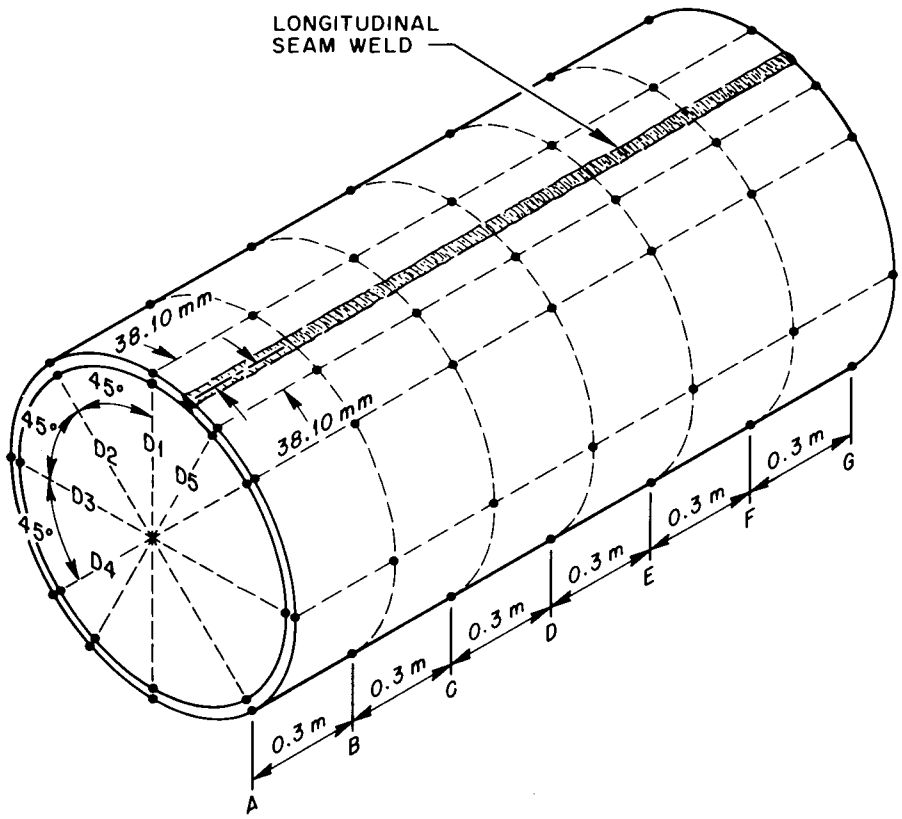

Fig. 14. Schematic sketch of dimensional inspection grid used to characterize the pipe.

After the grid points were located on the outside surface, ultrasonic techniques were used to locate the corresponding points on the inside surface. Diameters D1 through D5 were located 38.10 mm on either side of the weld centerline to enable detection of distortion in the weld region. The remaining diameters were located at 45° increments from D1. The planes perpendicular to the pipe axis were located at 0.3-m intervals along the length of the pipe. The following measurements were made on each of the pipes, using the previously described grid system:

1. Five inside and outside diameters were measured with a micrometer at each of seven planes perpendicular to the pipe axis.
2. The outside circumference was measured with a tape measure at each of the seven planes perpendicular to the pipe axis.
3. The wall thickness was measured using ultrasonic back reflection at each of the 70 points of intersection between the five diametral planes and the seven planes perpendicular to the pipe axis.
4. Camber measurements were made by placing a straightedge on the outside surface of the pipe aligned with each of the ten lines of intersection between the five diametral planes and outside surface. With the straightedge in contact with the pipe, the distance between it and the pipe surface was measured for each of the grid points along the line of intersection.

The dimensional measurements described above were evaluated in terms of three considerations: (1) how well the five pipes conform to their applicable manufacturing specifications; (2) how the pipes compare with the WARD requirements for CRBRP pipe; (3) which measurement techniques most adequately represent the dimensional condition of the pipe. The comparison with commercial specifications is important because it provides an indication of the capability of manufacturers of formed and welded pipe to meet a given specification. The comparison with the WARD requirements for CRBRP pipe can provide some indication of how much different commercial formed and welded pipe is from that required for BR applications. The evaluation of various measurement techniques provides an opportunity to rate their ability to characterize prototypic components.

Table 7 compares the measured dimensions of the five pipes and the requirements of SA-358[13] and SA-312[14] as specified in A530.[28] All measurements were made immediately after the pipes were removed from their shipping containers. Both SA-358 and SA-312 base their major dimensional requirements around outside diameter and wall thickness. The dimensional requirements apply throughout the length of the pipe. The OD requirements of SA-358 use an average OD calculated from circumference measurements in conjunction with a measured ovality, while SA-312 uses a directly measured OD, which inherently includes OD ovality limits. The method used by SA-358 will allow individual OD measurements to exceed the averaged limit and yet not exceed the ovality requirement. This situation cannot occur when the SA-312 requirement is used. The wall thickness requirement for both SA-358 and SA-312 is based upon a minimum

Table 7. Comparison of dimensional evaluation of formed and welded pipes with SA-358 and SA-312 requirements [nominal pipe dimensions 0.91-m OD by 12.7-mm wall by 1.83-m length (36 in. by 0.5 in. by 6 ft)]

Pipe	Measurements (in.)[a]														
	Wall thickness[b]			Outside diameter						Ovality[e]			Camber[f]		
				Calculated[c]			Measured[d]								
	min	max	av	min	max	av	min	max	av	min	max	av	min	max	av
E-13[g]	0.53	0.54	0.53	36.05	36.09	36.06	35.83	36.18	36.01	0.21	0.35	0.25	1/64	1/16	3/64
F-14[h]	0.49	0.52	0.51	35.93	36.01	35.97	35.70	36.15	35.96	0.25	*0.45*	0.33	1/32	5/64	3/64
G-16[i]	0.50	0.52	0.51	36.07	36.11	36.09	*35.88*	*36.21*	36.03	0.09	0.29	0.19	1/64	5/64	3/64
G-15[j]	0.50	0.53	0.52	36.05	36.15	36.12	35.68	36.31	36.03	0.21	*0.62*	0.32	3/64	*19/64*	1/8
H-22[k]	0.61	0.65	0.64	35.97	36.11	36.05	35.88	36.13	36.01	0.04	0.09	0.07	1/16	*9/64*	1/8
SA-358 requirements:															
	0.49			35.82	36.18						0.36			5/64[l]	
SA-312 requirements as specified in A530:															
	0.44						35.97	36.19					Reasonably straight		

[a]To convert to millimeters, multiply by 25.4. (Dimensions given in inches to facilitate comparison with existing specifications). Italicized values exceed specifications.

[b]Eight measurements, at 45° increments around the circumference, were made every 0.30 m (12 in.).

[c]Calculated from circumference measurements made every 0.30 m (12 in.).

[d]Five measurements, one on each side of weld and three at 45° increments from the weld, were made every 0.30 m (12 in.).

[e]Calculated from differences between major and minor OD measurements at planes every 0.30 m (12 in.).

[f]Eight measurements of the maximum camber, with a 1.83-m (6-ft) straightedge in contact with the pipe surface, were made at 45° increments around the pipe circumference.

[g]Pipe E-13, GTA welded with type 16-8-2 filler metal, dimensions to SA-358.

[h]Pipe F-14, GTA welded with type 16-8-2 filler metal, dimensions to SA-358 except maximum ovality on ends 0.5% OD [4.6 mm (0.18 in.)].

[i]Pipe G-16, GTA welded without filler metal, dimensions to SA-312 as specified in A530 except ±1% of OD [±9.1 mm (0.36 in.)].

[j]Pipe G-15, SA-GTA welded with type 316 filler metal, dimensions to SA-358 except ±1% OD [9.1 mm (0.36 in.)].

[k]Pipe H-22, SA welded with type 16-8-2 filler metal, dimensions to SA-358.

[l]The SA-358 camber allowance is given as 3.2 mm (1/8 in.) max in 3 m (10 ft); when it is scaled down for 1.8 m (6 ft) the maximum is about 2 mm (5/64 in.).

without any maximum specified. The absence of a maximum wall thickness requirement results in the plate specification controlling the tolerance. The italicized measurements in Table 7 indicate dimensions that exceed the tolerance allowed by the applicable specification. It should be noted that only pipe E-13 met all specified dimensional requirements. The manufacturer of pipe F-14 narrowed the ovality tolerance on the ends from 1% to 0.5% of the OD. However, the pipe failed to meet even the original 1% OD requirement. The manufacturer of pipes G-15 and G-16 broadened the tolerance from ±0.5% to ±1% OD for G-15 and from +4.8 −0.76 mm to ±1% OD for G-16. Pipe G-16 met the broadened OD tolerance but exceeded the original requirement. Pipe G-15 met the original OD requirement but failed to meet the ovality requirement. In addition, pipe G-15 exceeded the camber allowance. Although pipe H-22 exceeded the camber allowance, its ovality was greatly improved compared with the other four pipes.

The foregoing analysis indicates that the dimensional control of formed and welded pipe fabricated to current commercial specifications typically does not rigorously meet the requirements. In addition, the exceptions taken by one of the manufacturers indicate that in some cases it is normal practice not to attempt to meet the dimensional requirements. It also appears to be common practice to meet dimensional requirements on the ends of the pipe and not in the body. This is of course due to the sizing operation being performed on the ends and not the body, as previously discussed. However, the small amount of pipe that was procured for this evaluation may not accurately represent larger orders.

Before comparing the dimensional measurements of the pipes to the requirements of the WARD CRBRP specification for welded pipe, it is appropriate to examine the chronological sequence of changes which occurred to the dimensional requirements in this specification. Because this sequence of changes occurred during the procurement process, it provides a good indication of what the manufacturers' exceptions were to the given requirements. In addition, since design analyses had to be performed in some cases to justify these revisions, the final requirements should represent the most liberal dimensional tolerances allowed by current design rules.

Table 8 shows the chronological sequence of dimensional requirements for 0.91-m-OD pipe in WARD CRBRP specification E-953094.[26] The current revision of specification E-953094 (revision 4) bases its

Table 8. Chronological sequence of dimensional requirements for 0.91-m-OD pipe in WARD CRBRP specification E-953094 (ref. 26)

Revision, date	Wall thickness (in.)	Inside diameter (in.)	Inside diameter ovality (in.)	Camber
Rev. 0, 8/76	0.47 to 0.56 at any point measured by ultrasonic reflection	34.97 to 35.03 at resized ends; 34.82 to 35.18 over body; although no measurement technique is specified, direct measurement is implied	End requirement included ovality, therefore 0.06 max ovality at ends; 1% of ID over body; although no measurement technique is specified, direct measurement is implicit	1/8 in. over 10-ft span measured with 10-ft straightedge in contact with pipe surface
Rev. 1, 12/76	No change	No change	No change	No change
Rev. 2, 2/77	0.45 to 0.58, no measurement technique specified	35.03 to 35.09 within 3 in. of ends, measurement can be made either by calculation using circumference and average wall thickness or by average of four direct measurements;[a] the vendor is to choose a nominal ID for the body within the range of 35.92 to 35.20 in. and then apply a tolerance of ±0.5% to the chosen nominal, the measurement technique is the same as that for the ends	1% of average ID[a] for ends; 1% of the chosen nominal ID for body	Same as Rev. 0
Rev. 3, 4/77	No change	No change	No change	No change
Rev. 4, 10/77	0.45 to 0.58, no measurement technique specified	The acceptance limits remained the same as Rev. 2; however, the measurement technique was changed to allow only the average of four direct measurements with the pipe restrained to as nearly as possible a circular shape	The acceptance limit remained the same as Rev. 2; however, the measurement is now specified to be made in the unrestrained condition	Same as Rev. 0

[a]Although Rev. 2 did not specify it, the intent was that ID measurements were to be made in the restrained condition, while ovality measurements were to be made unrestrained (ref. 31).

major dimensional requirements on the inside diameter and wall thickness. The ID requirements use end and intermediate plane acceptance limits, which incorporate both ID and ovality measurements. The ID measurements are to be made with the pipe restrained to as nearly as possible a circular shape. The ID requirement is checked against the average of four direct measurements spaced 45° apart. The pipe ends are required to be measured within 76.2 mm from the end, while no requirement is placed on the location or frequency of the body measurement. The ovality measurements are to be made with the pipe unrestrained. The ovality requirement is checked against the difference between the maximum and minimum measurements described above. A restrained ID limit is used to simulate the conditions present during the fitup for welding. An unstrained ovality requirement is utilized to limit the maximum amount of rounding that will need to be applied for fitup. The acceptance limits at the resized ends are narrow to improve circumferential weld joint fitup and thereby reduce residual stress caused by alignment. The intermediate-plane acceptance limits are comparable with the OD tolerance range on the present commercial specifications, except that they are averaged direct measurements rather than indirect determination from circumference measurements. The wall thickness requirement for E-953094 uses both a minimum and a maximum requirement. As previously mentioned, SA-358 and SA-312 do not have a maximum wall thickness requirement and therefore depend upon the plate specification. The maximum plate thickness requirements of SA-240[12] as specified in A-480[29] allow between 1.5 and 2.3 mm over the nominal 12.77 mm, depending upon the plate width. In addition, the plate thickness is checked only up to 76.2 mm in from the edge, thereby enabling roll crown effects to cause undetected thickness increases in the center of the plate.

Table 8 shows that the WARD acceptance limits and/or measurement techniques were changed during the piping procurement process for wall thickness, inside diameter, and inside diameter ovality. The acceptance range for the wall thickness was broadened (0.47–0.56 to 0.45–0.58 in.), which resulted from the fabricators' inability to accurately control plate thickness as previously discussed. WARD had to perform additional stress analyses to establish that an increased wall thickness would not be detrimental.[49,50] This analysis evaluated the effect of the heavier wall thickness on fatigue damage resulting from postulated thermal transients. In addition, the decreased wall thickness had to be evaluated in terms of its effect on fitup for welding. With the decrease in the allowable as-manufactured pipe wall thickness, the margin between it and the minimum allowable as-fabricated thickness was reduced from 0.03 in. to 0.01 in. (ref. 30). This decreased margin means that there is a greater chance that counterboring during fitup will exceed the minimum wall thickness. This situation is acknowledged in the WARD shop fabrication specification[30] by allowing weld buildup to compensate for the decreased base-metal thickness.

The ID requirements changed in two ways. First, the nominal ID for both the end and intermediate planes has been shifted. In the case of the end ID, the shift was made to facilitate fitup with other components.[31] However, the provision to enable the vendor to select a "nominal inside diameter of the body of the pipe away from the ends"[32] within a specified range indicates the reluctance of manufacturers of formed and welded pipe to commit to specific body dimensional requirements. This again relates to the fact that it is not common practice to size the body region. Although there was a shift in nominal ID for both the end and intermediate planes, the actual tolerance for each region did not shift. The second change that occurred involved the measurement techniques. Whereas ID requirements were initially to be checked by direct measurement, averaged direct measurements or values calculated from wall thickness and circumference were next allowed, followed by use of only the averaged measurements. In addition, the direct measurements were to be made in the restrained condition. The change from direct to averaged measurements for acceptance indicates that the manufacturers are concerned that several different effects (such as handling and gravity) can alter the as-sized dimensions. This is further verified by the requirement to make these measurements in the restrained condition. The philosophy behind making the measurements in the

restrained condition is that it shows whether or not a pipe will be capable of being rounded within the acceptance limits for weld fitup. Since fitup for welding is normally performed in a restrained condition, it is more significant to evaluate the pipe in this condition. The use of averaged instead of direct measurements will be discussed in a later section. However, Table 8 does indicate that the use of an average ID calculated from wall thickness and circumference was eliminated. This is probably due to the fact that this averaging technique had the possibility of allowing too large a local deviation.

The end ID ovality requirement initially appears to have experienced the greatest change. This requirement changed from 0.06 in. maximum, with no measurement technique specified, to 1% of the average inside diameter (∿0.35 in.) in the unrestrained condition. However, it could be argued that since the initial ovality requirement was included in the ID, this measurement could have been made in the restrained condition (because no technique was specified) and therefore would be comparable with the later unrestrained ovality requirement in conjunction with a restrained ID requirement having a range of 0.06 in. In any event, this situation again indicates that the manufacturers generally felt that the tight end requirements for fitup could not be met without restraining the pipe. This again relates to concern about various effects altering the as-sized dimensions.

By comparing the dimensional evaluation of the five pipes procured in this program with the WARD CRBRP specification E-953094, it will be possible to some extent to see why the changes in the dimensional requirements had to be made. However, before examining this comparison, it is important to note that all measurements were made without restraining the cross section. This, of course, prevents an accurate comparison with the ID requirements. In addition, since the nominal ID for the WARD pipe was shifted, this further detracts from the ability to compare the inside diameter. Table 9 shows the comparison

Table 9. Comparison of dimensional evaluation of formed and welded pipes with WARD CRBRP specification E-953094 [nominal pipe dimensions 0.91-m OD by 12.7-mm wall by 1.83-mm length (36 in. by 0.5 in. by 6 ft)]

Pipe	Measurements (in.)[a]																	
	Wall thickness[b]			Inside diameter						ID ovality						Camber[g]		
				Ends[c]			Body[d]			Ends[e]			Body[f]					
	min	max	av	min	max	av	min	max	av	min	max	av	min	max	av	min	max	av
E-13[h]	0.53	0.54	0.53	34.81	35.11	*34.96*	34.80	35.02	34.92	0.23	0.35	0.28	0.20	0.22	0.22	1/64	1/16	3/64
E-14[i]	0.49	0.52	0.51	34.68	35.13	*34.94*	34.70	35.10	34.93	0.28	*0.45*	0.34	0.32	*0.37*	0.34	1/32	5/64	3/64
G-16[j]	0.50	0.52	0.51	34.88	35.20	*35.02*	34.86	35.13	34.98	0.10	0.28	0.19	0.10	0.27	0.18	1/64	5/64	3/64
G-15[k]	0.50	0.53	0.52	34.65	35.30	*34.98*	34.88	35.25	35.03	0.21	*0.65*	0.35	0.23	*0.37*	0.29	3/64	*19/64*	1/8
H-22[l]	*0.61*	*0.65*	0.64	34.62	34.81	*34.71*	34.71	34.78	*34.74*	0.02	0.05	0.04	0.05	0.06	0.05	1/16	*9/64*	1/8
WARD E-953094 requirements:																		
	0.45	0.58				35.03[m] to 35.09			34.88[m,n] to 35.24		0.35			0.35			5/64[o]	

[a]To convert to millimeters, multiply by 25.4 (dimensions given in inches to facilitate comparison with existing specifications). Italicized values exceed the specifications. All measurements made without restraining the cross section.

[b]Eight measurements, at 45° increments around circumference, were made every 0.30 m (12 in.).

[c]Five measurements, one on each side of weld and three at 45° increments from the weld, were made at each end and 0.30 m (12 in.) from each end.

[d]Five measurements, one on each side of weld and three at 45° increments from the weld, were made at three center locations 0.30 m (12 in.) apart.

[e]Calculated from differences between major and minor ID for end planes and planes 0.30 m (12 in.) from each end.

[f]Calculated from differences between major and minor ID for three center planes 0.30 m (12 in.) apart.

[g]Eight measurements of the maximum camber with a 1.83-m (6-ft) straightedge in contact with pipe surface were made at 45° increments around the pipe circumference.

[h]Pipe E-13, GTA welded with type 16-8-2 filler metal, dimensions to SA-358.

[i]Pipe E-14, GTA welded with type 16-8-2 filler metal, dimensions to SA-358 except maximum ovality on ends 0.5% OD [4.6 mm (0.18 in.)].

[j]Pipe G-16, GTA welded without filler metal, dimensions to SA-312 as specified in A530 except ±1% OD [±9.1 mm (0.36 in.)].

[k]Pipe G-15, SA-GTA welded with type 316 filler metal, dimensions to SA-358 except ±1% OD [±9.1 mm (0.36 in.)].

[l]Pipe H-22, SA welded with type 16-8-2 filler metal, dimensions to SA-358. Note that the ID values are low because of the heavy wall thickness.

[m]Entered in the average column because limits are based upon average of measured values.

[n]These limits were obtained by applying ±0.5% to the midpoint (35.06 in.) of the range of nominal body inside diameters that the vendor can choose from.

[o]The camber allowance is given as 3.2 mm (1/8 in.) max in 3 m (10 ft); when it is scaled down for 1.8 m (6 ft) the maximum is about 2 mm (5/64 in.).

between the dimensional evaluation of the pipes and the WARD requirements. The wall thickness measurements in Table 9 show that four of the five pipes met the original tighter tolerance range, while the fifth exceeded both the tighter and broadened ranges because it was intentionally made from heavier plate, which typifies the fact that the manufacturers of commercial pipe are accustomed to working with only a minimum wall thickness requirement. The results in Table 9 might tend to suggest that formed and welded pipe could meet the original tighter wall thickness requirements. However, the changes made to the CRBRP specification during the procurement process indicate that the manufacturers would not accept the tighter tolerance range.

Direct comparison of the ID measurements with the WARD requirements shown in Table 9 is not valid as previously discussed. However, it can generally be concluded that manufacturers should not have a problem meeting the body ID requirements as evidenced by four of the five pipes meeting the requirement. This is because the tolerance on this requirement is the same as the current commercial specification which they are accustomed to meeting. Although all five pipes failed to meet the end ID requirement, this situation could be greatly altered if measurements were made in the restrained condition.

The ID ovality appears to be the area for greatest concern as evidenced by the comparison in Table 9. Since this measurement is specified to be in the unrestrained condition, it provides a realistic comparison. Two of the five pipes failed to meet the requirement in both the end and body regions, and a third was on the borderline for the end region. However, it is important to point out that one pipe had excellent ovality control and was able to meet the original tighter tolerance on both the ends and body.

Based upon the foregoing analyses of dimensional considerations and earlier discussions of BR design requirements, it is apparent that two aspects of the dimensional control of the pipe are the most important. These are wall thickness and end inside diameter and ovality. The control of body diameter and ovality becomes important if pipe must be cut to a smaller length in the field, therefore requiring weld fitup in a body region. The discussion has indicated that wall thickness tolerances have been broadened to enable formed and welded pipe to meet the requirement. It is beyond the scope of this report to examine the justification for increasing the maximum allowable wall thickness. The relationship between lowering the allowable thickness and fitup for welding has already been discussed. However, it is important to examine the various techniques which can be used to characterize pipe ends for weld fitup.

A detailed examination of the ends of the five pipes was performed to determine the effectiveness of averaging direct ID measurements and calculating the ID from circumference and average wall thickness as compared with direct measurements. Table 10 shows the dimensional data which were used to make this

Table 10. Dimensional data for the ends of the five rolled and welded pipes

Pipe	Average end plane wall thickness[b]	Measurements[a]								
		End plane measured inside diameters[c]					End plane outside circumference	End plane inside diameter ovality	End plane average inside diameter[d]	End plane calculated inside diameter[e]
		D1	D2	D3	D4	D5				
E-13	0.528	35.086	34.855	34.828	35.054	35.033	113.250	0.258	34.971	34.993
	0.532	35.112	34.940	34.766	34.960	35.040	113.375	0.346	34.964	35.024
F-14	0.510	35.055	35.042	35.772	34.904	35.035	113.125	0.283	34.962	34.989
	0.507	35.132	34.853	34.684	34.856	35.093	112.875	0.448	34.924	34.915
G-15	0.504	34.677	35.299	35.051	35.025	34.649	113.250	0.650	34.940	35.041
	0.512	34.886	35.093	34.875	34.995	34.863	113.437	0.230	34.942	35.084
G-16	0.501	35.164	35.009	35.038	35.022	35.162	113.375	0.155	35.079	35.086
	0.507	34.975	35.012	35.196	34.994	34.969	113.375	0.227	35.029	35.074
H-22	0.627	34.717	34.665	34.686	34.696	34.711	113.125	0.052	34.695	34.755
	0.636	34.653	34.627	34.615	34.625	34.666	113.000	0.051	34.637	34.697

[a]All measurements are in inches and were made within 1 in. of the pipe end without restraining the cross section.
[b]The average of eight ultrasonic measurements.
[c]D1 and D5 were 1.5 in. on each side of weld centerline; D2, D3, and D4 were 45° increments from D1.
[d]The average of the five measured inside diameters.
[e]The inside diameter is calculated from the outside circumference and average thickness.

comparison. As previously mentioned, the WARD specifications require that end ID measurements are to be made "when the cross section is restrained to as nearly as possible a circular shape." Since there is no specific requirement on this restrained circularity, it is assumed that ovality could range from 0 to 0.35 in. (1% maximum allowable). As shown in Table 10, the ovalities on the ten ends evaluated ranged from 0.051 to 0.650 in. with an average of 0.270 in. Therefore, while these data were not taken in a restrained condition, they are representative of a portion of the range of possible restrained circular conditions. Eliminating data from ends for which the ovality exceeded 0.350 in. leaves a data base of eight ends with an ovality range of 0.051 to 0.346 in. with an average of 0.200 in.

Table 11 provides a comparison of averaged and calculated ID with directly measured values for the eight ends with acceptable ovality. The comparison is made by showing the maximum deviations that

Table 11. Comparison of averaged and calculated inside diameter with directly measured values

Pipe or elbow	Measurements[a]		
	Maximum deviation of average ID from direct measurements[b]	Maximum deviation of calculated ID from direct measurements[c]	End plane ID ovality[d]
E-13	−0.115 +0.143	−0.093 +0.165	0.258
	−0.148 +0.198	−0.088 +0.258	0.346
F-14	−0.093 +0.190	−0.066 +0.252	0.283
G-15	−0.151 +0.079	−0.009 +0.221	0.230
G-16	−0.085 +0.070	−0.078 +0.077	0.155
	−0.167 +0.060	−0.122 +0.105	0.227
H-22	−0.022 +0.030	 +0.038	0.052
	−0.029 +0.022	 +0.082	0.051

[a]All measurements are in inches.
[b]Maximum positive and negative deviation between average inside diameter and direct measurements in Table 10.
[c]Maximum positive and negative deviation between calculated inside diameter and direct measurements in Table 10.
[d]Reported ovality from Tables 1 and 2.

occurred between these two techniques and the direct measurements. Figures 15 and 16 show plots of these maximum deviations vs the unrestrained ID ovality. A linear regression analysis was used to fit the data in these figures to linear equations of the form $y = a + mx$. The linear equation along with the coefficient of determination, r^2, is shown on each line. The equations for Fig. 15 should have intersected the y axis at zero, because with no ovality there should be no deviation between actual measurements and the average. The failure to intersect the y axis at zero is probably due to the low coefficients of determination (r^2 = 0.0671 and 0.793, with r^2 = 1 indicating perfect fit) which establish the degree of data fit. It is not

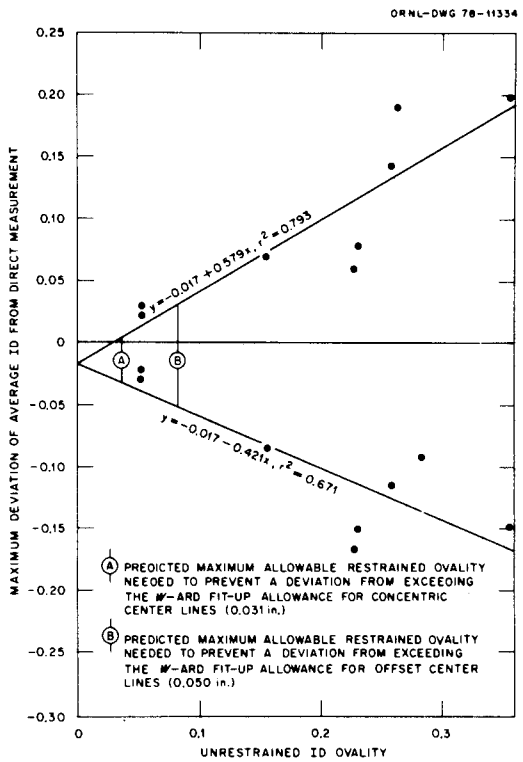

Fig. 15. Plot of maximum deviation of average inside diameter from direct measurements vs unrestrained inside diameter ovality.

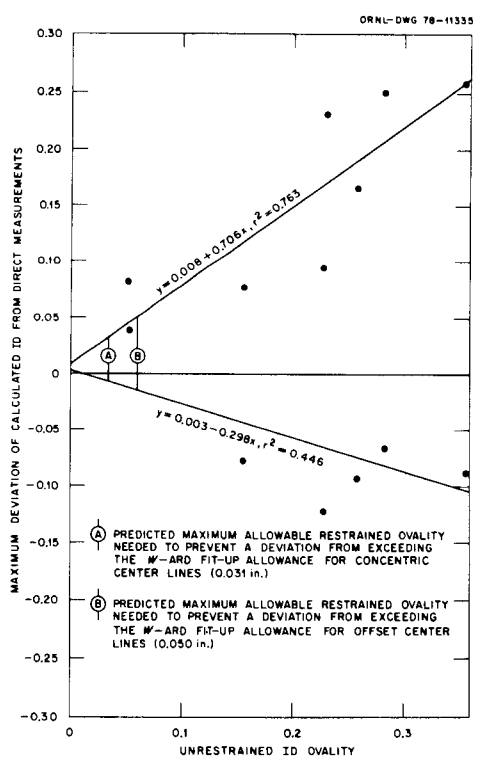

Fig. 16. Plot of maximum deviation of calculated inside diameter from direct measurements vs unrestrained inside diameter ovality.

expected that the equations for Fig. 16 should intersect the y axis at zero because of the use of average wall thickness to make the calculation of ID. However, the degree of data fit is also poor in Fig. 16 ($r^2 = 0.446$ and 0.763). Although the linear regression analysis for the data in Figs. 15 and 16 has been shown to be subject to some error, the following general conclusions can be drawn:

1. As ovality increases within the acceptable limits, significant deviations can occur between averaged or calculated ID and directly measured values.
2. The calculated ID values have a tendency to be larger than the average or directly measured values.
3. The predicted maximum allowable restrained ovalities needed to prevent a deviation from exceeding the WARD fitup allowances are relatively low.

These conclusions indicate that unless the pipe is restrained to very nearly a circular shape during measurement, the use of either averaged or calculated ID acceptance limits can allow deviations from the actual measurements which could exceed weld fitup requirements. Deviations that occur during fitup for welding may have to be corrected by special alignment procedures, counterboring, or weld buildup, depending upon the situation. Based upon the above considerations, it is therefore recommended that direct ID measurements made in the restrained condition be used as acceptance limits.

There are additional data available for four of the pipes which show the relationships between unrestrained and restrained end measurements, and between restrained end measurements and radial mismatch during weld fitup. These measurements were made by Idaho National Engineering Laboratory (INEL) on 0.6-m (2-ft) sections from the ends of four of the pipes (pipe identification numbers E-13, F-14, G-15, and G-16) as shown in Fig. 17. This work at INEL was part of a welding technology development program

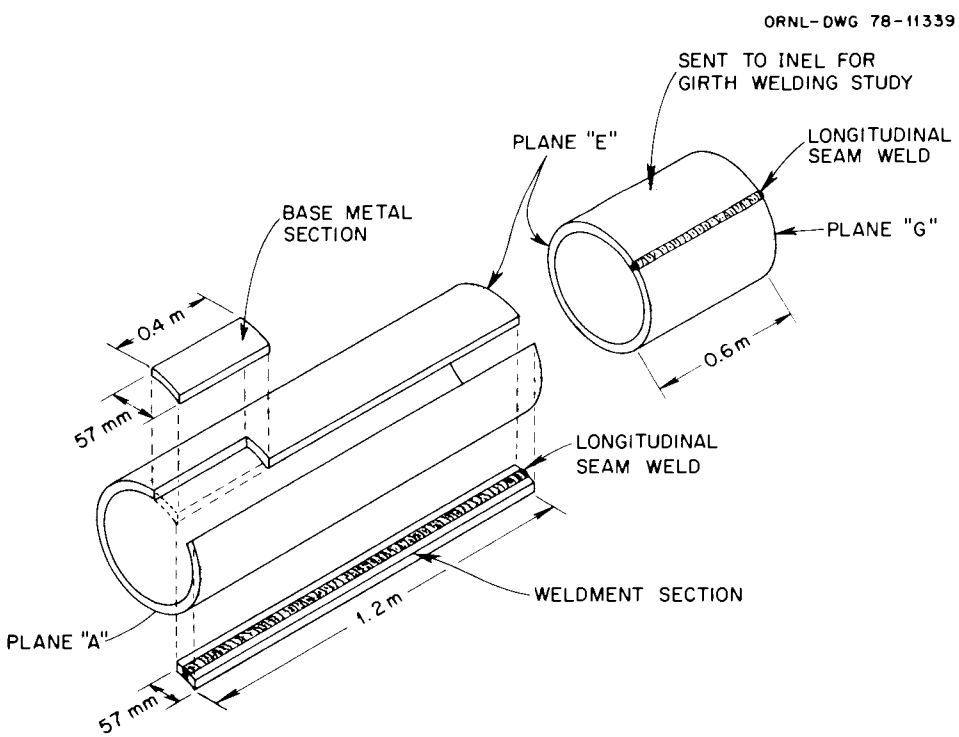

Fig. 17. Sectioning plan for all pipes.

which was evaluating joint preparation, alignment, and orbital welding techniques for BR piping.[51] Table 12 shows a comparison between pipe end OD ovality in unrestrained and restrained conditions. The restrained measurements were made using an internal lineup clamp to expand the inside surface to a round condition. The ovality data shown in Table 12 were obtained from the difference between the maximum and minimum of four OD measurements taken at 45° intervals at the end(s) of the pipe section. Measurements were made on the original pipe ends, remachined original ends, and an end which was in the body of the as-received pipe.[52] The data in Table 12 demonstrate that alignment equipment can round pipe to nearly a circular shape even when the unrestrained condition has excessive ovality (maximum of 0.436 in.). However, it must also be noted that the restrained ovalities varied from 0.022 to 0.082 in. and that in one case the internal rounding expansion increased the amount of ovality (0.060 to 0.082 in.). Using the latest tolerance range for end ID shown in Table 8 (0.060 in.), it must be realized that the additive effect of the difference in average pipe diameters and ovality must be accounted for to ensure that radial mismatch during weld fitup does not exceed the WARD allowance for concentric centerlines (0.031 in., ref. 30).

Table 12. Comparison between pipe end outside diameter ovality in unrestrained and restrained conditions[a]

Pipe end identification	End outside diameter ovality (in.)	
	Unrestrained	Restrained
E-13 (original end)	0.184	0.052
E-13 (remachined original end)	0.182	0.068
E-13 (2nd remachined original end)	0.193	0.075
F-14 (original end)	0.436	0.050
F-14 (original body)	0.277	0.047
G-15 (original end)	0.060	0.082
G-15 (remachined original end)	0.093	0.044
G-15 (2nd remachined original end)	0.123	0.043
G-16 (original end)	0.143	0.022
G-16 (remachined original end)	0.149	0.022

[a]Measurements made at INEL (refs. 51, 52).

Table 13 provides comparisons between restrained pipe end OD measurements and radial mismatch during fitup for four welds. Columns A and B in Table 13 provide the restrained ovality and average diameter based upon four OD measurements taken at 45° intervals. Column C provides the difference between the average diameters of the two ends being joined for each weld. Since the maximum tolerance range on ID is 0.060 in., the maximum difference between the outside diameters of two pipe ends being joined would not be much greater. Therefore, the welds with column C values exceeding 0.060 in. are not expected. Column D provides the maximum radial mismatch potential. There is a separate value for each end which is one-half the sum of the ovality of the end and the difference between the average diameters of the two ends. Since the column D mismatch potential represents the worst possible condition, significantly improved fitups can be obtained if the geometries of the ends are similar. Welds 2 and 3 in Table 13 show examples of predicted maximum radial mismatches (column D) closely predicting the actual radial mismatch (column E). The actual radial mismatch measurements are the "differences in the height of the root faces as measured with a depth micrometer from the outside surface of the pipe."[51] These fitup measurements were made with the two pipe ends butted together, using the internal lineup clamp to round the inside surface. In addition, welds 2 and 3 exceed the fitup allowance. Welds 4 and 5 show examples of predicted mismatches generally being much greater than the actual.

The fitup analysis described above indicates that there is a need to check ovality in the restrained condition as a part of the acceptance limit. The best way to do this is to use direct ID measurements made in the restrained condition. By specifying an acceptance range for ID measurements (four taken at 45° intervals), both the average diameter and ovality will be controlled.

Table 13. Comparison between restrained pipe end outside diameter measurements and radial mismatch during fitup for welding[a]

Weld No.	Identification of pipe ends being joined	A Ovality of restrained end outside diameter (in.)	B Average restrained end outside diameter (in.)	C Difference between average end outside diameters (in.)	D Maximum radial mismatch potential $\left(\frac{A+C}{2}\right)$ (in.)	E Actual radial mismatch measurements (in.)
2	E-13 (original end)	0.052	36.047	0.147	0.100	*0.090* *0.049* *0.048*
	E-14 (original end)	0.050	35.900		0.099	0.001
3	E-13 (remachined original end)	0.068	35.999	0.013	0.041	0.027 0.009 0.015 *0.038*
	G-15 (remachined original end)	0.044	35.986		0.029	*0.069*
4	E-14 (original body)	0.047	35.913	0.098	0.073	0.028 0.012 0.001
	G-16 (remachined original end)	0.022	36.011		0.060	0.027
5	E-13 (2nd remachined original end)	0.075	36.016	0.011	0.043	0.022 0.018 0.019
	G-15 (2nd remachined original end)	0.043	36.005		0.022	0.009

[a]Measurements made at INEL (refs. 51, 52).

Note: Italicized numbers in column E indicate those which exceed the WARD fitup allowance for concentric centerlines (0.031 in., ref. 30).

5.2 Determination of Weld Ferrite Number

Magnetic permeability measurements* were made on the inside and outside surfaces along the length of the welds in each pipe to determine the ferrite number (FN). It is important to note that the current magnetic permeability techniques (Ferritescope and Magnagauge) for measuring FN are not applicable to solution-annealed welds such as those present in the five pipes. This is because the calibration standards were only established for as-deposited welds,[33] although some allowance is made for cast material. However, since these were the only standardized techniques available, they were employed. Three measurements were made across the width of the welds at 0.3-m intervals along the length. The locations for the measurements correspond to the intersection with the weld of the seven planes perpendicular to the pipe axis (A through G) shown in Fig. 14. The three measurements were averaged to determine the FN for each location. Measurements of less than 0.1 FN were not reported. All of the measurements for pipes G-15, G-16, and H-22 were less than 0.1 FN, with most being zero. Therefore, no measurements are reported for these pipes, and the welds are assumed to have an FN of zero. Figure 18 shows the FN variation along the length of the welds in pipes E-13 and F-14. Because of the low ferrite content in the weld in E-13, base-metal dilution effects have not caused much of a difference between inside and outside measurements.

*Magnetic permeability measurements made with Twin City Testing Corp. Ferritescope, type FE8e2, model B, with probe type KF. Calibration was performed in accordance with AWS A4.2-74 (ref. 33), using Teledyne McKay weld metal secondary standards.

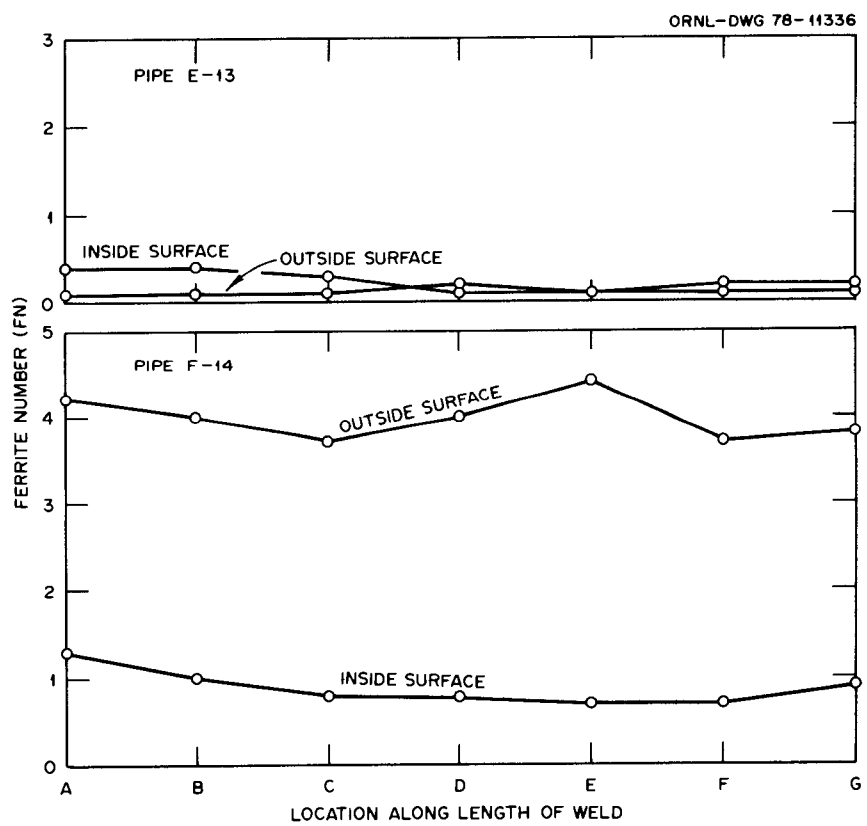

Fig. 18. Ferrite number variation along the length of the welds in pipes E-13 and F-14.

In fact, the normal trend for the inside surface (or root) of the weld to have a lower FN because of dilution is reversed. The FN is very uniform along both the inside and outside surfaces of pipe E-13. The plot for pipe F-14 clearly shows the expected effect of dilution on FN (i.e., the more diluted inside surface or root has a lower FN). Although the FN of the weld inside surface was relatively uniform, the outside surface exhibited some degree of variability. This variation could be the result of local variations in dilution. The results shown in Fig. 17 will be compared later with destructively determined values.

5.3 Radiographic Inspection

The welds in four of the five pipes were examined radiographically to verify compliance with the required quality levels. In addition, the manufacturer's radiographs from the pipe which was not reradiographed were reviewed. As shown in Table 3, the pipes manufactured in accordance with SA-358 (E-13, F-14, G-15, and H-22) had the additional requirement to radiographically examine the welds at two different angles at least 30° apart but not more than 150°. The intent of this requirement is to facilitate accurate characterization of defects which might be oriented such that their size could appear smaller or nonexistant if examined by a single radiograph at a critical angle. The welds in pipes F-14, G-15, and G-16 were reradiographed 25° from perpendicular on each side of the weld as shown in Fig. 19. No rejectable

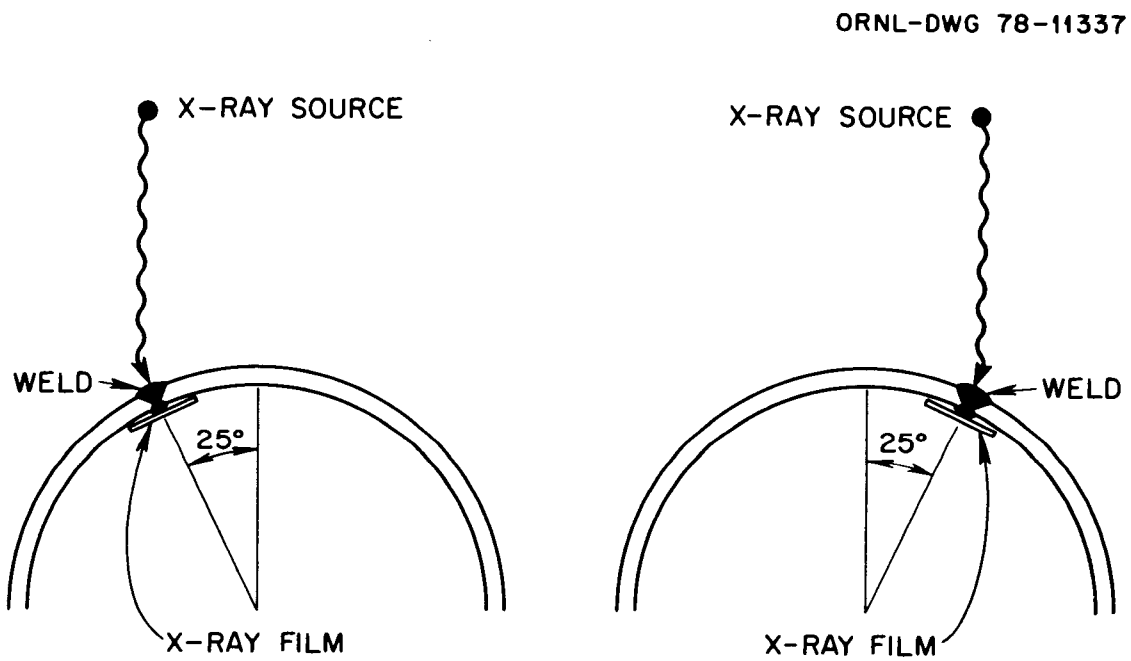

Fig. 19. Orientations between x-ray source and weld used for the radiographic examination of the welds in pipes F-14, G-15, and G-16.

defects were observed in the welds in either pipe F-14 or G-15. However, pipe G-16 had one rejectable line grouping of porosity. The defects appeared to be at the root of the outer pass. Discussions with the manufacturers indicated that their radiographs revealed the porosity, but it was not interpreted as being rejectable. Since both ORNL radiographs showed the same rejectable grouping of defects, it was concluded that the double-angle technique was not responsible for exposing the defects. The discrepancy was attributed to the ORNL radiographs having greater sensitivity than required.

To further evaluate the double-angle technique, the weld in pipe H-22 was reradiographed such that the x rays penetrated approximately normal to the planes of the weld bevels as shown in Fig. 20. In addition,

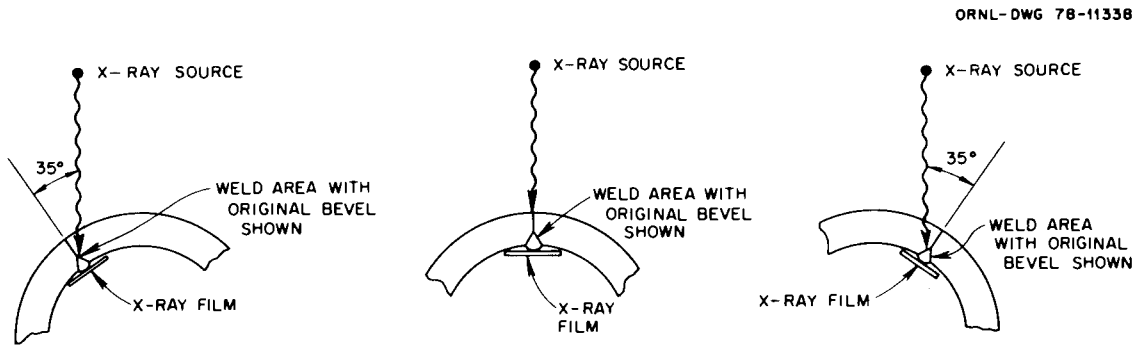

Fig. 20. Orientations between x-ray source and weld used for the radiographic examination of the welds in pipe H-22.

the weld was also radiographed with the x rays perpendicular to the weld. No rejectable defects were observed in any of the views.

Pipe E-13 was the one that was not reradiographed at ORNL. However, the manufacturer's radiographs were reviewed at ORNL, and no rejectable defects were observed.

6. DESTRUCTIVE EVALUATION

6.1 Sectioning of Pipes

In order to provide a uniform method for destructively evaluating the five pipes, a standard sectioning plan was established. Figure 17 shows the sectioning plan used on all of the pipes; each pipe had three sections removed for further evaluation. The base-metal and weldment sections were further processed at ORNL to provide specimens for metallographic examination and mechanical properties testing, while a 0.6-m section from each end was sent to INEL for use in a girth welding study, as previously described.

Figures 21 and 22 show the specimen removal plan for the base-metal and weldment sections. It should be noted that the removal of specimens from the pipes has been coordinated with the dimensional inspection grid shown in Fig. 14. The metallographic specimens shown in Fig. 21 were located where planes A

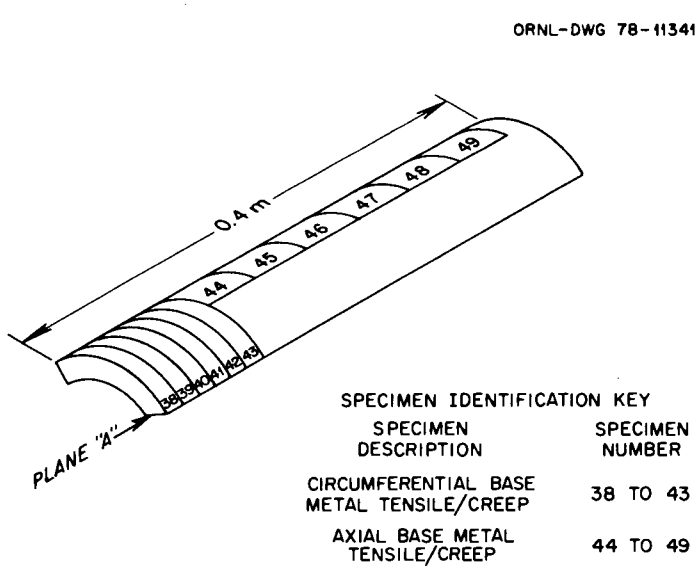

Fig. 21. Specimen removal from weldment section.

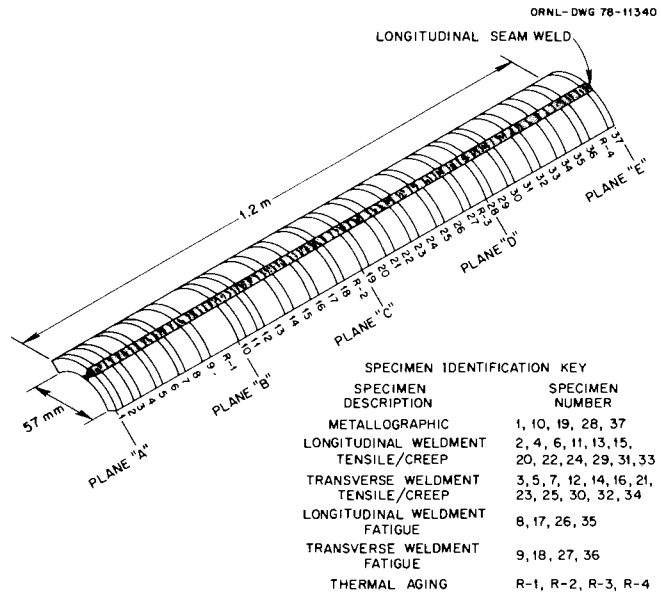

Fig. 22. Specimen removal from base-metal section.

through E intersect the weld. This was done so that the nondestructively determined ferrite measurements made at these locations could be directly compared with those obtained by destructive examination. In addition, the various types of specimens were equally distributed over the length of the weldment section to prevent any localized conditions from biasing the data.

6.2 Metallographic Characterization

As shown in Fig. 21, five metallographic specimens were removed from the weld in each pipe. All of the specimens from each pipe were given a macroscopic examination, while only one was examined for microstructural details. Figures 23 through 27 show typical macroetched cross-sectional views of the welds and sketches of joint design and welding pass sequence. The cross-sectional views of the welds in pipes E-13 and F-14 highlight the variation that can occur between different manufacturers using the same welding process. Both of these welds were made with the GTA process, except that pipe E-13 had a combination of hot- and cold-wire additions, while pipe F-14 was all cold-wire additions. Although the wall thickness was the same in both cases, the weld in pipe E-13 had six passes, while F-14 had only three. As a result, the large bead in F-14 had a coarser columnar grain structure. This structural difference could lead to differences in mechanical properties. The large passes used in pipes G-15 and G-16 also have coarse grain structure, which could lead to a variation in mechanical properties. Although the weld in pipe H-22 was made by the submerged-arc welding process, which has a high heat input, the structure of the weld does not appear to be too coarse in relation to the other welds. Two interesting situations were revealed during the examination of the macroetched specimens, one of which from the end of pipe G-16 is shown in Fig. 28. This specimen showed that there apparently was a gap between the longitudinal seam welds made from the outside and inside surfaces. A weld, which was likely to have been autogenous GTA, was used to fuse this gap. In making this weld, two arc strikes were created, with one of the strikes and the weld containing crater cracks. Figure 6 (*c*) shows this end as it was received from the manufacturer. It can be seen that grinding performed on the end has concealed this condition. Figure 29 shows the macroetched specimen from the end of pipe H-22.

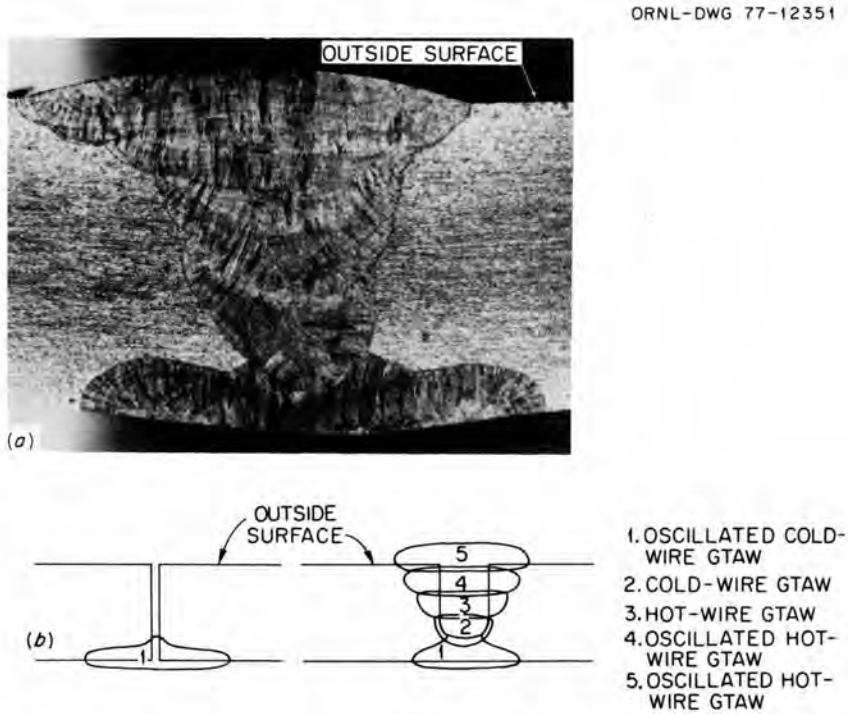

Fig. 23. (*a*) Typical macroetched cross-sectional view of GTA weld in pipe E-13, 7×, 50 HCl–10 HNO_3–5 H_2SO_4 etchant. (*b*) Joint design and welding pass sequence (Reduced 30%).

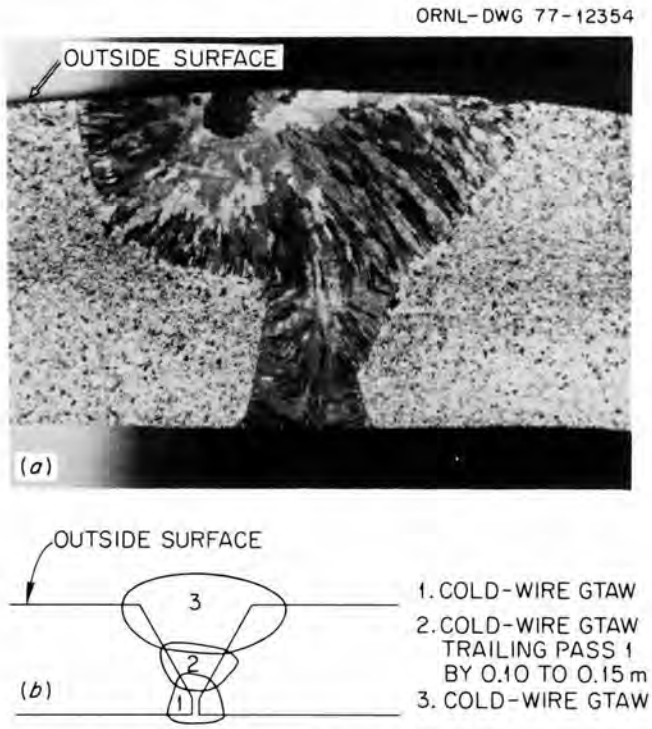

Fig. 24. (*a*) Typical macroetched cross-sectional view of GTA weld in pipe F-14, 7×, 50 HCl–10 HNO_3–5 H_2SO_4 etchant. (*b*) Joint design and welding pass sequence (Reduced 45%).

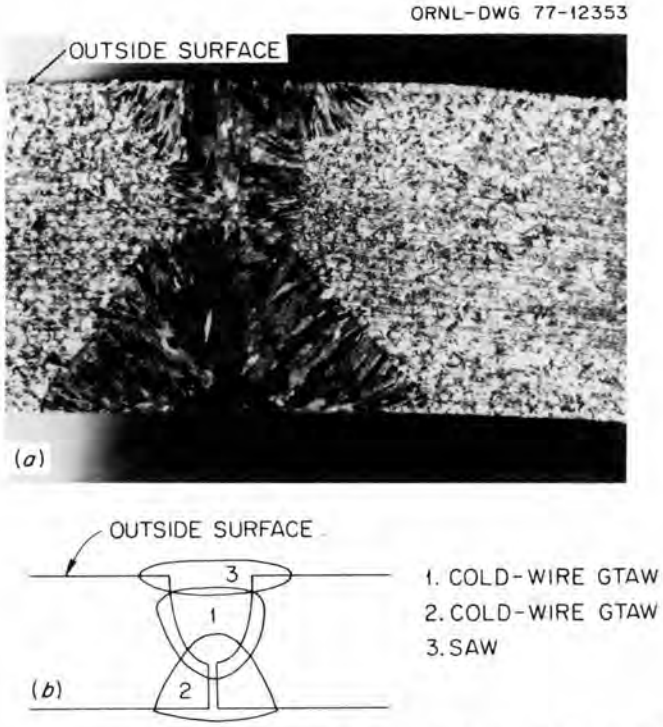

Fig. 25. (*a*) Typical macroetched cross-sectional view of SA-GTA weld in pipe G-15, 7×, 50 HCl–10 HNO_3–5 H_2SO_4 etchant. (*b*) Joint design and welding pass sequence (Reduced 40%).

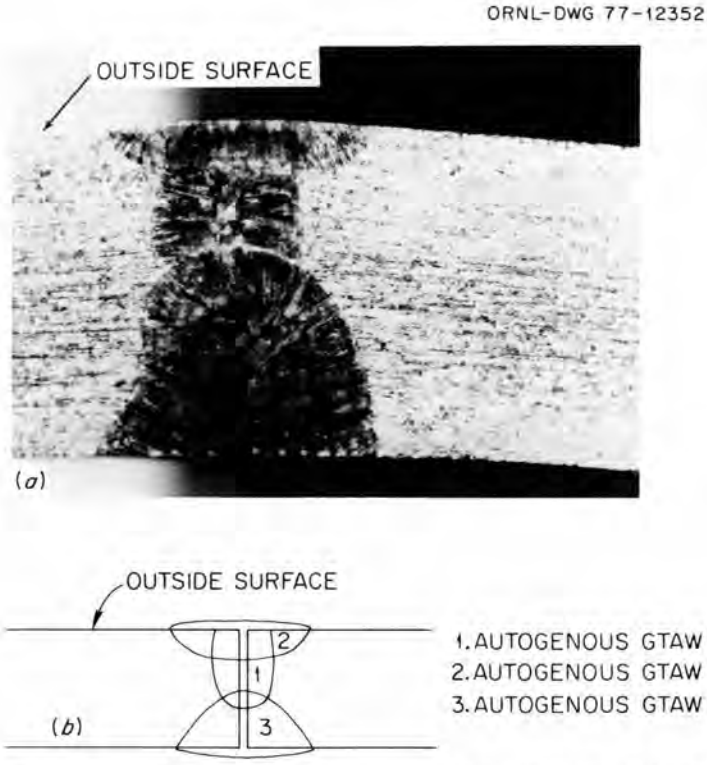

Fig. 26. (*a*) Typical macroetched cross-sectional view of autogenous GTA weld in pipe G-16, 7× 50 HCl–10 HNO_3–5 H_2SO_4 etchant. (*b*) Joint design and welding pass sequence (Reduced 50%).

ORNL-DWG 78-11342

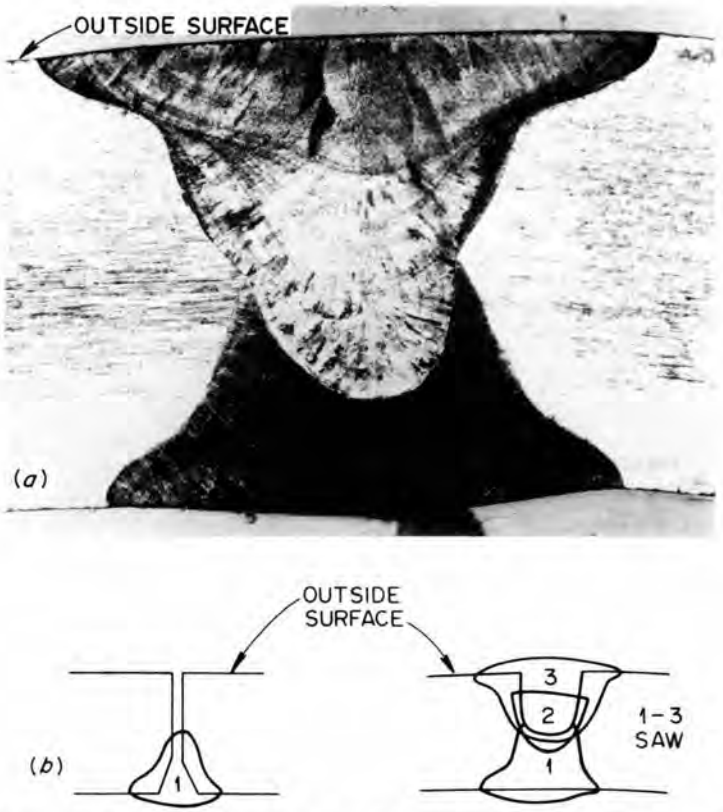

Fig. 27. (*a*) Typical macroetched cross-sectional view of SA weld in pipe H-22, 5×, 50 HCl–10 HNO_3–5 H_2SO_4 etchant. (*b*) Joint design and welding pass sequence (Reduced 50%).

Fig. 28. Macroetched cross-sectional view of the end of pipe G-16, showing arc strikes and GTA weld used to fuse an apparent gap between the seam welds, 6×, 50 HCl–10 HNO_3–5 H_2SO_4 etchant (Reduced 49%).

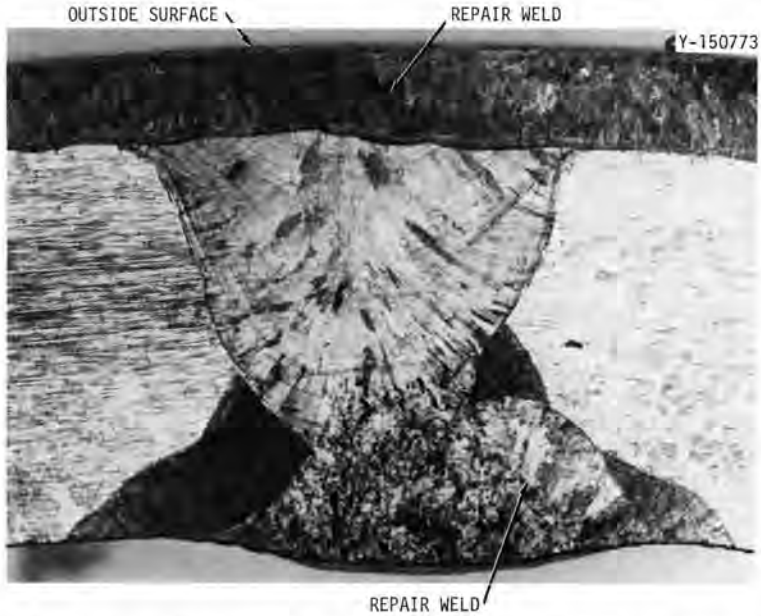

Fig. 29. Macroetched cross-sectional view of the end of pipe H-22, showing repair welds, 6× 50 HCl–10 HNO_3–5 H_2SO_4 etchant (Reduced 37%).

This specimen showed that two repair welds were performed on the end. This welding may have been related to repairing conditions which resulted from the removal of the runoff tab. However, the repair on the outside surface could be a wash pass used to achieve a surface finish. The conditions shown in Figs. 28 and 29 highlight the fact that discontinuities can be present in the weld ends. The presence of the crater cracks shown in Fig. 28 suggests that it is prudent to require a surface inspection, such as dye penetrant, of the pipe ends prior to girth welding.

Figures 30 through 32 show the typical microstructures of the weld, heat-affected zone (HAZ), and base metal for pipe E-13. Figure 33 shows a typical cross section of the weld region in pipe E-13 with the results of diamond pyramid hardness (DPH) traverses through the weld, HAZ, and base metal. As previously described from the macroetched specimens, the dendritic structure of the weld is fairly fine. In addition, only the HAZ appears to be significantly coarsened at the center of the weld. The base-metal structure is uniform except for a narrow coarsened band at the inner surface. The results of the DPH traverses are in good agreement with the microstructures, except that the measurement of the base metal at the inner surface appears to be high because it was not located in the coarsened band.

Figures 34 through 36 show the typical microstructures of the weld, HAZ, and base metal for pipe F-14. Figure 37 shows a typical cross section of the weld region in pipe F-14 with the results of DPH traverses through the weld, HAZ, and base metal. The dendritic structure of the weld is coarser than that for pipe E-13; the DPH values for the weld are also correspondingly lower for F-14 as compared with E-13. The HAZ for F-14 is coarsened throughout the thickness; the DPH traverse through the HAZ verifies this. The base-metal structure is relatively uniform. The coarser structures seen in the weld and HAZ of pipe F-14 are the result of the higher heat input used.

Figures 38 through 40 show the typical microstructures of the weld, HAZ, and base metal for pipe G-15. Figure 41 shows a typical cross section of the weld region in pipe G-15 with the results of DPH traverses through the weld, HAZ, and base metal. The weld in G-15 has a coarse cellular-dendritic structure.

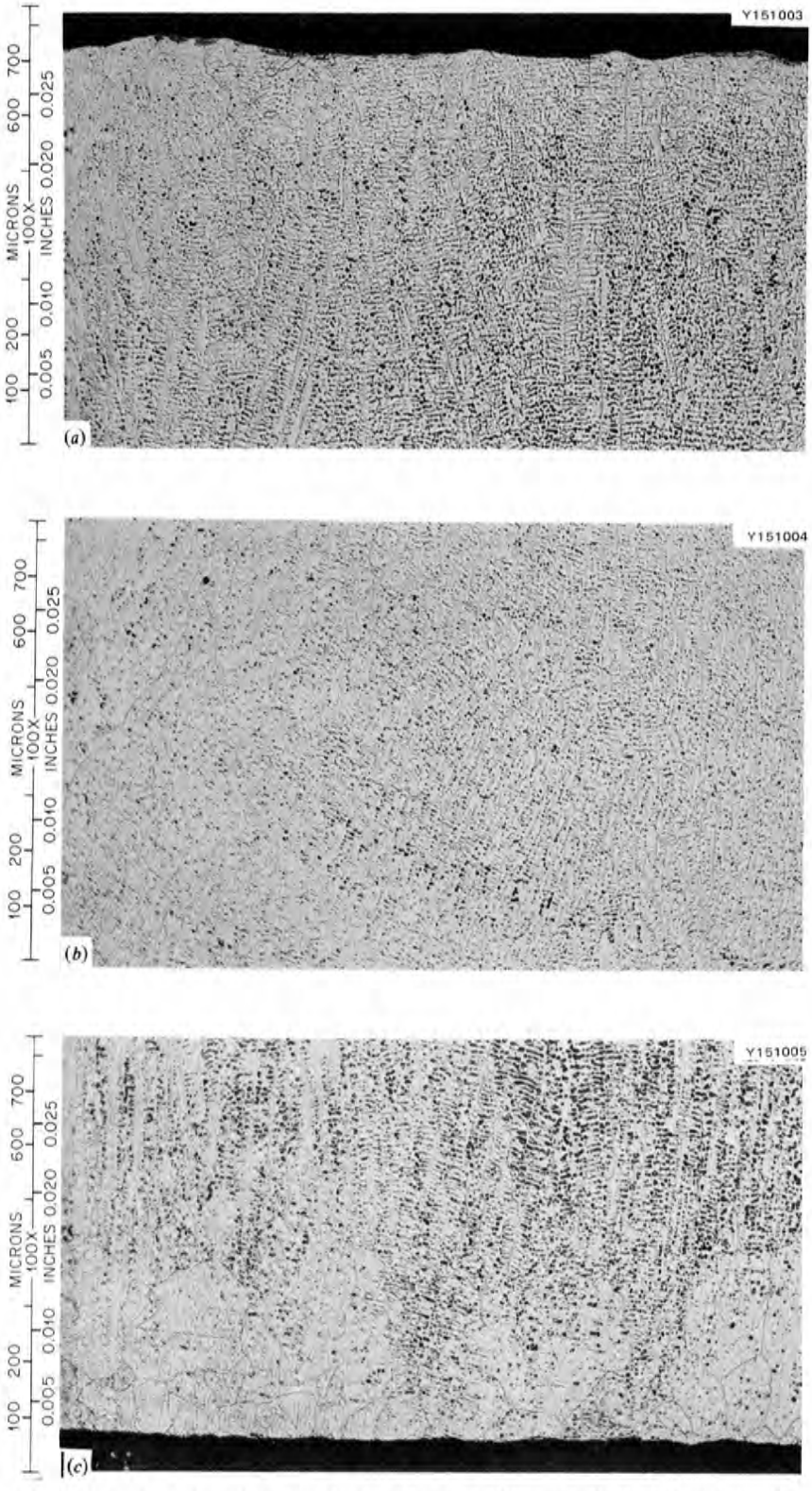

Fig. 30. Typical microstructure of weld in pipe E-13, etchant 50 HNO_3–50 H_2O applied electrolytically, 100X; (*a*) outside surface, (*b*) center, (*c*) inside surface.

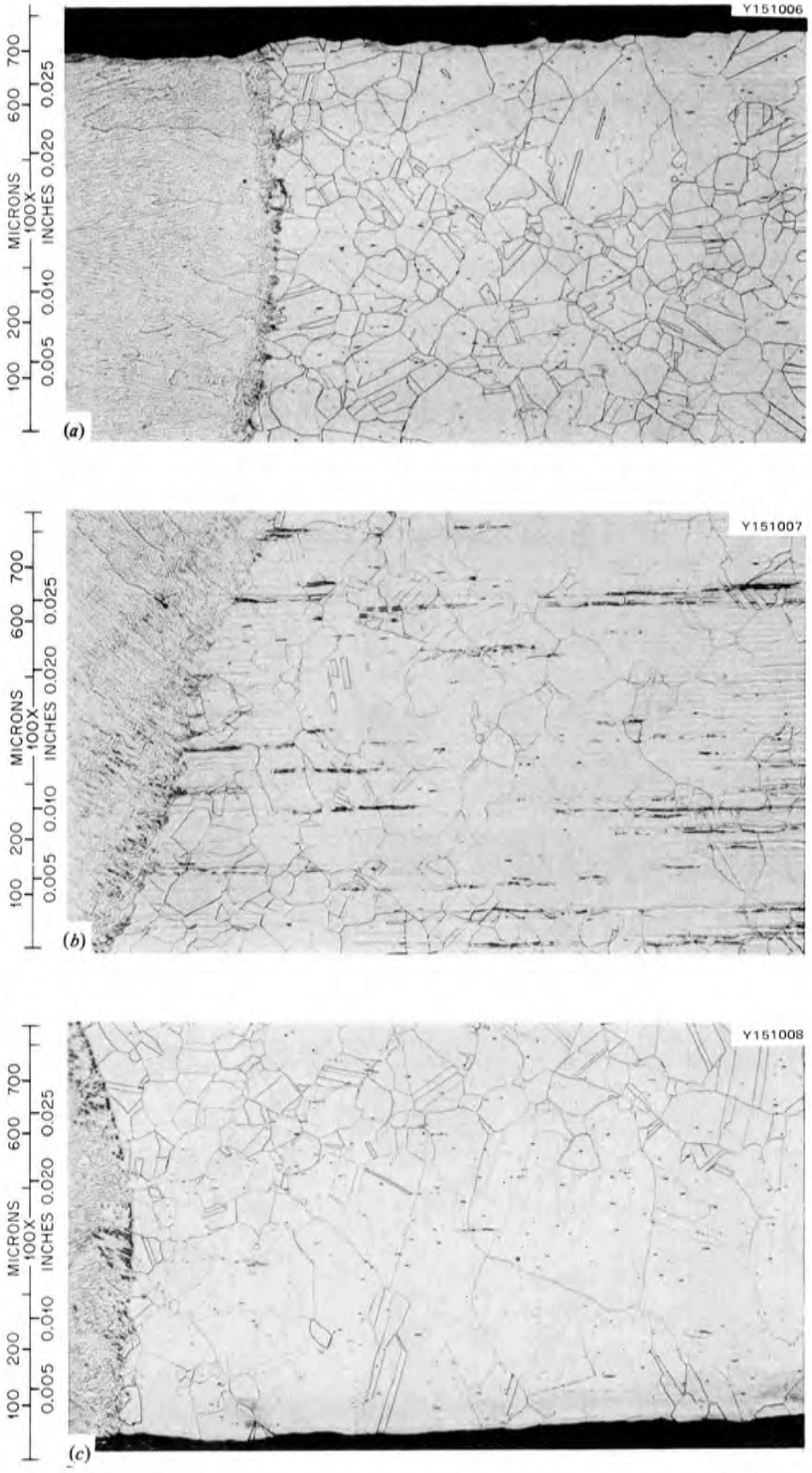

Fig. 31. Typical microstructure of fusion zone boundary and HAZ in pipe E-13, etchant 50 HNO_3 –50 H_2O applied electrolytically, 100×; (*a*) outside surface, (*b*) center, (*c*) inside surface.

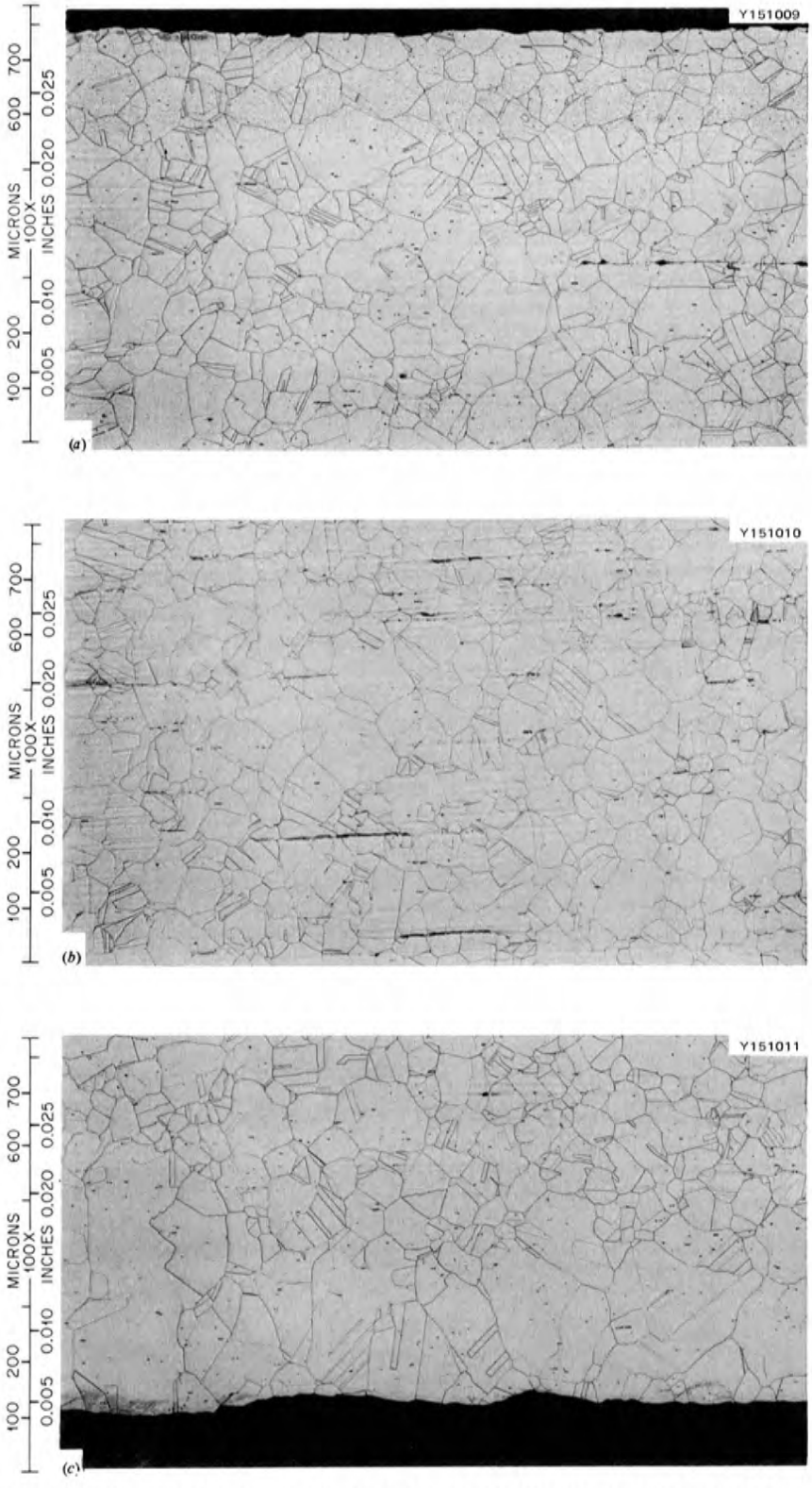

Fig. 32. Typical microstructure of base metal in pipe E-13, etchant 50 HNO_3 –50 H_2O applied electrolytically, 100×; (*a*) outside surface, (*b*) center, (*c*) inside surface.

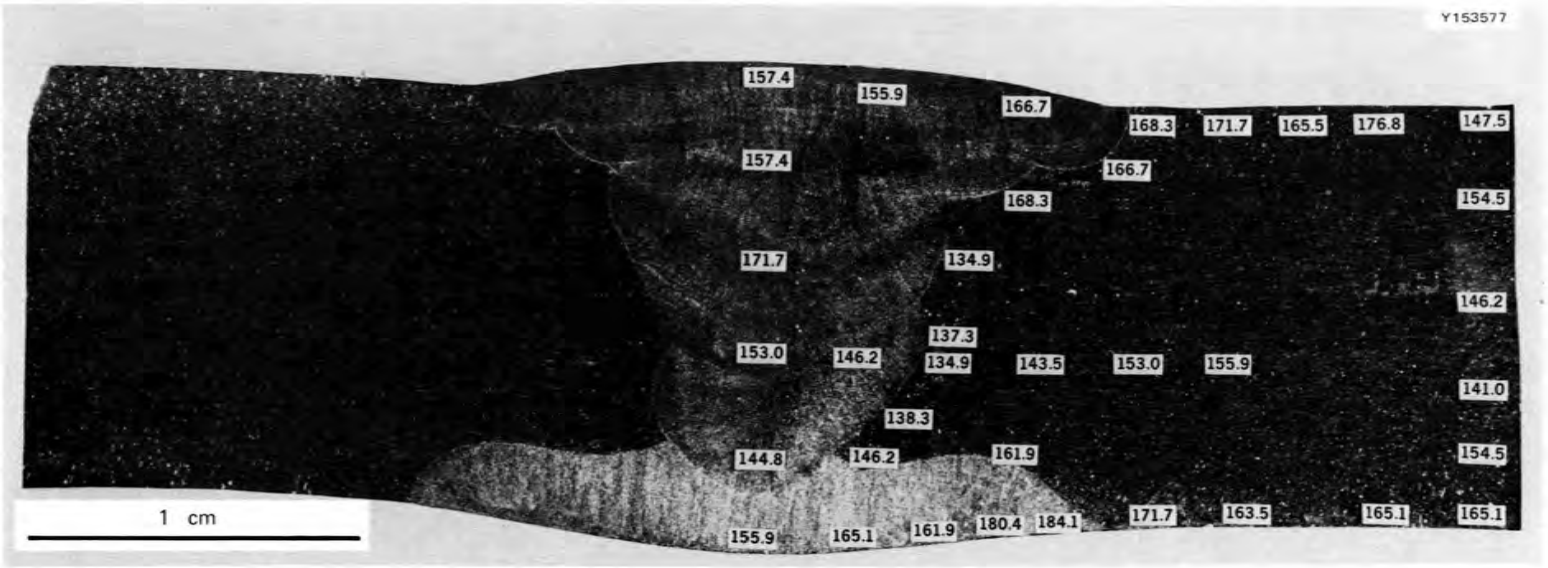

Fig. 33. Typical cross section of weld area in pipe E-13 showing the results of DPH traverses through the weld, HAZ, and base metal.

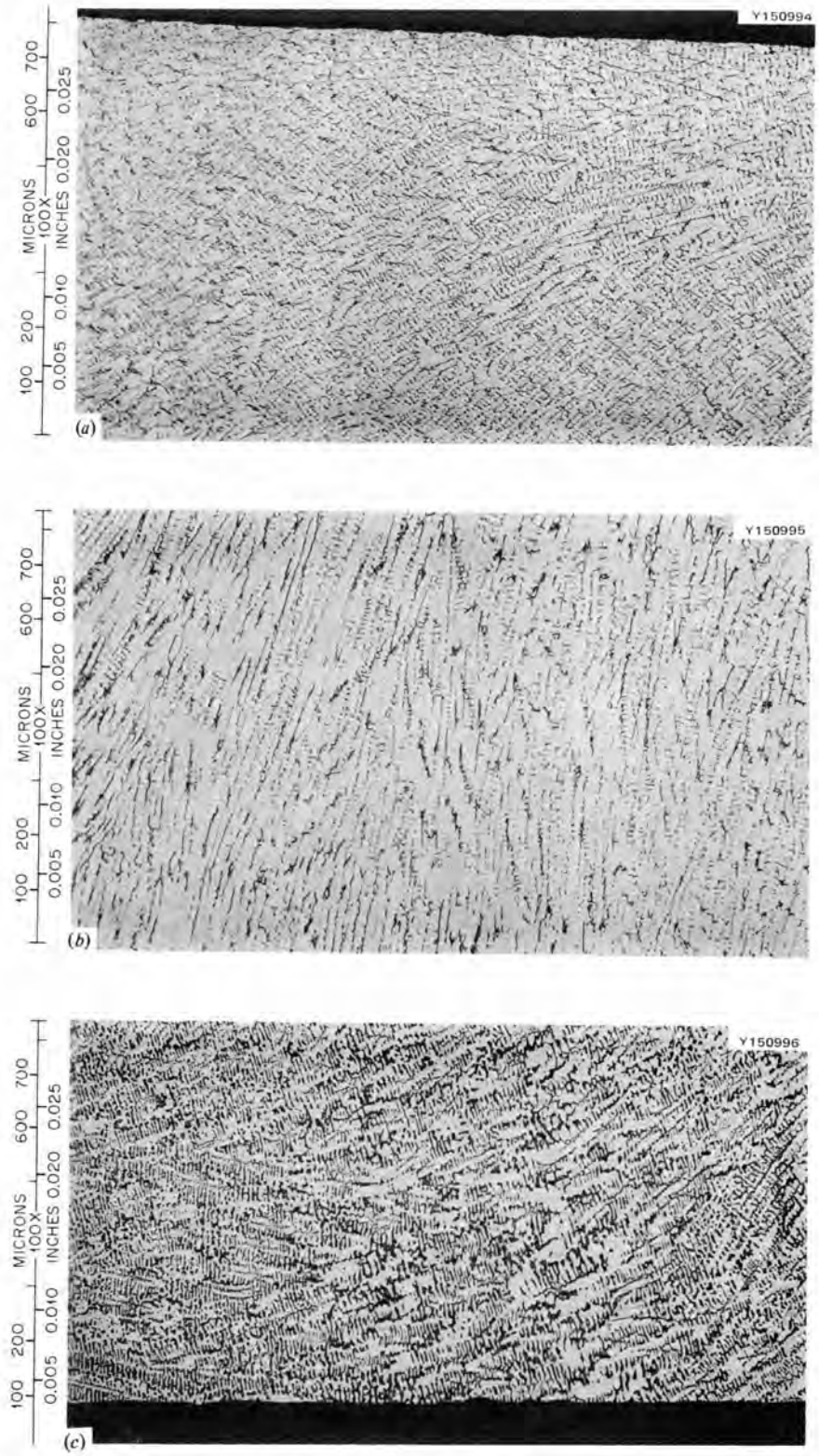

Fig. 34. Typical microstructure of the weld in pipe F-14, etchant 50 HNO_3–50 H_2O applied electrolytically, 100X; (*a*) outside surface, (*b*) center, (*c*) inside surface.

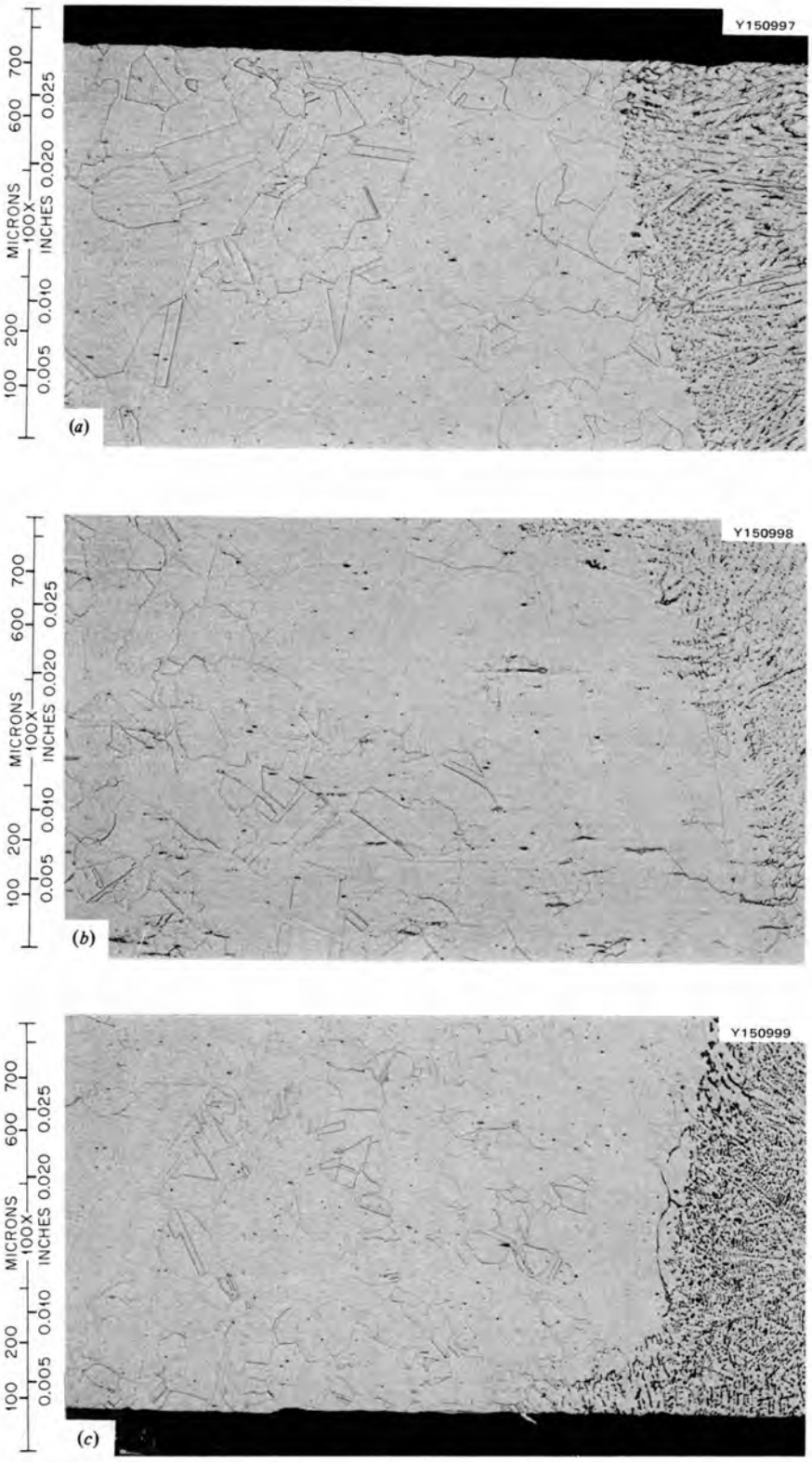

Fig. 35. Typical microstructure of the fusion zone boundary and HAZ in pipe F-14, etchant 50 HNO_3–50 H_2O applied electrolytically, 100×; (*a*) outside surface, (*b*) center, (*c*) inside surface.

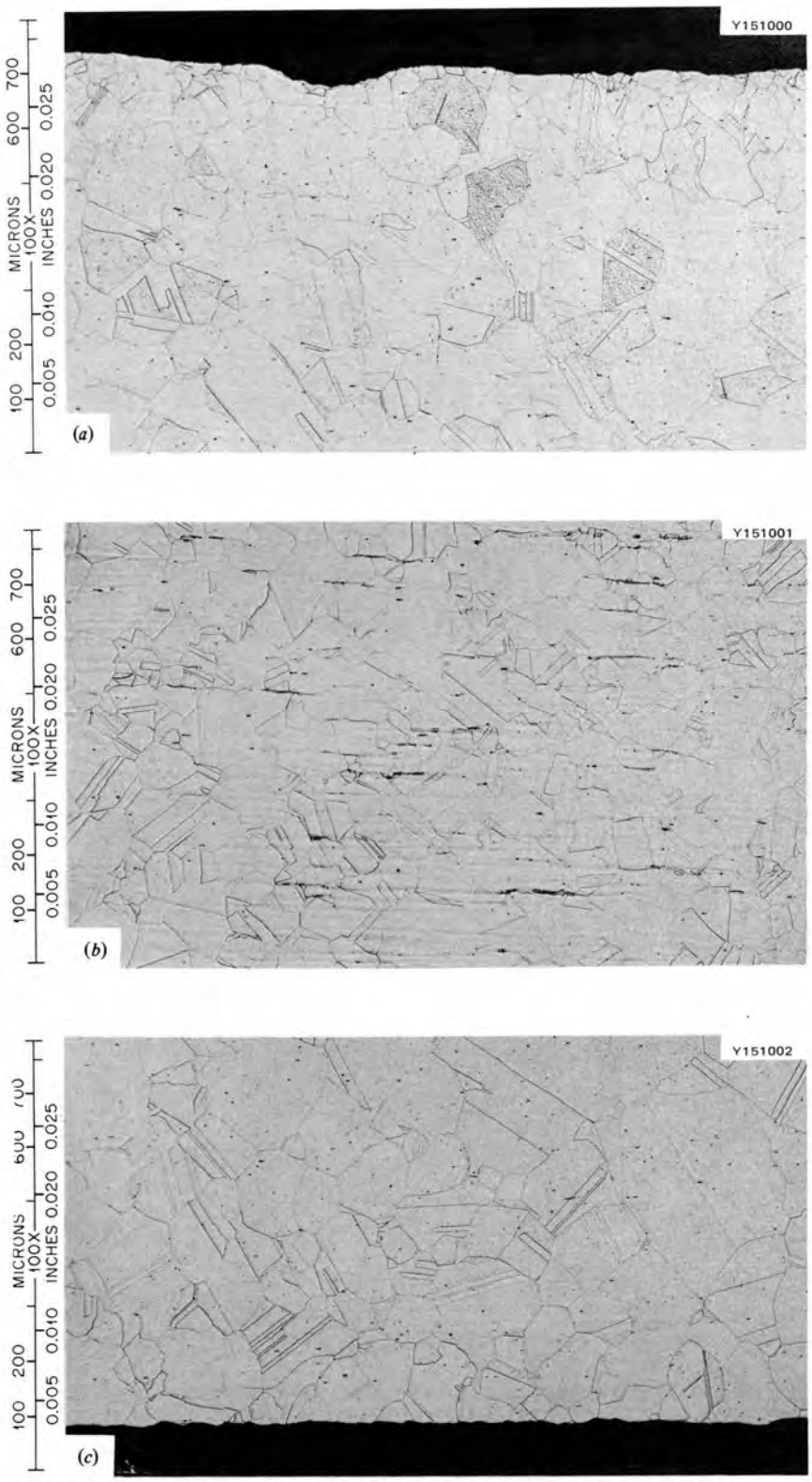

Fig. 36. Typical microstructure of the base metal in pipe F-14, etchant 50 HNO_3 –50 H_2O applied electrolytically, 100X; (*a*) outside surface, (*b*) center, (*c*) inside surface.

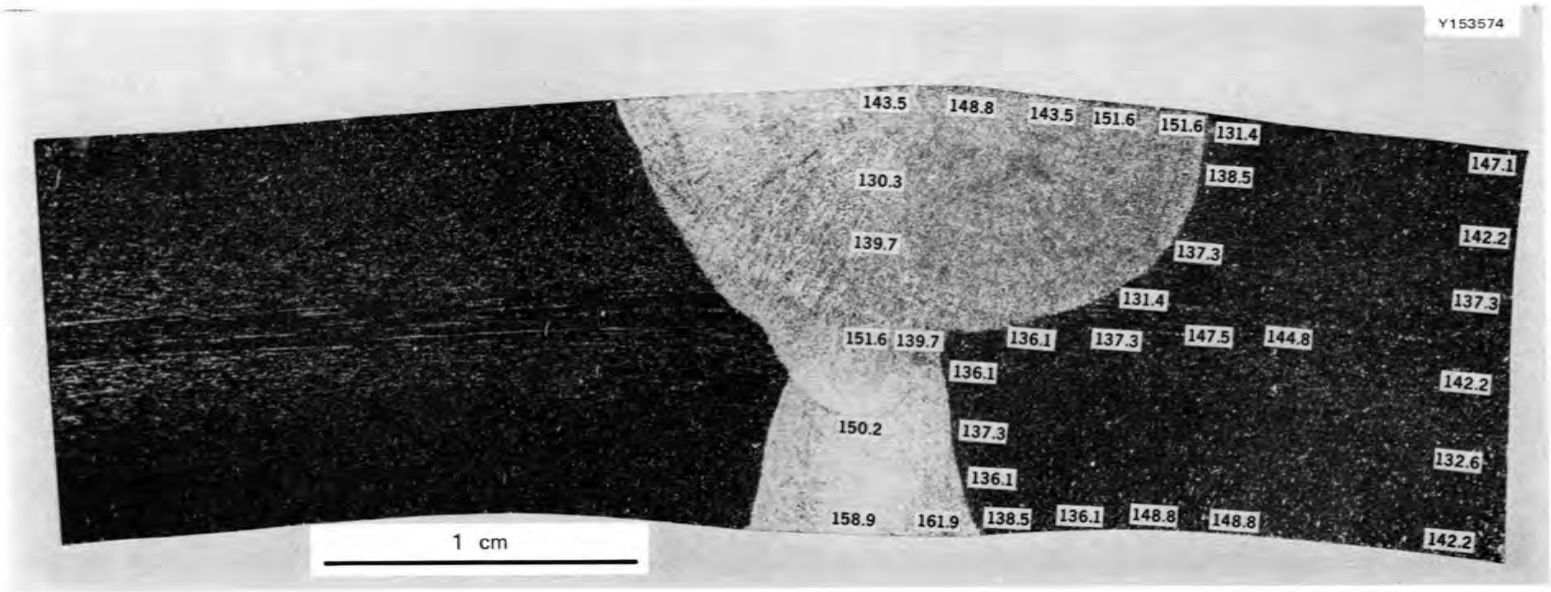

Fig. 37. Typical cross section of the weld in pipe F-14 showing the results of DPH traverses through the weld, HAZ, and base metal.

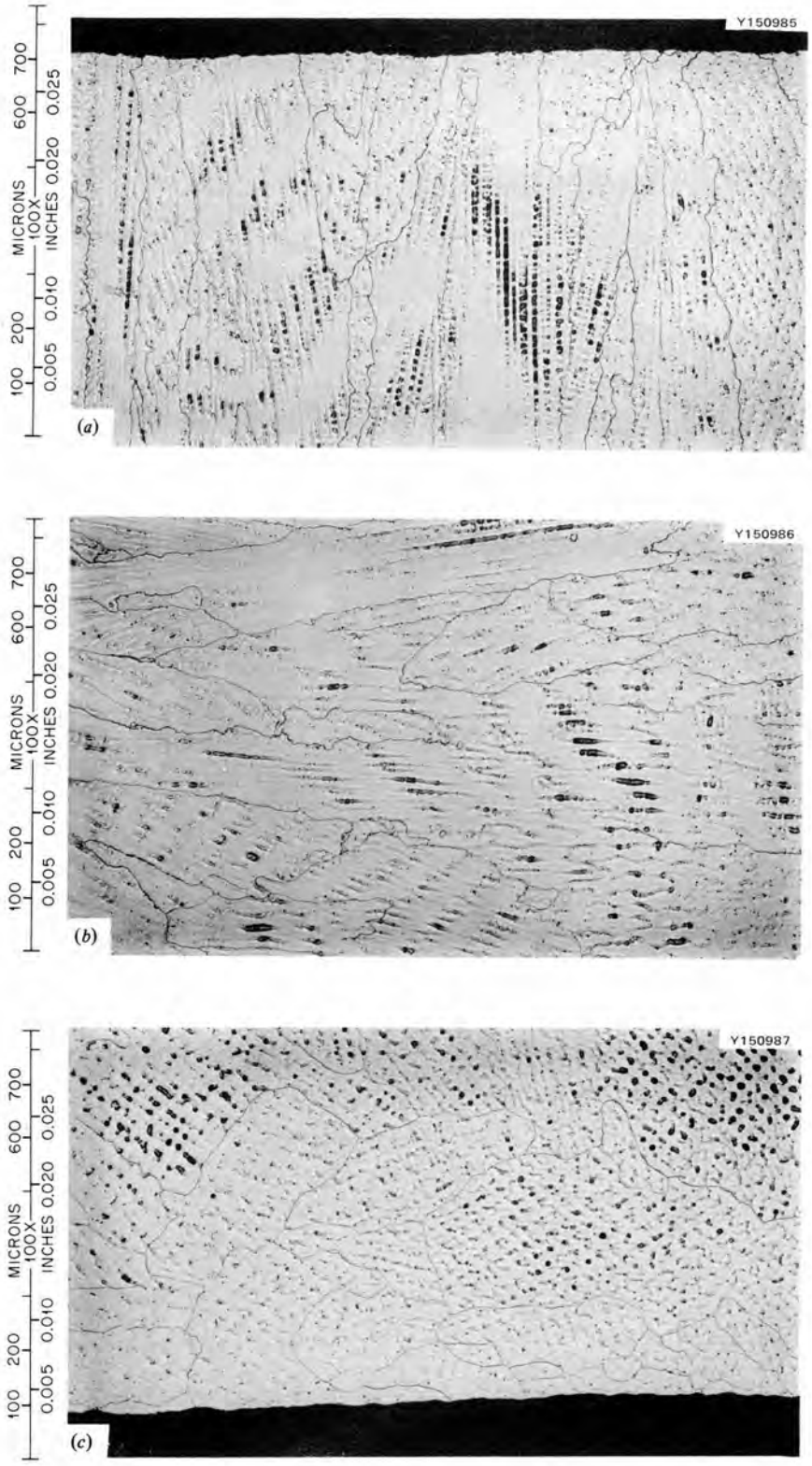

Fig. 38. Typical microstructure of weld in pipe G-15, etchant 50 HNO_3–50 H_2O applied electrolytically, 100X; (*a*) outside surface, (*b*) center, (*c*) inside surface.

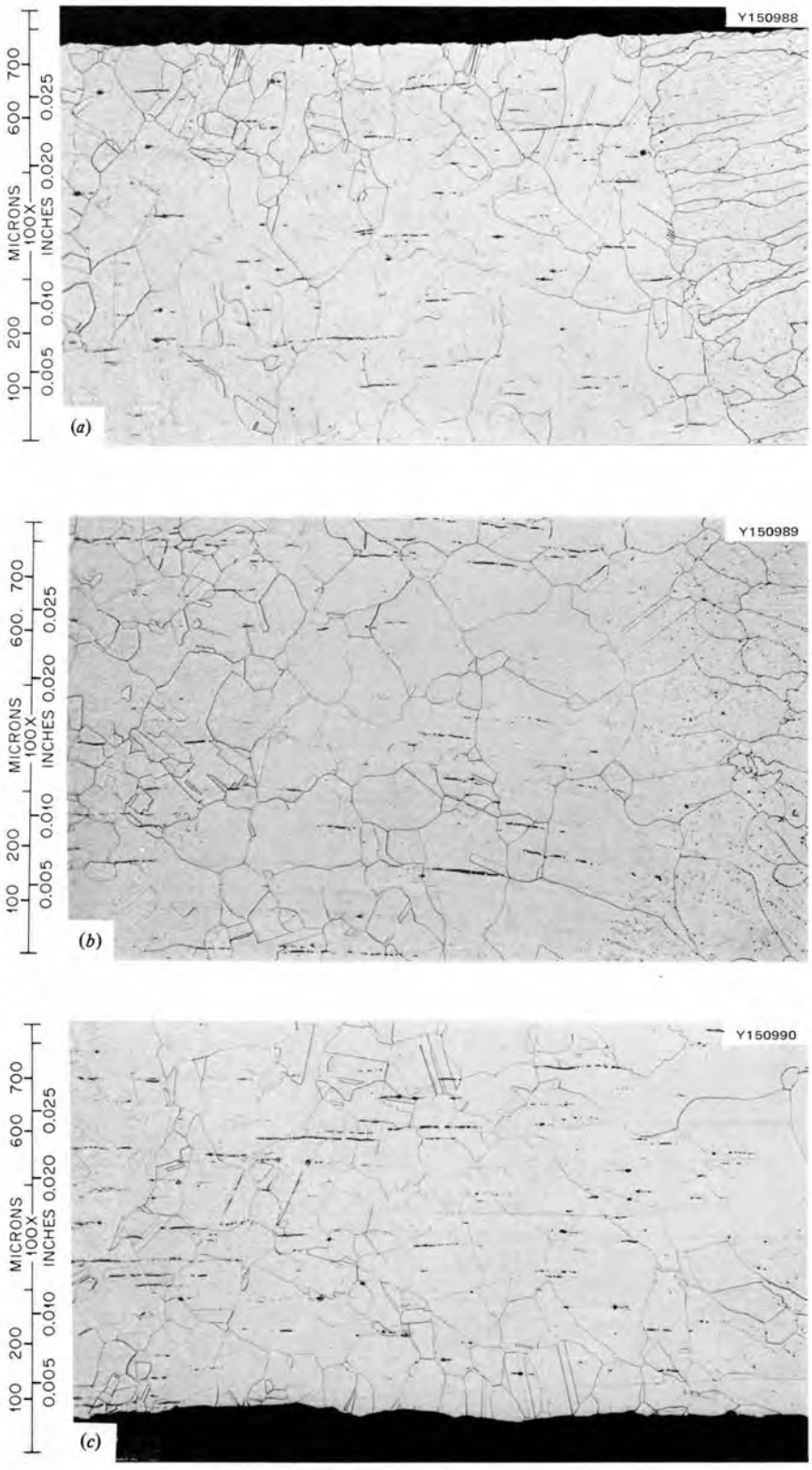

Fig. 39. Typical microstructure of fusion zone boundary and HAZ in pipe G-15, etchant 50 HNO_3–50 H_2O applied electrolytically, 100×; (*a*) outside surface, (*b*) center, (*c*) inside surface.

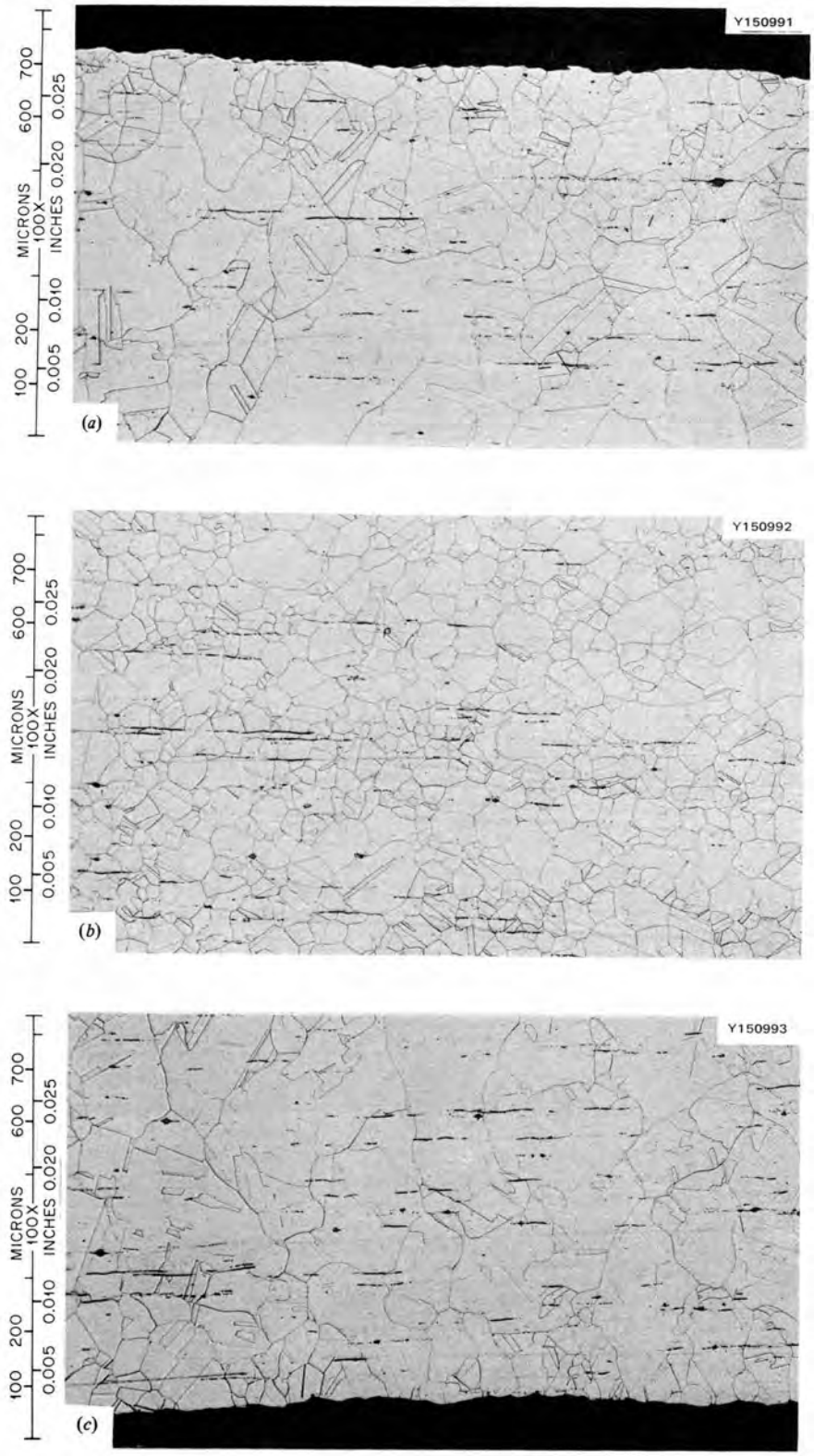

Fig. 40. Typical microstructure of base metal in pipe G-15, etchant 50 HNO_3 –50 H_2O applied electrolytically, 100X; (*a*) outside surface, (*b*) center, (*c*) inside surface.

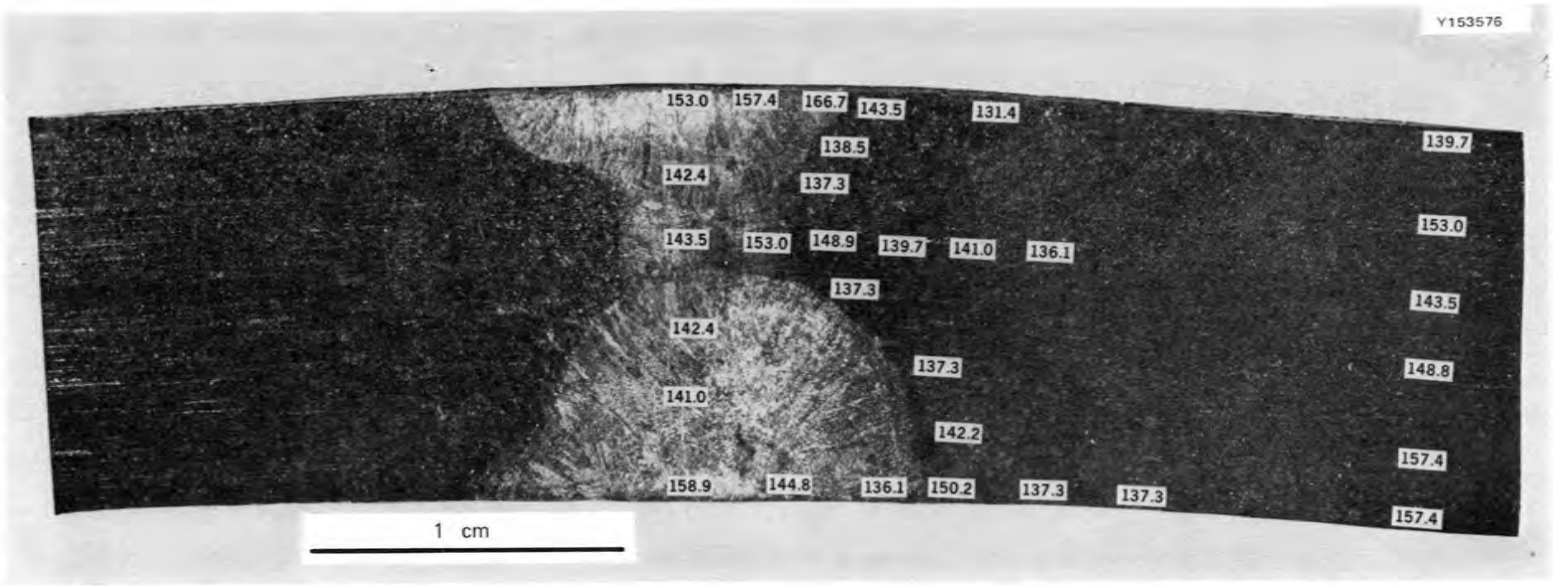

Fig. 41. Typical cross section of weld in pipe G-15 showing the results of DPH traverses through the weld, HAZ, and base metal.

The structure in the center of the weld was coarser as confirmed by the hardness traverse. In general, the weld structrue was much coarser than that of either E-13 or F-14. The HAZ appears to have experienced a greater degree of coarsening at the inside surface and center. The epitaxial growth of individual fusion zone grains from the base metal is more clearly observable than on the microstructures for either E-13 or F-14. The structure of the base metal does not correspond well with the hardness traverse. The microstructure indicates coarser grains at the inside and outside surfaces than at the center, while the hardness measurements indicate almost the opposite.

Figures 42 through 44 show the typical microstructures of the weld, HAZ, and base metal for pipe G-16. Figure 45 shows a typical cross section of the weld region in pipe G-16 with the results of DPH traverses through the weld, HAZ, and base metal. The weld has a coarse cellular-dendritic structure as was present in G-15. The weld structure at the inside surface appears to be the most coarse. The weld structure is columnar at the inside and outside surfaces, while it is relatively equiaxed at the center. The growth from the base metal into the fusion zone is again epitaxial as was the case in G-15. The coarsening of the HAZ appears to be most pronounced at the inside surface. This is because of the large heat input used to make the weld on the inside surface. The hardness values correlate with this conclusion. The base-metal structure was coarser on the inside and outside surfaces than it was at the center. This is the same variation seen in pipe G-15, because the plate used for both pipes was from the same heat of steel. The lack of correlation with the hardness measurements is also the same as reported for pipe G-15.

Figures 46 through 48 show the typical microstructures of the weld, HAZ, and base metal for pipe H-22. Figure 49 shows a typical cross section of the weld region in pipe H-22 with the results of DPH traverses through the weld, HAZ, and base metal. The inside surface of the weld has a fine dendritic structure. The structure of the center and outside surface of the weld is considerably different than that of the inside. This is probably due to the fact that the flux used to make the inside weld and that used to make the two outside welds were different (Lincoln 860 was used for the inside and Arcos S-11 was used for the outside two). The hardness traverse indicates that the outside pass was stronger. Epitaxial growth is more clearly observable at the fusion zone boundary at the center of the weld than at the boundary near the outside and inside surfaces. The HAZ appears to be most coarse near the outside surface. However, the hardness traverse does not agree with this conclusion. This is probably due to the fact that the outside weld pass had the highest heat input. The structure of the base metal is generally coarser than that for the other four pipes. The structure at the center of the base metal was finer than that at either the outside or the inside surfaces. However, the hardness traverse does not agree with this conclusion.

The above evaluation highlights the fact that the structure of a weldment is extremely variable, with significant variations occurring within the same weld, within welds made by the same process, and within welds made from the same filler material. Several programs are in progress at ORNL to study the relationship between weld structure and properties. It is beyond the scope of this report to make such complex correlations because of the limited number of welds tested. However, a later section will characterize the mechanical properties of the five weldments in the pipes.

6.3 Ferrite Evaluation

The ferrite content of the welds from pipes E-13, F-14, G-15, G-16, and H-22 has been destructively examined. Table 14 shows the vendor and ORNL overcheck chemical analyses. There are some differences between these analyses that affect the ferrite content calculation. Table 15 lists the weld ferrite numbers calculated with the DeLong diagram[34] from both vendor and overcheck chemical analyses, measured by magnetic permeability,[33] and the area percentage of ferrite determined by quantitative television microscope (QTM) analysis of specimens etched to identify the ferrite phase. It is again important to note that

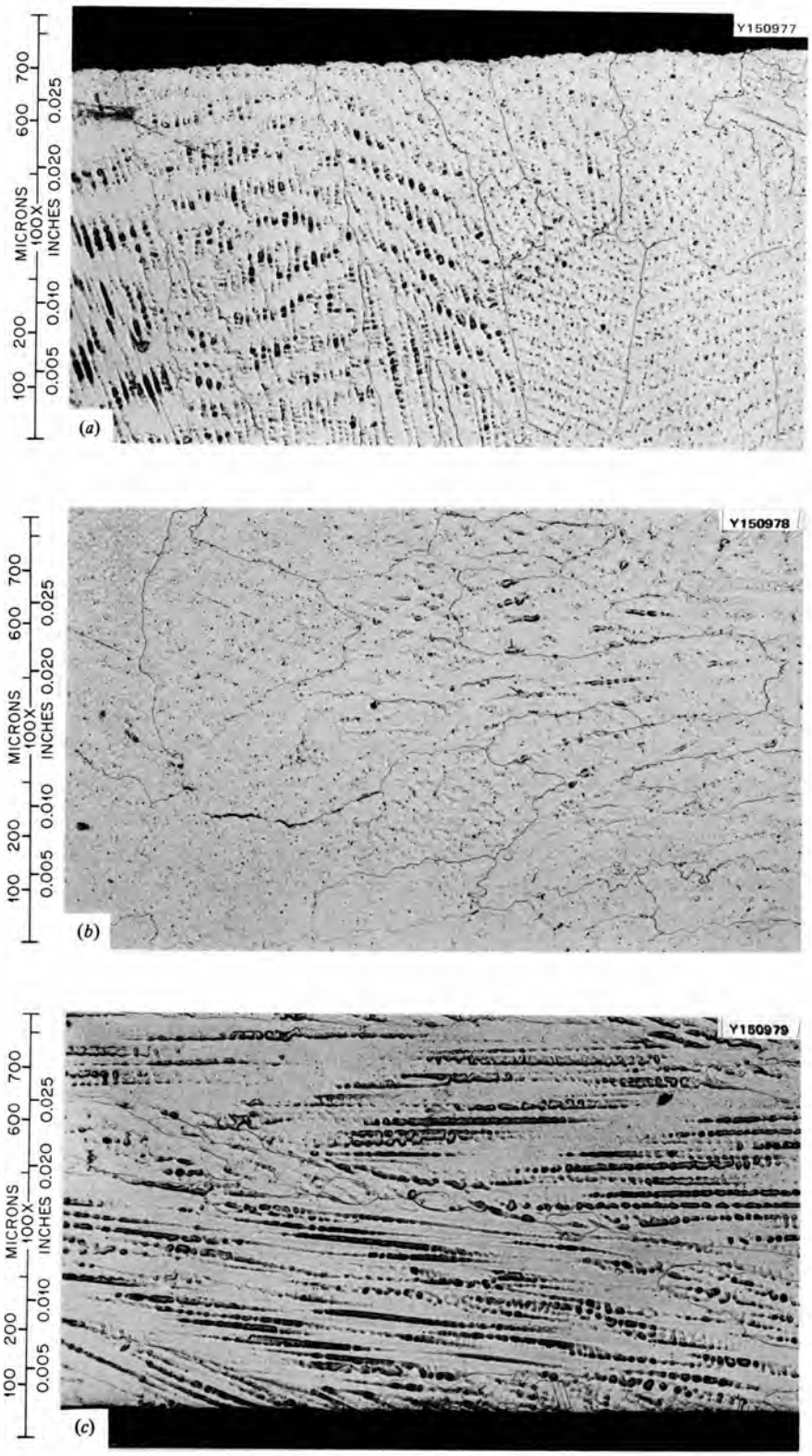

Fig. 42. Typical microstructure of weld in pipe G-16, etchant 50 HNO_3 –50 H_2O applied electrolytically, 100X; (*a*) outside surface, (*b*) center, (*c*) inside surface.

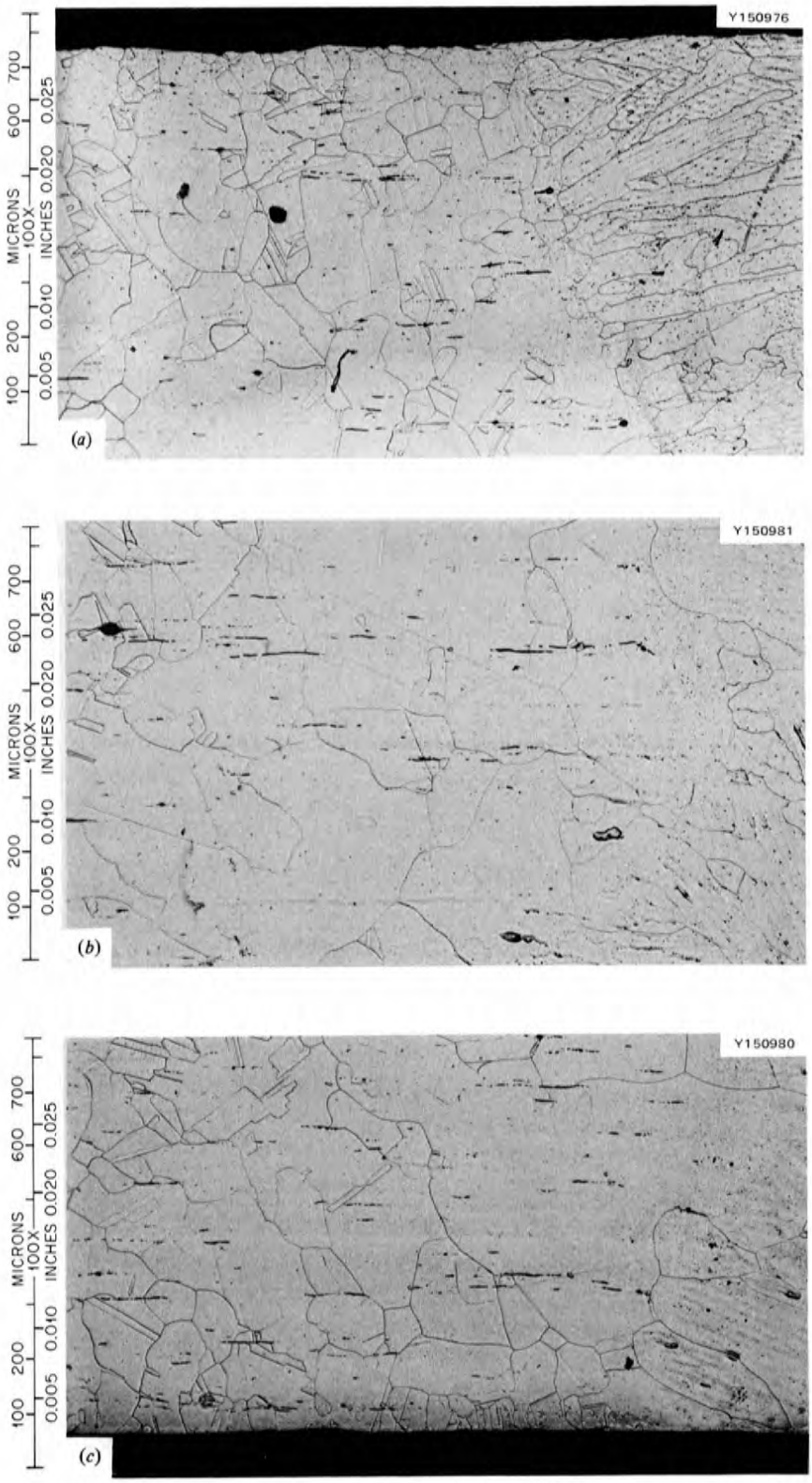

Fig. 43. Typical microstructure of the fusion zone boundary and HAZ in pipe G-16, etchant 50 HNO_3–50 H_2O applied electrolytically, 100X; (*a*) outside surface, (*b*) center, (*c*) inside surface.

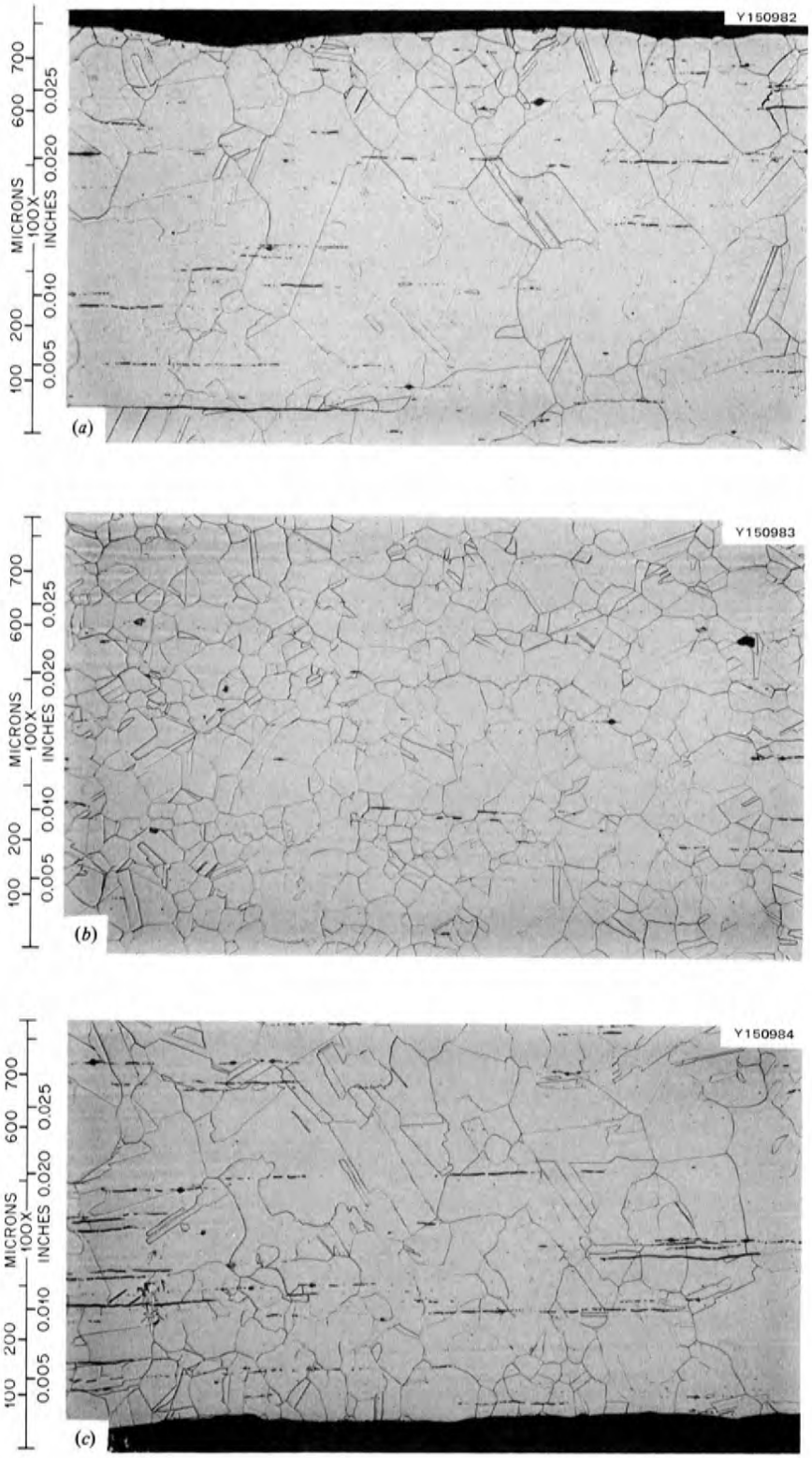

Fig. 44. Typical microstructure of base metal in pipe G-16, etchant 50 HNO_3 –50 H_2O applied electrolytically, 100X; (*a*) outside surface, (*b*) center, (*c*) inside surface.

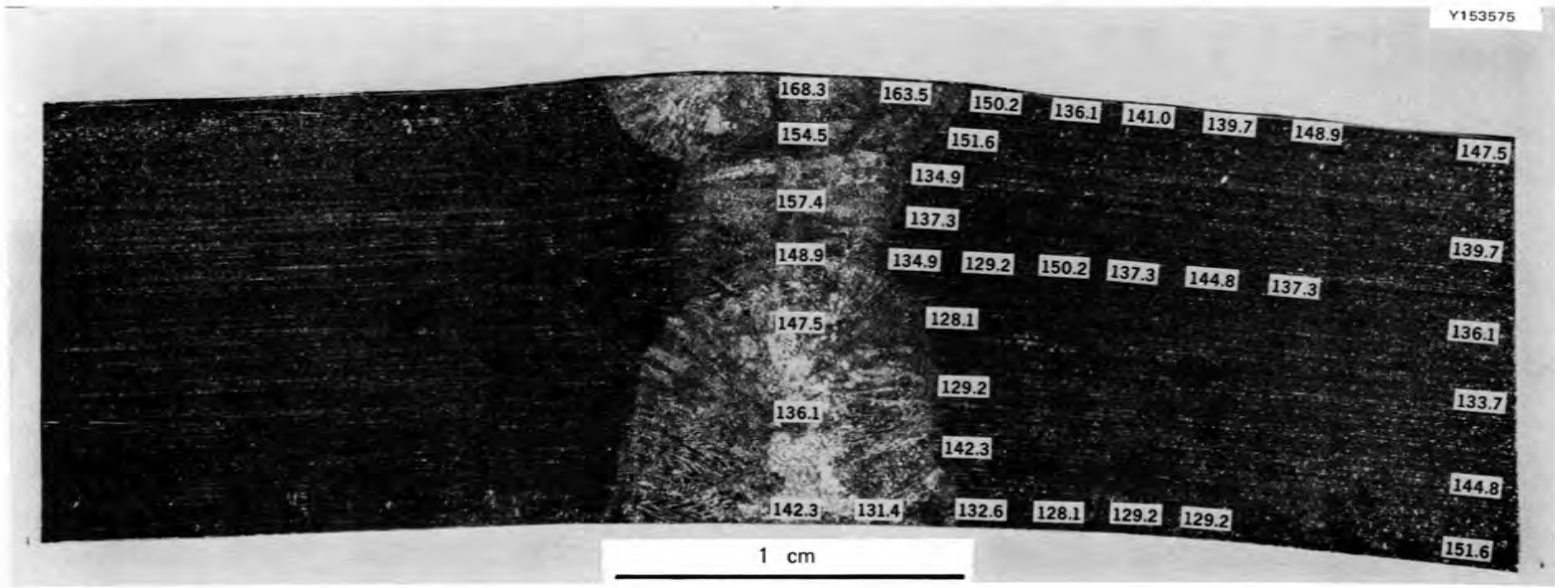

Fig. 45. Typical cross section of weld region in pipe G-16 showing the results of DPH traverses through the weld, HAZ, and base metal.

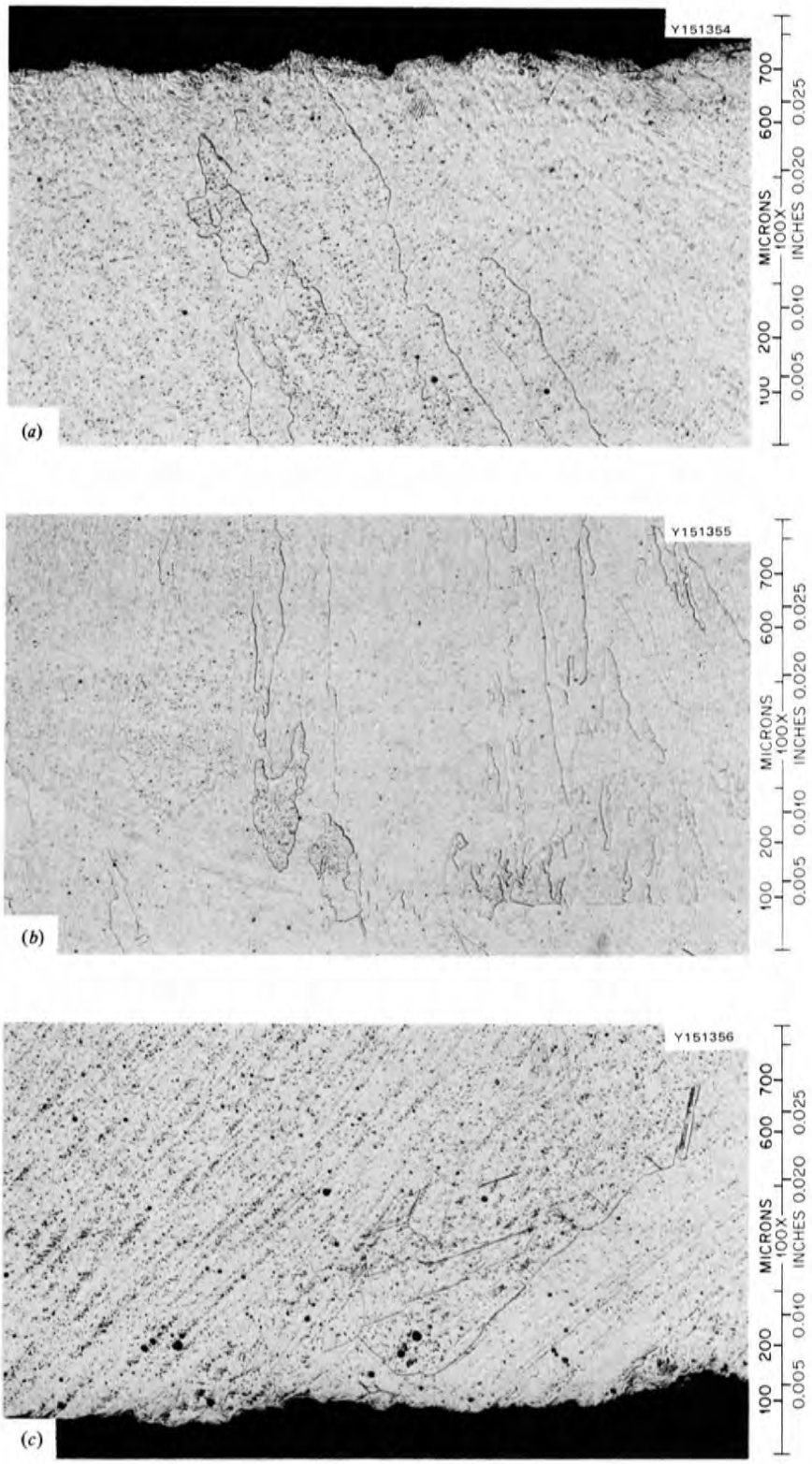

Fig. 46. Typical microstructure of weld in pipe H-22, etchant 50 HNO_3–50 H_2O applied electrolytically, 100X; (*a*) outside surface, (*b*) center, (*c*) inside surface.

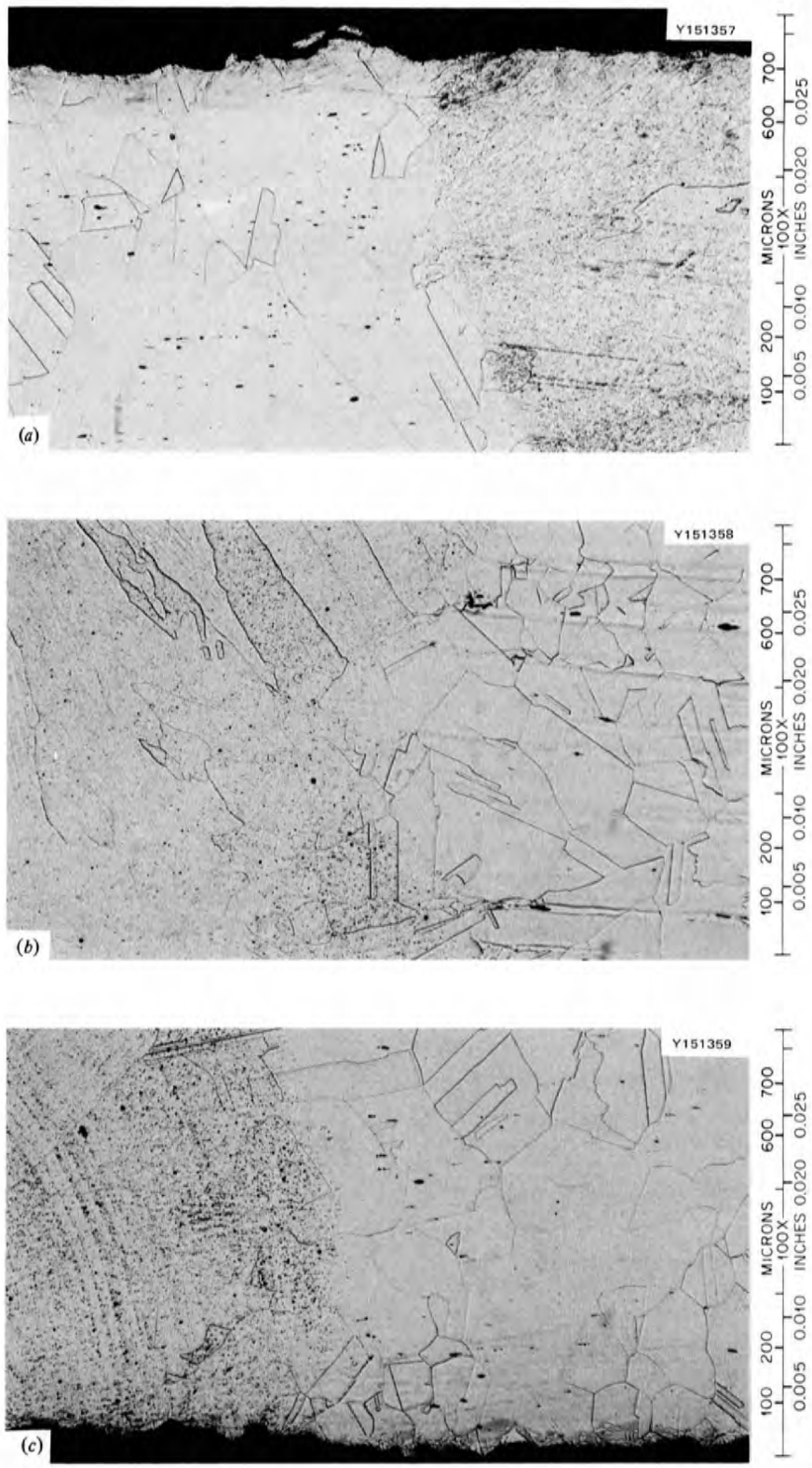

Fig. 47. Typical microstructure of fusion zone boundary and HAZ in pipe H-22, etchant 50 HNO_3 –50 H_2O applied electrolytically, 100×; (*a*) outside surface, (*b*) center, (*c*) inside surface.

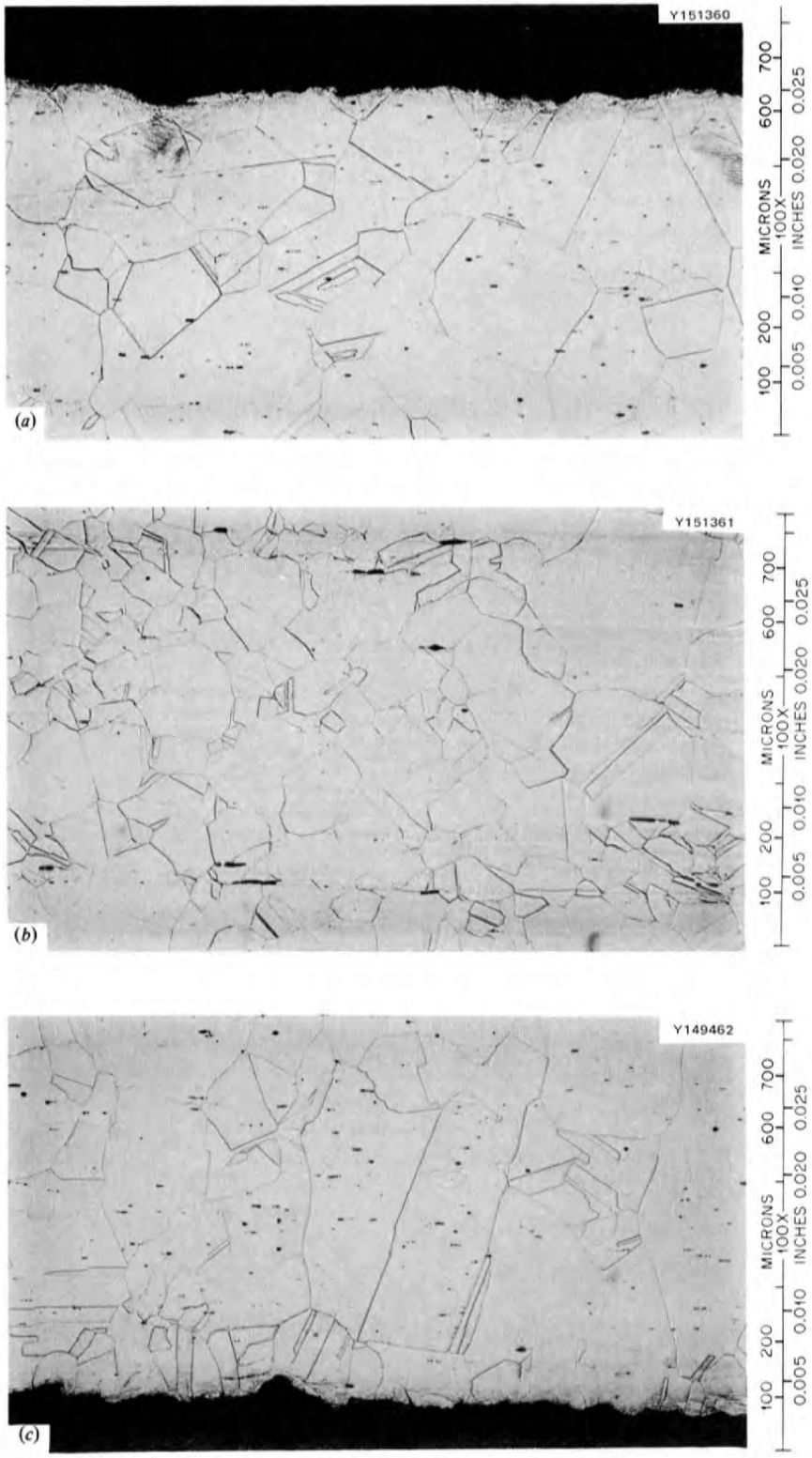

Fig. 48. Typical microstructure of base metal in pipe H-22, etchant 50 HNO_3–50 H_2O applied electrolytically, 100×; (*a*) outside surface, (*b*) center, (*c*) inside surface.

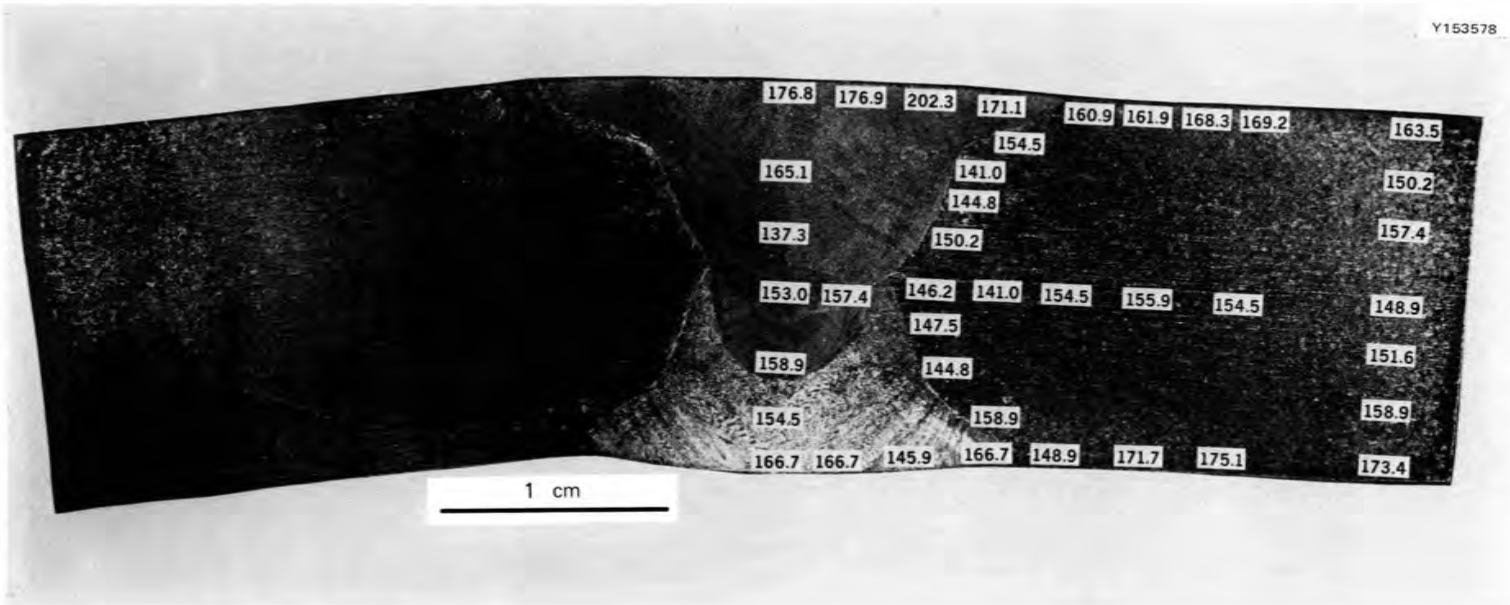

Fig. 49. Typical cross section of weld area in pipe H-22 showing the results of DPH traverses through the weld, HAZ, and base metal.

Table 14. Chemical analyses of formed and welded pipes

Pipe	Location	Content (wt %)															
		C	Mn	P	S	Si	Ni	Cr	Mo	V	Nb	Ti	Co	Cu	Al	B	N
								Vendor analysis									
E-13	Plate	0.074	1.78	0.020	0.012	0.91	11.48	17.18	2.01								
	Weld	0.060	1.66	0.012	0.012	0.49	10.79	16.43	2.00								
F-14	Plate	0.043	1.68	0.031	0.008	0.61	11.10	17.55	2.08								
	Weld	0.040	1.68	0.027	0.010	0.48	11.31	17.94	2.18								
G-15	Plate	0.055	1.63	0.025	0.024	0.45	12.10	16.40	2.15								
	Weld	0.055	1.58	0.026	0.025	0.46	12.20	16.40	2.20								
G-16	Plate	0.058	1.72	0.025	0.024	0.46	12.20	16.70	2.32								
	Weld	0.051	1.65	0.025	0.024	0.42	12.20	16.30	2.17								
H-22	Plate	0.053	1.82	0.020	0.012	0.50	13.30	16.65	2.28								
	Weld	0.060	1.65	0.024	0.019	0.55	10.06	15.33	2.04								
								Overcheck analysis[a]									
E-13	Plate	0.066	1.63	0.032	0.009	0.58	11.29	16.09	2.85	0.06	<0.01	0.01	0.17	0.22	0.01	0.001	0.039
	Weld	0.053	1.57	0.014	0.014	0.49	9.42	16.18	1.95	0.04	<0.01	0.01	0.06	0.13	<0.01	0.001	0.041
F-14	Plate	0.048	1.67	0.022	0.009	0.52	11.18	17.85	2.00	0.08	<0.01	0.01	0.21	0.19	<0.01	0.001	0.056
	Weld	0.026	1.57	0.020	0.009	0.51	11.62	17.88	2.08	0.08	<0.01	0.01	0.18	0.17	<0.01	0.001	0.037
G-15	Plate	0.064	1.57	0.029	0.026	0.47	12.63	16.39	2.19	0.05	0.01	0.03	0.22	0.26	<0.01	0.003	0.074
	Weld	0.051	1.50	0.026	0.021	0.53	12.68	16.19	2.17	0.05	0.01	0.02	0.23	0.27	<0.01	0.002	0.059
G-16	Plate	0.064	1.46	0.027	0.025	0.52	12.67	16.20	2.15	0.05	0.01	0.02	0.22	0.26	<0.01	0.003	0.083
	Weld	0.055	1.46	0.027	0.023	0.49	12.67	16.33	2.15	0.05	0.01	0.02	0.22	0.27	<0.01	0.002	0.062
H-22	Plate	0.057	1.84	0.030	0.018	0.60	13.17	16.37	2.21	0.07	<0.01	0.01	0.08	0.45	<0.01	0.002	0.076
	Weld	0.055	1.72	0.025	0.021	0.53	9.83	15.14	2.06	0.04	<0.01	0.01	0.08	0.21	<0.01	0.002	0.044

[a]Spectrographic chemical analysis performed by Combustion Engineering, Chattanooga, Tenn. Weld metal was analyzed in region where dilution effects were minimized.

Table 15. Ferrite content of formed and welded pipes

Pipe	Location	Ferrite number			Measured ferrite[d] (area %)
		Calculated vendor[a]	Calculated overcheck[b]	Measured[c]	
E-13	Outside	0	2.2	0.1–0.2	1.6
	Center			0.1–0.3	1.3
	Inside			0.2–0.4	2.4
F-14	Outside	4.5	6.0	3.2–4.8	7.2
	Center			2.4–2.8	5.8
	Inside			0.6–1.2	1.8
G-15	All	0	0	0	0
G-16	All	0	0	0	0
H-22	All	0	0	0	0

[a]Calculated from Delong diagram, using vendor chemical analysis shown in Table 14 and assuming 0.06% N.

[b]Calculated from Delong diagram, using overcheck chemical analysis shown in Table 14.

[c]Magnetic permeability measurements made with Twin City Testing Corp. Ferritescope, type FE8e2, model B, with probe type KF. Calibration was performed in accordance with AWS A4.2-74, using Teledyne McKay weld metal secondary standards. Measurements were made on five specimens sectioned at 0.3-m intervals along the weld.

[d]Quantitative television microscope analysis was made on one specimen per pipe, which was etched with 15 g $K_3Fe(CN)_6$ –15 g KOH–100 ml H_2O at 98°C to identify the ferrite phase. The area percentage of ferrite was averaged for six 0.150-mm^2 areas at the outside, center, and inside of the weld.

the diagram[34] and magnetic permeability[33] techniques are not applicable to solution-annealed welds. In addition, it would be expected that measured values should not agree too well with calculated values. This is again due to the effects of solution annealing.

Although the vendor chemical analysis of the weld from pipe E-13 predicts a zero ferrite number, the overcheck chemical analysis, magnetic permeability measurements, and metallographic examination indicated ferrite. This discrepancy is due to the use of an assumed nitrogen content (0.060% assumed vs 0.041% actual) and a higher reported nickel content (10.79% vs 9.42%) for the vendor analysis. This raised the nickel equivalent and therefore decreased the predicted ferrite content. Figure 50 shows the typical ferrite morphology of the weld in pipe E-13 near the outside surface, center, and inside surface. The fine globular ferrite morphology shown in Fig. 50 is a result of the low chemical potential for ferrite formation, the high cooling rates achieved by the previously described small-bead deposition sequence, and the solution heat treatment. These photomicrographs indicate no apparent significant difference in the ferrite morphology or content across the thickness of the weld. Figure 51 shows a continuous QTM scan across the weld thickness. This scan verifies the relative consistency of the ferrite content. The QTM ferrite measurement and the ferrite content predicted by overcheck chemical analysis unexpectedly agree fairly well. The difference between the QTM measurements of ferrite percentage and the magnetic permeability measurements of ferrite number is probably partially related to variation in the ferrite etching technique and the sensitivity adjustment of the QTM equipment. However, the reported[33] change in magnetic response of solution-heat-treated welds may also be involved.

The difference between the ferrite numbers calculated from vendor and overcheck chemical analyses for the weld in pipe F-14 is again due to the use of an assumed nitrogen content (0.06% assumed vs 0.037% actual) and a higher carbon content (0.040% vs 0.026%) for the vendor analysis, which raised the nickel equivalent and therefore decreased the predicted ferrite content. Figure 52 shows typical ferrite morphology in the weld in pipe F-14 near the outside surface, center, and inside surface. The variation in the ferrite morphology across the weld thickness can be related to the previously described weld bead deposition. The large, high-heat-input bead deposited from the outside produced a coarser ferrite morphology at the weld outside surface and center than on the inside surface. Figure 53 shows a continuous QTM scan across the weld thickness. The variation in ferrite content shown by this scan is typical of a single-groove joint. From the inside surface (root) of the weld to approximately one-third of the thickness, the ferrite content is low because of dilution of the weld metal with the fully austenitic base metal. However, as the outside surface (face) of the weld is approached, the dilution decreases and the ferrite content increases until it levels off at the maximum ferrite potential. The QTM ferrite measurements and the ferrite content predicted by overcheck chemical analysis are again in unexpectedly good agreement. There is again a deviation between the ferrite content as measured by magnetic permeability and QTM. The previously discussed reasons for the discrepancy again apply.

The weld in pipe G-15 had a calculated ferrite number of zero, using both vendor and overcheck chemical analyses, as shown in Table 14. This agrees with both the magnetic permeability measurements and the QTM analysis of the etched microstructure. However, a Delong diagram ferrite number of 7 is predicted from the chemical analysis of the filler wire, shown in Table 16. There are several reasons for the difference between the predicted ferrite number for the filler wire and the deposited weld. One reason is that the vendor chemical analysis of the filler wire did not report the nitrogen content, and therefore its effect as an austenite former could not be accounted for. A comparison of Tables 14 and 16 also shows a chromium content of 19.42% in the filler wire vs 16.40% for vendor and 16.19% for overcheck analyses of the deposited weld. This change in chromium content has a significant effect on the ferrite number calculation. The change in chromium content can be explained by dilution effects and some losses during welding. In addition, the pickup of nitrogen during welding increases the austenite forming potential.

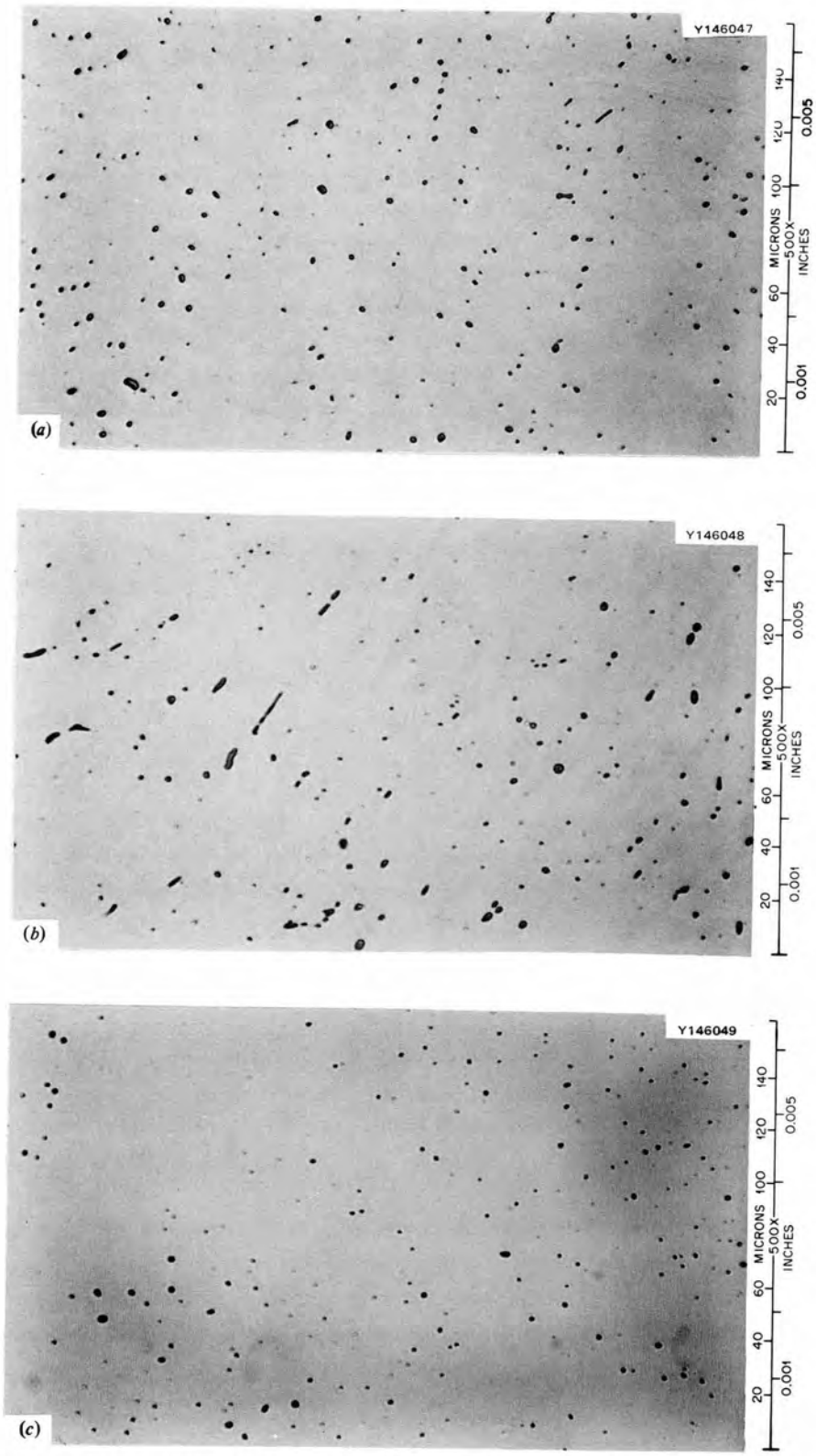

Fig. 50. Typical ferrite morphology in the GTA weld in pipe E-13. The outside surface is to the left in all photomicrographs. Etchant 15 g $K_3Fe(CN)_6$–15 g KOH–100 ml H_2O at 98°C. 500×. (*a*) Near outside surface, (*b*) near midthickness, (*c*) near inside surface.

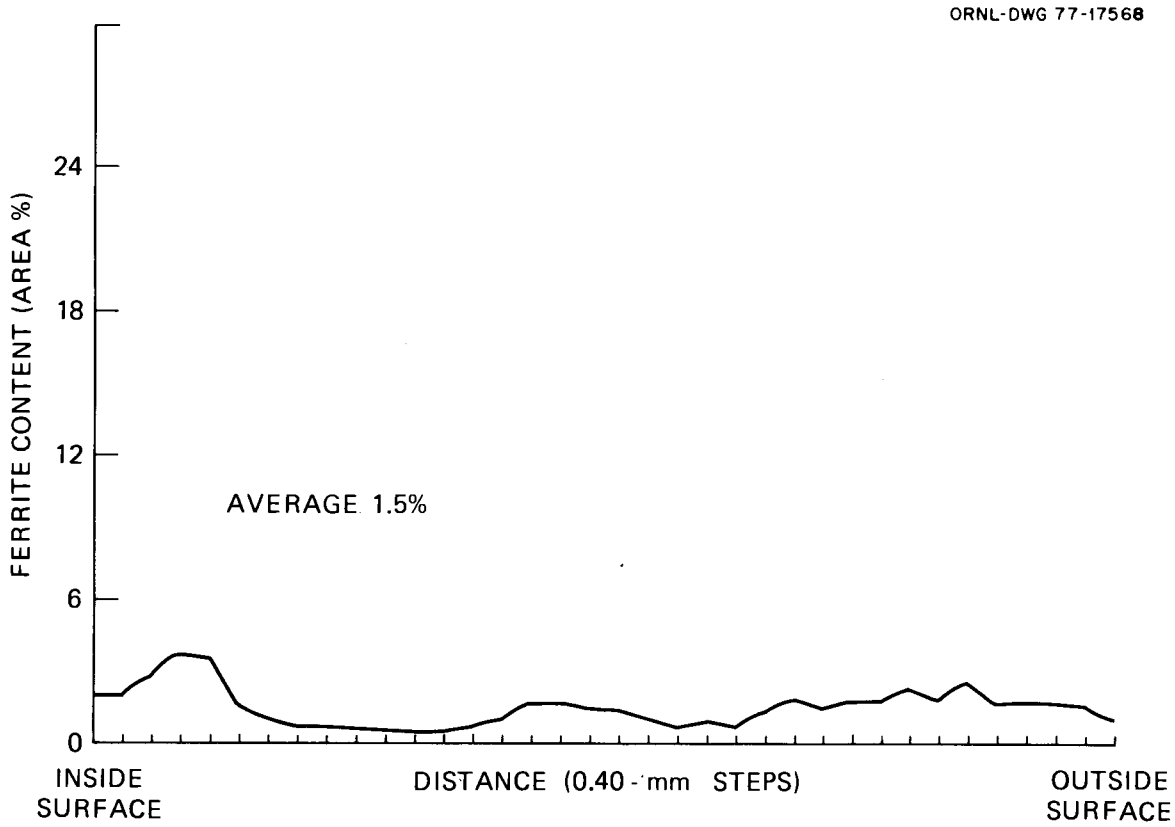

Fig. 51. Typical ferrite content variation across the thickness of the GTA weld in pipe E-13. Measured by quantitative television microscope analysis of a specimen etched with 15 g $K_3Fe(CN)_6$ –15 g KOH–100 ml H_2O at 98°C to identify the ferrite phase. Butted fields with an area 0.150 mm^2 were examined across the weld thickness.

The autogenous weld in pipe G-16 also had a calculated ferrite number of zero from both vendor and overcheck chemical analyses, as shown in Table 15. This is as expected since the base metal was fully austenitic. Both magnetic permeability measurements and QTM analysis of the etched microstructure confirmed the absence of ferrite.

Table 15 shows that the weld in pipe H-22 had both calculated and measured values which indicated no ferrite present. The situation with this weld is somewhat similar to that in G-15. Table 17 shows the vendor chemical analysis for the bare filler wire used to weld pipe H-22. Analyses were made on samples of the bare filler wire which were removed from the wire spool before and after welding. The Delong diagram[34] predicts a ferrite number of approximately 2, using the analyses shown in Table 17. The reason for the difference between the predicted ferrite number for the bare filler wire and the deposited weld is again due to changes in chemical composition. A comparison of Tables 14 and 17 shows a nickel content of 6.70% in the bare filler wire vs 10.06% for the vendor and 9.83% for the overcheck analyses of the deposited weld. This change has the effect of greatly decreasing the calculated ferrite number. Although there were other differences in the chemical content between the filler wire and the deposited weld, the change in the nickel content had the greatest effect. The change in nickel content probably resulted from dilution effects.

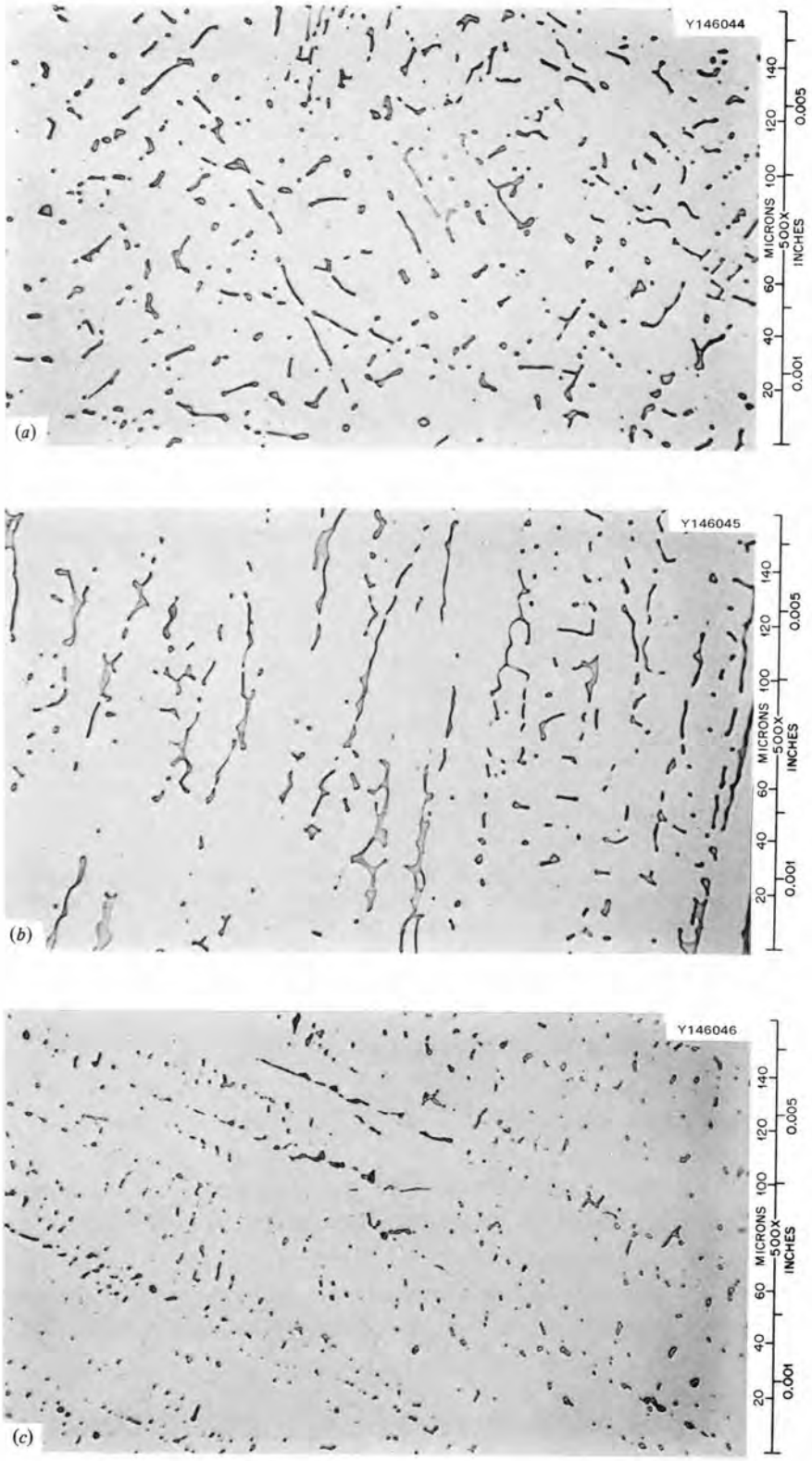

Fig. 52. Typical ferrite morphology in the GTA weld in pipe F-14. The outside surface is to the left in all photomicrographs. Etchant 15 g $K_3Fe(CN)_6$ –15 g KOH–100 ml H_2O at 98°C. 500×. (*a*) Near outside surface, (*b*) near midthickness, (*c*) near inside surface.

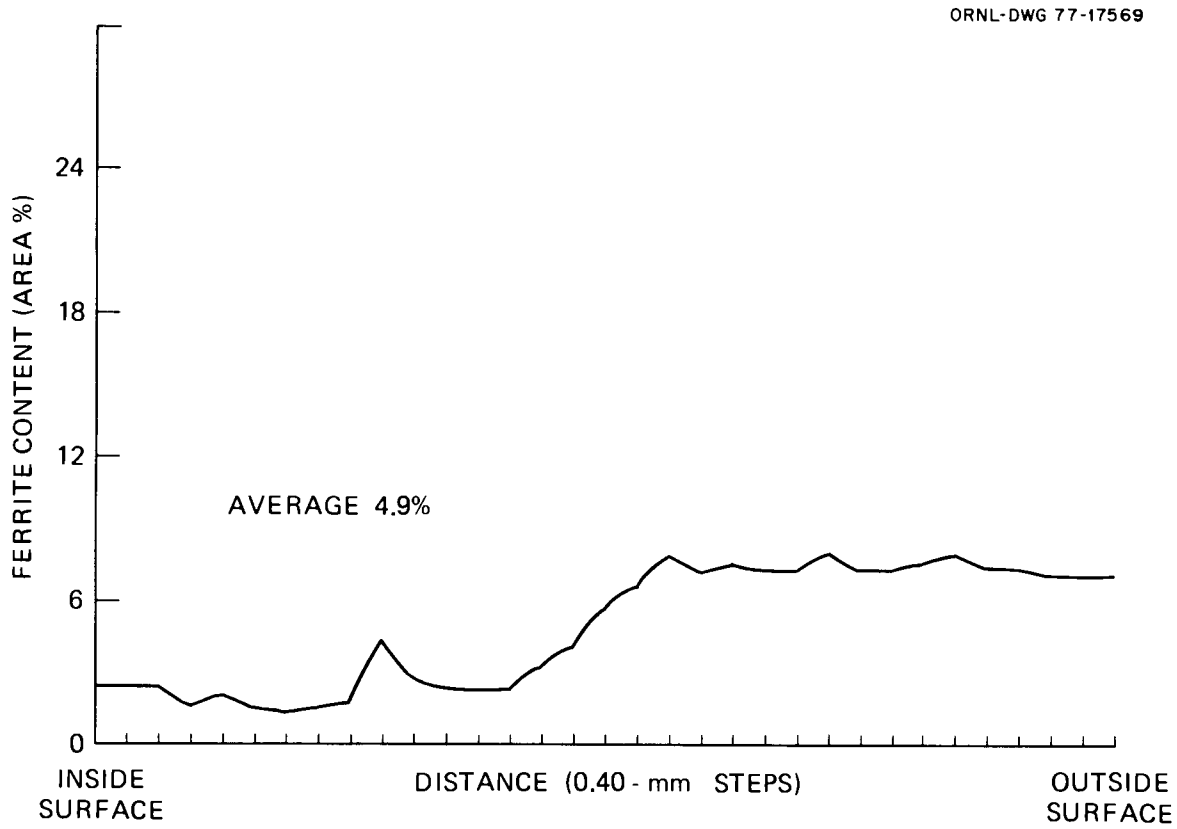

Fig. 53. Typical ferrite content variation across the thickness of the GTA weld in pipe F-14. Measured by quantitative television microscope analysis of a specimen etched with 15 g $K_3Fe(CN)_6$ –15 g KOH, 100 ml H_2O at 98°C to identify the ferrite phase. Butted fields with an area of 0.15 mm^2 were examined across the weld thickness.

In an earlier section, the results of a nondestructive evaluation of the ferrite content of the five welds were reported. Comparing the results of the destructive evaluation performed in this section with those of the nondestructive examination will provide some measure of the capability of the nondestructive technique to characterize the ferrite content of the welds. Table 18 shows a comparison of nondestructive measurements made on the inside and outside surfaces of the pipe and destructive measurements made across the thickness of specimens sectioned from the weld as shown in Fig. 21. The sectioned specimens correspond to the locations where the nondestructive measurements were made. The results shown in Table 18 indicate that there is generally good agreement between the nondestructive and destructive ferrite measurements. As previously discussed, the differences between the magnetically determined and QTM measurements could be related to several factors. It can be concluded that a nondestructive technique provides an adequate means of generally characterizing the ferrite content of solution-annealed longitudinal seam welds in formed and welded pipe.

7. MECHANICAL PROPERTY CHARACTERIZATION

As a part of mechanical property characterization, tensile tests were performed on all five pipes. Eight tests were conducted in the base-metal region of each pipe, four in the circumferential (*C*) and four in the axial direction (*A*). Eight additional tests were conducted in the weld-metal region of each pipe, four in the

Table 16. Vendor chemical analysis of filler wire used to weld pipe G-15

Element	Content (wt %)	Element	Content (wt %)
C	0.06	Si	0.36
Mn	1.68	Cr	19.42
P	0.025	Ni	13.02
S	0.008	Mo	2.34

Table 17. Vendor chemical analysis of bare filler wire used to weld pipe H-22

Element	Content (wt %)	
	Before welding	After welding
C	0.08	0.07
Mn	1.51	1.54
P	0.012	0.014
S	0.021	0.023
Si	0.20	0.20
Ni	6.70	6.78
Cr	14.48	14.41
Mo	1.85	1.82

Table 18. Comparison of nondestructive and destructive measurements of the ferrite content

Pipe No.	Location	Nondestructively determined (FN)[a]	Destructively determined	
			(FN)[a]	(Area)[b]
E-13	Outside	0.1–0.4	0.1–0.2	1.6
	Center		0.1–0.3	1.3
	Inside	0.1–0.4	0.2–0.4	2.4
F-14	Outside	2.8–4.5	3.2–4.8	7.2
	Center		2.4–2.8	5.8
	Inside	0.6–1.4	0.6–1.2	1.8
G-15	All	0	0	0
G-16	All	0	0	0
H-22	All	0	0	0

[a]Magnetic permeability measurements made with Twin City Testing Corp. Ferritescope, type FE8e2, model B, with probe type KF. Calibration was performed in accordance with AWS A4.2-74, using Teledyne McKay weld metal secondary standards. Measurements were made on five specimens sectioned at 0.3-m intervals along the weld.

[b]Quantitative television microscope analysis was made on one specimen per pipe, which was etched with 15 g $K_3Fe(CN)_6$ –15 g KOH–100 ml H_2O at 98°C to identify the ferrite phase. The area percentage of ferrite was averaged for six 0.150-mm^2 areas at the outside, center, and inside of the weld.

longitudinal weld direction (L) and the four in transverse weld direction (T). The transverse weld specimens had a composite of weld metal, HAZ, and base metal in the gage length, while the longitudinal specimens were generally all weld metal except for a few which had some composite areas. In order to sort out the chemistry and straightening effect on tensile properties, we reannealed (laboratory annealed) eight specimens from each of the pipes, four from the base metal (two axial and two circumferential) and four from the weld-metal region (two longitudinal and two transverse). The reannealing treatment consisted of holding the tensile specimens at 1065°C for 0.5 hr followed by air cooling. The annealing treatment was performed in a tubular furnace backfilled with argon gas. The test specimen and the sectioning procedure are illustrated in Fig. 54.

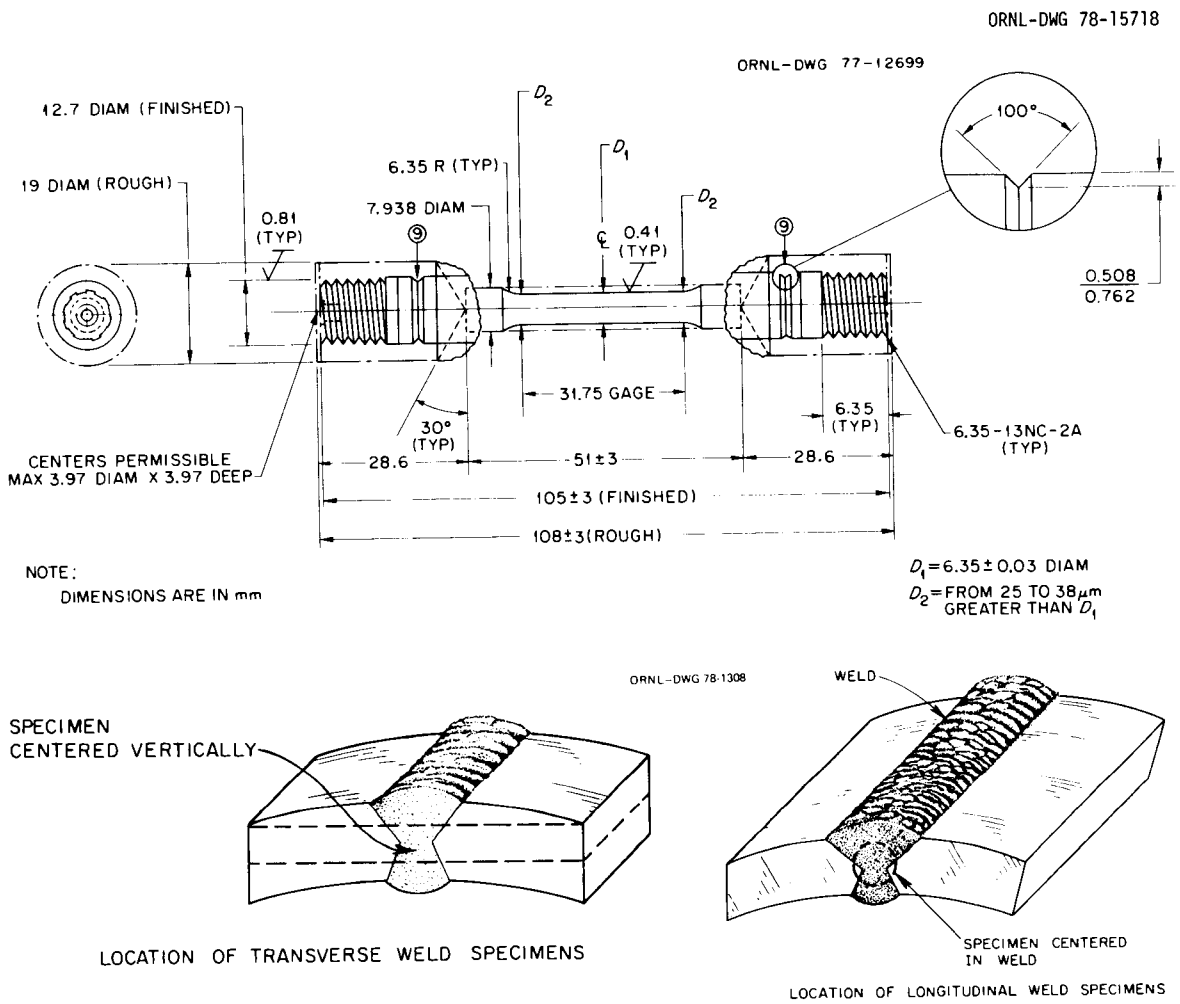

Fig. 54. Tensile test specimen design and its location and removal from blanks containing welds.

7.1 Test Procedure

Tensile tests were run on a 44-kN-capacity (10,000-lb) Instron Universal testing machine at a constant crosshead speed to give a nominal strain rate of 0.002 mm/sec (0.004 in./min). Strains measured by averaging extensometers and loads from cells in the load train were obtained for the first 0.05 strain, while

crosshead displacement vs load was graphed simultaneously and monitored continuously to rupture. The yield strength values were obtained from the extensometer chart (by the 0.2% offset method), and ultimate tensile strength was obtained from the load deflection chart. The total elongation values were measured from 25.4-mm gage marks on the gage section of the specimen.

7.2 Data

The tensile properties of the base metal and weld of the pipes in the as-received condition are summarized in Table 19. Tensile properties in the laboratory-annealed (reannealed) condition are summarized in Table 20. These tables also include the values of engineering toughness, which is the area under the curve up to maximum load.

7.3 Engineering Stress-Strain Curves

The engineering stress-strain curves for axial base-metal and longitudinal weld specimens are compared at room temperature, 427, 538, and 649°C in Figs. 55 through 59. These figures show that significant differences exist between the stress-strain curves of the base and the weld metal, with the most noticeable differences being in yield, ultimate tensile strength, and total elongation. The extent of the difference between the weld and base metal depends on the filler metal and the welding procedure. This point will be illustrated in detail in a later section of this report.

7.4 Comparison of Properties with Upper and Lower Bounds for the Wrought Material

The tensile properties of the base metal and weld of the pipes were compared with the upper and lower bounds (expected ±2 standard error of estimate) derived from ORNL data[35] on eight heats of wrought material. Plots showing the comparisons are presented in Figs. 60 through 64. These figures also include the minimum property curves computed by the ratio method.[36] The following observations can be made from these figures.

0.2% yield strength. The base metal showed essentially the same yield strength values in both circumferential and axial directions [Fig. 60(*a*)]. The scatter in data reflects slight heat-to-heat variation between various plates used in making the pipe (this will be discussed again in a later section). The base-metal region yield strength values of all pipes were close to or slightly below the average for the wrought material data. The corresponding yield strength values of the weld of all five pipes were slightly higher than those of the base metal [Fig. 60(*b*)]. However, there was more variation in the weld data than in the base-metal data. The weld in pipe G-15 (cold wire GTA and SA with type 316 filler metal) showed maximum anisotropy at room temperature, 538, and 649°C. At 427°C, the weld showed the same values in both the longitudinal and transverse directions. The autogenous GTA weld (G-16) and the SA weld with type 16-8-2 filler metal (H-22) showed isotropic yield strength values at all four test temperatures. The GTA weld with both hot- and cold-wire additions of type 16-8-2 filler metal (E-13) showed the same room-temperature yield strength values for both longitudinal and transverse directions. However, the longitudinal values at all higher temperatures were greater than the corresponding transverse values.

Among the five welds investigated, E-13 and F-14 were the only ones with a similar welding process and filler metal. A comparison of yield strength values for these welds showed that E-13 had consistently higher values than F-14 at room temperature, 427, and 538°C. However, at 649°C, these strength differences were relatively small. The higher values of the E-13 weld are a result of its higher C + N content of 0.094% as compared with 0.063% for the F-14 weld. This point will be explained in more detail in a later section.

Ultimate tensile strength. The base metal of all five pipes showed UTS values close to or slightly below the upper bound for the wrought material [Fig. 61(*a*)]. Significantly lower values at 649°C are due to a

Table 19. Tensile properties of five formed and welded pipes of type 316 stainless steel in the as-received condition
Tests were performed at a nominal strain rate of 0.004/min

Test	Specimen	Orientation	Test temperature (°C)	Test temperature (°F)	Stress [MPa (ksi)] Proportional limit		Yield 0.02%		Yield 0.2%		Tensile		Elongation (%) Uniform	Elongation (%) 1 in.	Reduction of area (%)	Engineering toughness (MJ/m³)	Engineering toughness (ft-lb/in.³)
Pipe E-13 base metal																	
18569	E-13-38	C	25	77	65	(9.4)	163	(23.7)	259	(37.6)	610	(88.4)	66.19	83.55	78.45	363	4387
18570	E-13-44	A	25	77	123	(17.8)	186	(26.9)	259	(37.5)	605	(87.7)	67.02	79.20	77.07	364	4395
18571	E-13-39	C	427	800	79	(11.4)	124	(28.0)	168	(24.3)	527	(76.4)	33.46	46.70	59.04	154	1856
18572	E-13-45	A	427	800	70	(10.2)	116	(16.8)	156	(22.6)	516	(74.9)	37.26	49.35	66.28	161	1945
18573	E-13-40	C	538	1000	67	(9.7)	105	(15.2)	139	(20.2)	481	(69.7)	42.61	55.45	69.33	174	2100
18574	E-13-46	A	538	1000	84	(12.2)	112	(16.3)	141	(20.4)	485	(70.4)	40.21	51.41	59.59	164	1985
18575	E-13-41	C	649	1200	77	(11.1)	136	(19.7)	172	(25.0)	332	(48.1)	20.23	45.85	69.83	68	824
18576	E-13-47	A	649	1200	81	(11.7)	102	(14.8)	134	(19.4)	311	(45.1)	29.69	75.90	70.50	89	1069
Pipe F-14 base metal																	
18578	F-14-38	C	25	77	140	(20.3)	193	(28.0)	252	(36.6)	593	(86.0)	64.17	78.00	82.80	343	4147
18579	F-14-44	A	25	77	121	(17.5)	194	(28.1)	253	(36.7)	603	(87.4)	62.20	79.60	78.47	338	4090
18580	F-14-39	C	427	800	84	(12.2)	115	(16.7)	148	(21.4)	490	(71.1)	38.47	44.80	70.50	158	1914
18581	F-14-45	A	427	800	62	(9.0)	115	(16.6)	143	(20.7)	494	(71.7)	35.18	47.50	61.12	147	1780
18582	F-14-40	C	538	1000	61	(8.8)	88	(12.8)	119	(17.3)	446	(64.7)	49.19	53.30	58.10[a]	191	2312
18583	F-14-46	A	538	1000	28	(4.1)	64	(9.3)	117	(17.0)	445	(64.6)	41.36	51.45	58.91[a]	157	1891
18584	F-14-41	C	649	1200	50	(7.3)	84	(12.2)	118	(17.1)	308	(44.7)	29.12	73.90	71.37	84	1011
18585	F-14-47	A	649	1200	42	(6.1)	84	(12.2)	121	(17.6)	309	(44.8)	27.21	69.65	71.38	79	957
Pipe G-15 base metal																	
18559	G-15-38	C	25	77	107	(15.5)	174	(25.2)	266	(38.6)	619	(89.7)	54.05	67.20	75.78	305	3691
18560	G-15-44	A	25	77	116	(16.8)	226	(32.8)	282	(40.9)	632	(91.7)	51.65	61.80	62.87	301	3639
18561	G-15-39	C	427	800	74	(10.7)	110	(16.0)	162	(23.5)	538	(78.0)		43.42	68.21	237	2860
18562	G-15-45	A	427	800	95	(13.8)	126	(18.2)	155	(22.4)	545	(79.1)	41.64	47.72	51.68	193	2328
18563	G-15-40	C	538	1000	73	(10.6)	115	(16.7)	150	(21.8)	508	(73.7)	34.96	41.90	66.41	151	1819
18564	G-15-46	A	538	1000	59	(8.6)	106	(15.3)	141	(20.4)	512	(74.3)	40.62	48.75	52.10	177	2140
18565	G-15-41	C	649	1200	71	(10.3)	99	(14.4)	137	(19.8)	363	(52.7)	26.78	56.65	57.60	91	1096
18566	G-15-47	A	649	1200	87	(12.6)	110	(16.0)	135	(19.5)	362	(52.5)	30.05	60.00	50.95	102	1234
Pipe G-16 base metal																	
18658	G-16-38	C	25	77	126	(18.2)	183	(26.6)	241	(34.9)	605	(87.8)	57.13	75.05	79.11	313	3777
18659	G-16-44	A	25	77	141	(20.5)	213	(30.9)	259	(37.6)	601	(87.1)	58.96	76.30	65.54	323	3906
18660	G-16-39	C	427	800	72	(10.4)	112	(16.3)	157	(22.7)	538	(78.0)	40.63	48.35	57.95	182	2204
18661	G-16-45	A	427	800	71	(10.3)	112	(16.3)	152	(22.0)	532	(77.2)	43.38	49.25	52.98	195	2351
18662	G-16-40	C	538	1000	68	(9.8)	117	(16.9)	154	(22.3)	494	(71.6)	38.17	41.80	58.63	154	1857
18663	G-16-46	A	538	1000	70	(10.2)	114	(16.5)	138	(20.0)	486	(70.5)	42.07	48.85	55.77	173	2091
18664	G-16-41	C	649	1200	70	(10.2)	101	(14.7)	131	(19.0)	361	(52.3)	29.41	52.00	56.26	98	1179
18665	G-16-47	A	649	1200	76	(11.0)	104	(15.2)	130	(18.9)	351	(50.9)	28.97	56.00	53.99	94	1140
Pipe H-22 Base metal																	
19141	H-22-38	C	25	77	93	(13.5)	229	(33.2)	336	(48.8)	610	(88.5)	43.40	63.65	76.13	249	3012
19142	H-22-44	A	25	77	141	(20.5)	226	(32.8)	300	(43.5)	600	(87.0)	54.03	70.32	74.52	299	3613
19143	H-22-39	C	427	800	94	(13.6)	151	(21.9)	194	(28.1)	533	(77.3)	39.35	44.24	58.96	182	2200
19144	H-22-45	A	427	800	94	(13.6)	142	(20.6)	178	(25.8)	519	(75.3)	43.23	47.77	57.52	192	2316
19145	H-22-40	C	538	1000	93	(13.5)	141	(20.5)	179	(25.9)	474	(68.8)	39.22	45.23	60.19	161	1949
19146	H-22-46	A	538	1000	70	(10.2)	120	(17.4)	166	(24.1)	490	(71.0)	42.53	48.64	60.28	179	2163
19147	H-22-41	C	649	1200	63	(9.1)	117	(16.9)	165	(23.9)	354	(51.4)	25.71	45.50	51.05	85	1032
19148	H-22-47	A	649	1200	59	(8.6)	108	(15.6)	156	(22.6)	341	(49.4)	27.67	45.21	42.36	89	1076
Pipe E-13 weld metal																	
18389	E-13-2	L	25	77	141	(20.4)	214	(31.1)	283	(41.1)	594	(86.1)	63.41	74.32	75.60	340	4106
18390	E-13-3	T	25	77	112	(16.3)	192	(27.9)	283	(41.0)	603	(87.5)	49.88	57.90	74.30	274	3313
18391	E-13-11	L	427	800	118	(17.1)	160	(23.2)	204	(29.6)	463	(67.1)	34.28	41.35	58.07	142	1710
18392	E-13-12	T	427	800	110	(15.9)	153	(22.2)	183	(26.6)	460	(66.7)	25.82	31.10	62.73	104	1262
18393	E-13-20	L	538	1000	85	(12.3)	135	(19.5)	183	(26.6)	414	(60.0)	32.06	40.42	49.08[a]	116	1407
18394	E-13-21	T	538	1000	105	(15.2)	132	(19.1)	168	(24.4)	428	(62.0)	25.50	30.01	56.21	96	1160
18395	E-13-29	L	649	1200	73	(10.6)	113	(16.4)	155	(22.5)	286	(41.5)	25.55	62.00	63.85	72	865
18396	E-13-30	T	649	1200	66	(9.5)	109	(15.8)	139	(20.2)	303	(43.9)	19.67	33.10	61.23	57	692
Pipe F-14 weld metal																	
18409	F-14-2	L	25	77	92	(13.4)	167	(24.2)	246	(35.6)	554	(80.3)	45.24	58.55	78.24	221	2674
18410	F-14-3	T	25	77	122	(17.7)	188	(27.2)	266	(38.5)	544	(78.9)	35.49	47.25	68.02	179	2164
18411	F-14-11	L	427	800	93	(13.5)	127	(18.4)	172	(24.9)	448	(65.0)	30.93	39.10	52.90[a]	123	1482
18412	F-14-12	T	427	800	80	(11.6)	124	(18.0)	166	(24.1)	448	(65.0)	26.39	32.50	46.52[a]	100	1207
18413	F-14-20	L	538	1000	83	(12.0)	129	(18.7)	170	(24.6)	403	(58.4)	16.69	27.50	64.57	63	761
18414	F-14-21	T	538	1000	48	(7.0)	104	(15.1)	154	(22.3)	408	(59.1)	25.55	34.20	59.12[a]	91	1097
18415	F-14-29	L	649	1200	48	(7.0)	91	(13.2)	135	(19.5)	272	(39.5)	22.10	60.55	63.77[a]	58	706
18416	F-14-30	T	649	1200	94	(13.6)	115	(16.7)	154	(22.3)	291	(42.2)	15.38	38.15	60.58[a]	45	539
Pipe G-15 weld metal																	
18517	G-15-2	L	25	77	170	(24.6)	261	(37.9)	325	(47.1)	558	(80.9)	29.65	46.50	68.26	164	1978
18518	G-15-3	T	25	77	143	(20.7)	212	(30.7)	265	(38.4)	533	(77.3)	30.65	38.90	61.34	151	1823
18519	G-15-11	L	427	800	90	(13.1)	135	(19.6)	175	(25.4)	468	(67.9)	34.60	40.05	55.51	138	1671
18520	G-15-12	T	427	800	86	(12.4)	134	(19.4)	174	(25.2)	450	(65.3)	23.97	29.25	55.30	95	1146
18521	G-15-20	L	538	1000	71	(10.3)	117	(16.9)	175	(25.4)	450	(65.3)	35.50	40.95	50.12	139	1675
18522	G-15-21	T	538	1000	76	(11.0)	112	(16.3)	148	(21.5)	428	(62.1)	28.57	34.70	51.29	105	1265
18523	G-15-29	L	649	1200	84	(12.2)	119	(17.3)	162	(23.5)	330	(47.8)	23.42	34.40	49.06	74	895
18524	G-15-30	T	649	1200	65	(9.4)	104	(15.1)	143	(20.8)	325	(47.1)	18.73	29.80	49.09	58	705
Pipe G-16 weld metal																	
18647	G-16-2	L	25	77	117	(17.0)	179	(25.9)	248	(36.0)	523	(75.9)	46.03	61.10	67.90	221	2675
18648	G-16-3	T	25	77	123	(17.8)	188	(27.3)	243	(35.2)	507	(73.5)	25.78	38.92	68.76	120	1453
18649	G-16-11	L	427	800	70	(10.2)	114	(16.5)	157	(22.8)	447	(64.8)	34.00	43.95	58.72	129	1561
18650	G-16-12	T	427	800	77	(11.2)	117	(17.0)	147	(21.3)	423	(61.3)	24.31	31.95	54.47[a]	87	1053
18651	G-16-20	L	538	1000	65	(9.4)	108	(15.6)	144	(20.9)	419	(60.7)	37.64	44.00	55.68	133	1609
18652	G-16-21	T	538	1000	90	(13.1)	117	(17.0)	143	(20.7)	403	(58.5)	23.05	28.65	59.29	81	979
18653	G-16-29	L	649	1200	78	(11.3)	104	(15.1)	138	(20.0)	319	(46.2)	28.81	39.80	51.11	81	982
18654	G-16-30	T	649	1200	79	(11.5)	100	(14.5)	132	(19.2)	319	(46.2)	18.68	30.70	51.12[a]	56	676
Pipe H-22 weld metal																	
19133	H-22-4	L	25	77	87	(15.6)	217	(31.5)	296	(42.9)	571	(82.8)	56.27	64.40	59.95	289	3491
19134	H-22-16	T	25	77	156	(22.6)	226	(32.8)	275	(39.9)	555	(80.5)	43.10	48.33	53.61	219	2645
19135	H-22-6	L	427	800	59	(8.6)	113	(16.4)	166	(24.1)	446	(64.7)	34.39	42.06	49.78	133	1605
19136	H-22-7	T	427	800	62	(9.0)	128	(18.5)	170	(24.7)	454	(65.9)	28.54	32.92	44.02	110	1333
19137	H-22-13	L	538	1000	70	(10.2)	110	(16.0)	148	(21.4)	381	(55.3)	32.63	36.41	42.53	111	1336
19138	H-22-25	T	538	1000	90	(13.1)	127	(18.4)	155	(22.5)	425	(61.7)	29.31	31.46	37.69	108	1307
19139	H-22-20	L	649	1200	46	(6.6)	93	(13.5)	139	(20.1)	261	(37.8)	22.43	41.88	41.67	57	680
19140	H-22-34	T	649	1200	63	(9.1)	97	(14.0)	140	(20.3)	296	(42.9)	16.45	25.78	46.60	47	564

[a]Specimen measured separately.

Table 20. Tensile properties of five formed and welded pipes of type 316 stainless steel in the reannealed (laboratory-annealed) condition
The reannealing was performed at 1065°C for 0.5 hr; tests were performed at a normal strain rate of 0.004/min

Test	Specimen	Orientation	Stress [MPa (ksi)]								Elongation (%)		Reduction of area (%)
			Proportional limit		Yield				Tensile		Uniform	1 in.	
					0.02%		0.2%						
Base metal, room temperature													
19535	E-13-42	C	119	(17.2)	171	(24.8)	220	(31.9)	590	(85.5)	62.15	72.29	81.85
19537	E-13-48	A	120	(17.4)	188	(27.2)	228	(33.0)	597	(86.6)	65.38	80.71	75.28
19539	F-14-42	C	135	(19.6)	185	(26.9)	222	(32.2)	585	(84.8)	62.83	74.10	82.67
19541	F-14-48	A	166	(24.1)	203	(29.4)	222	(32.2)	589	(85.4)	68.80	82.54	78.82
19543	G-15-42	C	154	(22.3)	219	(31.7)	250	(36.2)	623	(90.4)	60.64	71.05	78.09
19545	G-15-48	A	160	(23.2)	203	(29.5)	258	(37.4)	624	(90.5)	55.40	67.78	62.99
19547	G-16-42	C	107	(15.5)	192	(27.8)	241	(34.9)	604	(87.6)	52.53	62.87	76.83
19549	G-16-48	A	140	(20.3)	193	(28.0)	247	(35.8)	608	(88.2)	58.37	72.97	64.73
19551	H-22-42	C	145	(21.1)	218	(31.6)	246	(35.7)	584	(84.7)	50.93	68.59	73.72
19553	H-22-48	A	134	(19.4)	208	(30.1)	252	(36.6)	603	(87.5)	53.55	71.28	74.01
Base metal, 649°C													
19536	E-13-43	C	74	(10.8)	90	(13.1)	106	(15.5)	310	(44.9)	29.61	72.40	76.05
19538	E-13-49	A	57	(8.2)	92	(13.4)	106	(15.4)	323	(46.9)	31.54	70.00	69.75
19540	F-14-43	C	80	(11.6)	91	(13.2)	103	(15.0)	301	(43.6)	30.14	67.73	70.98
19542	F-14-49	A	41	(5.9)	78	(11.3)	97	(14.1)	302	(43.8)	31.59	59.43	68.98
19544	G-15-43	C	50	(7.3)	101	(14.6)	126	(18.3)	359	(52.1)	28.46	45.38	52.33
19546	G-15-49	A	70	(10.1)	105	(15.3)	128	(18.6)	359	(52.1)	30.43	51.30	51.20
19548	G-16-43	C	66	(9.6)	93	(13.5)	117	(17.0)	350	(50.8)	31.09	56.83	56.67
19550	G-16-49	A	59	(8.6)	92	(13.4)	119	(17.3)	340	(49.3)	28.07	55.28	53.92
19552	H-22-43	C	67	(9.7)	88	(12.8)	119	(17.2)	340	(49.3)	27.92	50.75	46.52
19554	H-22-49	A	66	(9.5)	99	(14.3)	117	(16.9)	339	(49.1)	29.31	51.72	41.45
Weld metal, room temperature													
19587	E-13-6	L	127	(18.4)	179	(26.0)	230	(33.4)	590	(85.5)	71.42	83.46	82.02
19588	E-13-7	T	105	(15.2)	177	(25.6)	232	(33.6)	592	(85.8)	67.40	70.89	82.40
19591	F-14-6	L	106	(15.4)	160	(23.2)	207	(30.0)	553	(80.2)	62.06	76.65	77.03
19592	F-14-7	T	124	(18.0)	153	(22.2)	210	(30.5)	543	(78.8)	46.98	58.63	80.60
19595	G-15-6	L	157	(22.7)	208	(30.1)	250	(36.2)	547	(79.3)	39.38	48.68	63.97
19596	G-15-7	T	168	(24.3)	203	(29.4)	238	(34.5)	552	(80.1)	38.84	47.31	64.79
19599	G-16-6	L	205	(29.7)	256	(37.1)	302	(43.8)	553	(80.2)	49.70	66.42	68.62
19600	G-16-7	T	145	(21.1)	202	(29.3)	236	(34.2)	538	(78.0)	33.41	43.03	68.70
19603	H-22-22	L	136	(19.7)	187	(27.1)	222	(32.2)	545	(79.0)	56.09	62.21	58.12
19604	H-22-23	T	114	(16.5)	185	(26.9)	234	(34.0)	532	(77.2)	34.88	42.33	67.14
Weld metal, 649°C													
19589	E-13-15	L	71	(10.3)	88	(12.7)	105	(15.2)	281	(40.7)	26.67	55.68	61.97
19590	E-13-16	T	69	(10.0)	92	(13.4)	110	(16.0)	296	(42.9)	23.18	35.01	64.20
19593	F-14-15	L	70	(10.2)	86	(12.5)	104	(15.1)	263	(38.2)	24.51	55.41	73.25
19594	F-14-16	T	42	(6.1)	77	(11.2)	91	(13.2)	276	(40.0)	21.58	39.24	71.23
19597	G-15-15	L	74	(10.8)	113	(16.4)	143	(20.7)	320	(46.4)	22.88	32.81	55.70
19598	G-15-16	T	59	(8.6)	96	(13.9)	118	(17.1)	315	(45.7)	22.37	31.43	47.20
19601	G-16-15	L	60	(8.7)	102	(14.8)	128	(18.6)	303	(44.0)	27.81	41.70	42.68
19602	G-16-16	T	66	(9.5)	94	(13.7)	114	(16.5)	301	(43.6)	19.95	29.84	56.63
19605	H-22-31	L	48	(7.0)	82	(11.9)	117	(17.0)	264	(38.3)	24.05	44.33	49.06
19606	H-22-32	T	71	(10.3)	92	(13.4)	112	(16.2)	280	(40.6)	18.20	25.65	51.65

lower strain rate (0.002 mm/sec) used in the present investigation as compared with the strain rate of 0.017 mm/sec used for the wrought material.[53] The base metal from all five pipes showed isotropic UTS values. The base metal in pipe F-14 was weaker than in other pipes at all test temperatures. The weld UTS values for all five pipes were below the lower bound for the wrought material. Some of the values even fell below the ratio method minimum curve (a method used in determining minimum values for ASME code cases).

At room temperature, UTS values for the weld showed more scatter than those for the corresponding base metal. However, at high temperature, the scatter in the base metal and weld appeared the same. A comparison of UTS values for the similar welds E-13 and F-14 showed consistently higher values for E-13 than for F-14.

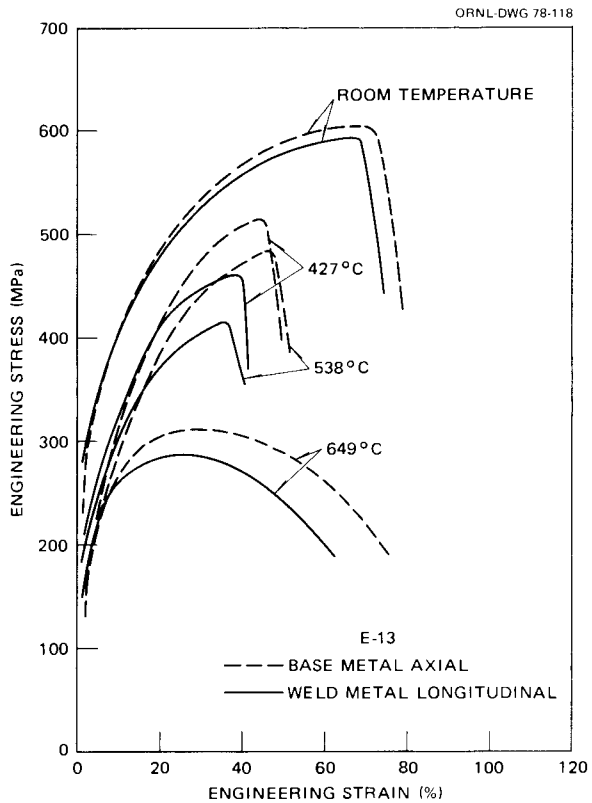

Fig. 55. Comparison of engineering stress-strain curves for the base- and weld-metal regions of pipe E-13 of type 316 stainless steel.

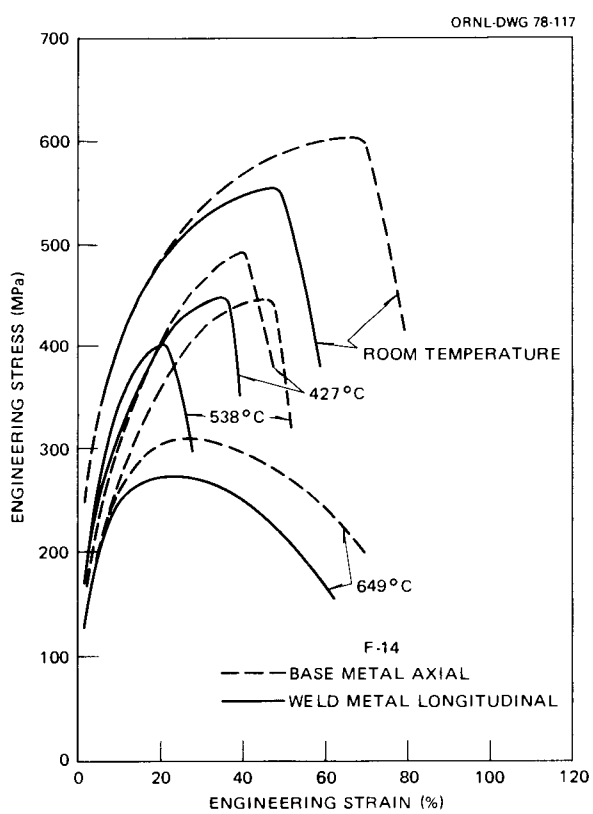

Fig. 56. Comparison of engineering stress-strain curves for the base- and weld-metal regions of pipe F-14 of type 316 stainless steel.

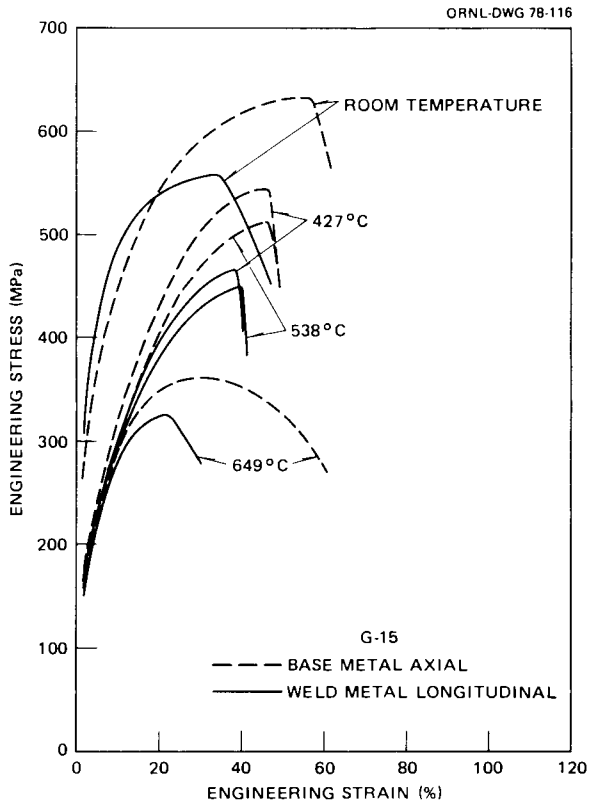

Fig. 57. Comparison of engineering stress-strain curves for the base- and weld-metal regions of pipe G-15 of type 316 stainless steel.

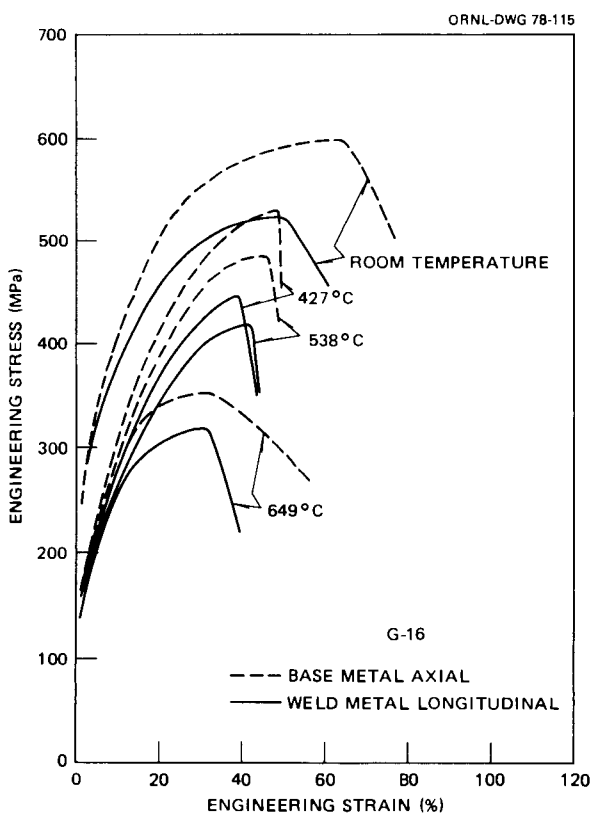

Fig. 58. Comparison of engineering stress-strain curves for the base- and weld-metal regions of pipe G-16 of type 316 stainless steel.

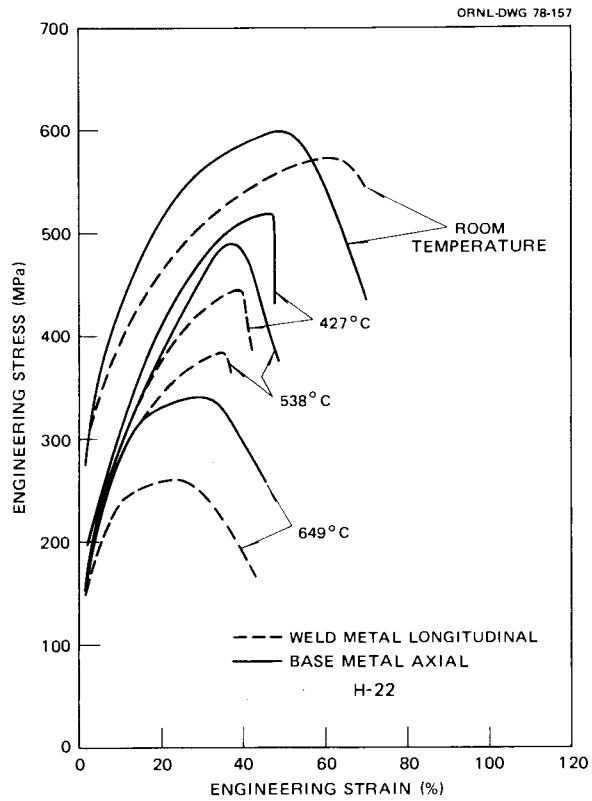

Fig. 59. Comparison of engineering stress-strain curves for the base- and weld-metal regions of pipe H-22 of type 316 stainless steel.

Uniform elongation. The base metal of all five pipes showed uniform elongation values close to average for the wrought material [Fig. 62(*a*)]. The weld values not only showed large scatter in the data, but several of them fell below the lower bound for the wrought material [Fig. 62(*b*)]. Some of the values even fell below the ratio method minimum. The transverse values were generally lower than the longitudinal values.

Total elongation. The base metal of all five pipes showed total elongation values from close to average to slightly above the upper bound for the wrought material [Fig. 63(*a*)]. The weld values showed large scatter [Fig. 63(*b*)]. Several transverse values fell below the lower bound for the wrought material. The weld in pipe G-15 (cold wire GTA and SA with type 316 filler metal) gave the most isotropic and highest values of total elongation.

Reduction of area. The base metal of all five pipes showed reduction of area within the range observed for the wrought material [Fig. 64(*a*)]. The circumferential values were generally higher than the axial values. The base-metal values from pipes G-15, G-16, and H-22 showed lower reduction-of-area values at 649°C than did the other pipes. The reduction-of-area data for the weld showed slightly more scatter than did the base metal. A significant amount of weld values fell below the lower bound for the wrought material.

7.5 Comparison of Weld Properties with Base-Metal Properties

One of the convenient ways of comparing weld properties with the base-metal properties is to plot one against the other on a linear scale. The line of slope unity through the origin will represent a weld with the same properties as those of the base metal. Divergence from this line indicates deviation of these properties

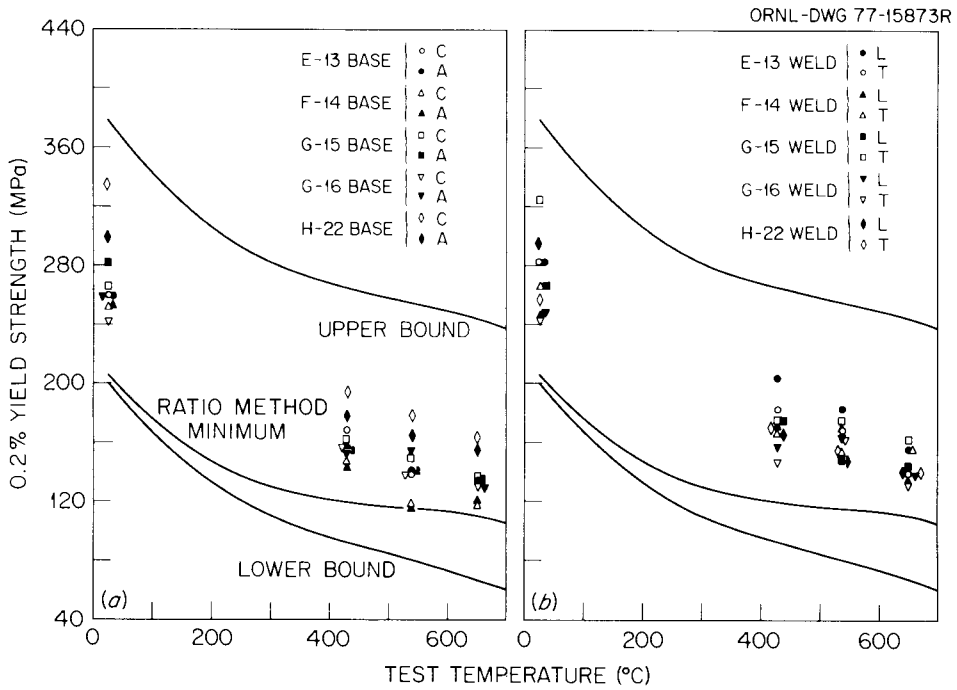

Fig. 60. Comparison of 0.2% yield strength values of base- and weld-metal regions of five formed and welded pipes of type 316 stainless steel with upper and lower bound curves for wrought material. (*a*) Base metal, (*b*) weld. Minimum value curves based on the ratio technique are also included.

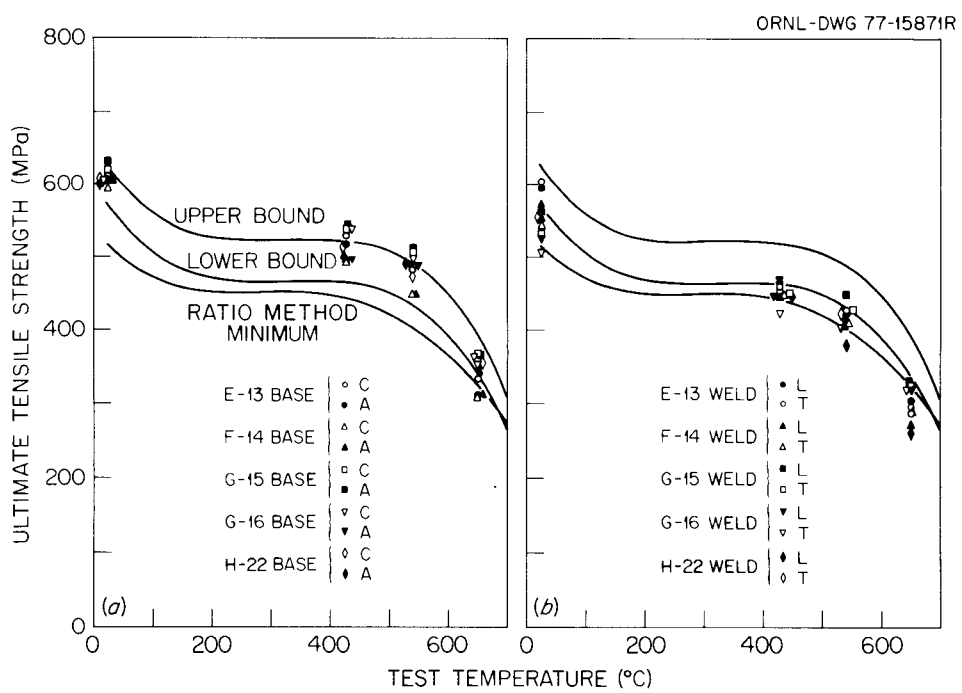

Fig. 61. Comparison of ultimate tensile strength values of base- and weld-metal regions of five formed and welded pipes of type 316 stainless steel with upper and lower bound curves for wrought material. (*a*) Base metal, (*b*) weld. Minimum value curves based on the ratio technique are also included.

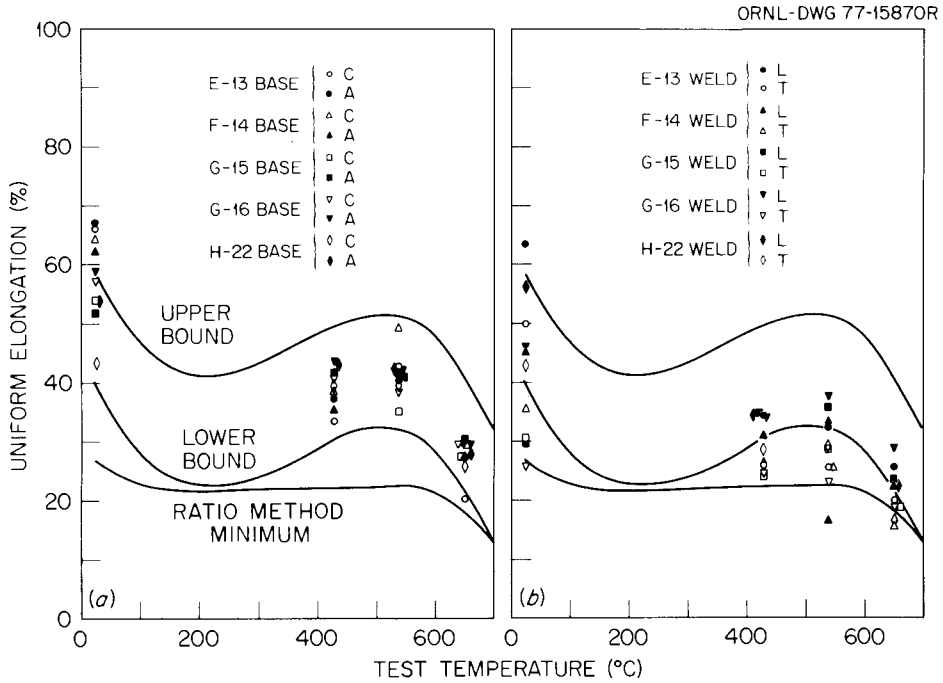

Fig. 62. Comparison of uniform elongation values of base- and weld-metal regions of five formed and welded pipes of type 316 stainless steel with upper and lower bound curves for wrought material. (*a*) Base metal, (*b*) weld. Minimum value curves based on the ratio technique are also included.

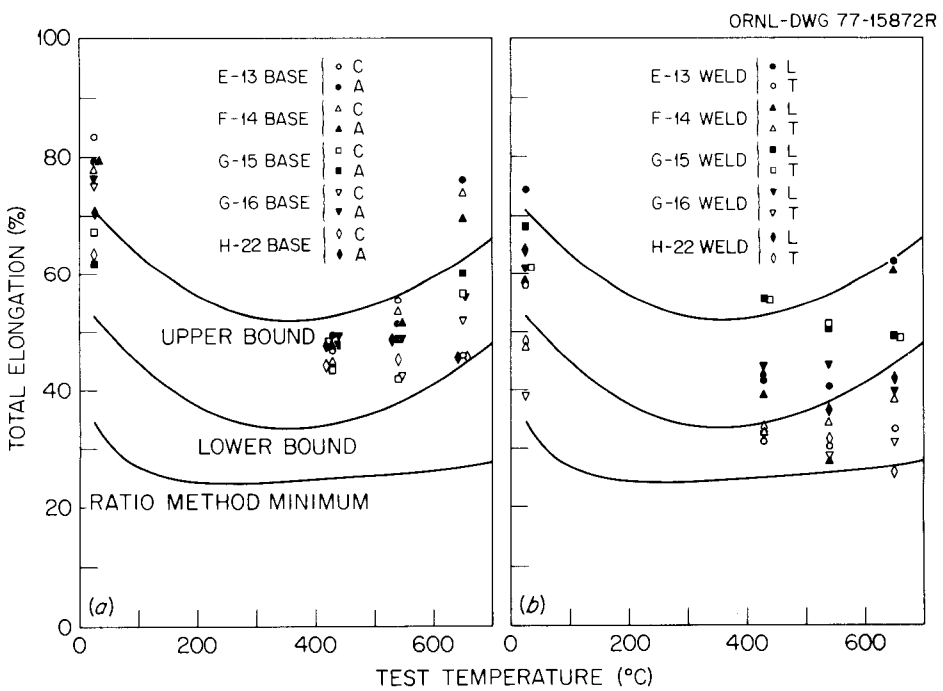

Fig. 63. Comparison of total elongation values of base- and weld-metal regions of five formed and welded pipes of type 316 stainless steel with upper and lower bound curves for wrought material. (*a*) Base metal, (*b*) weld. Minimum value curves based on the ratio technique are also included.

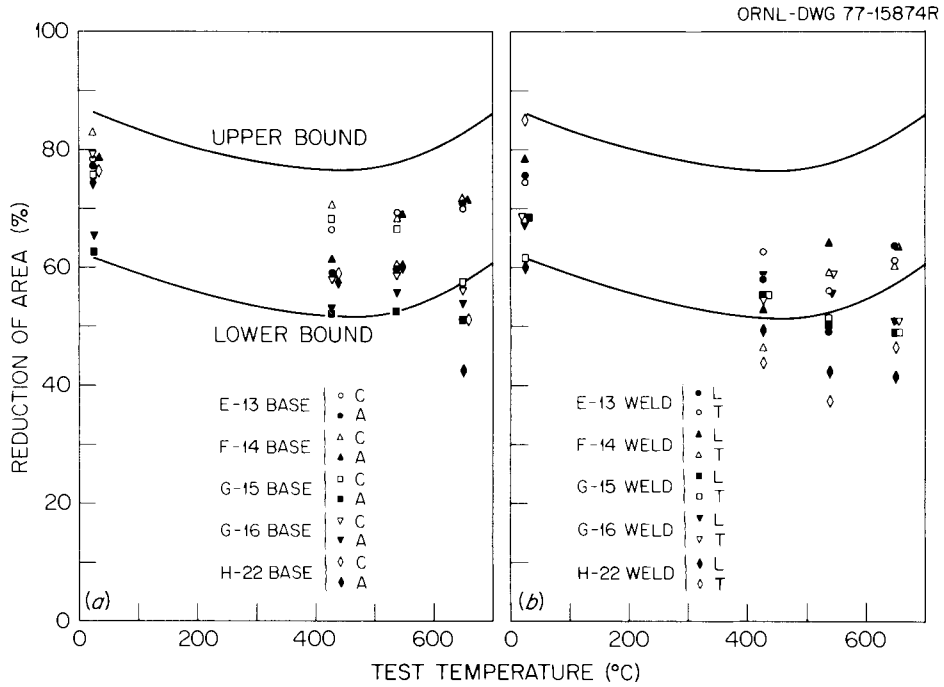

Fig. 64. Comparison of reduction-of-area values of base- and weld-metal regions of five formed and welded pipes of type 316 stainless steel with upper and lower bound curves for wrought material. (*a*) Base metal, (*b*) weld.

from the ideal behavior (equal property behavior). Figures 65 through 69 show the plots of weld yield, ultimate tensile strength, and uniform elongation vs the corresponding base-metal properties. These plots include data for both the as-received and reannealed conditions. The following observations can be made about the properties of the weld in each pipe.

E-13 (GTA with hot- and cold-wire additions of type 16-8-2). The C + N contents of the base metal and weld of this pipe were 0.105 and 0.094% respectively. The weld had a ferrite number of 0.1 to 0.4. Figure 65(*a*), (*b*), and (*c*) shows that GTA weld E-13 is characterized by the following properties:

1. Weld yield strength is *higher* than that of the base metal.
2. Weld ultimate tensile strength is *lower* than that of the base metal.
3. Weld uniform elongation is lower than that of the base metal.
4. Reannealing for 0.5 hr at 1065°C makes the yield strength of the base metal and the weld comparable.
5. Reannealing treatment has only a small effect on the ultimate tensile strength of the base metal and the weld.

F-14 (GTA with cold-wire addition of type 16-8-2). The C + N contents of the base metal and weld of this pipe were 0.104 and 0.063% respectively. This weld had an FN of 0.6 to 4.8 as compared with only 0.1 to 0.4 for the weld in E-13. Figure 66(*a*), (*b*), and (*c*) shows that GTA weld F-14 is characterized by the following properties:

1. Weld yield strength at room temperature is essentially the same as that of the base metal. At higher test temperature, the weld yield strength was higher than that of the base metal.

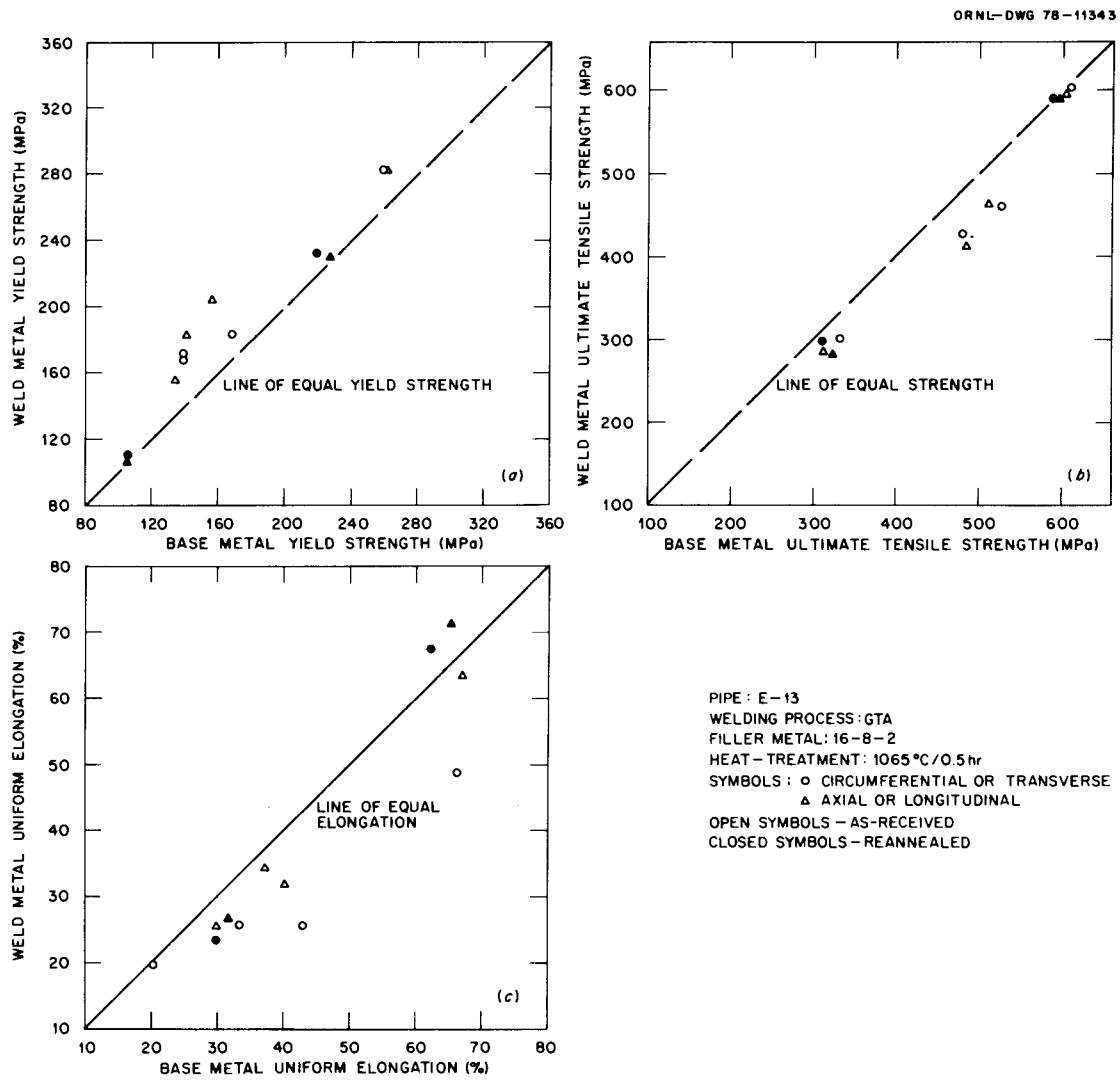

Fig. 65. Plot of weld tensile properties as a function of base-metal properties for pipe E-13 of the type 316 stainless steel; (*a*) yield strength, (*b*) ultimate tensile strength, (*c*) uniform elongation. These data are for tests in the temperature range room temperature to 649°C.

2. Weld ultimate tensile strength is lower than that of the base metal at all test temperatures.
3. Weld uniform elongation is significantly lower than that of the base metal. The transverse weld specimens showed more deviation from line of equal elongation than did the longitudinal specimens.
4. Reannealing made the weld yield strength equal to or slightly below the base-metal yield strength.
5. Reannealing has only a small effect on the ultimate tensile strength of the base metal and the weld.

G-15 (cold wire GTA and SA with type 316 stainless steel). The C + N contents of the base metal and weld of this pipe were 0.138 and 0.110% respectively. The weld had an FN of zero. Figure 67(*a*), (*b*) and (*c*) shows that this weld is characterized by the following properties:

1. The longitudinal weld yield strength is higher than that of the base metal at all four test temperatures. However, the transverse weld yield strength is the same as the base-metal yield strength at all test temperatures.

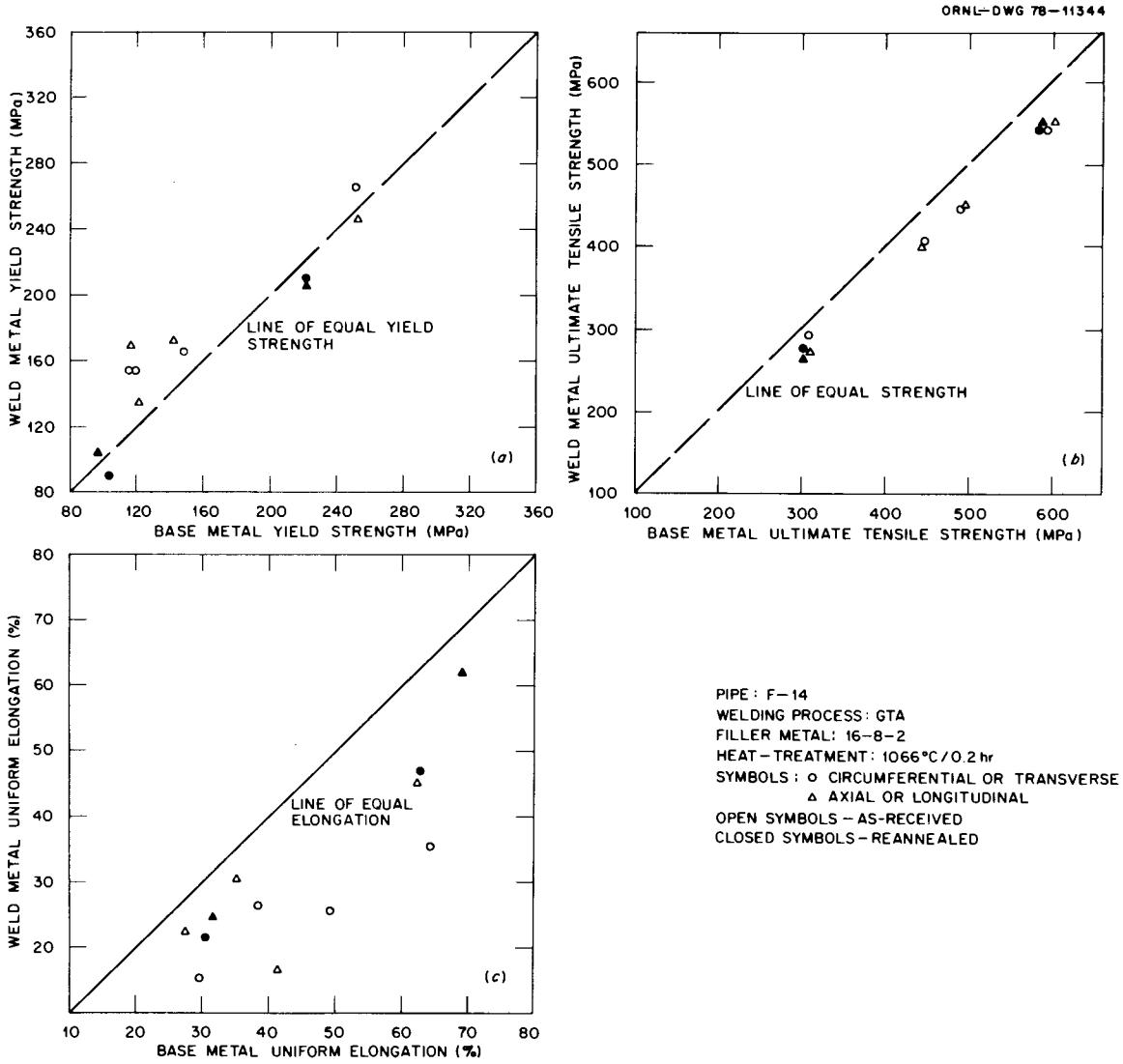

Fig. 66. Plot of weld tensile properties as a function of base-metal properties for pipe F-14 of type 316 stainless steel; (*a*) yield strength, (*b*) ultimate tensile strength, (*c*) uniform elongation. These data are for tests in the temperature range room temperature to 649°C.

2. Weld ultimate tensile strength (for both longitudinal and transverse specimens) is significantly lower than the base-metal ultimate tensile strength at all test temperatures. The longitudinal weld specimens appear to show slightly higher ultimate tensile strength as compared with transverse weld specimens.
3. Weld uniform elongation is 5 to 6% lower than that of the base metal at higher temperatures. At room temperature, the weld-metal uniform elongation is 15 to 20% lower than that of the base metal.
4. Reannealing made the weld yield strength equal to or slightly below the base-metal yield strength.
5. Reannealing has only a small effect on the ultimate tensile strength and uniform elongation of the base metal and the weld.

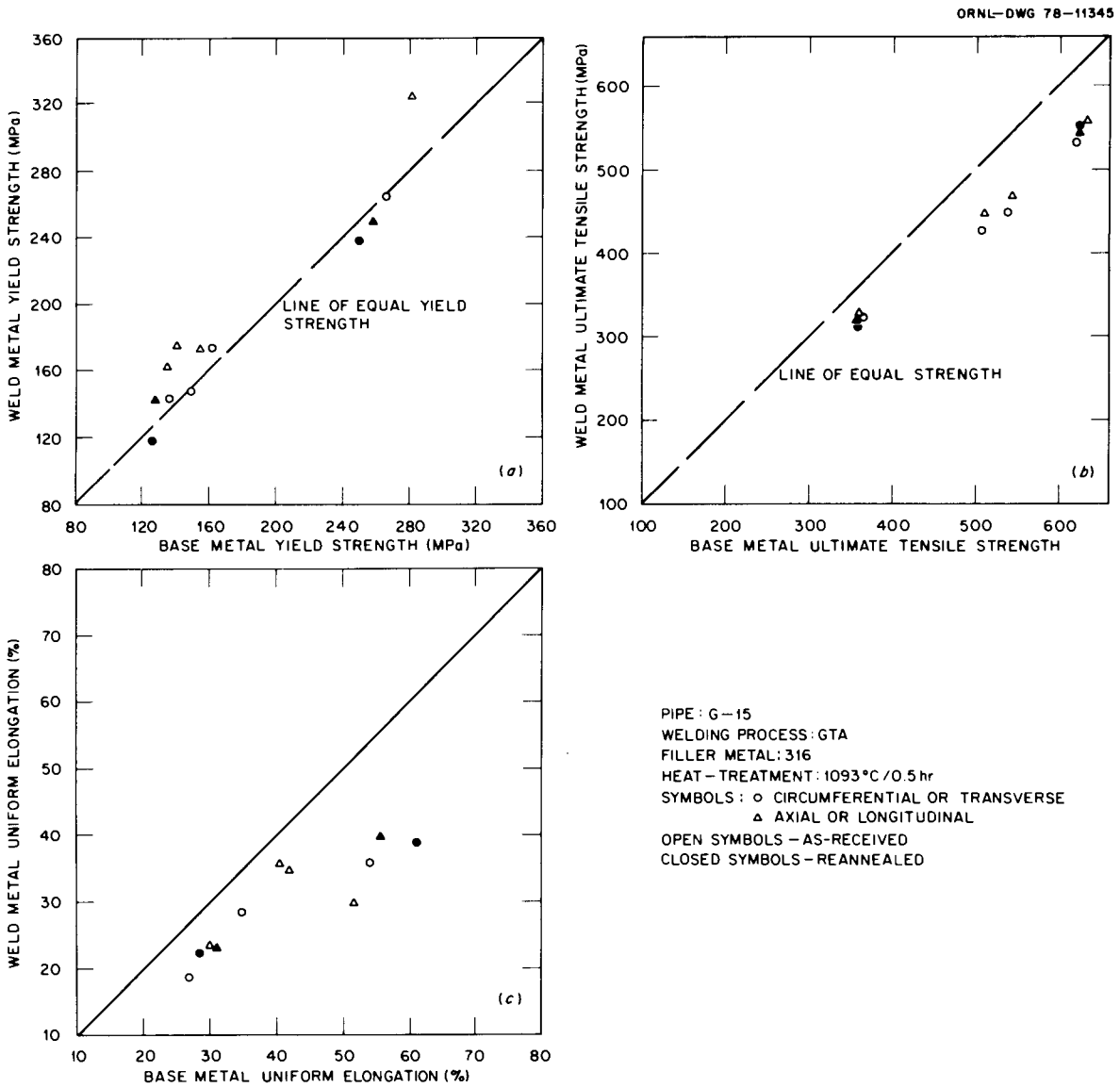

Fig. 67. Plot of weld tensile properties as a function of base-metal properties for pipe G-15 of type 316 stainless steel; (*a*) yield strength, (*b*) ultimate tensile strength, (*c*) uniform elongation. These data are for tests in the temperature range room temperature to 649°C.

G-16 (autogenous GTA). The C + N contents of the base metal and weld of this pipe were 0.147 and 0.117% respectively. The weld had an FN of zero. Figure 68(*a*), (*b*) and (*c*) shows that this weld has the following properties:

1. The weld yield strength for this pipe is the *same* as the base-metal yield strength.
2. Weld ultimate tensile strength is *lower* than that of the base metal at all four test temperatures.
3. Weld uniform elongation for transverse specimens is significantly lower than that of the base metal. The longitudinal weld uniform elongation is also lower than that of the base metal, but to a much lesser extent.
4. Reannealing has only a small effect on yield, ultimate tensile strength, and uniform elongation.

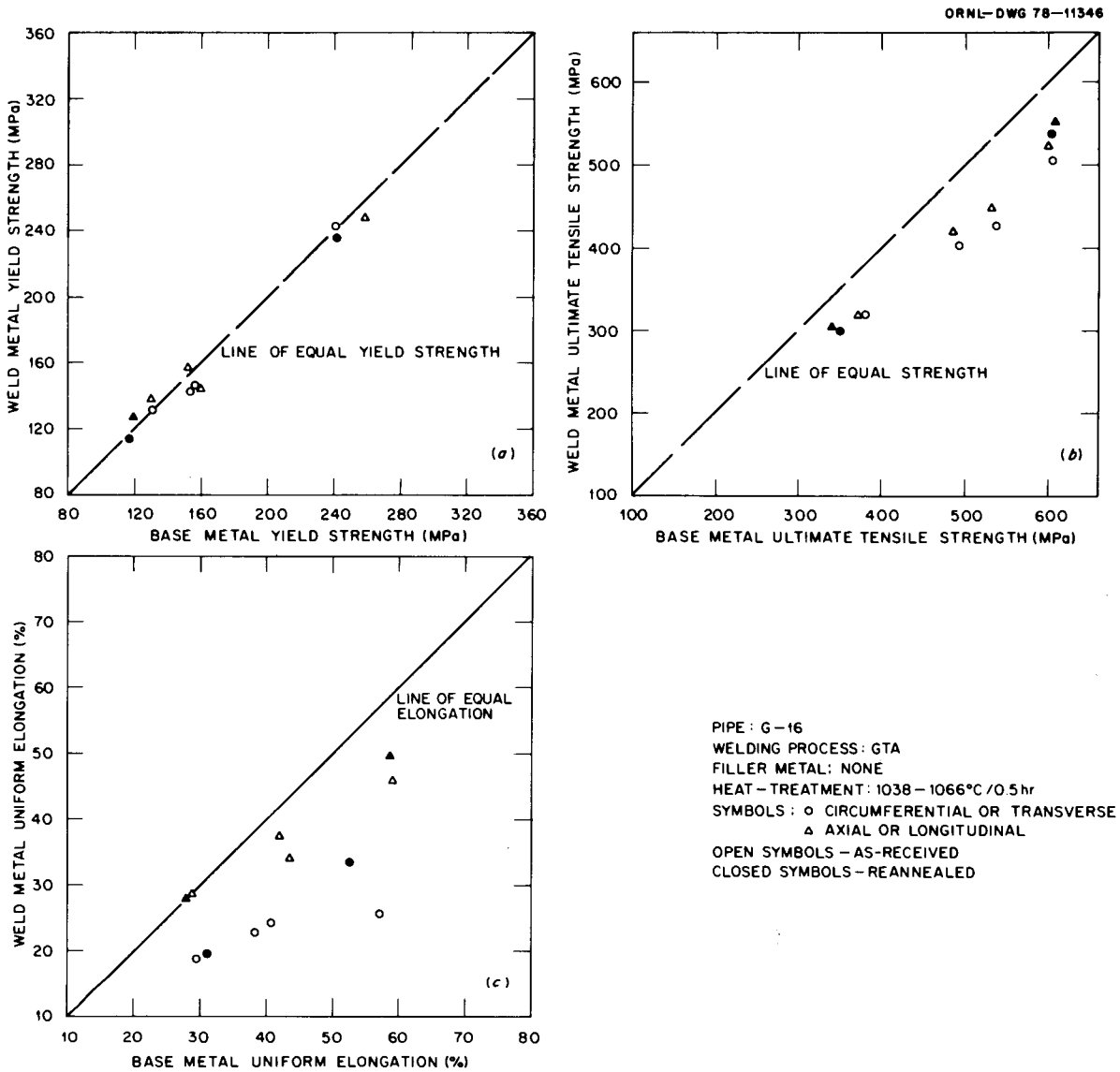

Fig. 68. Plot of weld tensile properties as a function of base-metal properties for pipe G-16 of type 316 stainless steel; (*a*) yield strength, (*b*) ultimate tensile strength, (*c*) uniform elongation. These data are for tests in the temperature range room temperature to 649°C.

H-22 (SA with type 16-8-2 filler metal). The C + N contents of the base metal and weld of this pipe were 0.133 and 0.099% respectively. The weld had an FN of zero. Figure 69(*a*), (*b*), and (*c*) shows that this weld metal has the following properties:

1. This is the only weld (among the five studied) whose yield strength is lower than that of the base metal.
2. The weld ultimate tensile strength is significantly less than that of the base metal.
3. The elevated-temperature uniform elongation of the weld is lower than that of the base metal. At room temperature they appear to be the same.

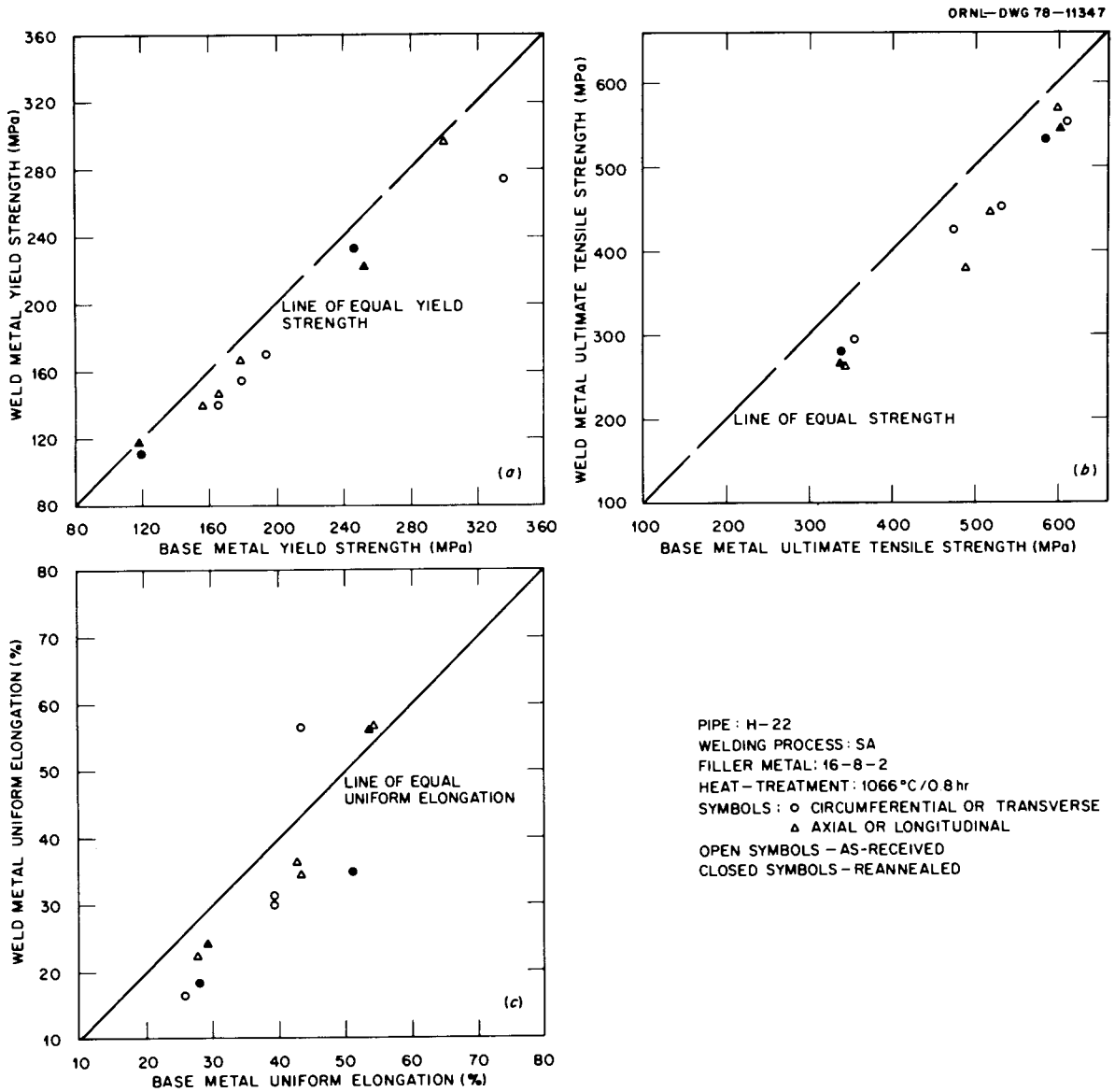

Fig. 69. Plot of weld tensile properties as a function of base-metal properties for pipe H-22 of type 316 stainless steel; (*a*) yield strength, (*b*) ultimate tensile strength, (*c*) uniform elongation. These data are for tests in the temperature range room temperature to 649°C.

4. Reannealing produced a significant lowering of both the weld and base-metal yield strength, with weld yield strength remaining lower than that of the base metal.

5. Reannealing produced only a small change in ultimate tensile strength and uniform elongation.

Summary

1. Yield strength is a strong function of welding process and the filler metal used. The GTA process with types 16-8-2 and 316 stainless steel filler metal results in yield strength values equal to or greater than the base-metal values. The SA process with type 16-8-2 filler metal is the only one which results in yield strength values lower than those of the base metal.

2. Ultimate tensile strength of the weld is always lower than that of the base metal. The extent of lowering is influenced by the welding process and the filler metal. Once again, the SA process produces the greatest difference between the base-metal values and weld values.

3. The uniform elongation (one measure of ductility) is generally lower for the weld as compared with the base metal. Among the two weld orientations studied, transverse specimens generally produced lower values than did the longitudinal specimens.

7.6 Comparison between GTA (E-13) and SA (H-22) Welded Pipes

The welds in pipes E-13 and H-22 were deposited using type 16-8-2 filler metal with resultant C + N levels of 0.094 and 0.099% respectively. The weld in pipe E-13 had an FN of 0.1 to 0.4, while the weld in pipe H-22 had an FN of zero. These welds therefore provide a reasonable data base for comparing the GTA and SA processes. However, it must be noted that the comparison is only valid for the specific parameters used to make each weld. In order to compare these processes, we have plotted SA properties (H-22) as a function of GTA properties (E-13) in Fig. 70. The following comments can be made from this figure.

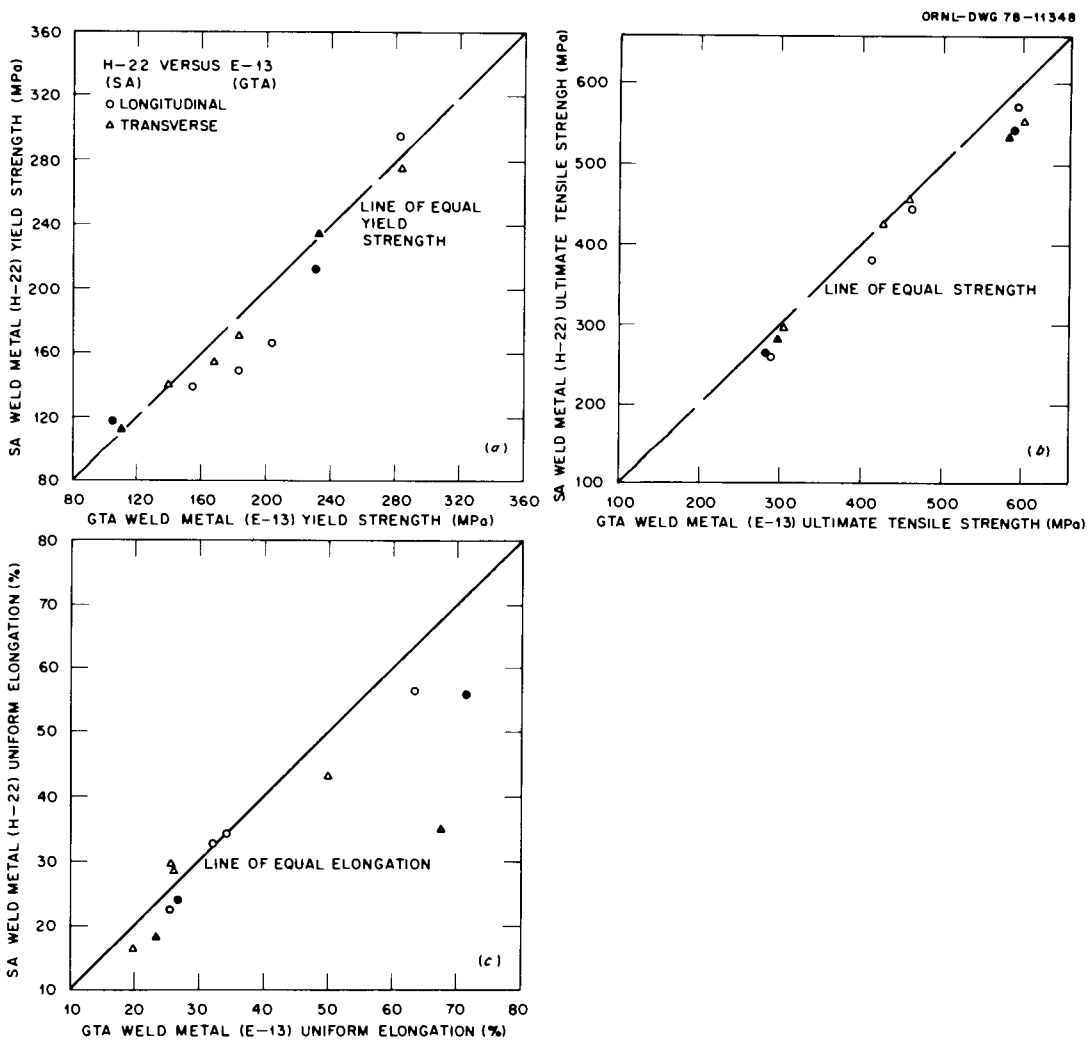

Fig. 70. Plot of SA weld tensile properties for pipes H-22 and E-13 of type 316 stainless steel; (*a*) yield strength, (*b*) ultimate tensile strength, (*c*) uniform elongation. These data are for tests in the temperature range room temperature to 649°C.

1. SA yield strength values are lower than GTA values at elevated temperatures. At room temperature they appear to be the same. The reannealed values for the two welds were the same at both room and high temperature.
2. The ultimate tensile strength of the SA weld is lower than that of the GTA weld at all test temperatures. Reannealed values maintained the same trend.
3. The uniform elongation (UE) of the SA weld is lower than that of the GTA weld, except at the testing temperatures of 538 and 427°C, where the situation is reversed. Reannealing did not affect elevated-temperature UE, while room-temperature values appeared to change significantly.

From what has been presented in Figs. 65 through 70 we can state that for the SA welded pipe, both plastic flow and failure will be controlled by the weld as compared with the GTA welded pipes, where the flow will be controlled by the base metal and the failure by the weld metal. The control of failure by the weld will become obvious from the photographs of tensile-tested specimens to be shown in a later section.

7.7 Estimate of Residual Cold Work in the Base Metal and Weld

As previously discussed, formed and welded pipes will typically have some level of residual cold work due to straightening. To estimate the amount of residual cold work in the pipes, we have plotted the 0.2% yield strength of the as-received material (Table 19) as a function of its values in the reannealed condition. These values are plotted in Fig. 71 for tensile tests performed at room temperature and 649°C. The linear bounds for these values are indicated by lines on Fig. 71. This figure indicates that as-received yield strength of both the base metal and weld can be linearly related to the reannealed yield strength. The following expression can be used to describe the linear relationship which is represented by the linear bound lines on Fig. 71:

$$Sy^{AR} = A + BSy^{RA} , \tag{1}$$

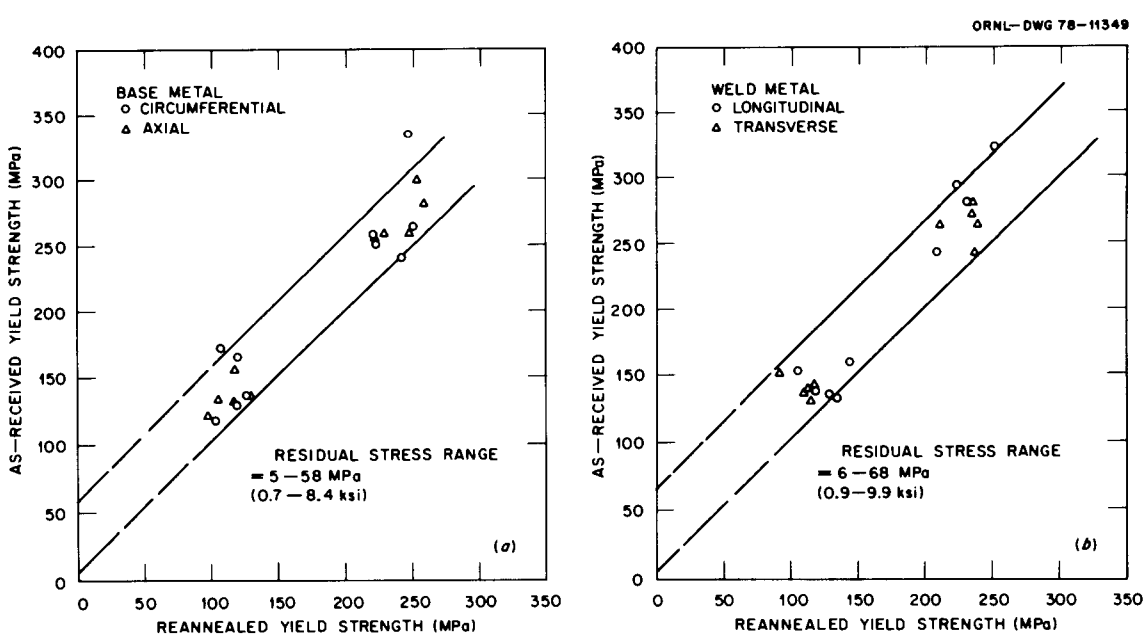

Fig. 71. Plot of as-received yield strength as a function of reannealed yield strength for five pipes; (*a*) base-metal, (*b*) weld. These data are at room temperature and 649°C. Lines represent linear bounds for the data.

where

Sy^{AR} = 0.2% yield strength in the as-received condition,

Sy^{RA} = 0.2% yield strength in the reannealed (laboratory-annealed) condition,

A, B = constants.

Previous work[37] has shown that A and B can be expressed as

$$A = S_0{}^{AR} - S_0{}^{RA} \sqrt{d_{RA}/d_{AR}} , \tag{2}$$

$$B = \sqrt{d_{RA}/d_{AR}} , \tag{3}$$

where

d_{AR} = as-received grain size,

d_{RA} = reannealed grain size,

$S_0{}^{AR}$ = frictional stress in the as-received condition,

$S_0{}^{RA}$ = frictional stress in the reannealed condition when grain size remains unaltered or for reannealing,

$$A = S^{AR} - S_0{}^{RA} , \tag{4}$$

$$B = 1 . \tag{5}$$

The constant A in Eq. (4) is the difference in frictional stresses opposing the dislocation movement in the as-received and reannealed condition and is therefore indicative of the residual stress. Since the constant A in Eq. (1) represents the intersection with the ordinate, residual stress values can be obtained from Fig. 71 from the intersection of the linear bound lines with the ordinate. The value of residual stress for the base metal of the five pipes is in the range of 5 to 58 MPa (0.7 to 8.4 ksi) [Fig. 71(*a*)], while for the weld it varies from 6 to 68 MPa (0.9 to 9.9 ksi) [Fig. 71(*b*)]. Figure 71(*a*) and (*b*) suggests that in general the residual cold work is slightly more in the weld than in the base metal of the formed and welded pipe. However, the base-metal specimens are not necessarily representative of all base-metal regions. Our previous work[38] on 711 × 10 mm type 316 stainless steel hot extruded and worked pipe gave a residual stress value of 8 MPa (1.2 ksi). Thus it appears that the formed and welded pipe contains more residual stress in the as-received condition than was observed in the hot extruded and worked pipe.

The yield strength relationship of Eq. (1) with constants given by Eqs. (4) and (5) is extended to the UTS data in Fig. 72(*a*) and (*b*). This figure shows a decrease of 0.28 MPa (0.4 ksi) in UTS of the base metal and 6 to 43 MPa (0.7 to 6.2 ksi) for the weld. These changes in UTS are relatively small as compared with the decreases in yield strength [Fig. 71(*a*) and (*b*)].

Previously published work[39–41] has shown that the elevated-temperature UTS at the creep test temperature is a pretty good index for estimating creep and creep-rupture behavior of wrought austenitic stainless steels. This result when extended to the welds in the formed and welded pipe yields the following observations:

1. The consistently lower ultimate tensile strength of the weld as compared with the base metal may produce lower creep rupture life for the weld as compared with the base metal.

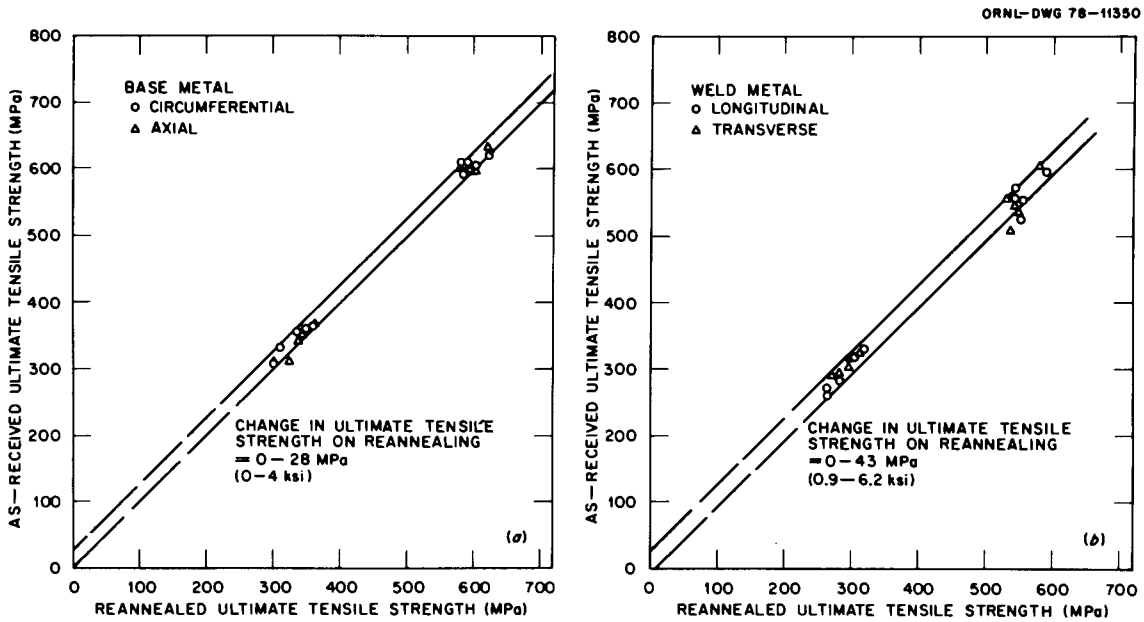

Fig. 72. Plot of as-received ultimate tensile strength as a function of reannealed ultimate tensile strength for five pipes; (*a*) base-metal, (*b*) weld. These data are at room temperature and 649°C.

2. Of the welding processes investigated, the SA weld may produce the lowest creep-rupture properties. The GTA process is expected to yield better properties.
3. The decrease in ultimate tensile strength on reannealing is expected to produce small decreases in the creep-rupture properties of both the base metal and weld.

Based on tensile and creep correlation, it appears that creep failure of the formed and welded pipe will also be controlled by the weld. This point will be illustrated by photographs of creep-rupture specimens in another report.[42]

7.8 Role of Carbon and Nitrogen on Tensile Properties

Carbon and nitrogen are the two elements recognized[43–45] in controlling the yield and UTS of austenitic stainless steels. Because of the wide range of C + N values that can be obtained from current commercial specifications, these elements play an important role in heat-to-heat variation in mechanical properties. It is the purpose of this section to demonstrate this variation and to compare the data from the five pipes against the currently available relationships between strength and C + N levels. One set of such correlations was developed by Soo and Horton[45] and is given by the following equations:

Yield strength (Sy^{AR}), ksi

$$Sy^{AR} = 88.474 + 211.640\,(\mathrm{C} + \mathrm{N}) - 0.206T\,(\mathrm{C} + \mathrm{N}) - 6.762T^{1/2} + 0.111T\,, \tag{6}$$

standard deviation = 2.806 ksi

[value for $297 \leqslant T \leqslant 977$ K (75–1300°F)] ,

where

(C + N) is in wt % ,

T is test temperature in K.

Ultimate tensile strength (Su^{AR}), ksi

$$Su^{AR} = 8.563 - 461.665\,(C + N) + 1064.154T^{-1/2} + 2.722T\,(C + N) - 2.330 \times 10^{-3}T^2\,(C + N)\,, \quad (7)$$

standard deviation = 6.458 ksi

[value for $297 \leqslant T \leqslant 977$ K (75–1300°F)] .

The superscript AR in Eqs. (6) and (7) indicates that these correlations were developed for data on material in the as-received condition.

The above equations are valid for C + N $\leqslant$ 0.10 wt %, but the authors[45] suggest that at room temperature, 593, and 704°C, the range of validity may be increased to 0.167, 0.141, and 0.141 respectively. These equations were derived from base-metal data and thus may not be applicable to welds.

Base-metal comparisons. The comparison of experimental yield strength data on the base metal of the five pipes with the predicted values from Eq. (6) is shown in Fig. 73. Parts (*a*) and (*b*) show comparisons at room temperature for data in as-received and reannealed conditions respectively. Parts (*c*) and (*d*) show similar comparisons for data at 649°C. The corresponding comparisons for UTS data are shown in Fig. 74.

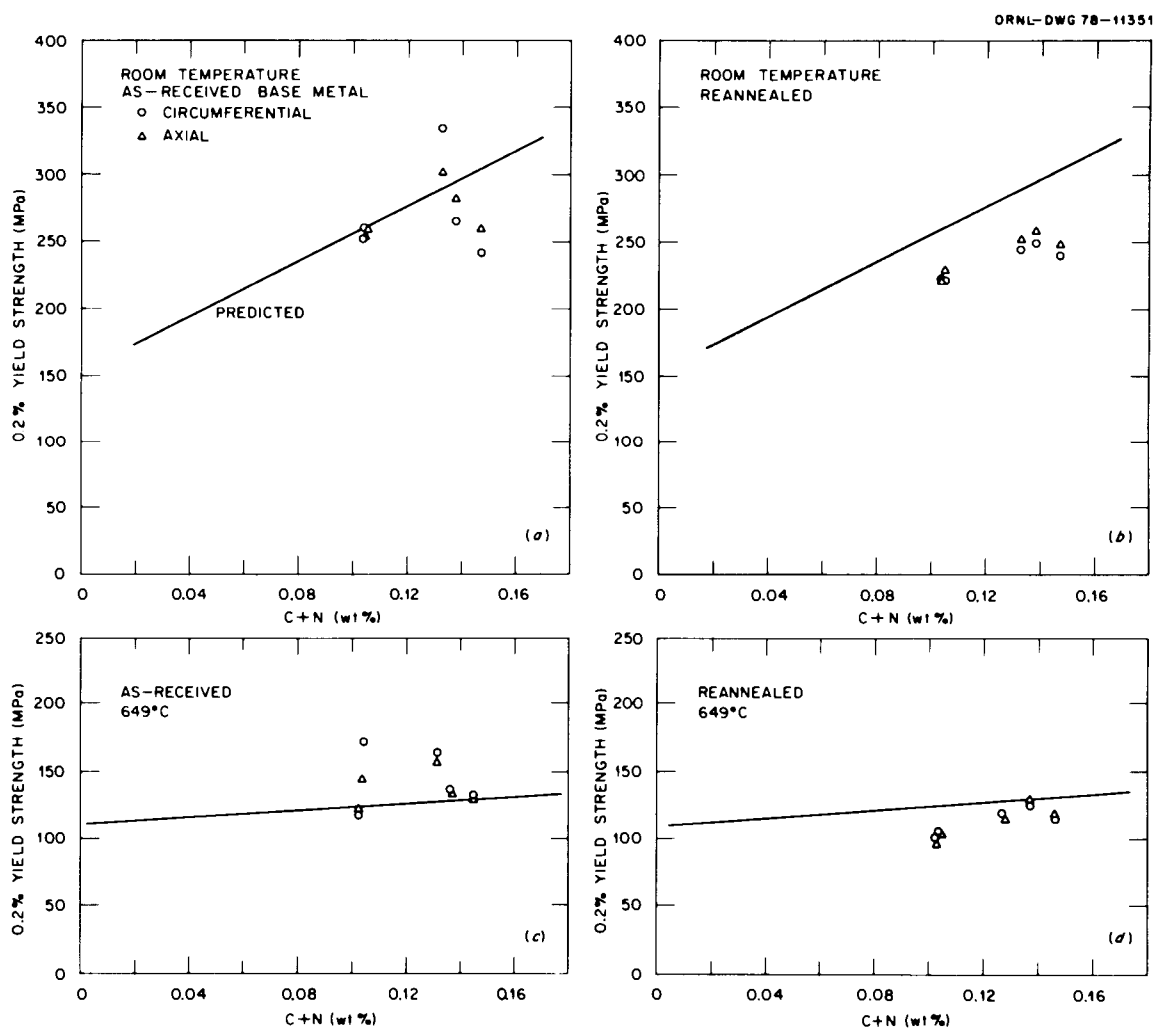

Fig. 73. Plot of yield strength as a function of the C + N content for the base metal of the five pipes. At room temperature; (*a*) as-received condition, (*b*) reannealed condition. At 649°C; (*c*) as-received condition, (*d*) reannealed condition. The solid line is predicted by ref. 45.

At room temperature, both the as-received and reannealed data showed the trend of increasing yield strength with increasing C + N [Fig. 73(*a*) + (*b*)]. However, the as-received data showed significantly more scatter than did the reannealed data. The greater scatter in as-received data is probably a consequence of varying degrees of residual cold work from straightening operations performed on these pipes (see the previous section for more details). When the residual cold work is removed by reannealing, the trend of increasing yield strength with C + N becomes more consistent with the slope of the predicted line [Fig. 73(*b*)]. Note, however, that the reannealed values are significantly below the predicted line, because the latter was derived from the data in the as-received condition.

The yield strength data at 649°C again shows more scatter in the as-received as compared with the reannealed condition [Fig. 73(*c*) + (*d*)]. Both the predicted and experimental values show that C + N dependence of yield strength is much less at 649°C than observed at room temperature. The reannealed values are again below the predicted line [Fig. 73(*d*)] but have a similar slope.

Figure 74 shows that the observed UTS dependence on C + N is generally less than the predicted line at room temperature and at 649°C. The values for as-received and reannealed specimens are comparable at both test temperatures. The data follow the trend of increasing UTS with increasing C + N.

Weld comparisons. Figure 75(*a*) and (*b*) shows that at room temperature both as-received and reannealed yield strength for the weld increases with increasing C + N content. The as-received data again show more scatter than the reannealed data. Furthermore, the as-received data tend to fall above and the

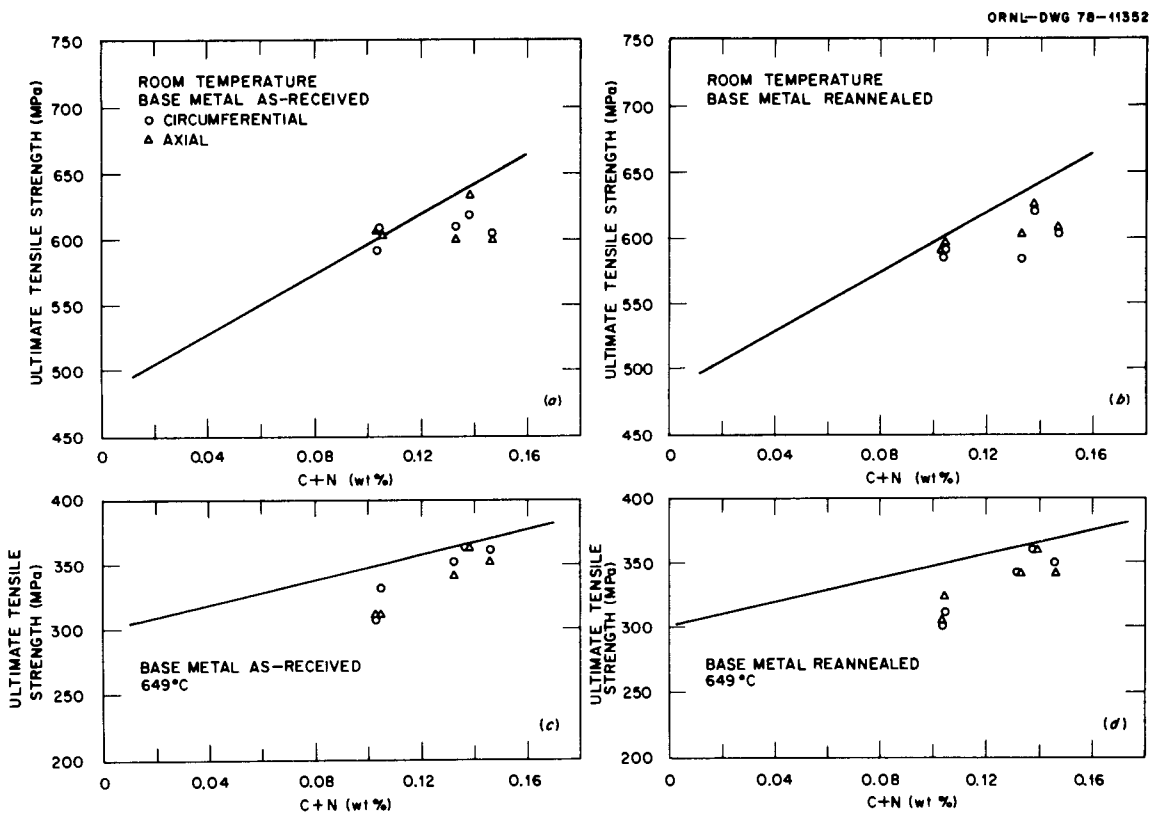

Fig. 74. Plot of ultimate tensile strength as a function of the C + N content for the base metal of the five pipes. At room temperature; (*a*) as-received condition, (*b*) reannealed condition. At 649°C; (*c*) as-received condition, (*d*) reannealed condition. The solid line is predicted by ref. 45.

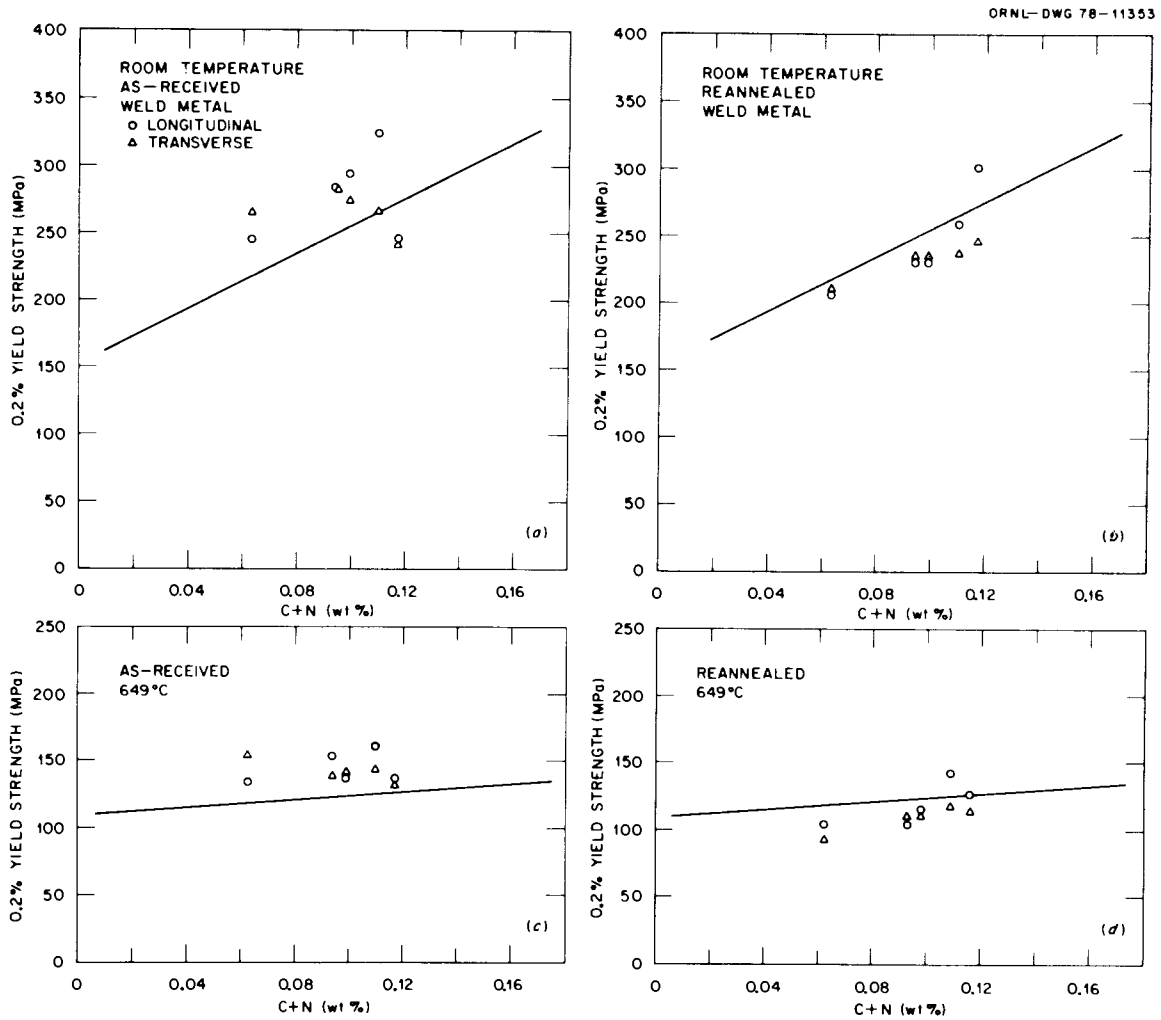

Fig. 75. Plot of yield strength as a function of C + N content for the weld of the five pipes. At room temperature; (*a*) as-received condition, (*b*) reannealed condition. At 649°C; (*c*) as-received condition, (*d*) reannealed condition. The solid line is predicted by ref. 45.

reannealed data below the predicted line. The reannealed data in Fig. 75(*b*) show that the predicted line [Eq. (6)], which uses entirely base-metal data, predicts a correct slope for the yield strength dependence on C + N of the weld.

The observations made for room-temperature data [Fig. 75(*a*) and (*b*)] are also true for data at 649°C [Fig. 75(*c*) and (*d*). Note again that the yield strength dependence on C + N is relatively much weaker at 649°C than at room temperature.

Figure 76(*a*) and (*b*) shows that at room temperature the experimental data on UTS experience a dramatic deviation in slope from the predicted line. The as-received data [Fig. 76(*a*) show an increase in UTS up to 0.095% C + N followed by a rapid drop in value at higher values of C + N. The reannealed data [Fig. 76(*b*)] also increase to 0.095% C + N and then drop. However, the values do not continue to decrease as did the as-received values. The reasons* for the behavior of the as-received and reannealed data are not clear at present.

*Probably results from the anisotropy of the weld and the influence of martensite formation after a certain C + N level.

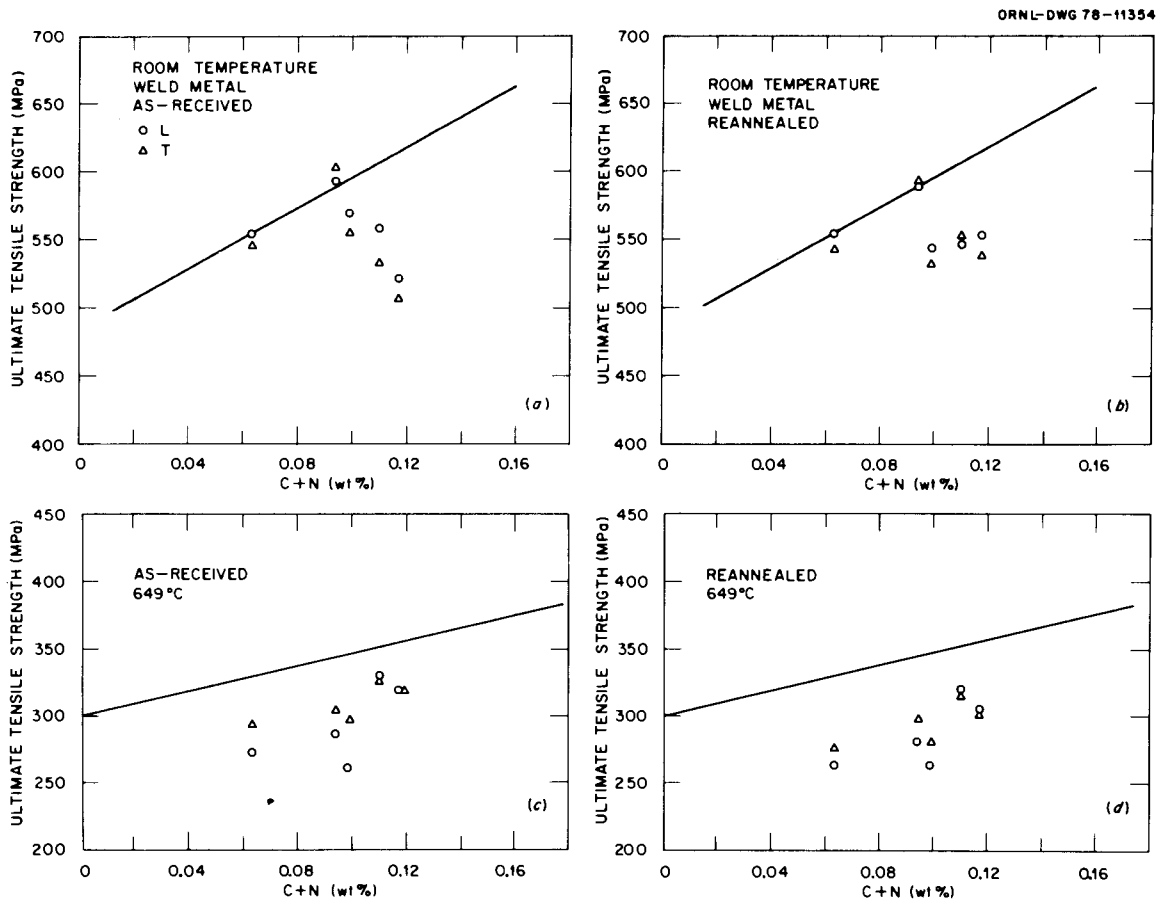

Fig. 76. Plot of ultimate tensile strength as a function of C + N content for the weld of the five pipes. At room temperature; (*a*) as-received condition, (*b*) reannealed condition. At 649°C; (*c*) as-received condition, (*d*) reannealed condition. The solid line is predicted by ref. 45.

At 649°C, the trend of increasing UTS with C + N content is again apparent. However, the experimental use of base-metal data. It is interesting to note that the two pipes with the highest C + N (G-15 and G-16) and UTS have stress-rupture lives (tests still in progress) that are currently as much as five times greater than for tests completed on the other pipes.

In summary, Figs. 73 through 76 have shown that the observed variations in the yield and UTS of the base metal and weld (except the room-temperature UTS of the welds) are related to the variation in C + N content. It therefore appears that these elements should be controlled within specific ranges to ensure that minimum property requirements can be obtained. The effect of C + N variation on the UTS is considered to be more important because of its relationship[39–41] with creep and creep-rupture behavior.

7.9 Stress-Strain Behavior (up to 5% Strain)

The monotonic stress-strain behavior (up to 5% strain) of austenitic stainless steel can be described by

$$\sigma - \sigma_{PL} = \frac{Cpe_p}{1 + Pe_p} + He_p \ , \tag{8}$$

where

C = measure of strength level and, as shown later, is related to yield strength,

H = steady-state hardening rate ($d\sigma/\epsilon d$),

P = parameter describing the shape of the stress-strain curve before reaching the steady-state hardening,

σ_{PL} = proportional limit of stress below which there is no plastic strain,

e_p = true plastic strain.

The value σ_{PL} was estimated to be $0.5\sigma_y$, where $0.5\sigma_y$ is the 0.2% offset yield strength. The constant H is 2758 MPa, while P is given by $500C$. The value of C is determined by the criterion that $\sigma = \sigma_y$ for e_p = 0.002. Since a knowledge of stress and Young's modulus yields the magnitude of the elastic strain, Eq. (8) can be used to calculate the total strain corresponding to a given stress by only knowing the yield strength of the material at a given temperature. The analysis of stress-strain behavior is fully described elsewhere.[46]

Sikka and Booker[47] and Hammond and Sikka[48] have found excellent agreement between experimental stress-strain curves and those predicted by Eq. (8) for several heats of types 304 and 316 stainless steel.

The purpose of this section is to check whether Eq. (8) can predict the stress-strain behavior of the base metal and weld for the pipes tested. Figures 77 through 81 show the comparisons between the predicted and observed stress-strain curves for the base metal of the five pipes. These comparisons are made for axial specimens and at test temperatures of room temperature, 427, 538, and 649°C. These figures show that the model, Eq. (8), accurately predicts the experimental behavior of the base metal at all test temperatures. Two of the tests for pipe G-15, one at room temperature and one at 649°C, are predicted with less accuracy than are the rest of the 18 tests. Thus it can be concluded that Eq. (8) is applicable in predicting the stress-strain behavior (up to 5%) of the base metal of large-diameter formed and welded pipes.

Figures 82 through 86 compare the predicted stress-strain curves with the experimental curves for longitudinal weld specimens from the five pipes. Once again these comparisons are for test temperatures of room temperature, 427, 538, and 649°C. The model, Eq. (8), appears to predict longitudinal weld stress-strain behavior less accurately than it does for axial base-metal behavior. In general, the observed steady-state hardening rate ($H = d\sigma/d\epsilon$) is less than predicted from Eq. (8). The difference in steady-state hardening rate appears to be the greatest for the autogenous weld (G-16) and the SA weld with type 16-8-2 filler metal (H-22). It therefore appears that the stress-strain model developed from base-metal data can be used to accurately predict weld behavior by modifying the steady-state hardening parameter, H. For example, the change of H from 2758 MPa for the base metal to 2200 MPa will predict the stress-strain curves more accurately for the welds from pipes G-16 and H-22.

It can be concluded that a model of the type given in Eq. (8) is capable of describing the general shape of the stress-strain curve (up to 5%) for both the base metal and weld from formed and welded pipes. However, for accurate prediction of weld stress-strain behavior, a modified hardening parameter, H, may need to be used.

7.10 Photographs of Tensile-Tested Specimens

Photographs of the tensile-tested specimens from the base metal and weld of each pipe are shown in Figs. 87 through 91. These figures show that the longitudinal weld specimens generally experienced uniform straining, as did the base metal. However, because the transverse weld specimens are composites of the weld, HAZ, and the base metal, the straining was concentrated in the weaker weld metal. These figures show that the tensile failure occurs in the weld of each of the transverse specimens as postulated in one of the previous sections of this report. In summary, the photographs of tensile-tested specimens have shown that in the formed and welded pipe, the weld is the weakest link in transverse specimens.

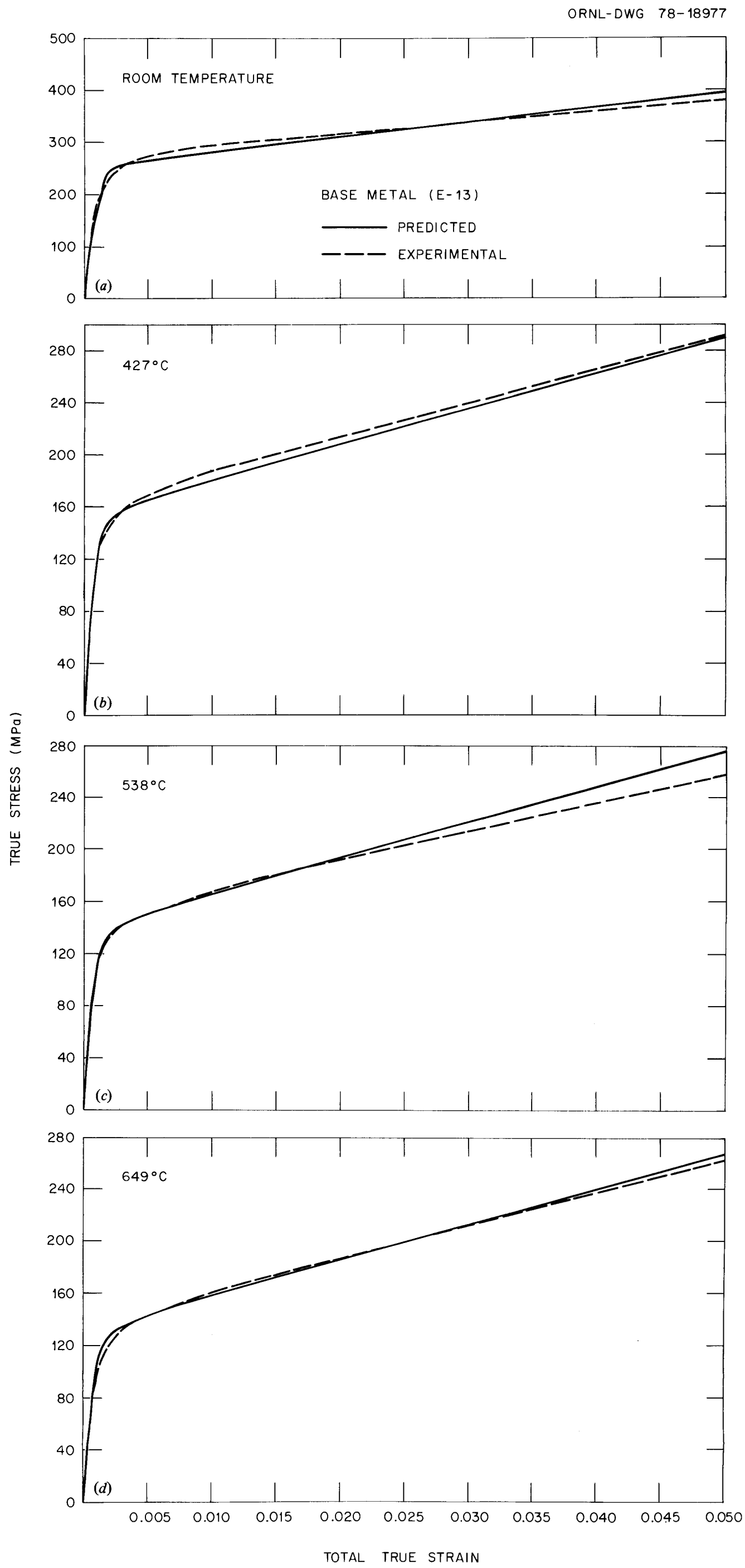

Fig. 77. Comparison of experimental vs predicted stress-strain curves for axial base-metal specimens from pipe E-13. The dashed line represents the experimental data; the solid line represents the predicted behavior. (*a*) Room temperature, (*b*) 427°C, (*c*) 538°C, (*d*) 649°C.

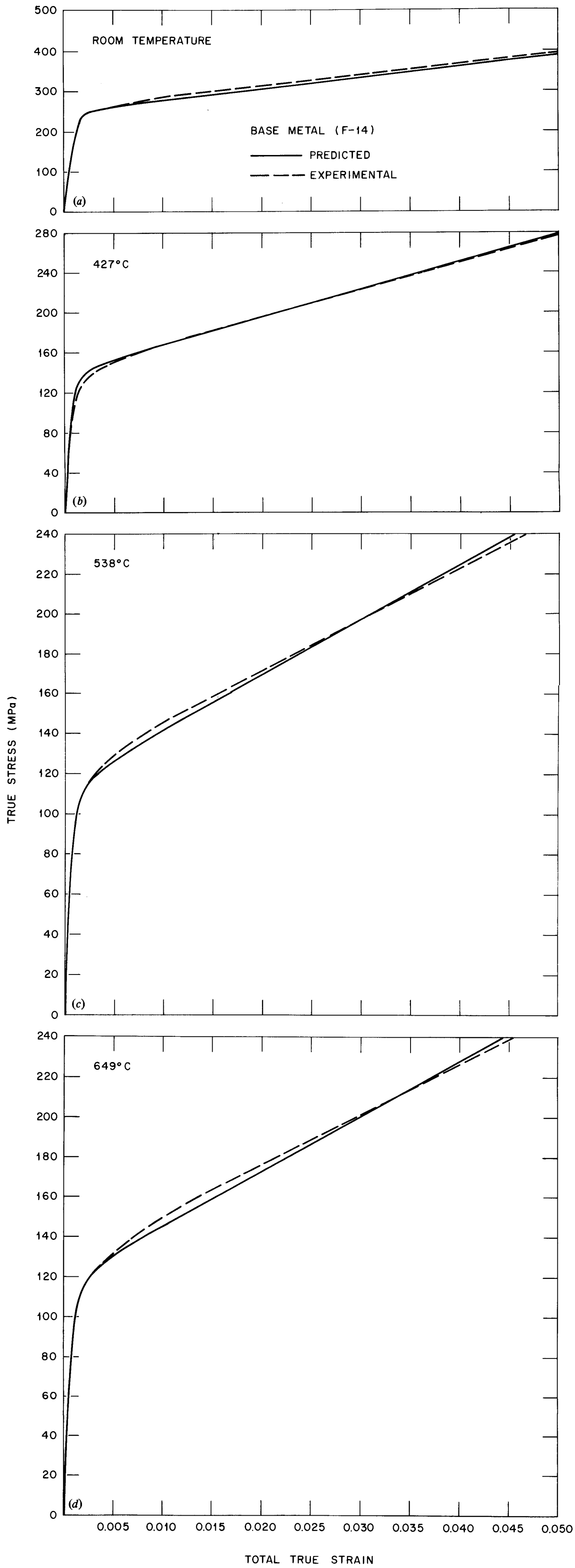

Fig. 78. Comparison of experimental vs predicted stress-strain curves for axial base-metal specimens from pipe F-14. The dashed line represents the experimental data; the solid line represents the predicted behavior. (*a*) Room temperature, (*b*) 427°C, (*c*) 538°C, (*d*) 649°C.

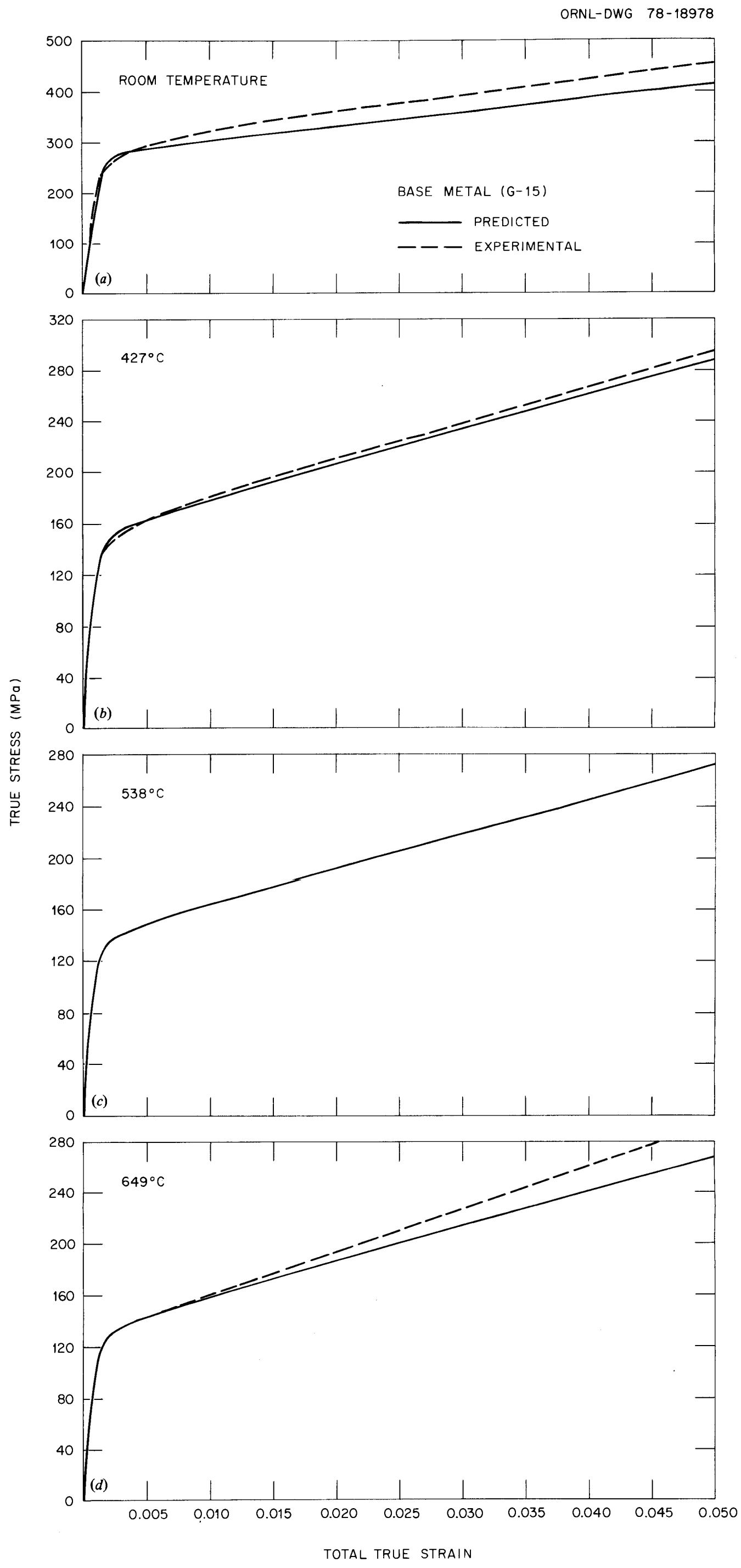

Fig. 79. Comparison of experimental vs predicted stress-strain curves for axial base-metal specimens from pipe G-15. The dashed line represents the experimental data; the solid line represents the predicted behavior. (*a*) Room temperature, (*b*) 427°C, (*c*) 538°C, (*d*) 649°C.

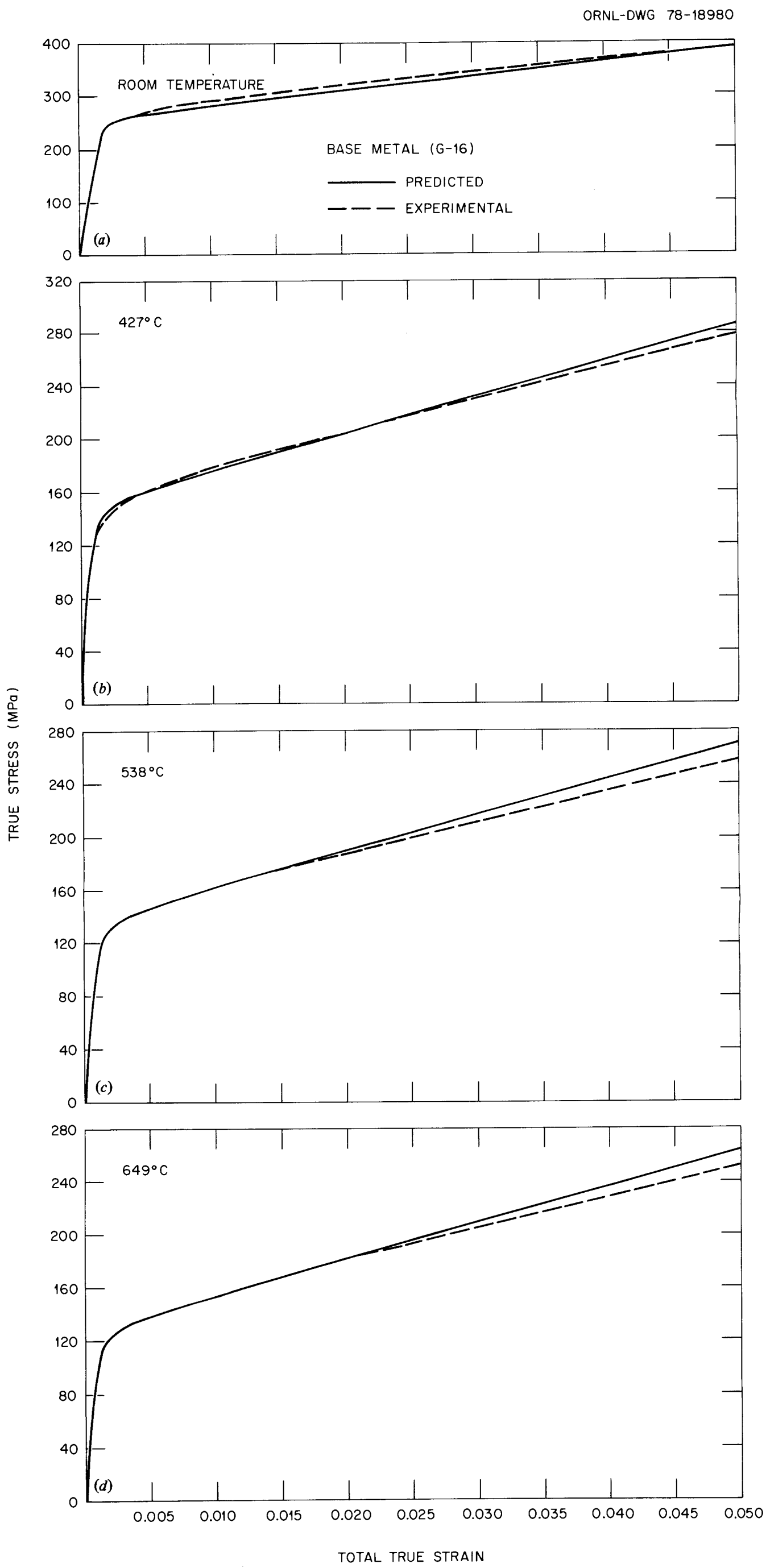

Fig. 80. Comparison of experimental vs predicted stress-strain curves for axial base-metal specimens from pipe G-16. The dashed line represents the experimental data; the solid line represents the predicted behavior. (*a*) Room temperature, (*b*) 427°C, (*c*) 538°C, (*d*) 649°C.

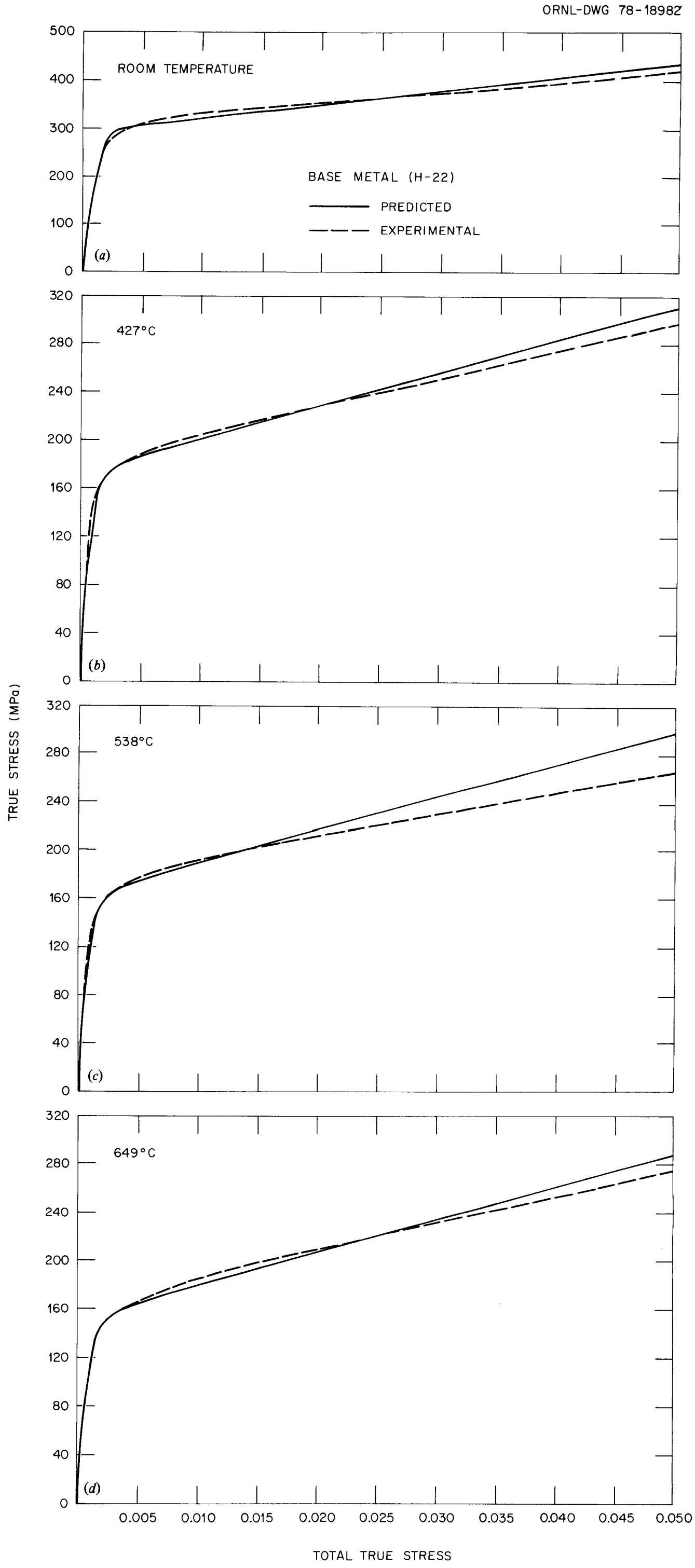

Fig. 81. Comparison of experimental vs predicted stress-strain curves for axial base-metal specimens from pipe H-22. The dashed line represents the experimental data; the solid line represents the predicted behavior. (*a*) Room temperature, (*b*) 427°C, (*c*) 538°C, (*d*) 649°C.

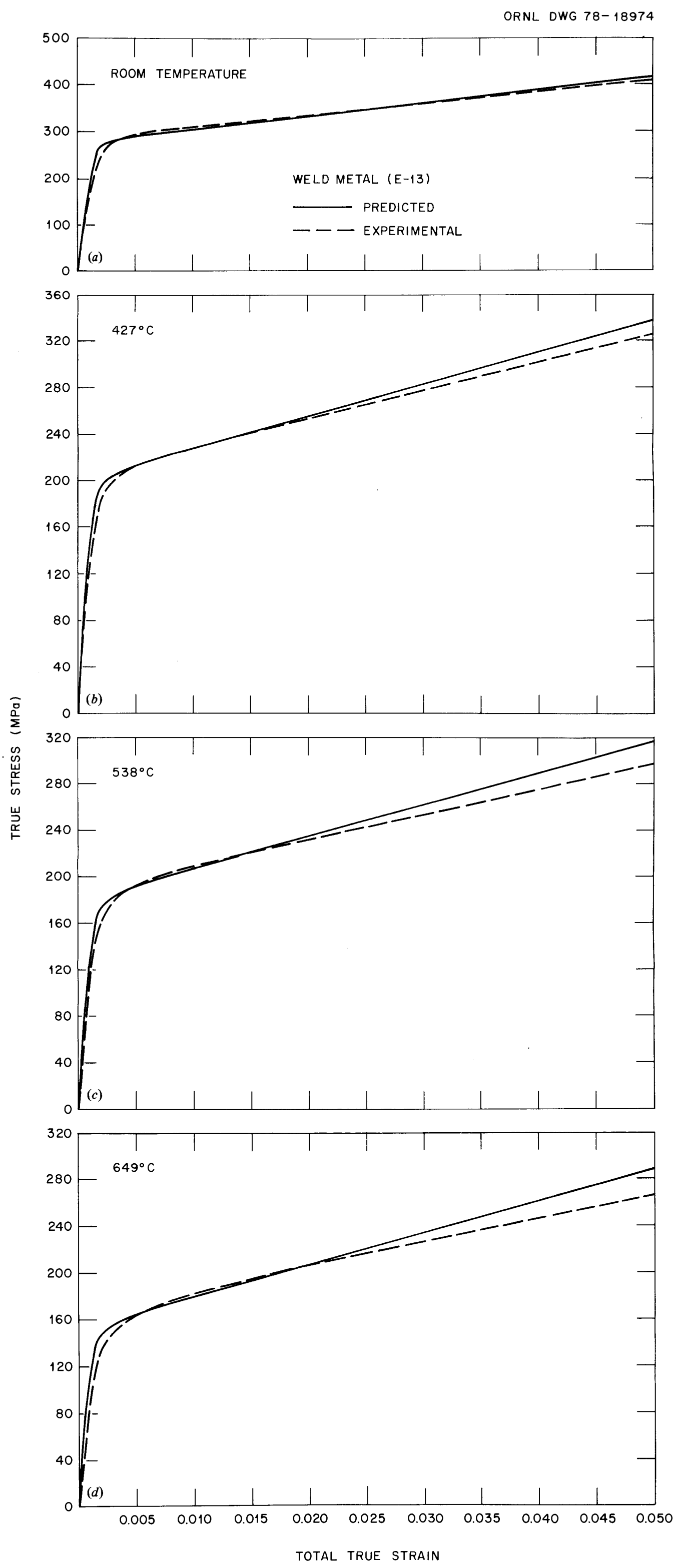

Fig. 82. Comparison of experimental vs predicted stress-strain curves for longitudinal weld specimens from pipe E-13. The dashed line represents the experimental data; the solid line represents the predicted behavior. (*a*) Room temperature, (*b*) 427°C, (*c*) 538°C, (*d*) 649°C.

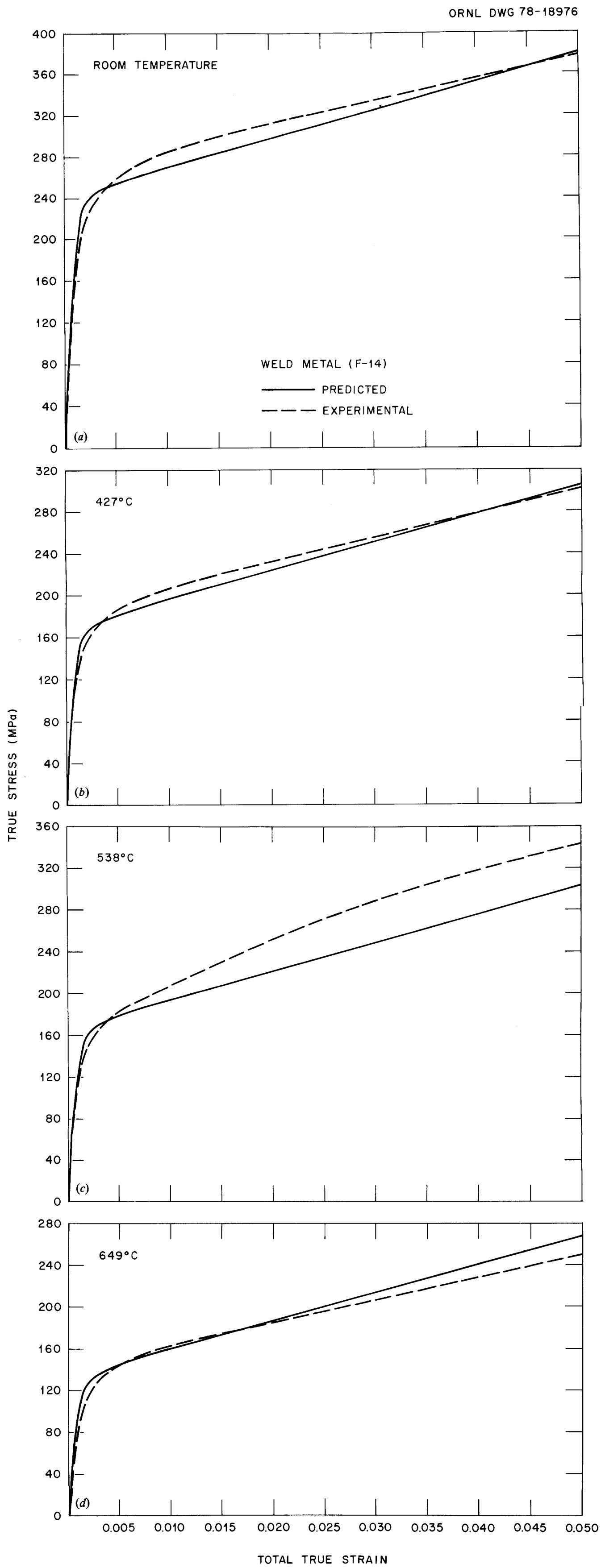

Fig. 83. Comparison of experimental vs predicted stress-strain curves for longitudinal weld specimens from pipe F-14. The dashed line represents the experimental data; the solid line represents the predicted behavior. (*a*) Room temperature, (*b*) 427°C, (*c*) 538°C, (*d*) 649°C.

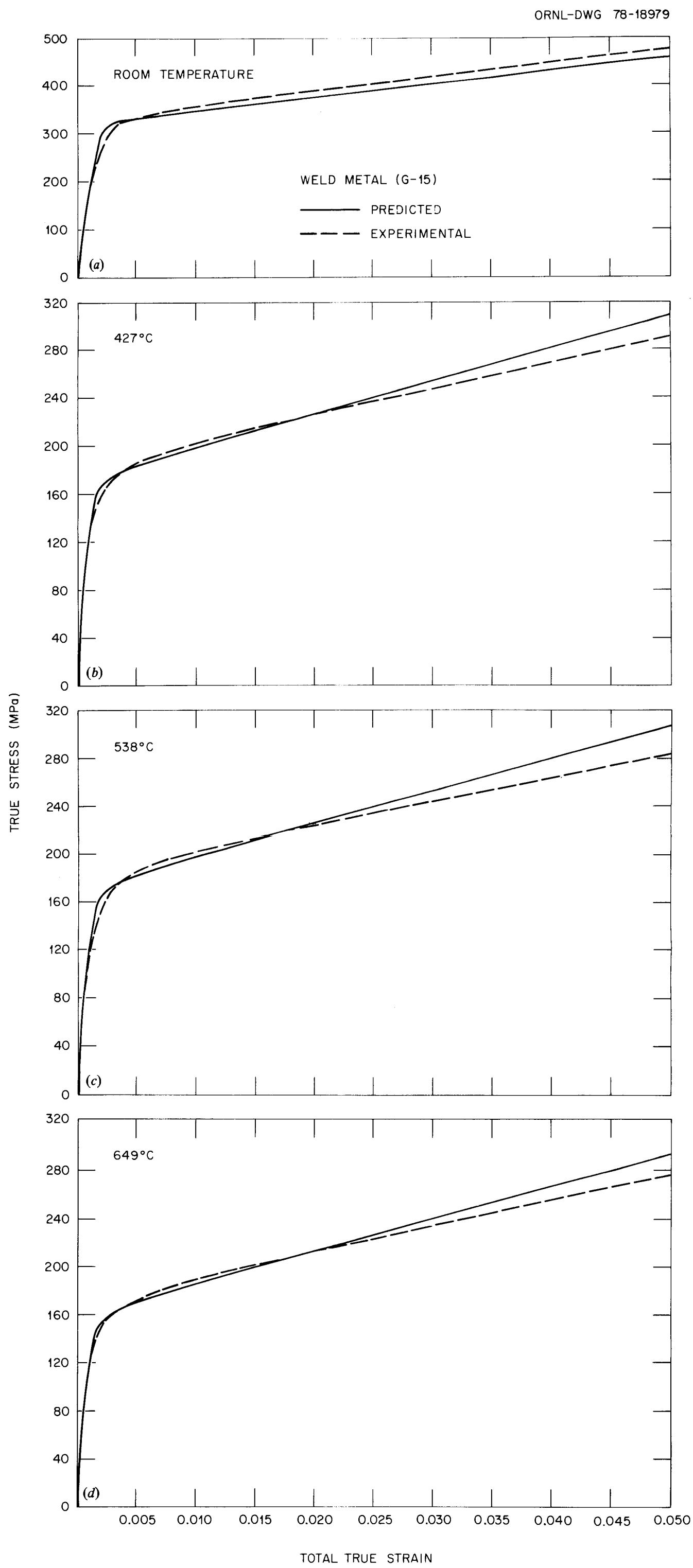

Fig. 84. Comparison of experimental vs predicted stress-strain curves for longitudinal weld specimens from pipe G-15. The dashed line represents the experimental data; the solid line represents the predicted behavior. (*a*) Room temperature, (*b*) 427°C, (*c*) 538°C, (*d*) 649°C.

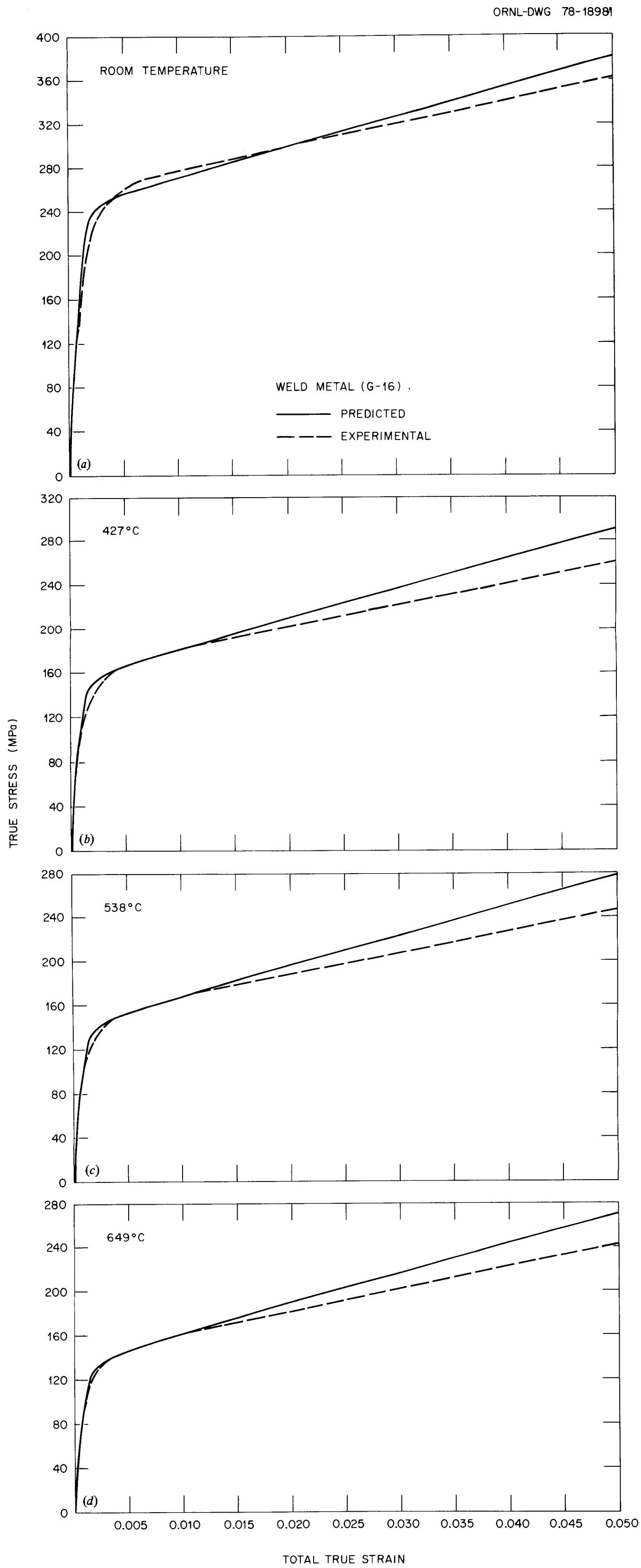

Fig. 85. Comparison of experimental vs predicted stress-strain curves for longitudinal weld specimens from pipe G-16. The dashed line represents the experimental data; the solid line represents the predicted behavior. (*a*) Room temperature, (*b*) 427°C, (*c*) 538°C, (*d*) 649°C.

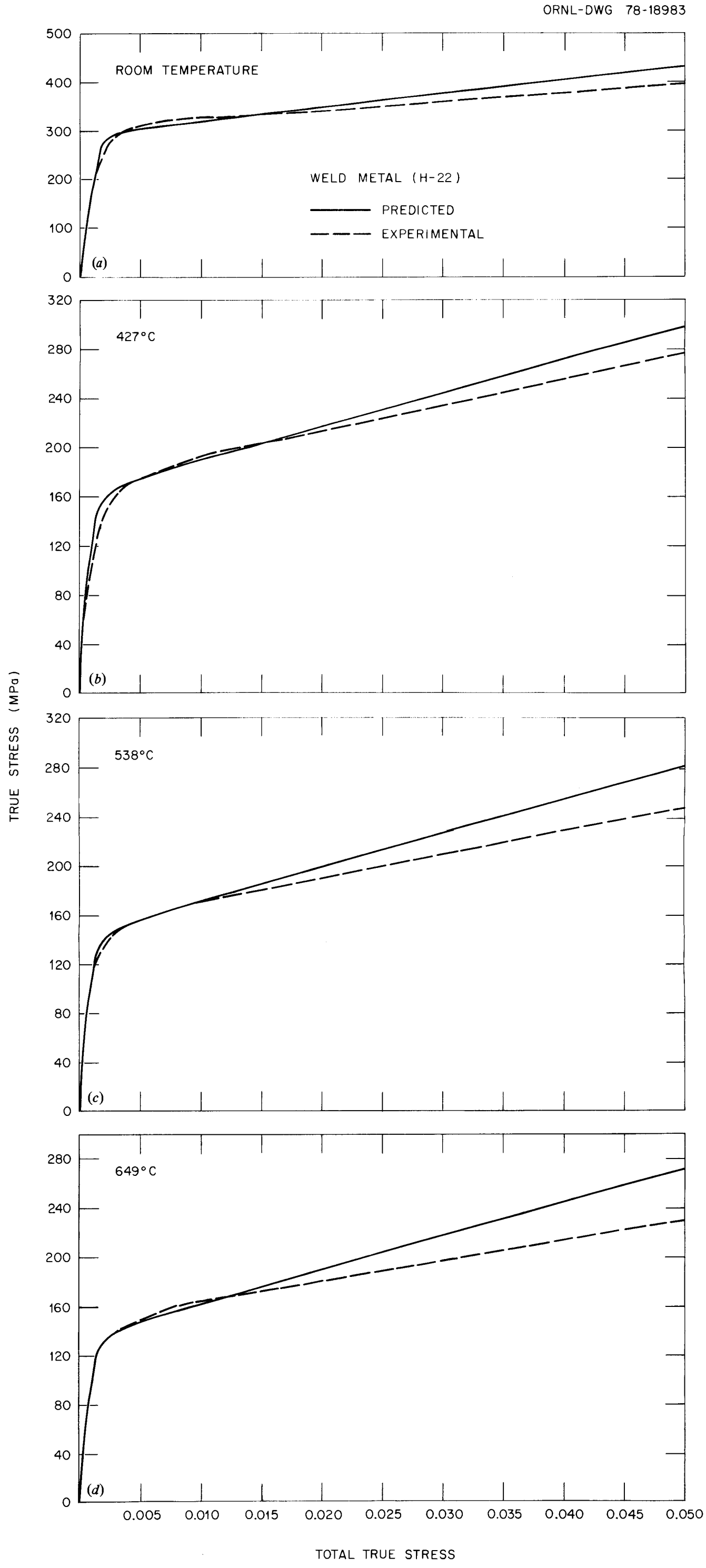

Fig. 86. Comparison of experimental vs predicted stress-strain curves for longitudinal weld specimens from pipe H-22. The dashed line represents the experimental data; the solid line represents the predicted behavior. (*a*) Room temperature, (*b*) 427°C, (*c*) 538°C, (*d*) 649°C.

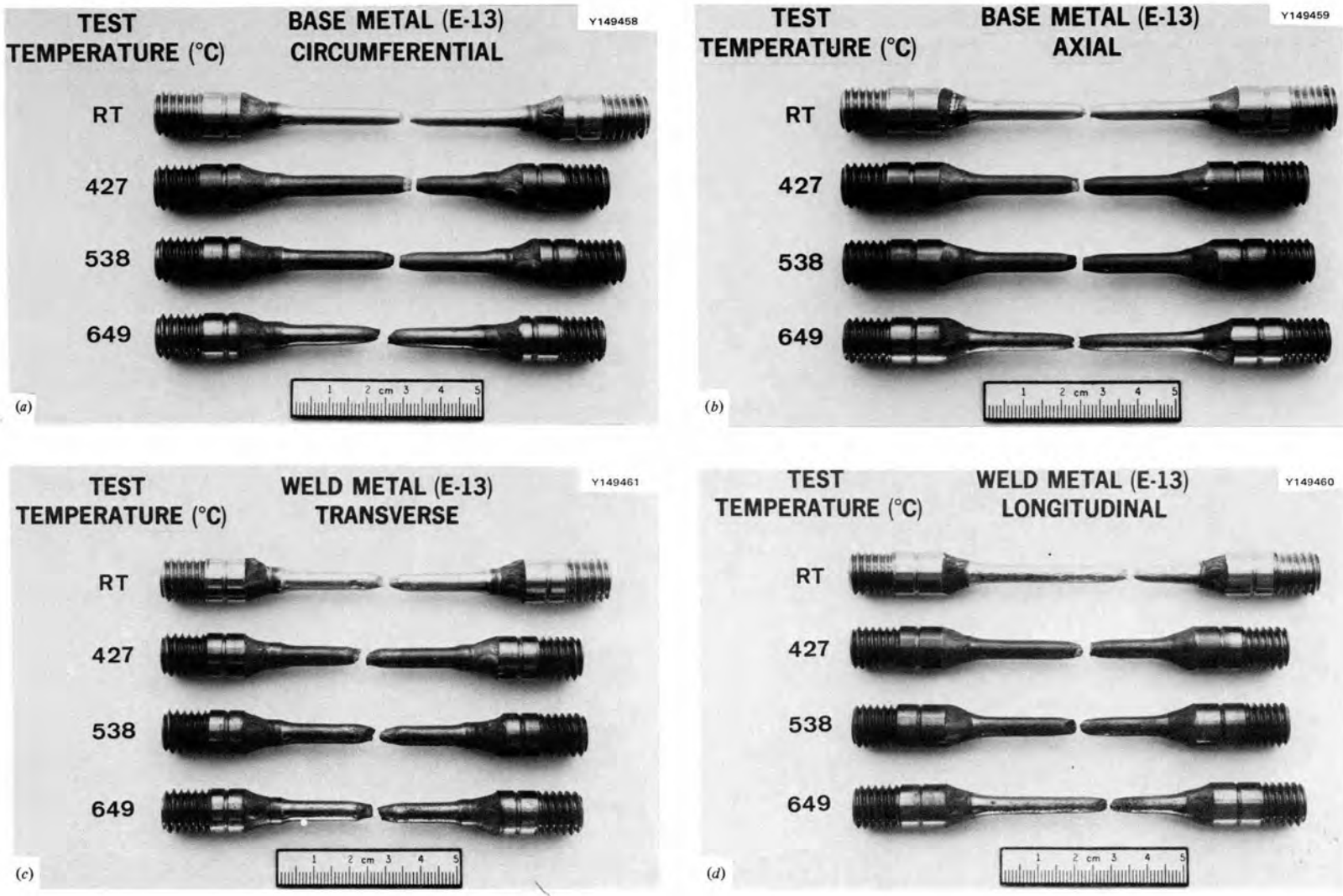

Fig. 87. Tensile specimens of E-13 pipe of type 316 stainless steel. (*a*) Base-metal circumferential, (*b*) base-metal axial, (*c*) transverse weld, (*d*) longitudinal weld.

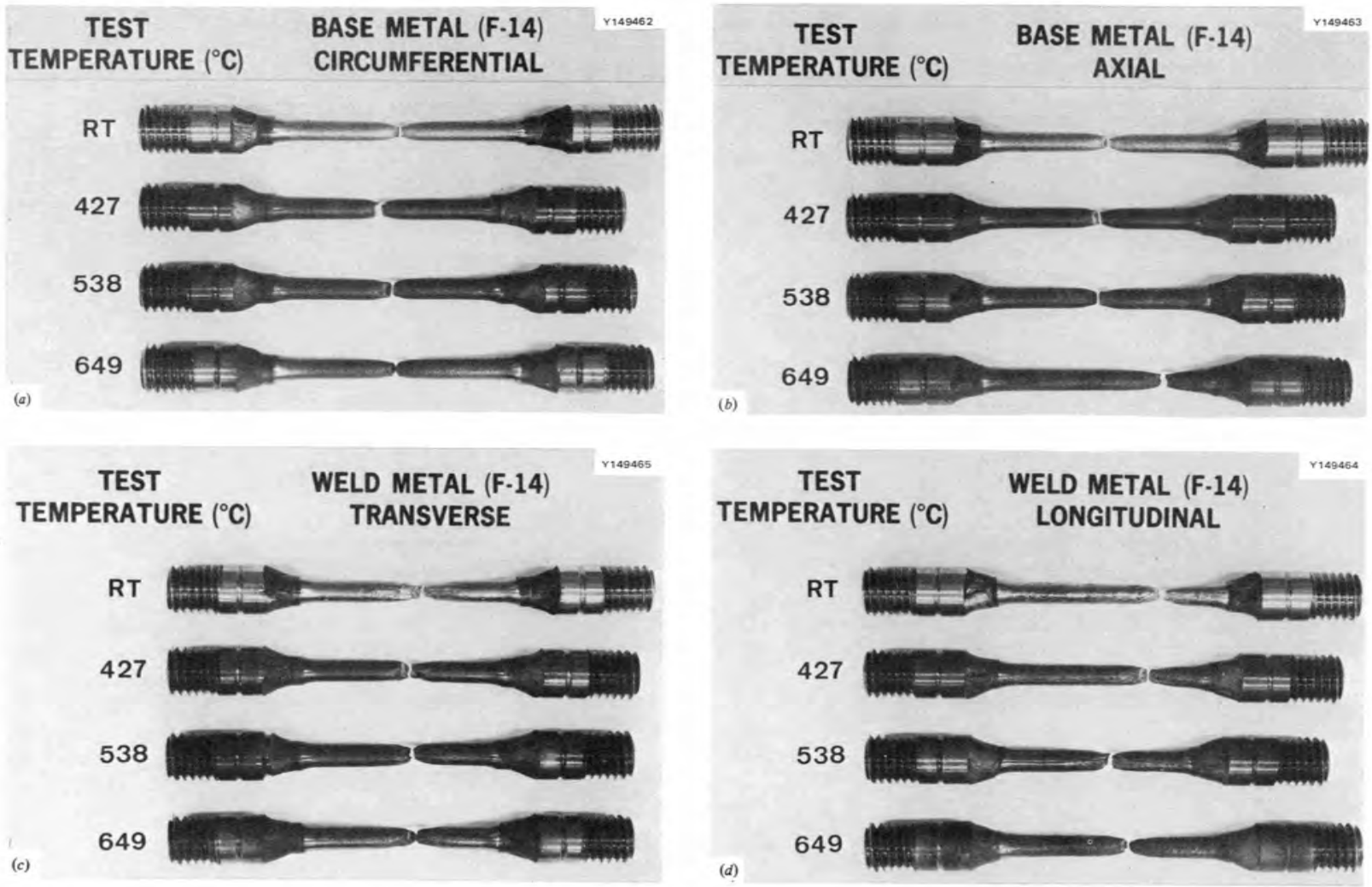

Fig. 88. Tensile specimens of F-14 pipe of type 316 stainless steel. (*a*) Base-metal circumferential, (*b*) base-metal axial, (*c*) transverse weld, (*d*) longitudinal weld.

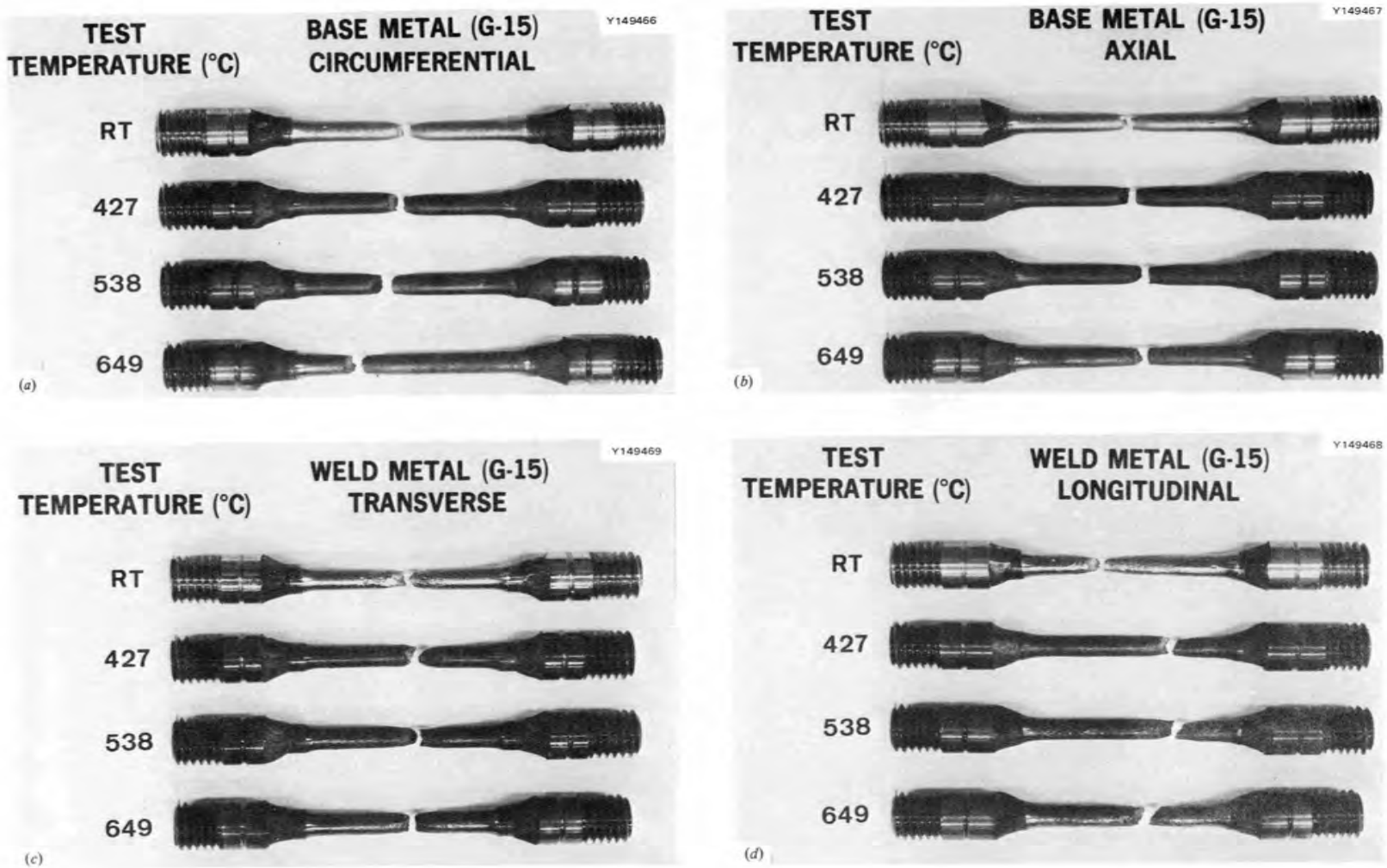

Fig. 89. Tensile specimens of G-15 pipe of type 316 stainless steel. (*a*) Base-metal circumferential, (*b*) base-metal axial, (*c*) transverse weld, (*d*) longitudinal weld.

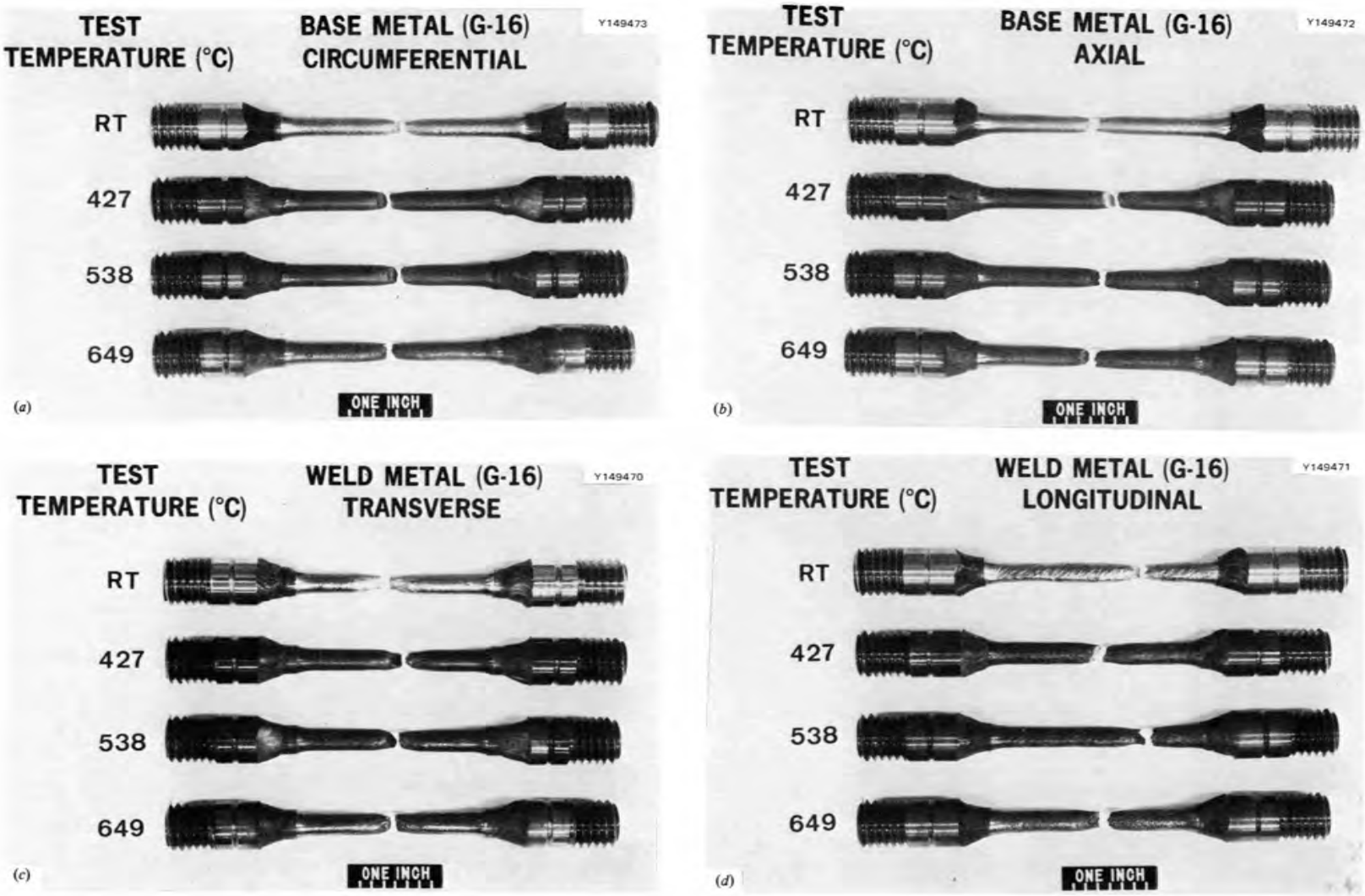

Fig. 90. Tensile specimens of G-16 pipe of type 316 stainless steel. (*a*) Base-metal circumferential, (*b*) base-metal axial, (*c*) transverse weld, (*d*) longitudinal weld.

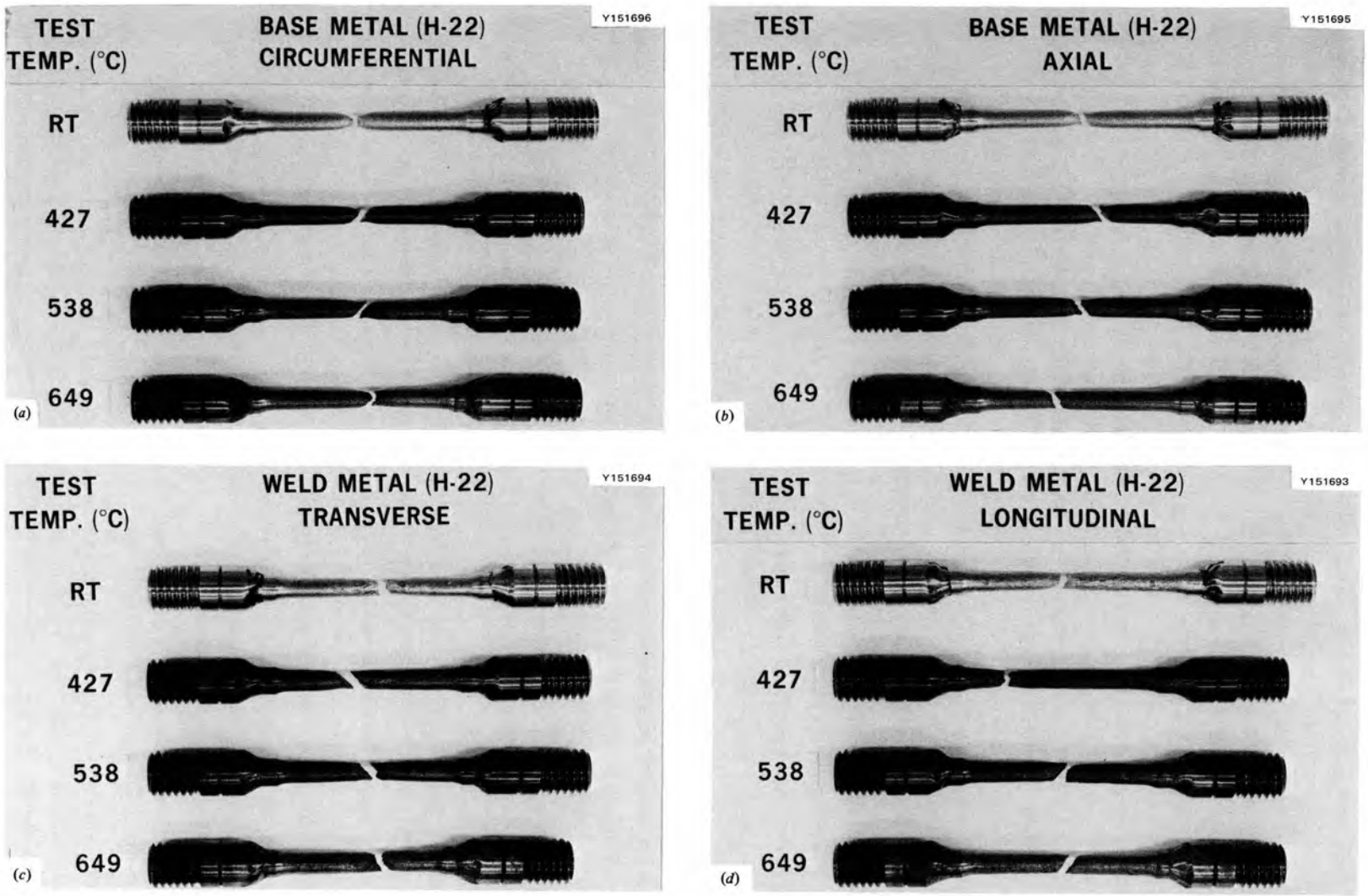

Fig. 91. Tensile specimens of H-22 pipe of type 316 stainless steel. (*a*) Base-metal circumferential, (*b*) base-metal axial, (*c*) transverse weld, (*d*) longitudinal weld.

7.11 Summary of Mechanical Property Characterization

Tensile data were reported on five formed and welded pipes of type 316 stainless steel. Tensile tests were performed on specimens taken from both the base metal and weld. The tensile tests were primarily carried out on material in the as-received condition. However, eight tests per pipe (four at room temperature and four at 649°C) were also performed on material in the reannealed condition. The reannealing treatment consisted in heating specimens at 1065°C for 0.5 hr followed by rapid cooling. The tensile tests were supplemented by photographs of the specimens to show the location of failure.

Tensile stress-strain curves for the base metal and weld were compared. The tensile properties were compared with the upper and lower bounds for the wrought material. The weld properties of each pipe were compared with the corresponding base-metal properties. The tensile properties of an SA weld were compared with a GTA weld to study the effect of welding procedure. The reannealed and as-received data were used to estimate the residual cold work (from straightening) in the base metal and weld of each pipe. The variation in tensile properties of the base metal and weld was examined in terms of currently available relationships between strength properties and the C + N content. A previously developed stress-strain model for the base metal was used to predict the stress-strain behavior (up to 5%) of the base metal and weld from each of the pipes. The following conclusions can be drawn from this work:

1. The yield strength values of the base metal of all five pipes were close to or slightly below the average for the wrought material, whereas those of the weld were close to or slightly above the average.
2. The ultimate tensile strengths of base metal from all five pipes were close to or slightly above the upper bound for the wrought material, whereas the weld values were close to or below the lower bound. Some of the weld values even fall below the minimum curve determined by the ratio method.
3. The uniform elongations of base metal from all pipes were close to the average for the wrought data, whereas the weld values fall below the lower bound. Several weld values were even below the minimum curve determined by the ratio method. The transverse weld specimens generally showed lower values than did the longitudinal specimens.
4. Total elongation values for the base metal were above average or close to the upper bound for the wrought material. However, several of the weld values were below the lower bound for the wrought material.
5. Reduction-of-area values for the base metal were within the range observed for the wrought material. A significant number of the values for the weld fell below the lower bound for the wrought material.
6. Yield strength was a function of the welding process. The GTA process with type 16-8-2 filler metal resulted in yield strength values equal to or greater than those of the base metal. The SA process with type 16-8-2 filler metal resulted in yield strength values lower than those of the base metal.
7. The ultimate tensile strength of the weld was always lower than that of the corresponding base metal. The extent of lowering was influenced by the welding process. The SA process produced the greatest difference between the base metal and the weld.
8. The uniform elongation of the SA weld with type 16-8-2 filler metal was lower than that of the corresponding GTA weld with 16-8-2 filler metal.
9. Based on yield strength data, the as-received base metal contained residual straightening stress (corresponds to increase in friction stress) in the range of 5 to 58 MPa (0.7 to 8.4 ksi) for the five pipes. The corresponding values for the welds were 6 to 68 MPa (0.9 to 9.9 ksi). Although reannealing may reduce the yield strength to values at or below the minimum requirement, the yield strength is not considered to be an important property in terms of creep and creep-rupture behavior.

10. Reannealing decreased the base-metal ultimate tensile strength in the range of 0 to 28 MPa (0.4 ksi). The corresponding decrease for the weld-metal regions was 6 to 43 MPa (0.7 to 6.2 ksi). These decreases are not considered to be significant in terms of the relationship between UTS and creep and creep-rupture properties.
11. The observed variations in the yield and ultimate tensile strength of the base metal and weld (except weld room-temperature ultimate tensile strength) were related to the variation in C + N content.
12. A previously developed stress-strain model could generally describe the stress-strain behavior (up to 5%) of the base metal and weld for all five pipes. However, for an accurate description of the weld, a modified steady-state strain-hardening constant is necessary.
13. On the basis of previous work, the lower ultimate tensile strength values of the weld as compared with the base metal are expected to produce reduced creep-rupture properties. The SA weld is expected to show poorer creep-rupture properties than those of the GTA welds.
14. Irrespective of the welding process and filler metal combinations tested, the weld was the weakest link in the formed and welded pipe for transverse tensile tests.

8. CONCLUSIONS

The results of this characterization indicate that formed and welded pipe can be manufactured at a lower cost than can the hot-extruded and -worked pipe used for the FFTF. However, the dimensional requirements as compared with the FFTF were shown to have been relaxed in order to allow the use of formed and welded pipe for the Clinch River Breeder Reactor. While stress analyses have been performed to justify the relaxed dimensional control, fitup for welding was shown to conceivably be affected. Therefore, the selection of formed and welded pipe over alternate manufacturing methods must weigh the loss of dimensional control against the potential cost reduction.

The tensile properties of the weldments in the five formed and welded pipes were shown to be generally weaker than those for the base metal. The most significant differences were for UTS and ductility. Since UTS has been used to predict creep and stress-rupture properties for base metals,[39–41] the weldments in these pipes are expected to have reduced time-dependent properties as compared with the base metal. Although ASME Code Case N-47[4] currently penalizes welds being used at elevated temperature to account for these reduced properties, the penalty factor was arbitrarily set by limiting the allowable strain for the weld region to one-half the value permitted for the base metal. If welded pipe is going to be used, it would appear that a more realistic method should be employed to account for the reduced weldment properties. One possible method would be to establish a design limit curve for weldment creep and stress-rupture properties which would enable correlation to acceptance testing of weld prolongations from actual components or from welding procedure qualification tests. The proposed method could provide a means to account for variations resulting from such factors as base metal, filler metal, flux, and arc atmosphere composition; dilution; heat input; welding travel speed; and heat treatment. One such method which utilizes UTS at the temperature of interest is being investigated at ORNL. It is important to remember that the sodium coolant system piping will contain non-heat-treated circumferential welds joining pipe sections even if seamless pipe is used. The use of the design method being investigated at ORNL would also be applicable to these welds.

ACKNOWLEDGMENTS

We would like to acknowledge D. P. Edmonds, G. M. Goodwin, R. T. King, and G. M. Slaughter for their work early in this program, R. J. Beaver for his efforts in writing the specifications for and procuring the pipe, T. G. Ramsey and J. L. Holbrook for performing the dimensional and radiographic inspections, C. W. Houck for performing the metallographic evaluations, L. Deroos and J. Green (Y-12 Plant) for performing the QTM examinations, D. P. Edmonds for obtaining the chemical analyses, L. T. Ratcliff for performing the tensile tests, R. Baldwin for his efforts in processing the mechanical properties data, K. Gardner for typing the draft of this paper, and R. T. King and R. E. McDonald for reviewing this paper. The report was edited and composed under subcontract with Adroit, Inc.

REFERENCES

1. *Clinch River Breeder Reactor Plant Design,* Breeder Reactor Corp., October 1975.

2. R. A. Moen, D. P. O'Keefe, J. E. Irvin, and J. C. Tobin, "Specifying and Manufacturing Piping for the Fast-Flux Test Facility," *ASME Congress on Pressure Vessels and Piping, Miami Beach, Fla., June 24–25, 1974.*

3. ASME Boiler and Pressure Vessel Code, Section III, Division 1, Nuclear Power Plant Components, Appendicies, *Am. Soc. Mech. Eng.,* 1977 edition.

4. ASME Boiler and Pressure Vessel Code, Code Cases, Nuclear Components, *Am. Soc. Mech. Eng.,* 1977 edition.

5. C. R. Brinkman, V. K. Sikka, and R. T. King, *Mechanical Properties of LMFBR Primary Piping Materials,* ORNL-5199 (November 1976).

6. E. C. Rodabaugh, *Stresses in Out-of-Round Pipe Due to Internal Pressure,* ORNL/TM-3244 (January 1971).

7. K. Thomas, *Effects of Nonuniform Geometry and Welding on Piping Elbow Design,* WARD-SD-3045-4 (April 1977).

8. FFTF dimensional inspection records provided by C. Bonham, Hanford Engineering Development Laboratory, Richland, Wash., December 14, 1976.

9. Specification 5853-M-106 for Seamless Austenitic Stainless Steel Pipe for Liquid-Metal Service for the Fast-Flux Test Facility of the U.S. Atomic Energy Commission, Richland, Wash., Rev. 3, June 19, 1974. (unpublished work)

10. J. M. Steichen, *Mechanical Properties of FFTF Primary Outlet Piping,* HEDL/TM-75-15 (January 1975).

11. J. M. Steichen, *FFTF Primary Piping Fabrication Comparison,* HEDL/TME-72-133 (October 1972).

12. ASME Boiler and Pressure Vessel Code, Section II, Material Specification Part A, Ferrous Materials, SA-240, "Specification for Chromium and Chromium-Nickel Stainless Steel Plate, Sheet, and Strip for Fusion-Welded Unified Pressure Vessels," *Am. Soc. Mech. Eng.,* 1974 edition, through summer 1975 addenda.

13. ASME Boiler and Pressure Vessel Code, Section II, Material Specification Part A, Ferrous Materials, SA-358, "Specification for Electric-Fusion-Welded Austenitic Chromium-Nickel Alloy Steel Pipe for High-Temperature Service," *Am. Soc. Mech. Eng.,* 1974 edition, through summer 1975 addenda.

14. ASME Boiler and Pressure Vessel Code, Section III, Material Specification Part A, Ferrous Materials, SA-312, "Specification for Seamless and Welded Austenitic Stainless Steel Pipe," *Am. Soc. Mech. Eng.,* 1974 edition, through summer 1975 addenda.

15. ASME Boiler and Pressure Vessel Code, Section III, Division 1, Nuclear Power Plant Components, Subsection NB – Class 1 Components, *Am. Soc. Mech. Eng.,* 1974 edition, through summer 1975 addenda.

16. ASME Boiler and Pressure Vessel Code, Section III, Division 1, Nuclear Power Plant Components, Subsection NC – Class 2 Components, *Am. Soc. Mech. Eng.,* 1974 edition, through summer 1975 addenda.

17. Specification ORNL MET-WB-MS-3, "Austenitic Stainless Steel Plate, Sheet and Strip (ASME SA-240 with Additional Requirements, Including RDT M5-1T Requirements)," January 26, 1976. (unpublished work)

18. Specification ORNL MET-WB-MS-2, "Austenitic Stainless Steel Welded Pipe, Large-Diameter (ASME SA-358 Including the Additional Requirements of RDT M3-7T)," January 26, 1976. (unpublished work)

19. Specification ORNL MET-WB-MS-4, "Austenitic Stainless Steel Welded Pipe (ASME SA-312 with Additional Requirements)," January 26, 1976. (unpublished work)

20. Bechtel Power Corporation Purchase Order No. 8776-M-106AC, March 10, 1972, provided by C. Bonham, Hanford Engineering Development Laboratory, Richland, Wash., December 14, 1976.

21. C. E. Veall, J. Donaldson, and D. H. Woodward, "Manufacture of Welded Steel Pipe and Tube," *Br. Weld. J.* **15**, 4 (April 1968).

22. ASME Boiler and Pressure Vessel Code, Section III, Division 1, Nuclear Power Plant Components, Subsection NB – Class 1 Components, *Am. Soc. Mech. Eng.* 1977 edition, through summer 1975 addenda.

23. "Three-Roll Forming," *Metals Handbook,* vol. 4, *Forming,* pp. 217–21, 8th ed. 1969.

24. "The Making, Shaping and Treating of Steel," *Manufacture of Steel Tubular Products,* pp. 887–89, ninth ed., 1971.

25. Private discussions with D. P. Edmonds, Oak Ridge National Laboratory, March 29, 1978.

26. "Clinch River Breeder Reactor Plant Specification, Pipe, Large-Diameter, Welded, Sodium Service," Specification No. 953094, Rev. 1, Para. 1.2.2.F, December 1976 and later revisions, Westinghouse Electric Corporation Advanced Reactors Division.

27. M. G. Fontana and N. D. Greene, *Corrosion Engineering,* p. 58, McGraw-Hill, New York, 1967.

28. Standard Specification for General Requirements for Specialized Carbon and Alloy Steel Pipe, A530-75, para. 10 and 12, pp. 536–37 in Part 1, *Steel Piping, Tubing, Fittings, 1976 Annual Book of ASTM Standards, ASTM,* Philadelphia, 1976.

29. "A-480-75, Standard Specification for General Requirements for Flat-Rolled Stainless and Heat-Resisting Steel Plate, Sheet, and Strip," para. 16, p. 356 in *Part 3, Steel Plate, Sheet, Strip, Wire; Metallic Coated Products, 1976 Annual Book of ASTM Standards,* ASTM, Philadelphia, 1976.

30. Clinch River Breeder Reactor Plant Equipment Specification, Shop Fabrication of Piping Sub-assemblies for Liquid-Metal Service, Specification No. E-953109, Rev. 0, April 1977, Westinghouse Electric Corporation Advanced Reactors Division.

31. Private communications with R. Newton, Westinghouse Electric Corp., Advanced Reactors Division.

32. "Clinch River Breeder Reactor Plant Specification, Pipe, Large-Diameter, Welded, Sodium Service," Specification No. E-953094, Rev. 2, Para. 1.2.2.F, February 1977, Westinghouse Electric Corporation Advanced Reactors Division.

33. AWS A4.2-74, *Standard Procedures for Calibrating Magnetic Instruments to Measure the Delta Ferrite Content of Austenitic Stainless Steel Weld Metal,* American Welding Society, Miami, 1974.

34. C. J. Long and W. T. DeLong, "The Ferrite Content of Austenitic Stainless Steel Weld Metal," *Weld. J. (Miami, Fla.)* **52**(7), 281-s–297-s (July 1973).

35. V. K. Sikka, *Tensile Properties of Type 316 Stainless Steel,* report in preparation.

36. G. V. Smith, *An Evaluation of the Yield, Tensile Creep, and Rupture Properties of Wrought 304, 316, 321, 321 and 347 Stainless Steels at Elevated Temperatures,* ASMT Data Series DS5-S2, Am. Soc. for Testing and Materials, Philadelphia (February 1969).

37. V. K. Sikka, R. W. Swindeman, T. L. Hebble, C. R. Brinkman, and M. K. Booker, "Residual Cold Work and Its Influence on Tensile and Creep Properties of Types 304 and 316 Stainless Steels," *Nucl. Technol.* **31**, 96–114 (1976).

38. V. K. Sikka, *Product Form Characterization of Reference Heat of Type 316 Stainless Steel,* ORNL-5384 (February 1978).

39. V. K. Sikka, H. E. McCoy, M. K. Booker, and C. R. Brinkman, "Heat-to-Heat Variation in Creep Properties of Types 304 and 316 Stainless Steel," *J. Pressure Vessel Technol.* **97**, 243–51 (1975).

40. V. K. Sikka and C. R. Brinkman, "Relation Between Short- and Long-Term Elevated Temperature Properties of Several Austenitic Stainless Steels," *Sci. Metall.* **10**, 25–28 (1976).

41. V. K. Sikka, M. K. Booker, and C. R. Brinkman, *Use of Ultimate Tensile Strength to Correlate and Estimate Creep and Creep-Rupture Behavior of Type 304 and 316 Stainless Steel,* ORNL-5285 (October 1977).

42. J. W. McEnerney and V. K. Sikka, *Time-Dependent Properties of Formed and Welded Pipe for Breeder Reactor Application,* report in preparation.

43. K. I. Irvine, T. Gladman, and F. B. Pickering, "The Strength of Austenitic Stainless Steels," *J. Iron Steel Inst.* **207**, 1017–28 (1969).

44. K. Natesan, T. F. Kassner, and Che-Yu Li, "Effect of Sodium on Mechanical Properties and Friction-Wear Behavior of LMFBR Materials," *React. Technol.* **15**, 244–77 (Winter 1972–73).

45. P. Soo and W. H. Horton, *The Effect of Carbon and Nitrogen on the Short-Term Tensile Behavior of Solution-Treated Types 304 and 316 Stainless Steels,* WARD-NA-3045-2 (July 1973).

46. V. K. Sikka, M. K. Booker, and J. P. Hammond, *Rational Polynominal Tensile Stress-Strain Equation for Low-Strain Behavior of Types 304 and 316 Stainless Steel,* report in preparation.

47. V. K. Sikka and M. K. Booker, "Influence of Laboratory Annealing on Tensile Properties and Design Stress Intensity Limits for Type 304 Stainless Steel," *Effects of Melting and Processing Variables on the Mechanical Properties of Steel,* MPC-6, ASME, New York (1977).

48. J. P. Hammond and V. K. Sikka, *Heat-to-Heat Variation of Total Strain (to 5%) at Discrete Stress Levels in Types 316 and 304 Stainless Steel from 24 to 316°C,* ORNL/NUREG/TM-57 (December 1976).

49. S. Kumar, "HTS Piping/Structural Analysis Calculation Summary Sheet," SARB No. LPE-PD-76-30 Rev. 0, Westinghouse Advanced Reactors Division, January 1977. (unpublished work)

50. R. M. Mello, "HTS Piping/Piping Tolerance-Fatigue Damage Study Calculation Summary Sheet," SARB No. LPE-PD-76-031 Rev. 0, Westinghouse Advanced Reactors Division, December 1976. (unpublished work)

51. G. D. Eichenberger, P. W. Turner, and D. W. Hood, *Tooling for Mechanized Welding of Large Diameter Pipe,* TREE-1258, Idaho National Engineering Laboratory, April 1978.

52. Private discussions with G. D. Eichenberger, Idaho National Engineering Laboratory, August 2, 1978.

53. V. K. Sikka, "Elevated-Temperature Ductility of Types 304 and 316 Stainless Steel," accepted for publication in Metals Properties Council book entitled *Ductility and Toughness Considerations in Elevated-Temperature Service,* 1978.

ORNL/TM-6609
Distribution
Category UC-79b, -h, -k

INTERNAL DISTRIBUTION

1–2. Central Research Library
3. Document Reference Section
4–5. Laboratory Records Department
6. Laboratory Records Department, RC
7. ORNL Patent Section
8. M. K. Booker
9. J. M. Corum
10. J. R. DiStefano
11. D. P. Edmonds
12. G. M. Goodwin
13. R. J. Gray
14–15. M. R. Hill
16. J. F. King
17. R. L. Klueh
18. K. C. Lui
19. H. E. McCoy
20–29. J. W. McEnerney
30. A. J. Moorhead
31. C. E. Pugh
32–36. V. K. Sikka
37. G. M. Slaughter
38. J. H. Smith
39. R. W. Balluffi (consultant)
40. W. R. Hibbard, Jr. (consultant)
41. M. J. Mayfield (consultant)
42. J. T. Stringer (consultant)

EXTERNAL DISTRIBUTION

43–44. DOE DIVISION OF REACTOR RESEARCH AND TECHNOLOGY, Washington, DC 20545
Director

45. DOE OAK RIDGE OPERATIONS OFFICE, P.O. Box E, Oak Ridge, TN 37830
Assistant Manager, Energy Research and Development

46–307. DOE TECHNICAL INFORMATION CENTER, Office of Information Services, P.O. Box 62, Oak Ridge, TN 37830

For distribution as shown in TID-4500 Distribution Category,
UC-79b (Fuels and Materials Engineering Development),
UC-79h (Structural Materials Design Engineering), and
UC-79k (Components).